INFORMATION TO USERS

This manuscript has been reproduced from the microfilm master. UMI films the text directly from the original or copy submitted. Thus, some thesis and dissertation copies are in typewriter face, while others may be from any type of computer printer.

The quality of this reproduction is dependent upon the quality of the copy submitted. Broken or indistinct print, colored or poor quality illustrations and photographs, print bleedthrough, substandard margins, and improper alignment can adversely affect reproduction.

In the unlikely event that the author did not send UMI a complete manuscript and there are missing pages, these will be noted. Also, if unauthorized copyright material had to be removed, a note will indicate the deletion.

Oversize materials (e.g., maps, drawings, charts) are reproduced by sectioning the original, beginning at the upper left-hand corner and continuing from left to right in equal sections with small overlaps. Each original is also photographed in one exposure and is included in reduced form at the back of the book.

Photographs included in the original manuscript have been reproduced xerographically in this copy. Higher quality 6" x 9" black and white photographic prints are available for any photographs or illustrations appearing in this copy for an additional charge. Contact UMI directly to order.

DESIGN METHODOLOGY, FABRICATION AND EVALUATION OF A BLOWER-RECIRCULATED, CLOSED VENTILATION SYSTEM AS A PLATFORM FOR ANESTHESIA DELIVERY

By

SAMSUN LAMPOTANG

A DISSERTATION PRESENTED TO THE GRADUATE SCHOOL
OF THE UNIVERSITY OF FLORIDA IN PARTIAL FULFILLMENT
OF THE REQUIREMENTS FOR THE DEGREE OF
DOCTOR OF PHILOSOPHY

UNIVERSITY OF FLORIDA

1992

UMI Number: 9838830

UMI

300 North Zeeb Road
Ann Arbor, MI 48103

Copyright 1992

by

Samsun Lampotang

I dedicate this work to the memory of my parents

"... that I may add my line of verse to the eternal song of humanity ..."

Robin Williams in
Dead Poet's Society

ACKNOWLEDGEMENTS

I thank Professor V.P. Roan, PhD, for his guidance in carrying out this work and for advocating a rigorous engineering methodology which, looking back, has indeed benefitted this interdisciplinary project. I also thank J.S. Gravenstein, MD, Dr. h.c., for his guidance and help and initiating this project and Drs. Doddington, Paulus, Schueller, van der Aa and Beneken for their encouragement and critically reading this dissertation.

I thank Daraius Hathiram, MSEE, Ron Carovano, BSEE, MBA, Hans van Oostrom, Ir., Jack Atwater, 2LT, USAF, MSEE and Gordon Gibby, MSEE, MD for introducing me to microcomputers and electronics, Paul Blanch, BS, RRT who shared his experience in clinical equipment maintenance and repair and M.J. Banner, RRT, PhD who taught me the finer points of respiratory therapy. Jim Brady, Eloy Villasuso, Kelly Spaulding and Lenny Hoag helped me in the final stages of this project.

I thank Professor J.H. Modell, MD and Michael L. Good, MD, and the Anesthesiology department personnel who made a true learning experience out of my stay in Gainesville. I thank Tom Clemens for advancing my professional development during my brief spell in industry, and Robert Tham, PhD for moral support.

Finally, special thanks to my relatives in Canada, Martina, Didi, Alain and Jeff and Debbie and Michael, my dear godson and his model parents, Mary and Ron. Their houses (and kitchens!) were always open to me at any time of the day (or night!). Their friendship, warmth and laughter sustained me through the hardest times of this endeavor.

v

TABLE OF CONTENTS

ix

x

LIST OF TABLES

xiv

LIST OF FIGURES

xvii

xviii

xix

xx

LIST OF ABBREVIATIONS AND SYMBOLS

1-D	One-dimensional
A/D	Analog to digital
ANSI	American National Standards Institute
APL	Adjustable pressure limiting (valve)
ATPD	Atmospheric temperature and pressure dry
BAS	Boston Anesthesia System
C	Compliance
C	A computer programming language
C++	An object-oriented extension of the C programming language
C_{circ}	Compliance of anesthesia circuit
CFAV	Continuous flow apneic ventilation
CFC	Chlorofluorocarbon
C_{gas}	Compliance of gas in anesthesia circuit
C_p	Specific heat at constant pressure
CPAP	Continuous positive airway pressure
C_v	Specific heat at constant volume
D/A	Digital to analog
EMI	Electromagnetic interference
ESWL	Extra-corporeal shock wave lithotripsy
ET	End tidal
$ETCO_2$	End tidal CO_2 concentration
ETT	Endotracheal tube
FGF	Fresh gas flow
FiN_2O	Inspired fraction of nitrous oxide
FiO_2	Inspired fraction of oxygen
FM	Frequency modulation
FRC	Functional residual capacity
GRADS	Gainesville recirculating anesthesia delivery system
HFV	High frequency ventilation
ICU	Intensive care unit
i.d.	Internal diameter
ISO	International Standards Organization
I:E	Inspiratory to expiratory (time ratio)
k	Specific heat ratio (C_p/C_v)
K	Kelvin
kPa	kiloPascal
MAC	Minimum alveolar concentration

MIB	Medical information bus
MTBF	Mean time between failures
MV	Minute ventilation
NAM	Nuffield anaesthetic machine
NIOSH	National Institute for Occupational Safety and Health
o.d.	Outside diameter
OR	Operating room
OS	Overshoot
Paw	Airway pressure
p	pressure
PEEP	Positive end expiratory pressure
P_b	Back pressure (pressure at outlet of a flow device)
P_{cr}	Critical pressure
PI	Proportional integral
PID	Proportional integral derivative
PIP	Peak inspiratory pressure
P_o	Stagnation supply pressure
ppm	parts per million, by volume
psi	Pounds per square inch
psia	Pounds per square inch absolute
psig	Pounds per square inch gauge
PVC	Polyvinyl chloride
PWM	Pulse width modulation
rpm	Revolutions per minute
R_g	Specific gas constant
R_{et}	Flow resistance of endotracheal tube
R	Flow resistance
Re	Reynolds number
RC	Rate of climb (e.g., of inspired anesthetic concentration)
RE	Ramp error (error in system response to a ramp input)
RR	Respiratory rate
RT	Rise time
SSE	Steady state error
St	Strouhal number
ST	Settling time
t	time
T	Temperature
T-piece	Also spelled tee-piece. The connector that links the inspiratory and expiratory hoses of a circle breathing circuit to the endotracheal tube. Differs from the Y-piece only in shape as the name implies.
T_{cr}	Critical temperature
T_i	Inspiratory time
UAW	Utah Anesthesia Workstation
UPS	Uninterruptible power supply

US	Undershoot
V_{abs}	Volume of CO_2 absorber
V_{circ}	Volume of anesthesia circuit
VIC	Vaporizer inside circuit
VOC	Vaporizer outside circuit
VT	Tidal volume
VT_d	Tidal volume actually delivered to patient
VT_s	Set tidal volume that the user wishes to deliver
WOB	Work of breathing
Y-piece	Also spelled wye-piece. The connector that links the inspiratory and expiratory hoses of a circle breathing circuit to the endotracheal tube

μ	Dynamic (or absolute) viscosity
η_{an}	Efficiency of anesthetic delivery
ρ	Density
τ	Time constant
$\tau_{washout}$	Washout time constant (e.g., of an anesthesia circuit)
ν	Kinematic viscosity

Abstract of Dissertation Presented to the Graduate School
of the University of Florida in Partial Fulfillment of the
Requirements for the Degree of Doctor of Philosophy

DESIGN METHODOLOGY, FABRICATION AND EVALUATION OF A
BLOWER-RECIRCULATED, CLOSED VENTILATION SYSTEM
AS A PLATFORM FOR ANESTHESIA DELIVERY

By

Samsun Lampotang

August 1992

Chairman: Dr. V.P. Roan
Major Department: Mechanical Engineering

An engineering methodology for designing a new type of anesthesia delivery
system is proposed. The design and fabrication of a prototype blower-recirculated,
closed ventilation system for anesthesia delivery were performed as part of this study of
the concept of a generalized methodical approach to anesthesia delivery system design.

Each module of the system has a single, clearly defined function, and
relationships between modules are explicit to avoid unintentional and undesirable
interactions. The prototype system is also used as a platform to demonstrate an
integrated design philosophy that enhances patient safety during laser surgery and
mechanical ventilation as well as facilitating the interface with external monitoring
systems such as alarm expert systems. The system is controlled in real time by a

xxiv

custom-designed, 12 MHz, Siemens 80535 microcontroller board, analog and digital electronics and software written in C.

A 2-stage, variable speed, centrifugal blower recirculates gases inside the closed anesthesia circuit and generates peak inflation pressures of up to 2 psig (140 cm H_2O). In a departure from present practice, the pressure sampling location used for airway pressure control during ventilation is moved to the distal tip of the endotracheal tube.

Among the advantages of the proposed design are: efficient volatile anesthetics delivery, low net gas consumption, high effective fresh gas flowrates, flexibility of mode of ventilation and decreased pollution by waste anesthetics. Another major benefit is that active control of airway pressure during spontaneous breathing reduces the work of spontaneous breathing. The potential drawbacks include the complexity of the control system and the dependence on uninterrupted electrical power.

In the course of formulating desired performance characteristics, a mechanical inspiration hypothesis, a lung classification scheme, new inspiratory flowrate and pressure waveforms and algorithms that convert a ventilator into a real-time, respiratory diagnosis platform were conceived and described. These concepts were assisted by a theoretical analysis of the effectiveness of inspiratory waveform shaping for an anesthesia ventilator using both a computer model and a mathematical analysis in the time domain.

Finally, using the proposed methodology, a prototype was successfully fabricated and tested. It was demonstrated that the system performed according to projections and offers the promise of significant advantages over conventional systems. The preliminary evaluations confirmed the methodology as well as the resulting prototype.

xxv

CHAPTER 1
INTRODUCTION

Present anesthesia delivery systems deliver expensive anesthetic gases inefficiently. In 87.5% of the cases in a study (Quinlan & Modell 1979), less than 5% of the gas output from currently-used anesthesia machines is taken up by the patient; 95% is spilled into the hospital scavenging system or the operating room (OR) ambient environment (Rodgers & Ross 1989). Numerous methods of quantifying anesthetic loss, the volume of anesthetic flowing out of an anesthesia delivery system that is not absorbed by the patient, have been proposed. In this work, the efficiency of anesthetic delivery, η_{an} will be defined as:

$$\eta_{an} = \frac{anesthetic\ output - anesthetic\ loss}{anesthetic\ output}$$

$$\eta_{an} = \frac{anesthetic\ absorbed\ by\ patient}{anesthetic\ output}$$

1.1

Depending on the definition of anesthetic loss that is used, different η_{an} are obtained. Using the definition of anesthetic loss of Mushin and Galloon (1960), experimental data for anesthetic loss collected by Herscher and Yeakel (1977), and the computed anesthetic loss based on the derivation of Schreiber (1972) respectively, anesthetic delivery efficiency is estimated at 5, 19 and 48% (Lampotang, Nyland & Gravenstein 1991).

1

The possible link between continued exposure to waste anesthetic gases and higher than average rates of spontaneous miscarriage (more than 3 times that of a control group in one study (Cohen, Belville & Brown 1971)), birth defects and cancer among OR personnel has also raised concerns about OR pollution (Cohen et al. 1974).

Further, anesthetic gases collected by a hospital scavenging system are ultimately vented to the atmosphere. Nitrous oxide (N_2O), an extensively-used anesthetic gas (estimated medical use of 100,000 tons/year worldwide representing about 1% of total worldwide emission mainly from industrial fertilizer production and soil microorganisms), depletes the atmospheric ozone layer (Waterson 1984). Modern volatile anesthetics (halothane, enflurane and isoflurane) are chlorofluorocarbons (CFCs) which contribute to both ozone layer depletion and the greenhouse effect (Waterson 1984; Norreslet et al. 1989). The amount of CFCs released into the atmosphere is estimated to be 2,020 tons from volatile anesthetics compared to 750,000 tons from industry (Brown et al. 1989). However, if proposed international legislature to ban industrial CFCs is ratified, ORs might become a major source of CFC emission in the future.

At the time of writing, the price per ml of liquid anesthetic bought by the University of Florida Department of Anesthesiology is $0.0462 for halothane, $0.433 for enflurane and $0.675 for isoflurane. Worldwide annual production is estimated to be 1,000 tons of halothane, 220 tons of enflurane and 800 tons of isoflurane (Rodgers & Ross 1989). The densities of the liquid anesthetics are 1.86 g/ml at 20°C for halothane, 1.517 g/ml for enflurane at 25°C and 1.496 g/ml for isoflurane at 25°C (Dorsch & Dorsch 1984). Assuming an operational anesthetic usage efficiency of 50%, about

$225,000,000/year is wasted worldwide, excluding the cost of N_2O and O_2 (Lampotang, Nyland & Gravenstein 1991). This estimate may increase sixteenfold if desflurane also known as I-653, a new, improved volatile anesthetic, reportedly 4 times as expensive as isoflurane and requiring 4 times the volumetric concentration of isoflurane to achieve the same anesthetic effect, becomes widely-used.

The anesthesia delivery system is above all else a life support system. Design flaws or equipment malfunction that endanger the patient are unacceptable. Consequently, conventional anesthesia equipment designs emphasize simplicity and robustness to promote mechanical reliability. The subsystems or building blocks (e.g., vaporizers, ventilators, CO_2 absorbers, breathing circuits) of current anesthesia delivery systems generally have standardized fittings which allow them to be assembled in different ways. However, this versatility in system configuration comes at the cost of incompatibility and the risk of misconnections.

Communication between subsystems is lacking when it should be present. For example, it is possible to switch on an anesthesia ventilator even though there is no inflow of gas to the breathing circuit. On the other hand, there are unintended and insidious interactions between the anesthesia machine subsystems which, although not obvious to the user, might jeopardize patient safety. For example, pediatric patients can receive a volume of gas up to 3 times as large as the set volume under certain conditions (Gravenstein, Banner & McLaughlin 1987). Multiple cases of anesthesia equipment malfunction have been reported (Cooper & Newbower 1975; Cooper, Newbower & Kitz 1984; Cooper et al. 1978) and simulated (Lampotang et al. 1992a, 1992b).

The influence of tradition on user acceptance of new designs is considerable. The pneumatic circuit of the modern anesthesia machine is fundamentally identical to the earliest anesthesia machines designed in 1914 when microcontrollers and gas analyzers were either unavailable or not as fast, reliable and inexpensive as they are today (Ream 1978; Jackson 1955). Modern technology has mostly been used to replace functional components (e.g., replacing pneumatic timing cartridges in anesthesia ventilators with electronic timers) and to implement anesthesia machine and patient monitors while leaving the overall design unchanged.

This work was motivated by the perceived potential for performance improvement over current anesthesia delivery system designs as well as the financial, environmental and health benefits to be derived from more efficient use of anesthetic gases.

The objectives of this dissertation were to construct a design checklist, establish and document an engineering design methodology, implement the ventilation part of the design prototype, and evaluate the feasibility of the prototype as a platform for an anesthesia delivery system that uses anesthetic gases efficiently. A bonus of using anesthetic gases efficiently is the reduced environmental pollution. The main design features of the prototype are a centrifugal blower for recirculating anesthetic gases in a closed system, sampling of the airway pressure at the endotracheal tube tip inside the patient, measurement of flowrate and tidal volume at the patient connection to the breathing circuit and computerized closed loop control of airway pressure in the anesthesia circuit. The processing power required to perform the above tasks in real-time is provided by a custom designed Siemens 80535 based microcontroller board.

Units of measure commonly used in anesthesia and respiratory care like cm H_2O and psig will be employed even though they are not Système International (SI) units. A units conversion table is listed in appendix A. In general, metric units will be used with the corresponding English units in parentheses. Unless otherwise stated, "concentration" will mean volumetric concentration in a gas mixture and all gas volumes will be at atmospheric temperature and pressure, dry (ATPD; 25°C, 760 mm Hg, relative humidity = 0%).

Chapter 2 provides a background in anesthesia delivery concepts, practice and equipment and ventilation and may be skipped without loss of continuity by readers familiar with the field of anesthesiology. Chapter 3 is a literature review of past research relevant to this present work. Chapter 4 establishes a comprehensive design checklist and documents in detail an engineering design methodology which, if systematically followed, leads to a design solution.

During the design phase, the benefits of shaping the inspiratory flowrate during mechanical ventilation in anesthesia were analyzed with both a computer model and a mathematical model. The novel concepts, features and algorithms resulting from these analyses are described separately in chapter 5.

Chapter 6 describes the actual physical implementation of the <u>ventilation</u> part of an anesthesia delivery system according to the design concepts that were developed in chapter 4. The preliminary performance data of the ventilator prototype of chapter 6 as a platform for an anesthesia delivery system are evaluated in chapter 7 and, finally, chapter 8 incorporates the conclusions and recommendations for further work.

CHAPTER 2
CONCEPTS, PRACTICE AND EQUIPMENT OF INHALATIONAL ANESTHESIA

The first sections of this chapter introduce general concepts relating to inhalational anesthesia and ventilation. The later sections address the design features and operating characteristics of existing inhalational anesthesia equipment subsystems and conclude with the description of a modern, commercial anesthesia delivery system.

2.1 Anesthesia

Surgical anesthesia was first performed by Crawford W. Long, in 1842, using diethyl ether vapor. The subsequent demonstration by William T.G. Morton, in 1846, brought anesthesia to public awareness and turned painless surgery into a practical reality (Thomas 1975). The anesthetics of the 1850's were primarily ether, nitrous oxide (N_2O), and chloroform. The first had the disadvantage of flammability, the last of toxicity. Subsequent anesthetic agents aimed at overcoming these drawbacks were only partially successful. During the 1950's, fluorine technology used in separating uranium isotopes for the atomic bomb was successfully applied to the manufacture of the current non-flammable and non-toxic volatile anesthetics: halothane (mid-1950's), enflurane (1963) and isoflurane (1965) (Eger 1985).

6
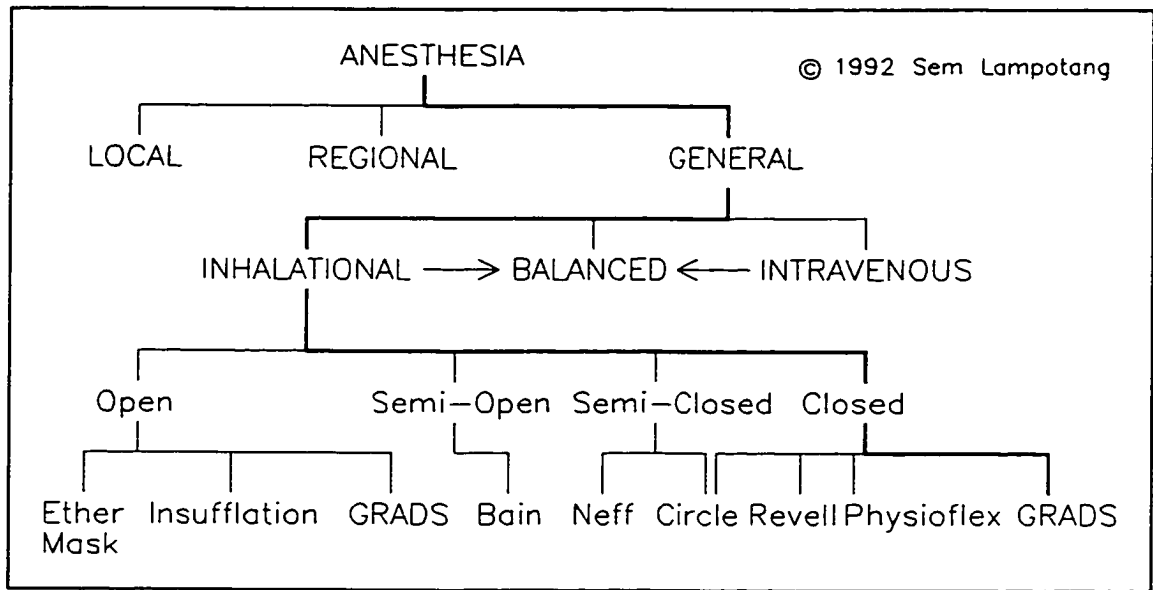
Figure 1. The field of anesthesia with emphasis on inhalational anesthesia and some of its circuits. The Gainesville Recirculating Anesthesia Delivery System (GRADS) is also included.

There are three types of anesthesia: local, regional and general (figure 1). Local anesthesia is administered via local drug injections directly into the affected tissues (e.g., excising a mole) while regional anesthesia is accomplished by injecting anesthetics into the tissues adjacent to the nerve supply of a specific region, thus anesthetizing the area of surgery (e.g., an arm or a leg). General anesthesia depresses the central nervous system; it is preferred for major operations and is often induced with intravenous anesthetics (non-volatile drugs) and maintained with inhalation (volatile) anesthetics. Intravenous anesthetics, once injected into the bloodstream, cannot be removed. Although their effect can be countered with reversal agents, the latter can produce unwanted side-effects. In contrast, agents administered by inhalation are said to be controllable as their level can be adjusted at will by ventilation of the lungs with gases

of known and controllable concentration. This dissertation will be concerned exclusively with general anesthesia performed via inhalation anesthetics.

Approximately 20 million general anesthetics are performed in the United States every year with an estimated anesthesia-related mortality rate of 0.8-1.0 per 10,000 anesthetics (Forrest 1988). A study of preventable anesthesia mishaps indicted human error in 82% of the cases and overt equipment failure in 14% (Cooper et al. 1978), emphasizing the need for human factors considerations in equipment design and layout. Recent developments in anesthesia simulators, similar in concept to flight simulators, are addressing the need to reduce the contribution of human error to anesthetic incidents (Lampotang et al. 1992a, 1992b; Good et al. 1988; Gravenstein 1988; Gaba & DeAnda 1989).

2.2 General Inhalational Anesthesia

General anesthesia is composed of three main components: analgesia, amnesia and paralysis (muscle relaxation). Analgesia is the pain-killing or pain-blocking property of a drug. Amnesia ensures that the patient has no recall, on waking up, of any pain or unpleasant experience that might have been felt during the operation. Amnesia is commonly obtained by rendering the patient unconscious, or with the help of specific drugs which may not cause sleep. Finally, a paralysed patient will not move under the stimulus of pain while muscle relaxation (decreased muscle tone) facilitates retraction of the surgical incision for easy access to internal organs. A paralysed patient cannot breathe spontaneously and is totally dependent on an anesthesia ventilator.

The three phases of general anesthesia are induction, maintenance and emergence (or recovery) (Dripps, Eckenhoff & Vandam 1982). Induction is the process of taking the patient from a conscious state to a depressed and unconscious state. During maintenance, the patient is kept in a relatively steady plane of anesthesia. Emergence is the reverse of induction and consists of bringing the patient back to a state of consciousness, once surgery is completed. Ideally, induction and emergence should be instantaneous (i.e., step functions in time), giving the anesthesiologist the possibility of practicing "square-wave" anesthesia. In practice, emergence and induction are of finite duration, lasting from 1-10 minutes for induction and 4-20 minutes for emergence, resulting in a trapezoidal anesthetic trajectory in time. During induction, an "overpressure" method is used to speed induction (Dripps, Eckenhoff & Vandam 1982). The anesthesiologist deliberately delivers a higher anesthetic concentration than the target concentration since the rate of anesthetic uptake by the patient is high, at induction. As clinical signs begin to indicate that the patient is anesthetized, the anesthesiologist starts to back off to the target concentration.

Inhalation anesthetics are absorbed via the alveoli in the lungs into the bloodstream of the patient and are thus transported to the site of action (the brain). To date, the exact mechanism of action of anesthetics has still not been determined. The well-established Meyer-Overton rule is based on the good correlation between anesthetic potency and lipid (olive oil) solubility which implies that the site of anesthetic action is hydrophobic (Koblin & Eger 1986). Microtubules have also been suggested as possible mechanisms of anesthetic action (Hameroff & Watt 1982).

However, it has been shown that partial pressure at the brain, rather than volume concentration, of the inhalational anesthetic determines the depth of anesthesia (Cullen 1986). At equilibration, the anesthetic partial pressure in the brain is assumed to be nearly the same as the anesthetic partial pressure in arterial blood (the arterial partial pressure). At equilibration, the anesthetic partial pressure in the alveoli (alveolar partial pressure) is assumed to be equal to the arterial partial pressure and hence the brain partial pressure, assuming that there are no ventilation/perfusion (blood flow) abnormalities in the lung.

End-tidal concentration is widely used in anesthesia to infer the alveolar concentration or partial pressure of a gas component. The end-tidal sample from a patient is the last portion of gas in each exhalation; it comes from the deepest parts of the lung (the alveoli) and has had the longest time to equilibrate with arterial blood via the blood/gas barrier (the alveolar membrane) due to the tidal nature of ventilation (first in, last out). Therefore, the end-tidal concentration is accepted as being representative of the alveolar and eventually the brain partial pressure at equilibration. However, the assumed equality between anesthetic end-tidal and arterial partial pressures only holds (acceptable maximum error of 10%) when the difference between anesthetic inspired and end-tidal partial pressures is small (less than 50% of the alveolar partial pressure) (Eger & Bahlman 1971).

The end-tidal anesthetic partial pressure is a useful, easily accessible and non-invasive indicator of the arterial anesthetic partial pressure. A more direct way of measuring arterial anesthetic partial pressure would be to insert a probe in the patient's

artery. However, this method is invasive (the patient's skin and artery have to be punctured leading to increased costs and risks of complications). Earlier investigators placed more emphasis on inspired anesthetic concentration as a means of controlling depth of anesthesia (Quasha, Eger & Tinker 1980). With the concept of equilibration now widely accepted, control of end-tidal anesthetic partial pressure is the preferred approach since brain anesthetic partial pressure and hence anesthetic depth is thereby inferred and controlled.

2.2.1 Partition Coefficients

The partition coefficient of a particular anesthetic gas or vapor is a measure of the relative affinity of the anesthetic for two different phases. It indicates how the anesthetic will divide (partition) itself between two phases when equilibrium (i.e., equal partial pressures) is achieved, at a specified temperature (usually, 37°C) (Eger 1986). For example, isoflurane has a relatively low blood/gas partition coefficient (numerically equal to the Ostwald solubility coefficient (Steward et al. 1973)) of 1.4, indicating that, at equilibrium, each ml of blood holds 1.4 times as much isoflurane as one ml of alveolar gas. Low blood/gas solubility in an inhalation anesthetic is desirable since induction and emergence are consequently rapid; the time constants for wash-in and wash-out, at induction and emergence respectively, are shorter since less anesthetics are in solution in the patient's blood. Short time constants bring the anesthesiologist closer to the ideal of "square wave" anesthesia and provide better control over the anesthetic procedure

since the anesthetic partial pressure is more responsive to inputs or changes in settings from the anesthesiologist.

The concept of a partition coefficient is also applicable to other substances. For example, the rubber/gas partition coefficient determines how much volatile anesthetic a rubber breathing circuit will absorb, at a specific temperature (usually 25°C) (Titel & Lowe 1968). Breathing circuits made of materials with high solid-gas partition coefficients are undesirable since the circuit acts as a sink for volatile anesthetics during induction and as a source of volatile anesthetics during emergence, increasing the time-constants and causing a departure from the ideal of square-wave anesthesia.

2.2.2 Anesthetic Uptake

The rate of anesthetic uptake (U) is the product of three parameters: blood/gas solubility or partition coefficient (S), cardiac output (Q, the flowrate of blood from the heart) and the difference between alveolar (P_A) and venous (P_V) anesthetic partial pressure (Eger 1986, 626). BP stands for barometric pressure.

$$U = S.Q.\frac{P_A - P_V}{BP} \qquad \qquad \textbf{2.1}$$

The rate of anesthetic uptake is initially high at induction and plateaus with time as the venous anesthetic partial pressure approaches the alveolar anesthetic partial pressure. As a rule of thumb, rate of anesthetic uptake is roughly proportional to the reciprocal of the square root of time in minutes (Eger 1986, 641).

$$U(t) \approx \frac{U(t=1)}{\sqrt{t}} \qquad\qquad \textbf{2.2}$$

The considerable variation in the rate of anesthetic uptake between patients (Westenskow, Jordan & Hayes 1983) precludes prediction of anesthetic uptake rate to determine the required inspired anesthetic concentration. Other anesthetic sinks include the anesthesia circuit, the soda lime in the CO_2 absorber, sampled gases (if the gas analyzer aspirates and does not return the sampled gases to the anesthesia circuit) and leaks in the anesthesia circuit.

2.2.3 Minimum Alveolar Concentration (MAC)

With inhalation anesthetics, the concept of Minimum Alveolar Concentration (MAC), introduced in 1963, is a useful indicator of potency (Merkel & Eger 1963). MAC, in humans, is defined as the volume concentration, at equilibrium and at a standard atmosphere (760 mm Hg), of an inhalation anesthetic at which 50% of patients will not move in response to surgical skin incision (Cullen 1986, 554). In general, 95% of patients do not respond at 1.3 MAC (de Jong & Eger 1975). A lower MAC implies a more potent agent. Although MAC is expressed as a percentage of a standard atmosphere, it is really a partial pressure. In practice, the volume concentration has to be altered when the ambient pressure deviates significantly from a standard atmosphere, to achieve the required anesthetic partial pressure. From this point of view, the term MAC is misleading since partial pressure, rather than concentration, is the invariant and, therefore, relevant parameter.

2.2.4 Physical Properties of Inhalational Anesthetics

The inhalation anesthetics in most common use at present are N_2O, halothane, enflurane and isoflurane. Nitrous oxide is a gas at room temperature and atmospheric pressure. The last three are volatile anesthetics and are liquids at room temperature and atmospheric pressure and their gaseous phase is called a vapor.

A by-product of fractional distillation of air, xenon is an inert gas with anesthetic properties (Cullen & Gross 1951; Adriani 1979). Xenon has a MAC of 71% for humans, a blood/gas partition coefficient of 0.14, a boiling point of -108°C and no undesirable side effects. However, xenon is prohibitively expensive for routine use in clinical anesthesia, even with low flowrate anesthesia techniques. Up to now, xenon has evoked interest mainly as a research tool to study and test proposed mechanisms of anesthetic action.

The physical properties of some gases and vapors used in inhalational anesthesia are listed in table 1. The Antoine equation is derived from the Clausius-Clapeyron equation (Wark 1983) and is used for deriving vapor pressure of a volatile anesthetic at a given temperature. The Antoine equation also allows determination of boiling point and is expressed as (Rodgers & Hill 1978):

$$\log_{10} P_{vap} = A - \frac{B}{T+C} \qquad\qquad 2.3$$

The constants A, B and C are called Antoine coefficients and are listed in table 1. P_{vap} is the vapor pressure in mm Hg and T the temperature in degrees Celsius.

Table 1. Physical properties of gases and vapors used in anesthesia.

Gas or Agent	Mol. Wt.	Density (kg/m³)	k	Boil. Point (°C)	B/G Part. Coef. 25°C	Human MAC in O₂ (% atm.)	Antoine Coefficients		
							A (mmHg)	B	C
Nitrous Oxide	44.0	1.8429	1.31	-89	0.47	105	7.57799	912.8988	285.309
Nitrogen	28.0	1.1648	1.41	-196	-	-	-	-	-
Oxygen	32.0	1.3310	1.4	-183	-	-	-	-	-
Helium	4.0	0.1663	1.66	-269	-	-	-	-	-
Xenon	131.3	5.85	1.67	-108	0.14	71	7.03040	705.9352	278.342
Halothane	197	8.90	-	50.2	2.5	0.77	6.76799	1043.697	218.262
Enflurane	184.5	7.54*	-	56.5	2.0	1.68	6.98840	1107.839	213.063
Isoflurane	184.5	7.54*	-	48.5	1.4	1.15	5.69778	536.4589	140.991
Desflurane	168.0	3*	-	22.8	0.42	6-7			

Approximate values at 20°C and 760 mm Hg; *=25°C (Hawkins 1978; Chemical Rubber Company 1990; Incropera & De Witt 1985). k is the specific heat ratio (C_p/C_v).

The most frequently used anesthetic gas is nitrous oxide. It has the lowest blood/gas solubility of all common inhalation agents (xenon is 3 times less soluble in blood but is rarely used) and a MAC of 105%. However, 100% N_2O is lethal because there is no oxygen to meet the metabolic oxygen requirement. Therefore, at a standard atmosphere ambient pressure, N_2O is always administered with at least 25%-30% oxygen mixed with it. Consequently, nitrous oxide has to be supplemented with intravenous or volatile anesthetics like isoflurane, halothane and enflurane because of its low potency (high MAC). MAC is additive when more than one anesthetic agent is used.

2.3 Ventilation

Ventilation is the process of bringing oxygen into, and washing out carbon dioxide from, the alveoli in the lungs. Ventilation is a process distinct from anesthesia. However, in the case of inhalation anesthesia, ventilation is the medium for delivery of anesthetics so that the two separate processes become coupled. During inhalation anesthesia, ventilation may be of three types: spontaneous, assisted or controlled. During spontaneous ventilation, the patient breathes, at his own pace, without any assistance from the anesthesiologist. In assisted ventilation (also known as manual ventilation or "handbagging"), the anesthesiologist manually squeezes a breathing bag attached to the anesthesia breathing circuit to supplement the spontaneous ventilation of the patient. If the patient does not breathe spontaneously, ventilation is controlled either manually (by squeezing a bag) or mechanically (by an anesthesia ventilator). Manually controlled ventilation is labor intensive and rarely used nowadays. During mechanically controlled ventilation, an anesthesia ventilator automatically ventilates the patient's lungs, thus freeing the hands of the anesthesiologist to perform other tasks.

During inspiration, pressure in the lung is sub-atmospheric with spontaneous ventilation while with assisted or controlled ventilation, inspiratory lung pressure is above atmospheric pressure (Mushin et al. 1980). The sub-atmospheric pressure during spontaneous inhalation is generated by the patient's respiratory muscles. The effort that the patient has to generate can be quantified in terms of the work of breathing (WOB; measured in Joules/breath) and is obtained from the area of a pressure-volume loop tracing. WOB is irrelevant during mechanical ventilation since a machine is generating

the pressure to drive the gas into the patient's lungs. Because circuits that are used with controlled ventilation are also used in spontaneous mode, the design of anesthesia circuits has to minimize WOB and thus flow resistance. The flow resistance of the uni-directional valves used in the circle system and the effort required to lift the passive valve leaflets contribute to the WOB.

2.3.1 Parameters of Ventilation

Movement of gas is tidal in the respiratory tract since it dead-ends into the alveoli and has only one opening to the atmosphere. Tidal volume is the volume of air delivered to the lungs during one breath while respiratory rate is the number of breaths per minute. Minute volume is the product of respiratory rate times tidal volume. During a respiratory cycle, the ratio of time duration of inspiration versus that for expiration is known as the inspiratory to expiratory time (I:E) ratio.

Table 2. Typical ventilation parameters for human neonate and adult under anesthesia.

Ventilatory Parameter	Neonate	Adult
Tidal Volume	20 ml	500 ml
Breathing Rate	36/min	12/min
Anatomical Deadspace	7.5 ml	150 ml
Metabolic O_2 Consumption	24-32 ml/min	200-250 ml/min
Compliance	0.01 l/cm H_2O	0.1 l/cm H_2O
Airways Resistance	19.2 cm H_2O/l/s	1.5 cm H_2O/l/s

Source: Cameron & Skofronick 1978; Lough, Chatburn & Schrock 1983.

Lung-thorax compliance is a measure of the stiffness of the respiratory system. Airways resistance is a measure of the ease with which gas can flow through the airways to, and from, the lungs. The concepts of compliance and resistance to flow are also applicable to the anesthesia breathing circuit.

Deadspace is space that does not participate in gas exchange. For example, the anatomical deadspace is the volume occupied by the conducting airways in the lung (trachea and bronchi) which are devoid of alveoli (Nunn 1987; West 1974). Breathing circuit design can also introduce deadspace and is termed mechanical, equipment or apparatus deadspace. Deadspace causes rebreathing of CO_2 when exhaled gas from the previous breath deposited in the deadspace is re-inspired due to the to-and-fro nature of gas movement during tidal breathing. Mechanical deadspace is generally undesirable, especially with pediatric patients, because larger tidal volumes are required to maintain normal gas exchange or induction and emergence are delayed. Typical ventilatory parameters for humans under general anesthesia are given in table 2.

2.3.2 Modes of Ventilation

Various modes of mechanical ventilation are currently used. High frequency ventilation (HFV) is characterized by high breath rates (up to 150 breaths/min) and small tidal volumes which may be lower than the deadspace. HFV is especially useful in extracorporeal shock wave lithotripsy (ESWL), a non-invasive way of pulverizing kidney stones with focused shock wave energy. The small tidal volume causes a smaller excursion of the kidney stone from the focus of shock energy leading to disintegration

of the stone with a smaller number of shocks (Whelan et al. 1988), reduced collateral healthy tissue damage and shorter patient turnaround time.

Continuous flow apneic ventilation (CFAV) introduces high flowrates of gas via catheters inserted in the patient's bronchi and lets the continuous flow of gas bring in O_2 and wash out CO_2 (Smith 1987; Smith et al. 1984). With CFAV, kidney stone movement during ESWL would be eliminated. However, CFAV is not a mature technique and requires high fresh gas flowrates of humidified gas so that the mucus does not dry up. CFAV is not presently used during ESWL.

Controlled ventilation in patients not requiring anesthesia (e.g., in intensive care (ICU) units) is typically done with higher flowrates of fresh gas as the gas mixture is typically not recirculated and there is no CO_2 absorber in the breathing circuit.

An elevation of the baseline pressure above atmospheric pressure is sometimes required to maintain lung volume and hence improve gas exchange (the so-called "pressure splint"). This elevation is called positive end expiratory pressure (PEEP) and is accomplished by a variety of mechanical devices (PEEP valves) placed in the expiratory path (Kacmarek et al. 1982).

Flow resistance in the expiratory path is undesirable especially in patients with emphysema or who might cough. The high transient flowrates generated during a cough (up to 400 l/min) (Gal 1980) generate a sudden rise in pressure which might cause barotrauma (Banner et al. 1986; Ulyatt et al. 1991).

2.3.3 Anesthesia Ventilators

Anesthesia ventilators were introduced to relieve the anesthesiologist from having to squeeze the breathing bag. This was achieved by enclosing a cylindrical bellows inside a transparent, rigid cylindrical housing. By periodically pressurizing the space between the bellows and the housing, the patient is ventilated. To date, anesthesia ventilators still use the same design whereas many ventilators used in the intensive care unit (ICU) do not use bellows. Modern ICU ventilators typically use proportional flow control valves which outlet directly into the breathing circuit; they are able to ventilate patients with very stiff compliance that anesthesia ventilators cannot ventilate (Gravenstein & Lampotang 1990).

There are two bellows configurations: ascending and hanging. With an ascending bellows (bellows ascend during exhalation as shown in figure 4 (p 28)), a leak in the anesthesia circuit can be visually detected since the bellows will progressively collapse. A hanging bellows is essentially an ascending bellows upside down and might not collapse if there is a leak in the anesthesia circuit because gravity pulls the bellows down. Hanging bellows are therefore not recommended. Bellows are also helpful as a visual indication of tidal volume delivered to the patient. The inspiratory flowrate waveform during inspiration is "square-wave" in anesthesia ventilators, i.e., flowrate rises in a step function to a constant level for the duration of inspiration and then drops to zero again in a stepwise fashion. ICU ventilators on the other hand permit selection of different inspiratory flowrate waveforms that are intended to distribute ventilation more uniformly in lungs with unequal time constants.

2.3.4 Inspiratory Waveform Shaping During Mechanical Ventilation

The introduction of microprocessor-controlled intensive care unit (ICU) ventilators in the 1980's facilitated implementation of user-selected inspiratory flowrate shaping during mechanical ventilation (Lampotang 1990b). At the time of writing, only four inspiratory flowrate shapes are available on current ICU ventilators: the constant, increasing, decreasing and half-sine(0-π) ("sinusoidal") waveforms (Banner & Lampotang 1992) (figure 2). In contrast, anesthesia ventilators typically provide only one waveform shape (square inspiratory flowrate) (Gravenstein & Lampotang 1990), sometimes with the option of adding an inspiratory pause (a time period when, by definition, the flowrate is zero in the endotracheal tube (ETT) and the gas in the lungs can redistribute).
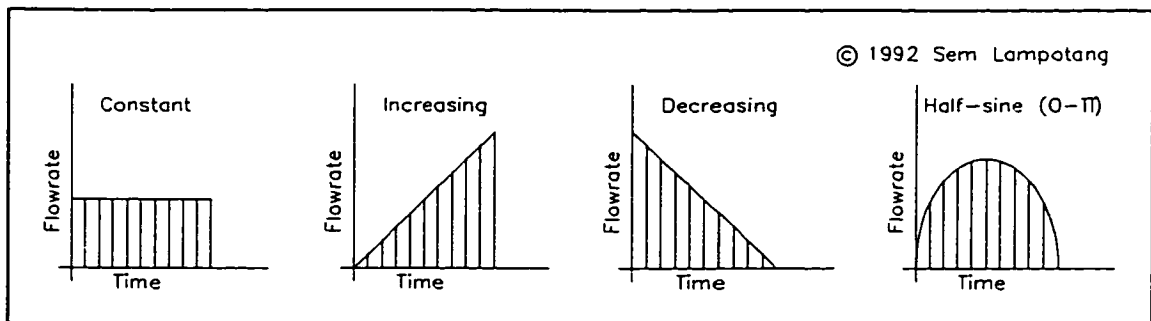
Figure 2. The different flowrate shapes presently available in modern intensive care unit (ICU) ventilators. The shaded areas under each curve are equal and represent the tidal volume.

It is interesting to note that historically the inspiratory flowrate shapes were to a major extent selected on the basis of how easily they could be implemented with the technology available in the 1960's and 70's. For example, the sinusoidal flowrate shape is the output of a piston eccentrically mounted on its driving crankshaft while the

decreasing flowrate waveform is obtained from a spring-driven bellows which delivers flow to the patient via a flow resistor (Dupuis, 1986). Although the advent of inexpensive electronics in the 80's has allowed the implementation of radically different inspiratory flowrate shapes, the four basic shapes in figure 2 are still the only ones available on current microprocessor-controlled ventilators.

The purpose of inspiratory flowrate shaping and the inspiratory pause is to reduce the maldistribution of ventilation that occurs in sick or injured lungs because of marked regional differences in the mechanical parameters of compliance (C) and resistance to gas flow (R) that lead to unequal time constants (τ = RC) for the inflation of different lung regions. It is postulated that a more uniform distribution of ventilation will reduce the ventilation/perfusion mismatch occurring during anesthesia with mechanical ventilation (Rehder et al. 1979). Numerous studies using theoretical (Fourier analysis), experimental (mechanical or electrical analogs, computer models, animals and healthy human volunteers) and clinical data on the various factors that can influence the distribution of ventilation with the objective of making distribution of ventilation more uniform have been performed (Banner & Lampotang 1988; Al-Saady & Bennett 1985; Bergman 1984; Baker, Colliss & Cowie 1977; Dammann, McAslan & Maffeo 1977; Sullivan, Saklad & Demers 1977; Fuleihan, Wilson & Pontoppidan 1976; Johansson & Löfström 1975; Baker & Hahn 1974; Baker, Wilson & Hahn 1974; Hedenstierna & Johansson 1973; Jansson & Jonson 1972; Herzog & Norlander 1968; Otis et al. 1956).

The results of these studies sometimes conflict with each other. For example, the results reported by Banner and Lampotang (1988) using a modified mechanical lung

model (Lampotang et al. 1986) indicate that the shape of the inspiratory flowrate can improve the distribution of ventilation. But Rehder et al. (1981, 396) concluded from their experiments with healthy human volunteers that "... manipulating flow during anesthesia-paralysis and mechanical ventilation is not a useful tool to improve pulmonary gas exchange...". These conflicting results from different researchers have raised questions about the clinical benefits of inspiratory flowrate shaping during mechanical ventilation. The benefits of a better understanding of the interaction between the different parameters of mechanical inspiration are significant and will have immediate clinical applications but have been elusive up to now.

This subject will be explored in more detail in chapter 5 where past research in the area of mechanical inspiration will be extensively surveyed. A mechanical inspiration hypothesis will be proposed on the basis of a theoretical analysis performed with a computer model.

2.4 "Typical" Inhalation Anesthesia Procedure

During a "typical" inhalation anesthetic, the inspired gas concentrations vary from 100% O_2 during preoxygenation to 70% N_2O, 25-30% O_2 and volatile anesthetics during induction and back to 100% O_2 during emergence. Preoxygenation (also known as denitrogenation) is performed by facemask in case there are complications during endotracheal intubation (gives some coast time during which blood oxygen levels at the brain will remain adequate even though the patient's lungs might not be ventilated). Ventilation is usually spontaneous at induction and is then supported manually by the

anesthesiologist as the patient's respiratory drive or muscle power fades away. During maintenance, ventilation is usually performed by the anesthesia ventilator while during emergence, ventilation is assisted and then spontaneous ventilation is re-established at high fresh gas flowrates.

2.5 Anesthesia Delivery Subsystem Design

In this part of the chapter, anesthesia delivery subsystem designs are described and analyzed. An anesthesia delivery system is essentially a life support system as well as a gas blender designed to create and deliver a life-sustaining and yet anesthetizing gas mixture. Reliable control of the delivered gas composition, especially anesthetic vapor concentrations is essential since anesthetics are lethal in overdose.

The term "anesthesia machine" will be consistently used for the assembly that includes the gas blending and vaporizing subsystems and the term "anesthesia circuit" for the breathing circuit (corrugated hoses and, if present, breathing bag, valves and CO_2 absorber). The "anesthesia delivery system" is the combination of the anesthesia machine, the anesthesia ventilator, the anesthesia circuit and the scavenging system. "Fresh gas flow" (FGF) is the flowrate, in l/min, from the anesthesia machine into the anesthesia circuit.

2.5.1 Anesthesia Circuits

The anesthesia circuit delivers gas from the anesthesia machine to the patient and may be classified into four broad categories: open, semi-open, semi-closed and closed

(figure 1) (Orkin 1986). Numerous other classification schemes exist (Conway 1982); the present one is widely used but can be confusing (e.g., the circle system can fall under all of the classes depending on the way it is used and the magnitude of the FGF, as will be discussed later).

2.5.1.1 Open anesthesia circuits

In open-drop administration, drops of highly volatile anesthetic (diethyl ether or chloroform) are deposited onto layers of gauze supported on a hemispherical wire frame held over the patient's mouth and nose. Patients breathe spontaneously and the liquid anesthetic is vaporized by the airstream. Delivered anesthetic concentration is unknown. Simplicity, portability, negligible respiratory resistance and low cost are heavily outweighed by lack of control over delivered anesthetic concentration, inability to control ventilation, ambient air pollution, humidity and heat loss and freezing due to evaporative heat loss. If inspired anesthetic concentration increases, spontaneous ventilation decreases resulting in a further increase in anesthetic concentration since the anesthetic vapor becomes less diluted by inspired ambient air. Similarly, light anesthesia will tend to get lighter. This positive feedback characteristic renders control of anesthetic depth difficult. Further, with flammable anesthetics, ambient air pollution generates a fire hazard.

With the technique of "insufflation," a premixed gas mixture from an anesthesia machine is delivered via the anesthesia circuit to a face mask (similar to an aviator's mask) held slightly above the patient's face or to a tube through which the anesthetic is

blown into the patient's mouth or airway. Insufflation is especially useful for induction of anesthesia with halothane (least pungent of the anesthetics) in pediatric patients but shares some of the drawbacks of open drop administration (Dripps, Eckenhoff & Vandam 1982, 317).

2.5.1.2 Semi-open anesthesia circuits
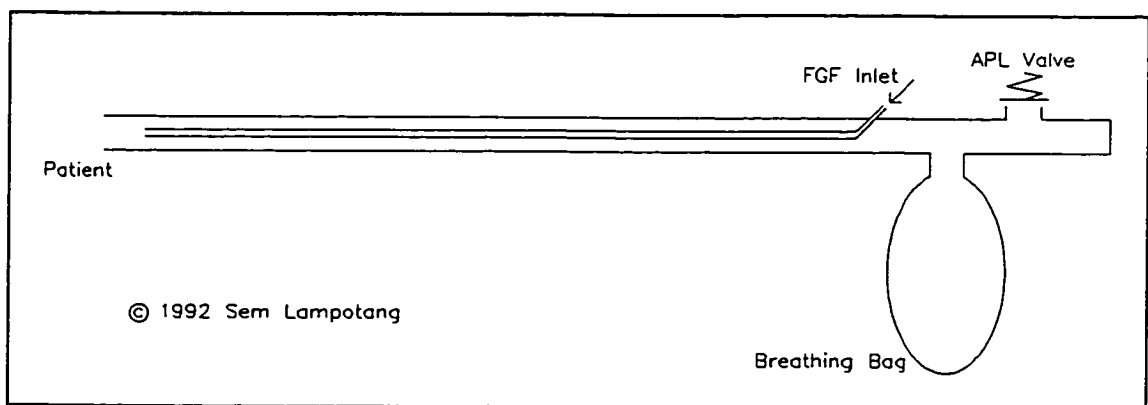
Figure 3. The Bain circuit, a semi-open anesthesia circuit.

Semi-open systems are characterized by the absence of a CO_2 absorber and high FGFs (greater than minute volume) to prevent rebreathing. Control of inspired gas concentration is straightforward since it approximates the concentration delivered to the anesthesia circuit from the anesthesia machine. Further, the presence of a breathing bag allows assisted or manually controlled ventilation, as well as tactile assessment of pulmonary compliance and airways resistance. However, expensive anesthetics, respiratory moisture and heat are spilled via the adjustable pressure limiting (APL) valve. The APL valve (commonly known as the "pop-off" valve) is simply a spring-loaded

pressure relief valve; the pressure at which the APL valve will start spilling gases ("pop-off") is manually adjusted by the anesthesiologist. Anesthetic waste is excessive because of the high FGFs. Some semi-open anesthesia circuits also incorporate unidirectional valves to prevent rebreathing.

The Bain circuit is the most widely used semi-open anesthesia circuit (figure 3). It is essentially a coaxial breathing circuit. The internal tube brings fresh gas to the patient. Claimed advantages of the Bain circuit are its simplicity, light weight, low flow resistance and retention of humidity and warmth. However, the Bain circuit is more complex than it appears to be and will cause CO_2 rebreathing at low FGFs (Gravenstein, Lampotang & Beneken 1985; Beneken et al. 1985; Beneken et al. 1987).

2.5.1.3 Semi-closed anesthesia circuits

These systems are characterized by the presence of a CO_2 absorber, unidirectional valves and moderate FGFs (typically 1 to 3 l/min in adults, i.e., less than the minute volume but greater than the metabolic O_2 consumption rate). A CO_2 absorber allows partial rebreathing of exhaled gases. A breathing bag permits manual ventilation and tactile assessment of lung compliance and resistance. If net flowrate (typically a FGF of 3 l/min) into the anesthesia circuit is higher than the net outflow rate (oxygen and anesthetic consumption rate of about 200-250 ml/min) in an airtight system, pressure will build up due to gas accumulation. The APL valve is designed to spill excess gas out of the anesthesia circuit to maintain a desired peak pressure selected by the anesthesiologist. During spontaneous or manual ventilation, excess gas leaves the circuit via the APL

valve. During mechanical ventilation, excess gas is spilled via the ventilator exhaust valve and the APL valve is closed or mechanically isolated from the anesthesia circuit in newer systems.
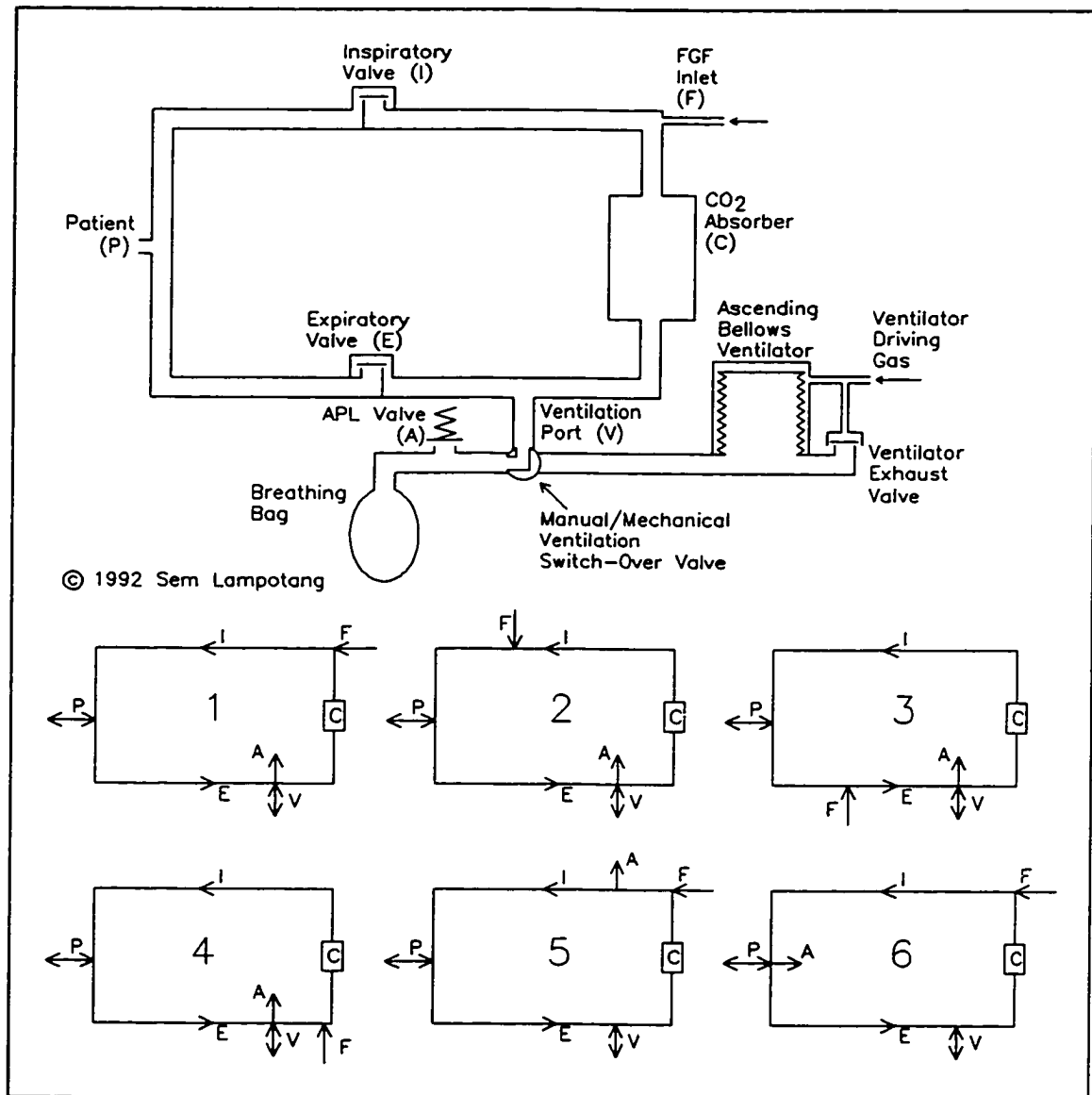
Figure 4. The circle system and its different configurations. The optimal configuration (1) is shown in detail. The scavenging system is not shown.

The components (APL valve, inspiratory and expiratory valves, CO_2 absorber, fresh gas inlet and reservoir bag) can be configured in many ways (Eger & Ethans 1968) (figure 4). Optimization parameters are efficient use of FGF, anesthetics and CO_2 absorbent and the time delay before user-initiated changes in the delivered gas mixture effectively appear at the patient's airway. The optimal configuration (1) in figure 4 is the most widely-used anesthesia circuit for adults and larger children and is known as a "circle" system (Schreiber 1972, 104).

Claimed advantages of the semi-closed circle system are conservation of moisture and heat, reduced anesthetic and fresh gas consumption as well as reduced operating room pollution. The drawbacks are increased flow resistance, greater bulk and complexity, decreased portability, risk of valve leaflets sticking with attendant increase in flow resistance, long time delays before changes in delivered gases concentration are effective as well as the inability to predict inspired oxygen concentration at low FGFs.

Although FGFs for semi-closed systems can be lower than minute volume, a 3 l/min FGF is still routinely used for mainly historical reasons (Petty 1987), explained later. Also, past vaporizer designs were inaccurate at low flowrates which also encouraged the continued use of a 3 l/min FGF in circle systems (Mushin & Jones 1987). Current vaporizers have adequate accuracy at low flowrates but use of high FGFs still persists. Furthermore, high FGFs will mask the existence of a leak in the anesthesia circuit resulting in OR pollution even if a scavenging system is available.

2.5.1.4 Closed anesthesia circuits

The introduction in 1933 of explosive and expensive cyclopropane as an anesthetic promoted the circle system and its use as a closed anesthesia circuit. A closed anesthesia circuit is simply a circle system used with very low FGFs. Ideally, FGF exactly matches metabolic O_2 consumption rate (roughly 250 ml/min for adults) and anesthetic uptake rate. There is no pollution when no excess gases are vented. A bonus of closed circuit anesthesia is that, at equilibrium, the metabolic O_2 consumption is equal to the O_2 inflow rate, which is known. Knowledge of metabolic O_2 consumption is clinically useful since it will warn of metabolism abnormalities (like malignant hyperthermia) which can be lethal. CO_2 production is absorbed by the CO_2 absorber. The term "closed" is slightly misleading since the system is not closed in the engineering sense, because of the inflow of metabolic oxygen and anesthetics and the emission of carbon monoxide and methane from the patient.

The circle anesthesia circuit can be classified into any of the four classes, depending on the way it is used. When used with a face mask for insufflation, the circle system can be considered as an open system. With high FGFs, the CO_2 absorber is effectively not required since most of the exhaled CO_2 is spilled via the APL valve and the circle system behaves as a semi-open system. With FGFs less than minute ventilation and greater than metabolic O_2 consumption rate, the circle system is used as a semi-closed system; this is the mode most commonly used.

There has been controversy in the anesthesia community over low versus high flowrate anesthesia techniques and the economy of low flowrate anesthesia has been

questioned, especially when the cost of CO_2 absorber is included (Rendell-Baker 1968; Edsall 1981; Jones 1982; Patel & Milliken 1982; Virtue & Aldrete 1981; Spain 1981). Further, current vaporizers deliver a maximum anesthetic concentration of 5% (7% for enflurane). If the rate of anesthetic uptake is, for example, 20 ml/min of halothane, O_2 inflow will have to be greater than the metabolic O_2 consumption rate of 200 ml/min (approximately 380 ml/min) to meet the anesthetic uptake rate and maintain the desired anesthetic concentration in the anesthesia circuit. In other words, the delivery of anesthetic is limited by the delivery of oxygen. The O_2 concentration in the inspired gas mixture during closed system anesthesia can be hard to predict, particularly during induction. The use of an oxygen analyzer is therefore mandatory to ensure adequate oxygenation of the patient, during closed-circuit anesthesia.

In the United States, the majority of the anesthesia circuits used are of the disposable, single use type despite inconclusive evidence of cross contamination between patients with non-disposable breathing circuits (Garibaldi et al. 1981; Feeley et al. 1981; du Moulin & Hedley-White 1982). In Germany, re-usable breathing circuits are used in some institutions for the entire week and are then sterilized over the weekend, with no apparent harm to the 15 or so patients who thus end up sharing the same circuit. The circle system is most widely used followed by the Bain circuit.

2.5.2 Anesthesia Circuit/Patient Interface

The interface between the anesthesia circuit and the patient can be the delivered anesthetic gas mixture itself (during "insufflation", section 2.5.1.1), a well-fitting face mask or an endotracheal (ET) tube.

2.5.2.1 Face mask

A good seal may be difficult to achieve with mass-produced face masks because of the diversity in facial features. A face mask also contributes to deadspace through the space between the patient's face and the mask (approximately 12-80 ml depending on the model).

2.5.2.2 Endotracheal tube

Anesthetics cause loss of muscle tone of the tongue which can then flop back and obstruct the airway in a prone patient (Cheney 1988). Laryngospasm (contraction of the muscles of the true and false vocal chords that inhibits gas flow to the lungs) will also endanger oxygen supply to the lungs. An ET tube is therefore inserted into the trachea to secure access to the lungs so that ventilation and inhalation anesthetics can always be delivered. A patient with an endotracheal tube inserted is said to be intubated. Endotracheal tubes have various internal diameters and lengths.

Adult ET tubes have a cuff that is inflated after insertion to provide a seal between the trachea and the external wall of the ET tube. The cuff also protects the lungs from aspiration (acidic gastric contents refluxing up the esophagus and down the

trachea into the lungs). Pediatric ET tubes are uncuffed since an adequate seal can generally be obtained in children by careful selection of ET tube diameter (Dorsch & Dorsch 1984, 363). Endotracheal intubation reduces anatomic deadspace but increases the flow resistance and therefore the spontaneous work of breathing. Natural humidification and warming of inspired air are lost because the nostrils are bypassed, which is especially a problem with children.

2.5.3 Vaporizers

Vaporizers are designed to introduce anesthetic vapor into the anesthesia circuit in a controllable and predictable way. Complete vaporization is critical since anesthetics in a liquid state in the lungs may be lethal. There are two main designs of commercial vaporizers: bubble-through and flow-over.

2.5.3.1 Bubble-through vaporizers

In this design, a small, independently-metered flowrate of oxygen is passed as fine bubbles through liquid anesthetic and is completely saturated with anesthetic vapor at the vaporizer outlet (figure 5A). Thermal inertia is provided by the high heat capacity and thermal conductivity of copper used in the vaporizer body (hence, the term "copper kettle" for one particular model). Temperature stability is desirable so that the saturation vapor pressure does not vary significantly. A bubble-through vaporizer is not agent-specific, i.e., the same device can be used to administer different anesthetic agents.
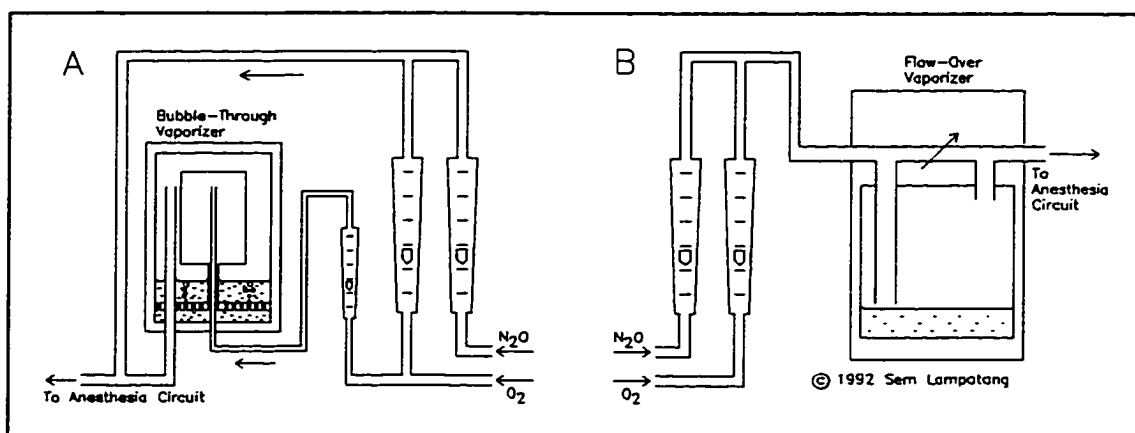
Figure 5. The two main types of vaporizers. A) the bubble-through vaporizer; B) the flow-over vaporizer.

With halothane in bubble-through vaporizers, a total FGF of 5 l/min allowed easy mental conversion of the oxygen flowrate through the vaporizer into delivered halothane concentration (division of the flowrate of O_2 in ml/min through the bubble-through vaporizer by 100 gave an approximation to the delivered percent (%) halothane concentration) (Quinlan & Modell 1979). This is the historical reason mentioned earlier why a 5 l/min FGF was widely-used in semi-closed anesthesia circuits. With the introduction of enflurane and isoflurane, a FGF of 3 l/min became common for the same reasons.

2.5.3.2 Flow-over vaporizers

The blended gases from the O_2 and N_2O flowmeters are directed to the vaporizer where the majority of the gas flows through a variable bypass (figure 5B). The remainder of the inlet gases flows over liquid anesthetic and picks up the saturated

anesthetic vapor. Anesthetic concentration is modulated by varying the bypass ratio. Bimetallic strips that alter the bypass ratio automatically compensate for temperature drop due to evaporation. There is no need for mental arithmetic from the user in setting delivered concentrations, as in the bubble-through vaporizer,. However, the flow-over vaporizer is agent-specific and the patient can be harmed if an anesthetic of higher volatility is inadvertently introduced into a vaporizer designed for a lower-volatility agent. Most modern vaporizers are flow-over vaporizers.

A vaporizer can be either inside the anesthesia circuit (VIC: vaporizer inside circuit; no longer recommended) or outside (VOC: vaporizer outside circuit) (Hill 1967). A VIC vaporizer must have low flow resistance since the patient must breathe through it. VIC vaporizer output is unpredictable since the unused anesthetic is recirculated through the VIC vaporizer. VIC vaporizers are no longer recommended. A VOC vaporizer, on the other hand, must be capable of delivering a higher concentration of anesthetics since the gases only pass through the VOC vaporizer once.

The "pumping effect" increases the anesthetic output concentration when pressure in the anesthesia circuit due to mechanical ventilation is transmitted back to the vaporizer outlet, causing gas to reflux into the vaporizer and pick up more anesthetic vapor (Dorsch & Dorsch 1984, 88). On the other hand, the "pressurizing effect" decreases the anesthetic output concentration from a vaporizer when pressure increases inside the vaporizer (Dorsch & Dorsch 1984, 91). The increase in total pressure decreases the relative anesthetic concentration since the anesthetic partial pressure remains constant if isothermal conditions prevail (partial pressure is dependent on temperature only).

2.5.4 Carbon Dioxide Absorbers

CO_2 absorbers are present in semi-closed and closed anesthesia circuits and remove CO_2 from the previously exhaled gases before they are rerouted to the patient. The modern CO_2 absorber is basically a transparent cylinder in which two canisters of soda lime are vertically stacked. Soda lime is made of granules of a mixture of sodium hydroxide and calcium hydroxide. The granules contain an indicator (usually ethyl violet) and turn from off-white to violet when their CO_2 absorption capacity is exhausted, providing a visual cue that they should be replaced. Soda lime also absorbs volatile anesthetics, especially when dry (Grodin, Epstein & Epstein 1982). The absorption of CO_2 by CO_2 absorbent is an exothermic chemical reaction that involves a reduction in gaseous volume (Orkin 1986, 124):

$$CO_2(g) + H_2O(l) \rightleftharpoons H_2CO_3(l)$$

$$H_2CO_3(l) + 2NaOH(s) \rightleftharpoons 2H_2O(l) + Na_2CO_3(s)$$

2.4
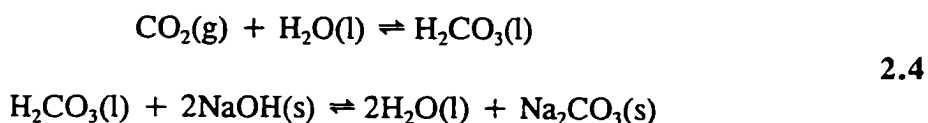
2.5.5 Scavenging Systems

Following a government report recommending a maximum of 25 parts per million, by volume (ppm) of N_2O and 2 ppm of halogenated agent in the OR environment, scavenging systems were introduced (NIOSH 1975). Current scavenging systems require either a vacuum source for active scavenging (figure 6B) or a non-recirculating air-conditioning system for passive scavenging (figure 6A).

Scavenging systems collect the excess gases spilled from the anesthesia circuit either via the APL valve or the ventilator exhaust valve and channel them out of the OR to prevent contamination of the OR environment. In a modern hospital scavenging

system, waste anesthetic gases are suctioned into a central vacuum source and vented to atmosphere from the hospital roof.
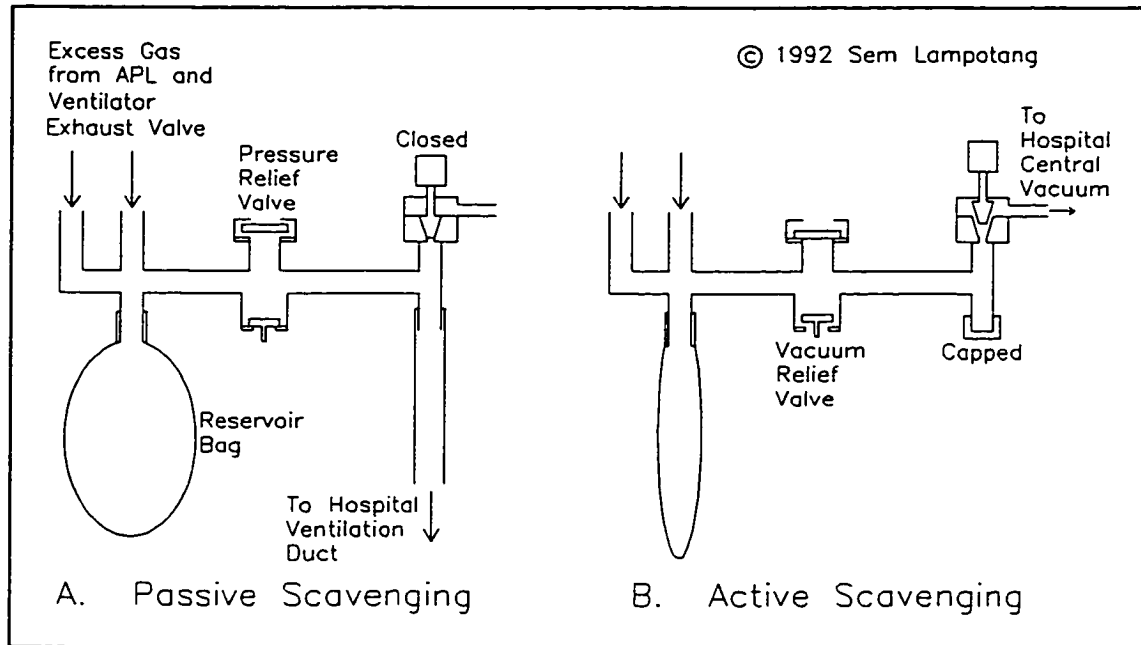
Figure 6. A current scavenging system design

Different scavenging system designs exist. The representative commercial design shown in figure 6B uses a needle valve to control the vacuum in the scavenging system. A gravity-operated pressure relief valve opens if the scavenging system pressure exceeds a certain threshold, venting waste gases into the OR (figure 6A). A gravity-operated vacuum relief valve admits room air into the scavenging system if the vacuum inside the scavenging system is excessive, to prevent the vacuum from being transmitted via the anesthesia circuit to the patient's lungs (figure 6B). An elastic scavenging bag temporarily accommodates any sudden surge in the rate of inflow of gases into the scavenging system.

The "vacuum" adjustment mechanism in the scavenger design of figure 6 (the needle valve) adjusts flowrate whereas vacuum in the scavenging system is the variable that actually has to be controlled. The significant vacuum level fluctuations from a central hospital source will change the vacuum level in the scavenging manifold for a given needle valve position. A device specifically designed to control vacuum like a vacuum regulator (back pressure regulator) will control the pressure upstream of it irrespective of the downstream pressure (vacuum supply) and is better indicated for this application. Scavenging systems are usually out of sight of the anesthesiologist in current anesthesia machine configurations and are often neglected and improperly set.

2.5.6 Gas Humidification and Warming

Humidification and warming of gases during inhalation anesthesia is desirable for the following reasons: (a) gases from the central hospital supply or cylinders must be dry because wet gases may freeze when expanding through the pressure regulators, (b) endotracheal intubation bypasses the heating and humidifying tissues in the naso-pharynx, (c) electron microscopy reveals extensive desiccation of mucus and defoliation of the cilia in the trachea which can favor postoperative pulmonary complications, when high FGFs of dry gas are used for extended periods of time (Kleemann 1989), (d) humidity loss causes clinically significant heat loss via the latent heat of vaporization, especially with babies and (e) warming of the gases increases their water vapor carrying capacity.

Humidification of anesthesia gases is performed by water vaporizers which can be classified into 5 groups (Petty 1987, 96; Andrews 1990): (a) pass-over vaporizer

which is simply a heated version of a volatile anesthetic draw-over vaporizer, (b) bubblers which pick up water vapor by passing the gases, as a stream of bubbles, through a jar of water, (c) heated cascade humidifiers (essentially a heated bubbler) which are the most effective and commonly-used, (d) ultrasonic nebulizers and humidifiers and (e) "artificial nose". The artificial nose is a filter attached to the endotracheal tube. The patient's saturated exhaled gas moistens the filter which then imparts the moisture back to the next inspired tidal volume of gas. Cascade humidifiers deliver 100% humidity at body temperature but will allow misconnection of the inlet and outlet ports, resulting in no flow through the anesthesia circuit because of the check valve that prevents retrograde flow of humidity back into the anesthesia machine.

Existing humidifiers are cumbersome, perform unsatisfactorily (poor control of humidity leads to rainout in the anesthesia circuit or in the patient's lungs, causing complications like stuck unidirectional valves and excessive fluid in the lungs as well as frequent false alarms and wide temperature swings) and increase the risk to the patient of a misconnection. Consequently, anesthesiologists usually choose to perform cases of less than 2 hours, without humidifiers because the ensuing postoperative patient discomfort (feeling of dryness in the mouth) is considered a worthwhile tradeoff against the increased risk of humidifier-induced anesthesia circuit malfunction.

2.5.7 Monitoring

Integrated circuit technology has allowed significant advances in monitoring, during anesthesia. The monitored parameters fall into two categories: patient and

machine variables. Pulse oximetry (non-invasive, optical determination of the degree of oxygen saturation of blood) and automated, oscillometric, non-invasive blood pressure measurement are examples of monitored patient variables while circuit pressure and inspired gas and volatile anesthetic compositions are machine variables.

Some monitors function as both a machine and patient monitor. For example, the capnograph will help the anesthesiologist detect an incompetent inspiratory valve via a distinctive capnogram but will also detect patient problems like malignant hyperthermia through an elevated end-tidal CO_2 value.

For obvious safety reasons and in accordance with proposed European standards, the sensors and transducers ($ETCO_2$, Paw, VT, FiO_2, FiN_2O, ET agent, etc) used for feedback and control in an automated anesthesia delivery system should not be used to drive monitor displays. The machine monitors should use separate transducers so that an independent assessment of the anesthesia delivery system performance can be obtained.

There is a current trend towards integration of monitors into the anesthesia machine. However, monitoring and the human factors associated with it are outside the scope of this work. Although monitoring is becoming an integral part of the anesthesia delivery system, it will not be discussed at length except where it impacts the mechanical design of the system. On the other hand, the monitors that will be used to control the operation of the anesthesia delivery system will be discussed.

2.5.8 Modern Commercial Design
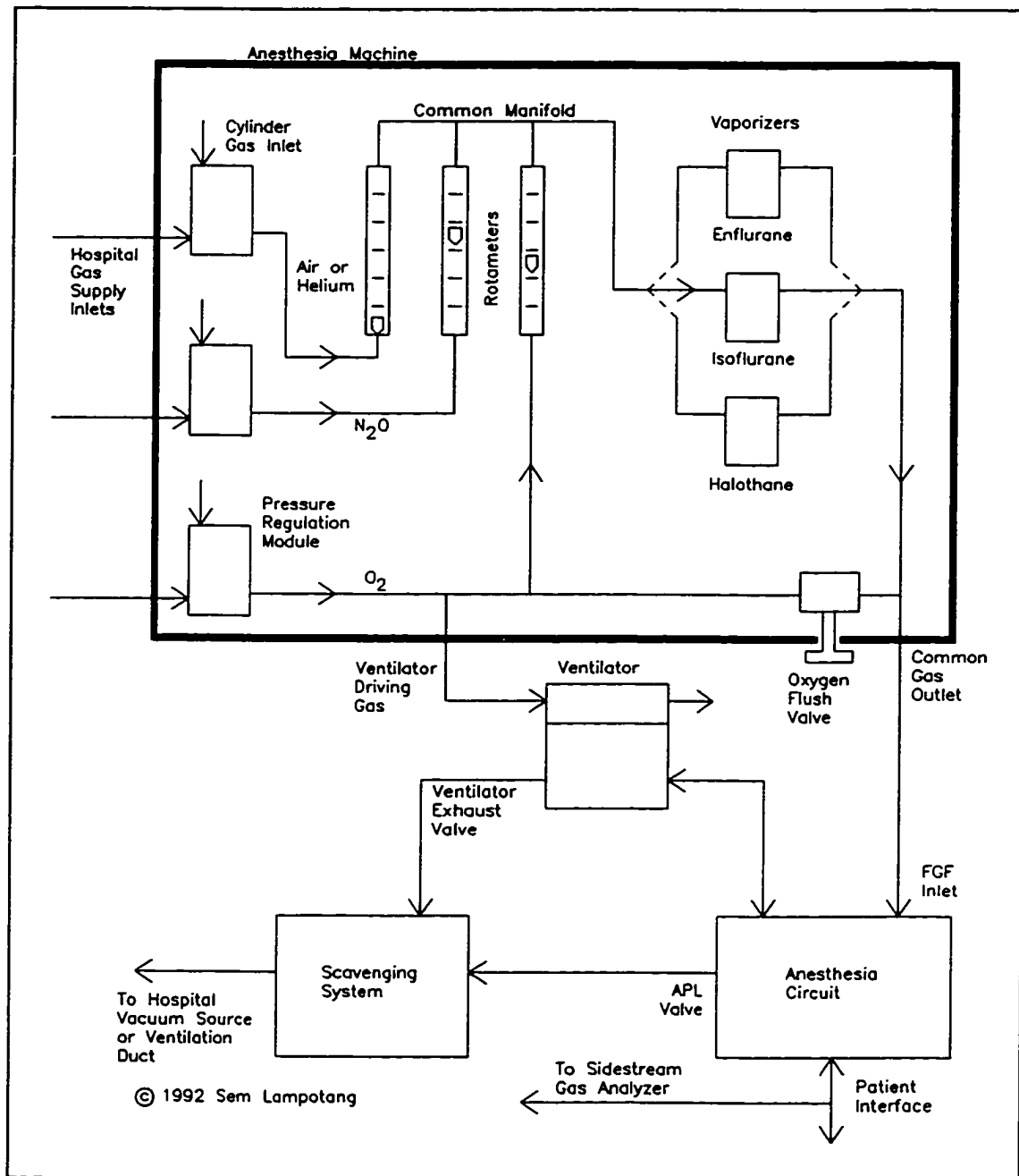
Figure 7. A modern, commercial anesthesia delivery system design

Figure 7 illustrates a commercial design representative of a modern anesthesia delivery system (Ohmeda 1986). Rotameters provide independent metering of O_2, N_2O and air(or helium, e.g., for laser surgery). The O_2 rotameter is always furthest downstream. If the O_2 rotameter is upstream of the N_2O rotameter and a crack develops in the manifold between the two rotameters, O_2 will leak out to ambient air and a hypoxic (oxygen-deficient) gas mixture would be delivered to the patient (Eger & Epstein 1964). The gases mix in the common manifold and are then passed through a flow-over vaporizer. The FGF leaves the anesthesia machine at the common gas outlet. The anesthesia circuit can be either a circle system or a Bain circuit. The ventilator uses a proportional flow control valve to drive an ascending bellows and is controlled by an Intel 8031 microcontroller. The scavenging system is similar to the one described in the previous section on scavenging systems.

The O_2 flush valve is a mechanically actuated poppet valve that delivers between 50 to 70 l/min of O_2 to the anesthesia circuit when it is manually depressed (Petty 1987). The high flowrate of O_2 rapidly washes out the pre-existing gas composition in the anesthesia circuit and replaces it with 100% O_2. However, according to the "helium protocol", a 100% O_2 environment will increase the risk of an "airway fire" during laser microsurgery of laryngotracheal lesions, if the laser beam accidentally strikes an ETT made of polyvinyl chloride (PVC) (Pashayan et al. 1988) when an O_2 flush is occurring.

2.6 Summary

This chapter has briefly introduced the state of current anesthesia delivery equipment. Anesthesia delivery is essentially an open loop process with the anesthesiologist providing the feedback, indirectly, via clinical signs. The lack of a definitive and measurable indicator of depth of anesthesia remains a significant hurdle to development of reliable closed loop anesthesia controllers.

Many other unsolved problems in anesthesia equipment remain. Tradition also has a strong influence as witnessed by the continuing use of bellows in anesthesia ventilators. Inadvertent equipment malfunctions, like stuck valve leaflets or leaks, may go unnoticed and jeopardize patient care. Although iterated in 1974, this statement by an anesthesiologist is still relevant and serves as a reminder of the challenges still facing the designer of anesthesia equipment (Morris 1974, 192):

The fact that survival is usual regardless of the system used is not an index of merit; rather, it reflects the normal hardy ability of patients to withstand assault and to invoke inherent biological compensatory mechanisms. Furthermore, anesthesiologists are quite often intuitively adept at compensating for deficiencies in equipment, even when they have not objectively recognized the existence or extent of those deficiencies.

CHAPTER 3
LITERATURE REVIEW

This chapter reviews experimental work carried out from the late 1940's to the present towards improving anesthesia delivery system performance, efficiency and safety. The earliest attempts in 1947 consisted of simple additions to the circle system like circulators aimed at reducing equipment deadspace.

Later efforts (late 50's - mid 70's) focused on automated (programmed or controlled) anesthesia delivery. During that period, the two predominant approaches to automated anesthesia delivery were (a) closed loop control using some form of feedback from the patient to induce and maintain depth of anesthesia and (b) open-loop control using digital computer models of the "typical" patient to predict the optimal <u>inspired</u> anesthetic concentration for maximum practical speed of induction.

In the late 70's, the emphasis started shifting to closed-loop control of <u>end-tidal</u> anesthetic concentration as a means of automating anesthesia delivery with closed circle systems. The late 70's also witnessed the introduction of an experimental, fully-integrated, microprocessor-controlled anesthesia delivery system which started the trend towards increasing use of electronics and microcontrollers in anesthesia delivery equipment and monitors that is still continuing today. Finally, numerous electronic monitors (pulse oximetry, multi-gas analyzers, etc.) became available in the 80's with

44

a trend towards integration of these devices into the anesthesia machine, both for monitoring and control purposes, emerging.

3.1 Circulators

Circulators are add-on mechanical devices (usually placed on the inspiratory port of the CO_2 absorber in a circle system) that reduce or eliminate deadspace in semi-closed or closed anesthesia via face mask, by increasing gas circulation in the breathing circuit (Morris 1974; Neff, Sullivan & Poulter 1979). The first closed anesthesia circuit designed in 1914 actually incorporated a circulator in the form of an air pump driven by an electric motor (Jackson 1955).
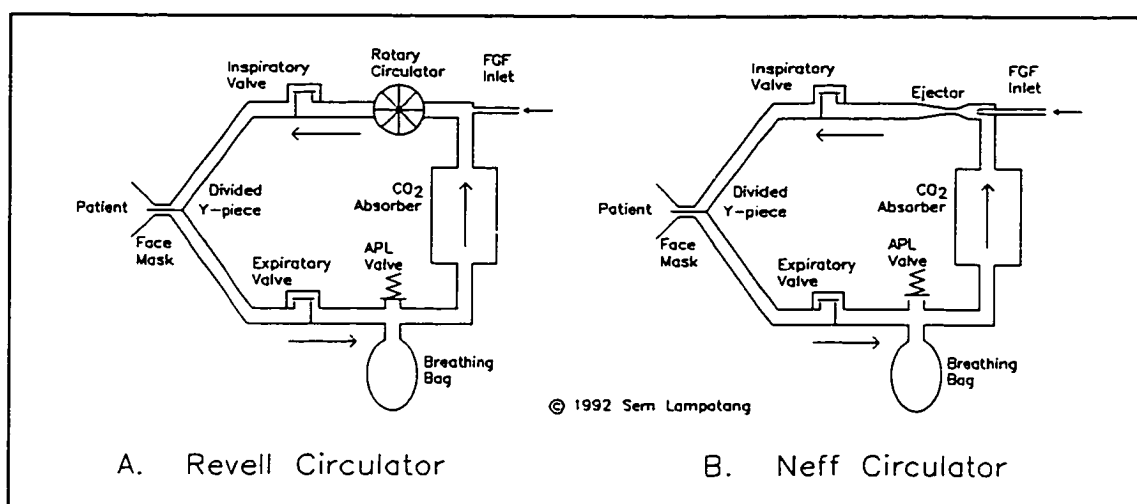
Figure 8. The Revell and Neff circulators

A divided chimney Y-piece is essential to ensure that the deadspace under the mask is continuously flushed by the high flowrate of recirculating gases, preventing buildup of CO_2 (Revell 1959a). The unidirectional valves in the breathing circuit are

usually retained (figure 8) and provide visual warning that the circulation flowrate is too low when the valve leaflets seat. The recommended circulation flowrate should be just high enough that the valves are always floating throughout the breathing cycle but not so high that residence time of the exhaled CO_2 in the absorber is too short for CO_2 absorption to take place. Due to the increased circulation flowrate, however, the gases also pass through the CO_2 absorber more times per minute. The increased rate of CO_2 absorber passage cancels the shortened residence time of the exhaled gases in the CO_2 absorber and inspired CO_2 level is unaffected (Revell 1959b).

A drawback common to the Revell (Revell 1959a; figure 8) and Neff (Neff, Burke & Thompson 1968; figure 8) circulators is the increased mean pressure under the facemask which tends to accentuate any leak in the seal between the mask and the face (Roffey, Revell & Morris 1961). Also with VIC vaporizers, the risk of overdosing the patient with volatile anesthetics increases since the gases pass through the VIC vaporizer more often and anesthetic concentration can consequently reach dangerously high levels (Morris 1974).

3.1.1 Revell Circulator

The high cost of cyclopropane combined with its explosive nature dictated its use with closed anesthesia circuits. However, the attendant drawbacks of deadspace and flow resistance made closed anesthesia circuits unsuitable for pediatric patients who are especially susceptible to these two factors. The Revell circulator (circa 1947, figure 8A) was designed to allow the use of cyclopropane in pediatric patients breathing

spontaneously on closed or semi-closed adult breathing circuits although its use on adults and intubated patients is also advocated (Revell 1959a).

When the circulation flowrate is set at 100 l/min, recirculation flow stops if back pressures exceed 3.5 cm H_2O (Revell 1959b). This would be a problem if the circulator was used during mechanical ventilation where the peak inspiratory pressure (PIP) can be 10-20 cm H_2O and as high as 100 cm H_2O but the Revell circulator was designed for use during spontaneous breathing only. If recirculating flow is present in the pause between expiration and mechanical inspiration, then recently exhaled alveolar CO_2 from the lungs will be washed away before the next inspiration. Pressure below the face mask is about 0.2 cm H_2O (Revell 1959b). Flowrates up to 50 l/min are attainable in adult anesthesia circuits (Roffey, Revell & Morris 1961). Recirculation flowrate required to just float the valve leaflets was 12-15 l/min . The Revell circulator has been shown to decrease deadspace, flow resistance (and hence work of breathing) and minute volume in mechanical models of spontaneously breathing pediatric patients using adult circuits via face mask (Morris 1974, 187). The Revell circulator does not interfere with the movement of the bag as an indicator of lightness of anesthesia (Revell 1959a).

3.1.2 Neff Circulator

The Neff circulator (circa 1968, figure 8B) employs an ejector (incorrectly called a "Venturi circulator") to pump the anesthesia gases around a circle system used as a semi-closed anesthesia circuit. It is designed for use with facemasks during spontaneous, assisted or controlled ventilation and is claimed to conserve halothane (Morris 1974).

The FGF (3-4 l/min) issuing from the bank of rotameters is supplied to the high pressure nozzle of the ejector (Neff, Burke & Thompson 1968). The flow resistance of the ejector nozzle orifice causes a back pressure of 80 mm Hg (1.6 psig) to be transmitted to the rotameters and the halothane vaporizer resulting in a 10% decrease in output for both devices (Neff, Burke & Thompson 1968). (This effect might have been eliminated with choked sonic nozzles interposed as baro-isolators between the components and the back pressure). Breathing circuit pressure increased by 0.3-1.0 cm H_2O with the circulator in use (Neff, Burke & Thompson 1968). The entrainment ratio of the ejector with zero back pressure is approximately 14:1 but the ejector is sensitive to back pressure especially at low primary gas flowrates (Jones & Prosser 1973). Effective entrainment ratio during operation was 5 (15 l/min entrained flowrate at a 3 l/min primary flowrate) (Morris 1974).

Significant economy in anesthetics consumption is claimed (Neff, Burke & Thompson 1968) but is probably unfounded since the FGF is 3-4 l/min. An independent study found that (a) facemask deadspace was reduced and even eliminated with one facemask design (b) no advantage is apparent with intubated patients and (c) work of breathing with conscious volunteers was markedly reduced (Jones & Prosser 1973).

3.2 Experimental Anesthesia Delivery System Designs

The following sections present a chronological overview of past research and developments in experimental anesthesia delivery systems. In general, the basic mechanical layout of the anesthesia machine and anesthesia circuit have been left

unmodified. Innovation has been mostly in the form of replacing functional components by their modern counterparts and the application of digital computers.

3.2.1 Early Experiments in Programmed Anesthesia

Bickford (1950) described an attempt to automate anesthesia that used closed loop control of patient variables (e.g., arterial blood pressure, electroencephalogram) as a form of feedback to induce and maintain depth of anesthesia. Subsequently, Cowles et al. implemented a four-compartment ("lung-blood", visceral including the brain, lean tissue and fatty tissue) model of anesthetic uptake and distribution in Fortran IV on an IBM 360-50 computer (Cowles, Borgstedt & Gillies 1972). This computer model was aimed at predicting the optimal **inspired** anesthetic concentration that would provide speedy induction and maintenance for an indefinite time period. For the sake of simplicity, a non-rebreathing anesthesia circuit was assumed in the model. A simple proportional controller predicted the required inspired anesthetic partial pressure (P_{insp}). P_{br} is the brain anesthetic partial pressure which is the same as the anesthetic partial

$$P_{insp} = P_{des} + k(P_{des} - P_{br}) \hspace{2cm} \textbf{3.1}$$

pressure at the visceral compartment. P_{des} is the desired brain anesthetic partial pressure (1.0% atm. for halothane) and k is the proportional gain determined by trial and error (32 for halothane). Inspired anesthetic concentration was constrained to a maximum safe level whose value depended on the type of anesthetic (3% atm. for halothane and 50% for cyclopropane). The model was tested on the computer only and was not validated. The predicted time course for the optimal inspired halothane concentration was 0-12 min:

3% atm., 12-15 min: 2% atm., 15-115 min: 1.5% atm. and 115+ min: 1.25% atm. for a normal "standard" 70 kg man, with an induction time of 11 minutes (Cowles, Borgstedt & Gillies 1972).

Chilcoat (1973) noted that, in clinical practice, the anesthesiologist actually uses a combination of the closed loop control advocated by Bickford and the predictive model, open loop control implemented by Cowles at al. Based on his experience and training, the anesthesiologist has in mind some plan of attack for induction (the predictive open-loop component) which he revises as feedback in the form of clinical signs from the patient becomes available.

Consequently, Chilcoat implemented an adaptive computer program that initially obtained its numeric coefficients for a simple mathematical model of halothane uptake from preprogrammed constants. Based on the initial model coefficients, halothane vaporizer settings were recommended. When feedback becomes available in the form of arterial or end-tidal anesthetic partial pressures, the numeric coefficients of the model are modified to adapt the initial plan to the particular patient. The feedback measurements were also used to modify the model so that it effectively "learned" from its past experience, to improve its performance. The program was only tested against another computer program that simulated a patient. It is claimed that desired control was successfully achieved and that system performance improved with "learning" (Chilcoat 1973). Further details are not available since the author did not publish a complete description of his work.

Concurrently, Mapleson et al. were experimenting with Alsatian dogs on a non-feedback computer technique that required precise, detailed information on the physiology (e.g., body weight and blood/halothane solubility) of each dog (Mapleson, Allott & Steward 1974). The goal of the exercise was to rapidly increase the arterial anesthetic partial pressure to a desired level and maintain it. The measured arterial anesthetic partial pressure or "tension" was deliberately not fed back to the computer program. Updated measurements of alveolar ventilation and cardiac output had to be supplied to the model at 10 minutes intervals. Arterial anesthetic partial pressures within 1 mm Hg of the target of 4 mm Hg were achieved when the inspired anesthetic concentrations delivered by the flow-over vaporizer were determined by the model (Mapleson, Allott & Steward 1974). Although impractical (because precise physiological data were continually required), this system had the merit of being the first that was validated with live animals instead of being tested via software. The error of up to 25% in the desired arterial anesthetic partial pressure was considered acceptable.

The adaptive approach (Chilcoat 1973) and the non-feedback technique (Mapleson, Allott & Steward 1974) for automated anesthesia were combined into the "black box" method (Mapleson et al. 1980) where the working premise was that only the anesthesiologist can assess if the depth of anesthesia is adequate. Instead of setting the inspired anesthetic concentration, the anesthesiologist sets the desired brain anesthetic concentration in MAC units on the black box which consists of a computer model that translates this instruction into vaporizer settings that will bring about the desired brain anesthetic tension rapidly and maintain it. The system used overpressure induction and

required measurements of inspired N_2O and anesthetic concentrations and alveolar ventilation at 10 seconds intervals and cardiac output at 10 minutes intervals. In mechanically-ventilated Alsatian dogs rendered unconscious via intravenous injection of pentobarbital, halothane anesthesia was "induced" in 2 minutes and maintained for 50-110 minutes (Mapleson et al. 1980).

In general, the experimental approaches to automated or computer controlled anesthesia delivery up to the late 70's used non-rebreathing anesthesia circuits since the emphasis was on prediction of optimal inspired anesthetic concentration. Inspired and FGF anesthetic concentration are similar in a non-rebreathing circuit whereas, in a closed circuit, inspired concentrations are harder to predict due to rebreathing. However, the simplicity of a non-rebreathing circuit has a cost, beyond the waste of expensive anesthetics. Assuming that the computer model accurately predicts the required inspired anesthetic concentrations for a desired anesthetic trajectory, alveolar ventilation must be sufficient to ensure that the inspired anesthetic concentrations actually reach the alveoli. In closed circuit anesthesia on the other hand, the anesthetic uptake process is not as dependent on alveolar ventilation (Salamonsen 1978), since any anesthetic that is not delivered to the patient on the first "pass" repeatedly comes around again, until it is finally absorbed.

3.2.2 Boston Anesthesia System (BAS)

This experimental design (circa 1976) was controlled by an 8-bit Intel 8080 microprocessor (Cooper et al. 1978). Most of the functions of the anesthesia machine

were integrated and performed under electronic control (figure 9). For example, digital valves metered O_2 and N_2O flowrates. The digital valves consisted of orifices of increasing sizes. The flowrate in an orifice at a constant supply pressure (50 psig) was double that for the next smaller orifice. In this way, 256 discrete flowrate settings were achievable (Langill, Friedland & Limbacher 1969).
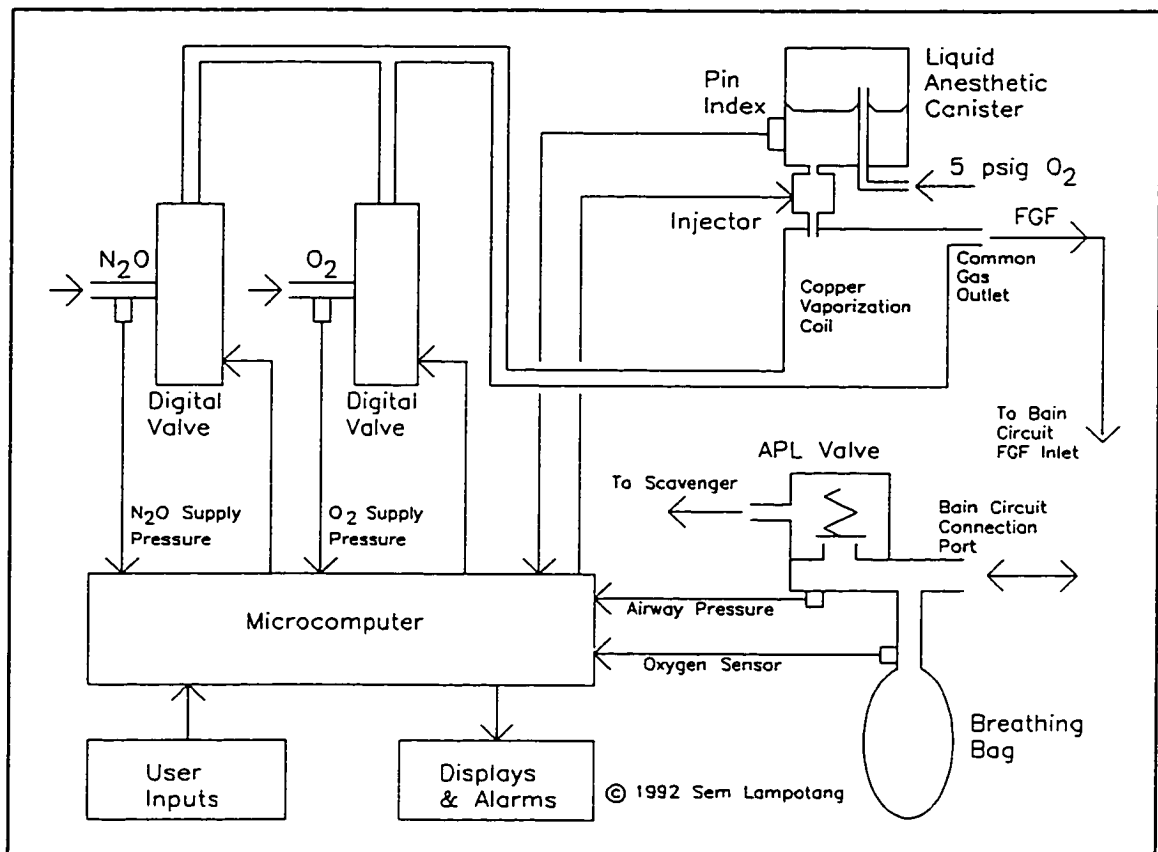
Figure 9. The Boston Anesthesia System. The first completely integrated electronic anesthesia delivery system.

The orifices were designed as fixed geometry sonic nozzles that would operate in the choked flow regime if the ratio of back pressure to stagnation supply pressure was less than 0.8. Consequently, the output of the digital valve orifices were independent of

the back pressure (anesthesia circuit pressure typically fluctuates from atmospheric to 20 cm H_2O with each mechanical inspiration from the ventilator).

Another noteworthy feature of the BAS was a modified automobile fuel injector supplied with liquid volatile anesthetic pressurized with oxygen at 5 psig. The injector was operated in pulsed mode (pulse width was constant in time), each pulse delivering approximately 5 microliters of liquid anesthetic (Cooper, Newbower & Trautman 1975).

The BAS departed from convention by allowing the user to set total FGF and the N_2O concentration (the balance gas being O_2; the microprocessor took care of the mathematics) rather than adjust two independent rotameters independently to arrive at the desired FGF and N_2O/O_2 mixture. The BAS approach removed the possibility of user miscalculation and was inherently more user-friendly.

The prototype of the BAS had no CO_2 absorber and was designed for use with high flowrate techniques and a Bain circuit. A conventional scavenger and anesthesia ventilator were used. Due to the expense of accurate gas sensors at the time, closed loop control of gas composition was not attempted.

3.2.3 Automated Closed and Semi-Closed Experimental Anesthesia Delivery Systems

In 1978, Salamonsen published results of a dog experiment with an electronically-controlled, VOC, vaporizing system for programmed anesthesia (Salamonsen 1978). The dog breathed spontaneously on a circle anesthesia circuit with a FGF of 0.5 l/min. End-tidal anesthetic concentration was the controlled variable. The displacement rate of a syringe pump filled with liquid halothane was electronically controlled by the output from

a pulsed oscillator circuit. The liquid halothane was nebulized by a 250 ml/min jet of a 50 psig mixture of O_2 and N_2O into a bowl with an inlet and outlet ports. Using a seven-compartment computer model tailored to the dog to predict the liquid anesthetic injection rates, the arterial and end-tidal anesthetic concentrations in the dog remained stable (variation of about 15%) at approximately 1.2 MAC (the target brain halothane concentration) (Salamonsen 1978).

In 1981, Tatnall et al. rejected predictive (pre-programmed) control of inspired anesthetic concentration based on an "average" patient computer model as unacceptable (Tatnall, Morris & West 1981). Recognizing the considerable variation in rate of anesthetic uptake among the patient population (Westenskow, Jordan & Hayes 1983a), the investigators set out to establish the feasibility of identifying in real time individual patient characteristics during induction (with or without N_2O) with controlled ventilation, using breath-by-breath measurements of inspired and end-tidal anesthetic concentrations. The algorithm required estimation of mixed venous anesthetic partial pressure which was assumed to be zero in the initial stages of induction. Alveolar anesthetic concentration, assumed to be identical to end-tidal anesthetic concentration, was controlled via modulation of the inspired anesthetic concentration.

The system was first tested against a multi-compartmental computer model of anesthetic uptake and distribution in pediatric and adult patients. Later "clinical" tests were performed "off-line" using collected pediatric patient data, during halothane anesthesia where the vaporizer setting was continuously, manually adjusted to maintain the desired alveolar halothane partial pressure. The type of anesthesia circuit was not

specified but was presumably a non-rebreathing circuit since inspired anesthetic concentration was the modulated variable. By comparison of the inspired halothane concentrations actually delivered in the clinical cases and those recommended by their control system (maximum difference of 0.1% halothane), the investigators concluded that their approach to controlled anesthesia was feasible (Tatnall, Morris & West 1981).

3.2.4 The Harrow I Controlled Anesthesia Delivery System
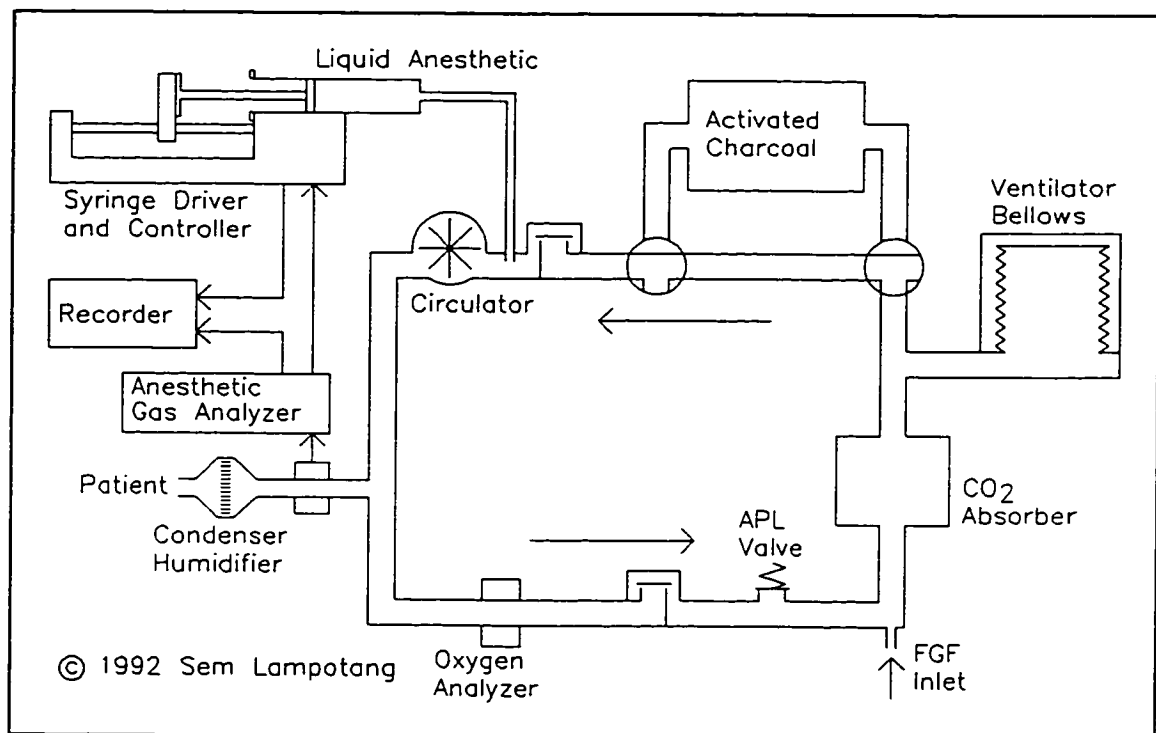
Figure 10. The Harrow I controlled anesthesia delivery system

Around the same time, Hawes at al. (1982) were working on closed-loop control of closed circuit anesthesia. Novel features included direct injection of liquid anesthetic by an electronically-controlled syringe pump into the closed anesthesia circuit

immediately upstream of a Revell circulator (figure 10) and an activated charcoal canister to quickly absorb the volatile anesthetic during emergence. The mixing action of the Revell circulator fan was presumed to help anesthetic vaporization. Anesthetic concentration was measured by an electronic anesthetic gas analyzer. End-tidal anesthetic concentration was maintained at a preset value via an analog, electronic feedback loop. The system was not computer based.

3.2.5 The Utah I Controlled Closed Circuit Anesthesia Delivery System

Control of end-tidal anesthetic concentration as an indirect means of controlling anesthetic depth was established as the preferred method in the early 80's. Surprisingly, Westenskow, Jordan and Hayes (1983b) reported no statistically significant difference in enflurane uptake, heart rate, blood pressure or cardiac output between end-tidal and inspired anesthetic concentration control during feedback control of enflurane/N_2O anesthesia in dogs. In one group of 7 dogs, the end-tidal enflurane concentration was held constant at 2%; during a 4 hour period, inspired enflurane concentration dropped from a maximum of 3.7% to 2.1%. The second group of 7 dogs were supplied a constant inspired enflurane concentration of 2%. Both groups were mechanically ventilated by an ascending bellows ventilator on a closed anesthesia circuit.

Enflurane was introduced into the circuit by a bubble-through (copper kettle) vaporizer (figure 11). Three electronic, analog proportional-integral-derivative (PID) feedback control loops were simultaneously in effect. One controlled inspired O_2 concentration to 50%. Another controlled enflurane concentration (inspired or end-tidal)

to 2.0% by modulating the flowrate of O_2 through the bubble-through vaporizer while the third maintained anesthesia circuit volume at a constant level by electronically controlling N_2O inflow rate.
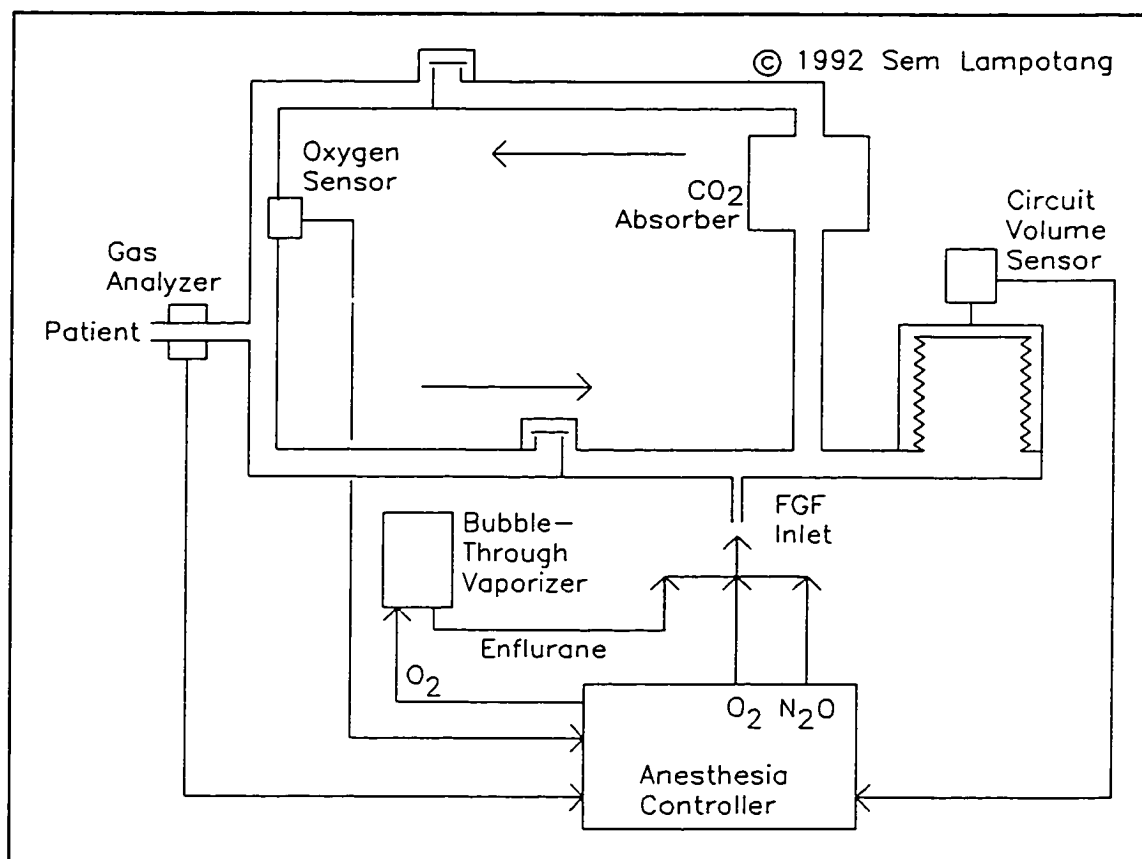
Figure 11. The Utah I controlled, closed-circuit, anesthesia delivery system

The sensors for the feedback loops were a polarographic O_2 sensor and an infrared gas analyzer for anesthetic concentration. The circuit volume sensor consisted of a linear, vertical array of 10 photodetectors on one side of the transparent upright bellows casing, diametrically opposite a fluorescent lamp. The voltage coming out of the linear array is proportional to the bellows position and hence the circuit volume

(Westenskow et al. 1977). The anesthesia circuit was primed for at least 20 minutes to allow equilibration of the material in the anesthesia circuit and of the soda lime. The leakage rate from the circuit averaged 32 ml/min (13-68 ml/min range).

3.2.6 The Harrow II Controlled Anesthesia Delivery System
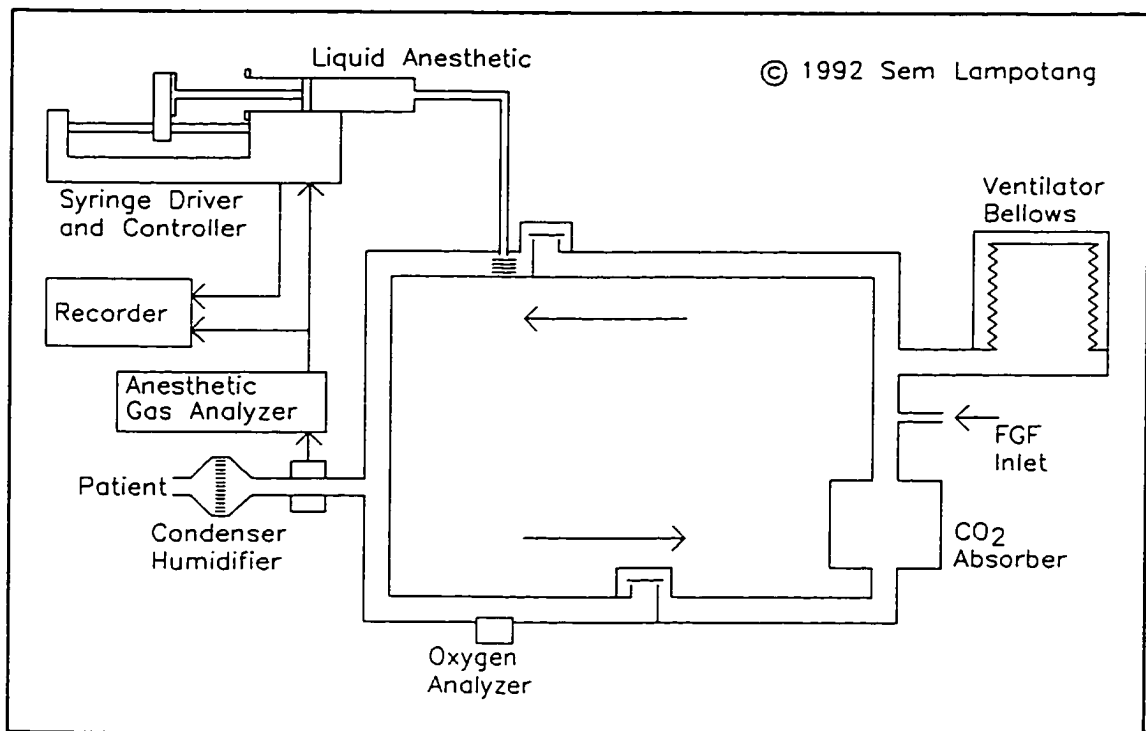
Figure 12. The Harrow II controlled anesthesia delivery system

The Harrow II system (circa 1983, figure 12) injected liquid anesthetic directly onto a wad of non-occlusive cotton material placed immediately downstream of the inspiratory valve of a completely-closed circle system (Ross et al. 1983). The brass housing material at the anesthetic injection site was in thermal contact with the large thermal inertia of the valve, canister and FGF inlet, to ensure adequate heat supply for

anesthetic vaporization. Using halothane/O_2 (no N_2O) anesthesia, end-tidal halothane concentration was automatically controlled by feedback via a simple proportional controller. The anesthetic agent sensor was a vibrating quartz crystal coated with silicone antifoam liquid (DC190). Volatile anesthetics are soluble in DC190 and will increase the mass of the vibrating arrangement and hence decrease its vibration frequency, by an amount proportional to the anesthetic concentration.

The Harrow II system went to considerable effort to reduce leaks. All permanent connections were sealed with silicone rubber compound. Leakage rate still occurred at about 0.48 to 0.61 ml/min/cm H_2O. Absorption of anesthetic agent by the circuit was 16.4 microliters of liquid isoflurane/min from 5-10 minutes dropping to 13.12 microliters after 10 minutes. The circuit was intended to be equilibrated for 5 minutes prior to connection to the patient. Anesthetic uptake rate was about 42 microliters/min of liquid isoflurane with wet soda lime and 140 with dry soda lime.

The system was clinically tested on twelve patients. Due to the proportional control law, an offset of 0.1% from the desired end-tidal halothane concentration was observed. O_2 was manually added to the circuit as needed to keep the circuit volume constant. At a constant end-tidal halothane concentration of 0.8%, vapor uptake was 114 ml/min at 1 minute from the start of anesthetic administration, 36 ml/min at 5 minutes, 29 ml/min at 10 minutes and between 22 and 18 ml/min at 20-35 minutes (Ross et al. 1983).

3.2.7 Salford System
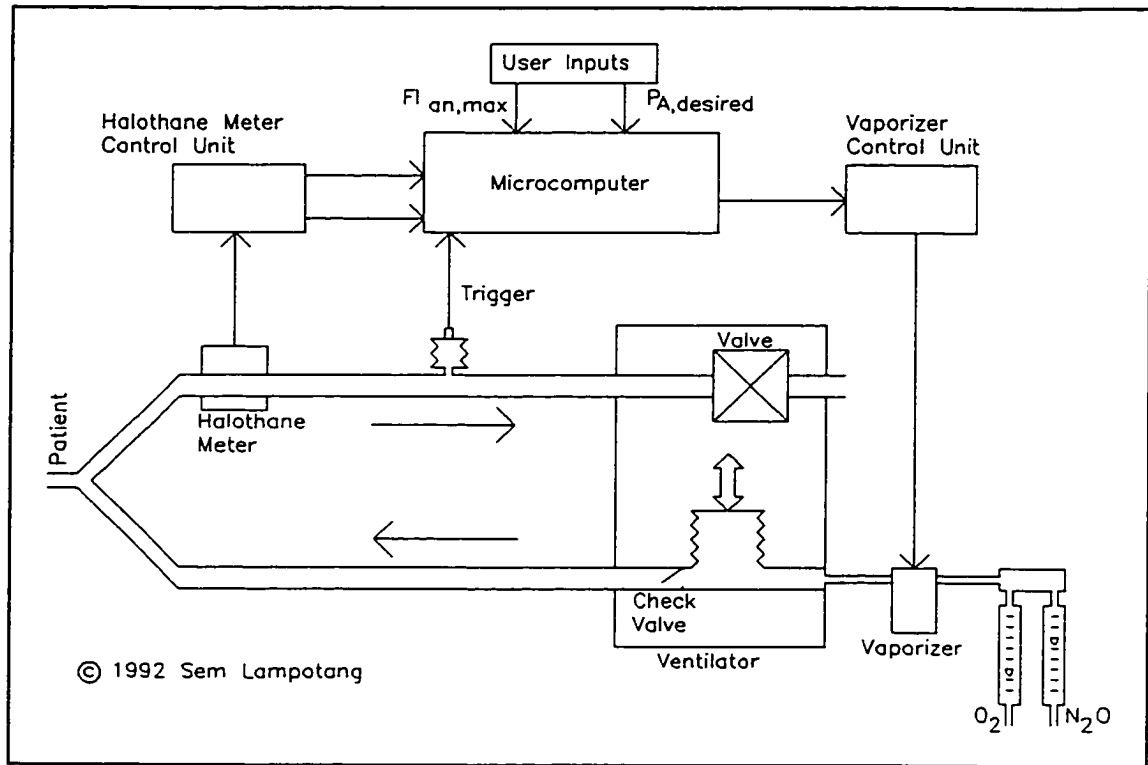
Figure 13. The Salford non-rebreathing controlled anesthesia delivery system

This system was a development of the study by Tatnall, Morris and West (1981) regarding the feasibility of identifying and quantifying individual patient anesthetic uptake characteristics, in real time during induction. Halothane anesthesia (with or without N_2O) using the overpressure method and controlled ventilation was performed on 80 patients ranging from 7 months to 62 years old undergoing routine surgery (Morris, Tatnall & Montgomery 1983). Initial settings were based on the extensive body of knowledge on MAC and how it is affected by patient variables such as age. A miniature bellows in the expiratory limb signalled the onset of each new respiratory cycle (figure

13). Patient uptake characteristics were identified and quantified in real time during the first 9 mechanical breaths delivered via a non-rebreathing anesthesia circuit (minute volume divider type, (Mushin et al. 1980, 135).

After 90 respiratory cycles, proportional-integral (PI) control was implemented. An Apple II 48K microcomputer was used for patient characteristic identification and vaporizer control. A geared DC servomotor adjusted the position of the control spindle on a flow-over vaporizer, allowing a range of 256 positions over a range corresponding to delivered halothane concentration of 0 to 2.5%. A potentiometer supplied feedback of the spindle position to the vaporizer control mechanism and a calibration table was used to correlate spindle position to vaporizer output concentration. High frequency filters, digital smoothing and a diathermy detection circuit protected the system from measurement noise. The maximum allowable inspired anesthetic concentration was set at 3 times the desired alveolar anesthetic concentration. Administration of halothane was delayed by 2-3 minutes whenever N_2O was also used to avoid the second gas effect which would enhance the uptake of halothane initially and affect the determination of the individual patient uptake characteristics.

The system overshot when only O_2 was used because calibration was done with an O_2/N_2O mixture, resulting in increased halothane output. The system was stable and reliable in a clinical environment as well as resistant to diathermy.

3.2.8 Utah II Controlled Anesthesia Delivery System
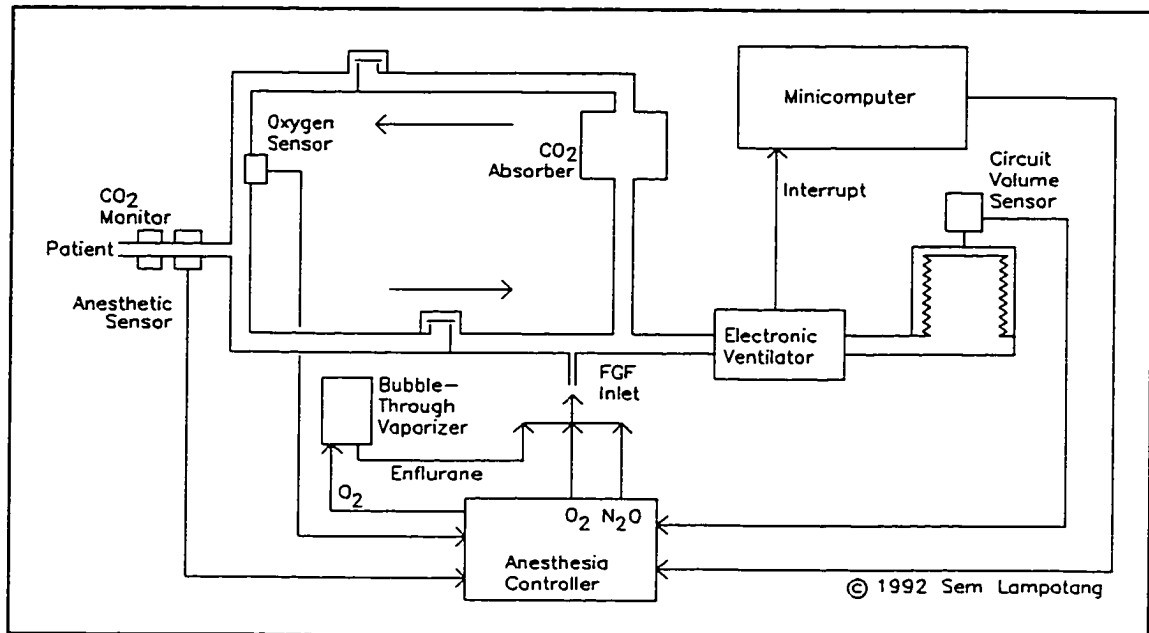
Figure 14. The Utah II controlled anesthesia delivery system

This system (figure 14) was a digital version of the Utah I system. PID software algorithms implemented in BASIC on a PDP 11/03 minicomputer digitally controlled end-tidal anesthetic agent concentration (± 0.1 v/v%), inspired O_2 ($\pm$ 0.2) and breathing circuit volume ($\pm$ 30 ml) (Hayes et al. 1984). Enflurane/N_2O anesthesia was successfully performed in a closed anesthesia circuit on 7 dogs for 4 hours.

3.2.9 Alabama Closed-Loop Control Anesthesia Delivery System

This system demonstrated closed loop automatic control of ventilation, oxygen, nitrous oxide and anesthetic agent delivery into a closed anesthesia circuit (Ritchie et al. 1987). The system is used with closed anesthesia circuits only (figure 15). End-tidal

anesthetic agent and CO_2 concentrations, inspired oxygen concentration and gas volume in the anesthesia circuit are regulated. A syringe pump injected liquid anesthetic agent into the anesthesia circuit. N_2O and O_2 flowrates were controlled by mass flow controllers. The control functions were implemented on a Zilog Z-80 based microcomputer. The control law for regulating exhaled end-tidal anesthetic concentration was proportional in the first 3 minutes and PI afterwards.
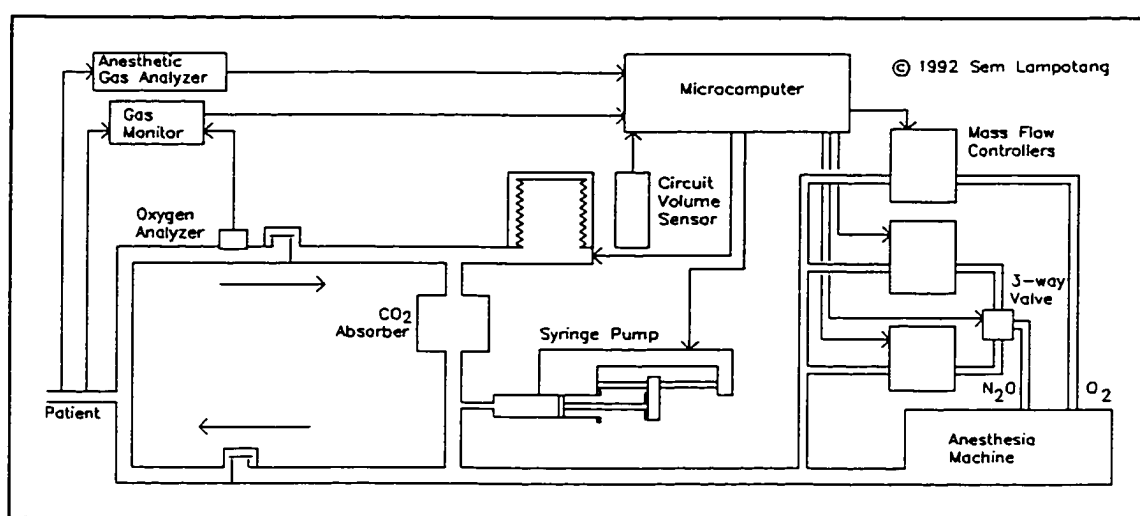
Figure 15. The Alabama closed circuit, controlled anesthesia delivery system

3.2.10 Utah Anesthesia Workstation (UAW)

The experimental UAW (circa 1987) used electronic instrumentation and monitors extensively for implementation of an alarm expert system (figure 16). Other distinctive features included three mass flow controllers (O_2, N_2O and O_2 flowrate to a bubble-through vaporizer) and a selectable anesthesia machine controller mode (Loeb et al. 1989). In "electronic" control mode, the anesthesiologist sets the desired O_2 and N_2O flowrates as well as the O_2 flowrate to the bubble-through vaporizer to control anesthetic

concentration as in conventional systems except that the flow controllers are electronically operated. In "autopilot" mode, the anesthesiologist sets FGF, oxygen concentration and exhaled end-tidal anesthetic concentration.
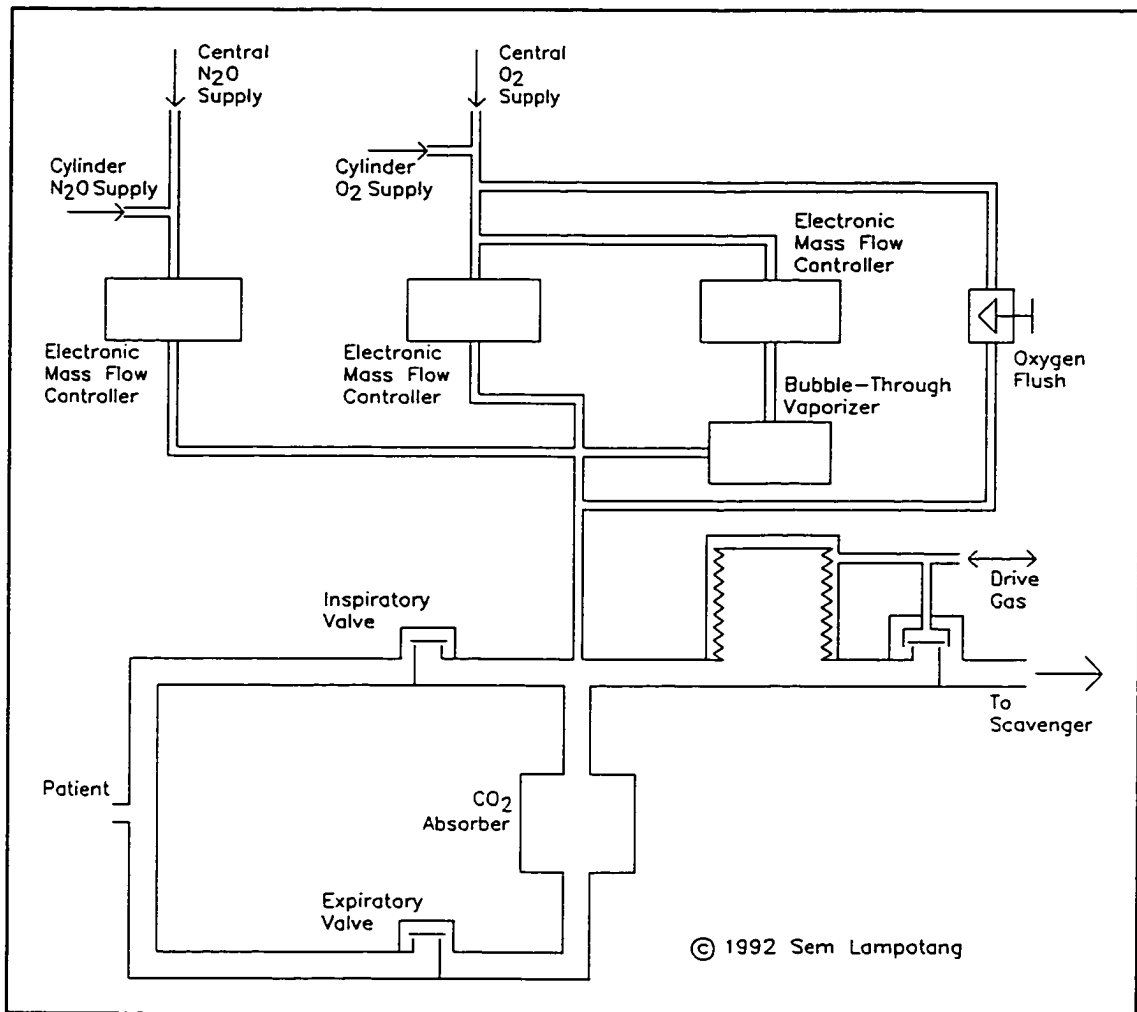
Figure 16. The Utah anesthesia workstation

The UAW used a conventional bellows ventilator, scavenging system and circle breathing circuit. Although some mechanical components were novel (e.g., the mass flow controllers), the mechanical layout of the anesthesia machine itself was left

unchanged. A Motorola 68000 microprocessor and a MacIntosh Plus controlled the operation of the UAW.

3.2.11 Nuffield Anaesthetic Machine (NAM)

In this British experimental, microprocessor-controlled machine, the flowmeter control valves are pulsed at a constant-time pulse width to deliver a constant volume of gas per pulse (Sykes et al. 1989). The desired gas composition is obtained by pulsing the desired flowrates of O_2 and N_2O or air into a mixing chamber (figure 17). An interesting feature is the possibility of using a mixture of 5% CO_2 in O_2. At the end of anesthesia, CO_2 may be desirable in the inspired gases to enable mechanical hyperventilation of the lungs to accelerate removal of anesthetic from blood without lowering the arterial pressure of CO_2. Saturated anesthetic vapor was added by pulsing gas from the mixing chamber through a bubble-through vaporizer. Unlike the UAW, the gas passing through the bubble-through vaporizer is not oxygen, but the mixture set by the user. The temperature within the vaporizer is measured and since the vapor pressure curve for each volatile anesthetic is known, the flowrate required to obtain a given anesthetic concentration can be predicted.

Sonic nozzles are placed at the outlet of the flow control valves to ensure insensitivity of the output to downstream pressure variation. The mixing chamber is maintained at a constant pressure by a variable-orifice, constant pressure valve which also acts as a rotameter, i.e., the position of the plunger controlling the orifice size is an indication of the flowrate.
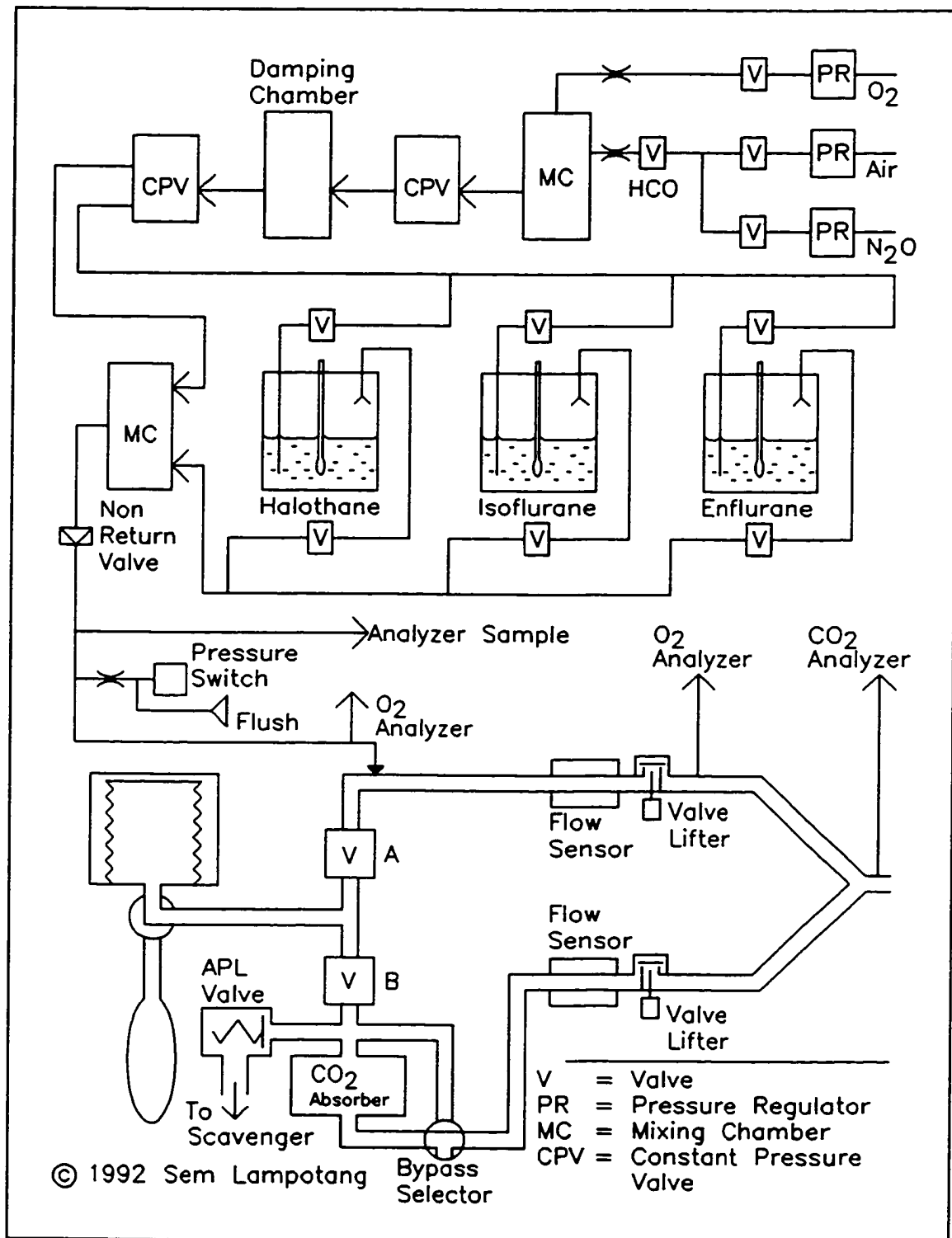
Figure 17. The Nuffield electronic anesthesia delivery system

The FGF range is 2-20 l/min with an O_2 concentration range of 25-100%. The NAM can be readily configured into different breathing circuits. The ventilator is a conventional time-cycled flow generator compressing an ascending bellows and can deliver a breathing rate of 8-40 bpm, a tidal volume of 0.2-1.5 l and a minute volume of 3-16 l/min. An end inspiratory pause is also featured in the ventilator cycle and allows assessment of lung-thorax compliance and airways resistance.

FGF augments the delivered tidal volume during mechanical ventilation since FGF from the anesthesia machine keeps flowing into the anesthesia circuit while the ventilator is delivering its tidal volume (VT).

$$VT_{delivered} = VT_{set} + (FGF * inspiratory\ time) \qquad 3.2$$

This insidious effect of FGF may double the tidal volume (Gravenstein, Banner & McLaughlin 1987) and cause barotrauma in pediatric patients. The NAM automatically compensates tidal volume by accounting for the contribution from FGF.

Even though each machine function has its own monitor, it is not used for closed loop control. The monitors are used for display and to warn the user via alarm algorithms. The unidirectional valves in the anesthesia circuit are passive (gravity-operated) but may be rendered inoperational by valve lifters that prevent the valve leaflets from reseating when they are energized. Flow transducers are installed on each limb of the anesthesia circuit. Five subsystems (gas mixing, vaporizer, ventilator, gas analyzer and monitor) are each controlled by a microcontroller.

3.2.12 Boquet Anesthesia Machine

Only a full-sized cardboard mock-up of this machine concept was built following a time and motion study of the anesthesiologist's routine activities in the operating room (Boquet, Bushman & Davenport 1980). The study was performed with the help of a device for tracking the direction in which the anesthesiologist's eyes were looking and was mainly geared at man-machine interaction and human factors. A modular approach to system design was emphasized in this conceptual machine. The work surface and storage units were separated from the control/display modules. One surprising finding was that the breathing bag was the most frequently checked visual display. It should be noted that the study was performed in 1980 in England and may not necessarily apply to the United States.

3.2.13 Physioflex Anesthesia Delivery System

This experimental system (figure 18) is not well-known in the United States. The initial literature search did not uncover any material on the Physioflex system and its existence was accidentally unearthed when a German textbook on humidity conservation in anesthesia was consulted (Erdmann, Veeger & Verkaaik 1989).

A fixed speed blower, similar in concept to the Revell circulator, continuously circulates gas around a circular closed circuit at approximately 70 l/min (Verkaaik & Erdmann 1990; Versichelen & Rolly 1990). One, two or four bellows (metal diaphragms with an outer concentric band of elastic material attached to them) are connected into the breathing circuit according to patient size so that compliance is kept at a minimum,

especially for neonates with small tidal volumes and low compliances (high PIPs). The metal diaphragms also act as capacitive transducers; the axial displacement and displacement rate of the bellows are transduced as volume and flowrate respectively into or out of the lungs. The added complexity of multiple bellows and their associated valving, controls and transduction are necessary because the system does not compensate for the amount of gas that is "stolen" by the compliance of the breathing circuit. Furthermore, the remoteness of the flowrate transducers (the metal diaphragms) from the variable that they are monitoring (flowrate into the lungs) means that the number of potential leak sites and sources of error is increased.

Using end-tidal anesthetic concentration as the feedback variable, liquid anesthetic is injected into the expiratory limb of the system via a computer-controlled syringe. An activated charcoal canister, when switched into the breathing circuit, allows rapid removal of volatile anesthetics while maintaining a closed circuit. A CO_2 absorber on the suction side of the blower removes exhaled CO_2. However, the CO_2 absorber cannot be cut out of the breathing circuit. If present, this feature would allow intentional rebreathing of CO_2 during deliberate hyperventilation with a closed circuit and the charcoal canister cut into the circuit so that the $PaCO_2$ is not excessively lowered (which would lead to clinical problems like acid/base balance in the blood). Neither can CO_2 be introduced into the circuit in cases where the CO_2 production rate is already too low and will not cause significant rebreathing even with the CO_2 absorber cut out of the closed breathing circuit.
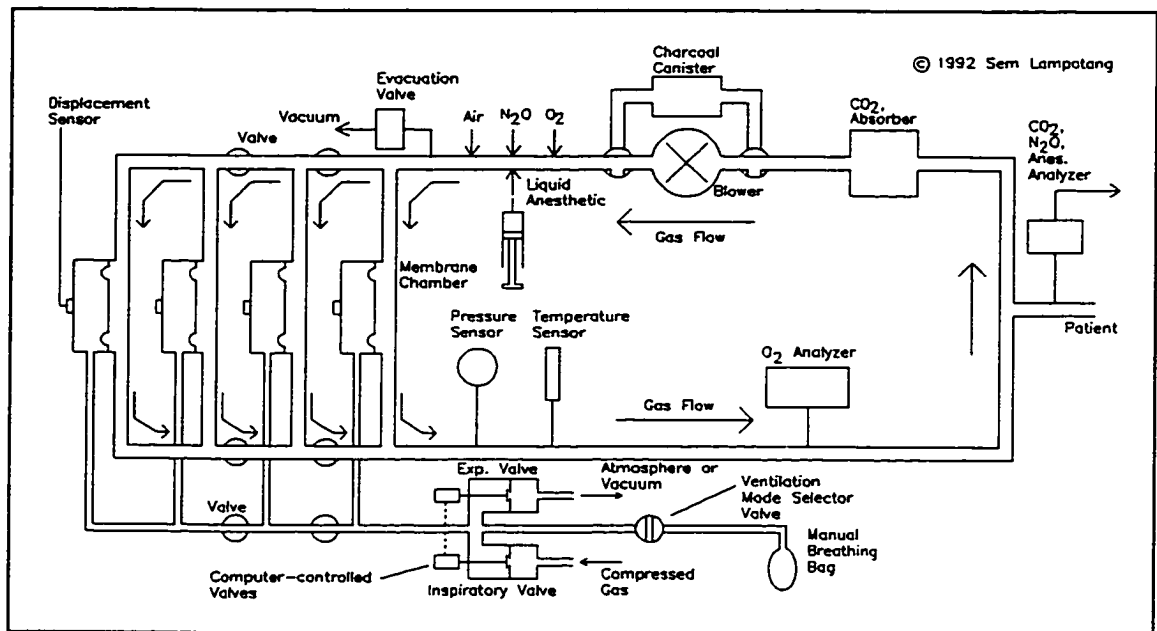
Figure 18. The Physioflex anesthesia delivery system shown in adult, mechanical ventilation mode

Spontaneous, assisted and mechanical ventilation are possible. The system requires compressed air or oxygen to power the bellows for mechanical ventilation. A vacuum source is required to assist exhalation, i.e., apply NEEP (negative end-expiratory pressure) to the airway. However, manual ventilation of the patient's lungs during mechanical ventilation, which is a desirable design feature, is not possible. The physical separation of the gas in the manual ventilation bag from that in the patient's lungs by the metal diaphragms in the bellows may reduce the sensitivity of the bag as an indicator of lightness of anesthesia, lung compliance and airway resistance. A maximum PIP of 6 KPa (60 cm H_2O) and a PEEP range of 0 - 30 cm H_2O are possible. The respiratory rate ranges from 5 - 40 bpm (Physio Medical Systems 1990).

An evacuation valve allows gases to be flushed from the system, especially when N_2, CH_4 and CO from the patient start accumulating in the closed circuit. A flush program admits 2.5 l/min of O_2/N_2O in the preselected ratio for 2 minutes when the N_2 concentration exceeds 10% because the accumulation of the undesirable gases excreted from the patient decreases the concentration of the balance gas by the same amount. The flush program is also used to increase the O_2 concentration in the circuit. Surprisingly, there is no O_2 flush button per se and the rise time to 100% O_2 is slow at 10 minutes (Versichelen & Rolly 1990) which will be a significant problem in an emergency since rapid attainment of 100% O_2 is a mandatory safety feature.

The Physioflex system does not provide the possibility of heating or cooling the gases as a means of maintaining the desired inspired gas temperature or removing heat from the patient in case of malignant hyperthermia, respectively. Airway pressure is sampled in the breathing circuit, far from the patient connection to the circuit. Again, the remoteness of the sensor from the monitored variable renders the design vulnerable to incidents like disconnects, kinks, obstructions and leaks. Gases sampled for gas analysis at the patient interface are not returned to the breathing circuit thus creating a departure from true closed circuit anesthesia.

3.2.14 Other Anesthesia Delivery System Designs

The initial design of the recirculating anesthesia delivery system that is the subject of this dissertation has been patented by the University of Florida (US Patent 4,702,241: Gravenstein & Lampotang 1987). During prosecution of the patent, the United States

Patent Office presented several anesthesia delivery system/breathing circuit patents (US

Patents 4,573,462; 4,543,951; 4,520,812; 4,481,944; 4,463,756; 4,281,652; 4,245,633;

4,188,946; 4,082,093; 4,007,737; 3,815, 593; 3,485,243; 3,385,295; 3,378,005;

3,003,196; 2,830,583; 2,325,049; 1,635,101; 1,630,501) as prior art. Since these

patents have not been implemented or commercialized, they will not be described further

in this review.

3.3 Summary

This chapter has examined the historical development of automated anesthesia

delivery and the relevant literature pertaining to experiments in improving and automating

anesthesia. Despite the multitude of experimental systems presented in this chapter,

automated closed-circuit anesthesia delivery is still not a reality in anesthesia. User

resistance to change, impracticality, cumbersomeness and lack of user-friendliness of past

system designs, computer-phobia as well as the perception of complexity leading to the

risk of more failure modes have combined to prevent the full-scale adoption of

automated, closed-circuit anesthesia.

In addition, expired gas partial pressures may not reflect blood partial pressures

if the ventilation/perfusion ratio of the patient is not optimal. Shunts and alveolar

deadspace ventilation are common during anesthesia. Closed-loop anesthesia must await

reliable methods of measuring depth of anesthesia and/or blood gas partial pressures.

However, the lack of these reliable measures does not interfere with the design process

for an anesthesia delivery system which will be addressed in the next chapter.

CHAPTER 4
ENGINEERING DESIGN METHODOLOGY FOR A VENTILATOR AS A PLATFORM FOR ANESTHESIA DELIVERY

The emphasis in this chapter is on the design process and the engineering, safety and user constraints for an anesthesia delivery system which, when systematically applied in a design methodology, lead to a solution. Historically, the design of anesthesia equipment and delivery systems has been a process of evolution by trial and error and enlightened inspiration rather than the result of a deliberate, systematic and well-documented analysis and engineering design methodology. Indeed, most anesthesia breathing circuits have been conceived by individuals who were, by profession, medical doctors, e.g., the circle (Jackson 1955), Revell (Revell 1959a, 1959b), Neff (Neff, Burke & Thompson 1968), Waters and Bain circuits.

There are undeniable benefits to an evolutionary approach and user-conceived designs; some of these early circuits are reliable, sturdy and elegantly simple designs and are still used. These circuits (e.g., the circle and Bain) still have a strong influence on system design today. However, the design synthesis of these circuits is not well documented and may not have taken into account design parameters which are now better understood or have since become relevant (like heat and humidity conservation, cost containment, operator overexposure to waste anesthetics and ozone layer depletion). Furthermore, relatively new technology like inexpensive and reliable microcontrollers and

74

electronics, and proven digital control algorithms were not available when the early anesthesia delivery systems were conceived (1917-1960).

Consequently, a design reappraisal of the anesthesia delivery system according to a top-down engineering design methodology is a worthwhile, necessary and overdue undertaking. As an academic dissertation free of the proprietary requirements of industry, part of the objective is also to establish a freely-accessible and thoroughly-documented engineering design methodology that is open to discussion and criticism while also serving as a framework for future follow-up work as new or initially overlooked technology becomes available or apparent. Indeed, a design reappraisal every 10 years according to the methodology outlined in this chapter would not be unreasonable in light of the rapid pace of technological progress in microelectronics, transducer technology and digital control algorithms.

In this chapter, we start by briefly reviewing the design history of anesthesia delivery systems. The design guidelines, objectives and options for an anesthesia delivery system are then grouped in order of approximate priority[1] into a design checklist. The terminology consistently used throughout this work will be:

Guidelines: a generalized, non-quantitative, design philosophy

Objectives: a specific and necessary design requirement, usually quantifiable

Options: a desirable but not necessary design aspect

---

[1] Establishing priorities is an inexact process since it involves subjective judgements which may vary somewhat with individuals. However, it is a necessary step in a systematic design methodology.

If it is possible to do so without gross oversimplification, the biomedical design guidelines, objectives and options are also translated into concise engineering terms. Examples of possible solutions are also included in the checklist to further illustrate the concepts. Then, the design path adopted to arrive at a design solution is thoroughly documented. Finally, the engineering design methodology is formalized into a flow chart diagram that can be used as a template for future design efforts and enhancements.

4.1 Design History

The design history of anesthesia delivery systems can be classified into three design generations which are also chronologically ordered.

The earliest, first generation designs were characterized by open or semi-open systems with varying degrees of control of anesthetic concentrations and the absence of a work surface or an anesthesia ventilator, e.g., the ether mask and the Morton inhaler (section 2.5.1.1).

The second generation designs exhibit a modular approach to system design and the absence of electricity or electronics. The four modular subsystems (high pressure, low pressure, breathing and scavenging circuits) are present as well as an anesthesia ventilator, a CO_2 absorber, a chassis frame with racks to hold anesthesia related equipment, a work surface and storage drawers, e.g., the Ohmeda Unitrol and Modulus II and the Dräger Narkomed anesthesia delivery systems which predominantly use the circle and Bain anesthesia circuits (section 2.5.8).

Third generation designs are typified by the same modular mechanical layout as second generation designs but analog and digital electronics replace functional components like pneumatic timers in anesthesia ventilators. Human factors and integration of electronic monitoring of the anesthesia breathing circuit and the patient are attempted (e.g., Ohmeda Central Display, North American Dräger Narkomed 4, Drägerwerk Cicero, Engström Elsa and the experimental Boston (sec. 3.2.2), Nuffield (sec. 3.2.11), Harrow II (sec. 3.2.6) and Utah anesthesia workstations (sec. 3.2.10).

What is in store for the future? The next generation of anesthesia delivery systems, which we shall call the fourth generation designs, are likely to be distinguished by extensive system integration of electronic, pneumatic and mechanical components from the start of the design process. Integration of mechanical function (the anesthesia ventilator and breathing circuit will be integral parts of the system, e.g., the experimental Physioflex prototype (Physio Medical Systems 1990; sec. 3.2.13)) will result in a different mechanical layout from second and third generation designs.

Information about internal events, especially those initiated by the operator, like an O_2 flush, will be readily accessible, in real time, to external systems like a laser surgery unit or an alarm expert system shell. An open information architecture will promote communication and therefore patient safety, by making data available to intelligent alarms expert systems (van der Aa 1990). The emphasis will be on top-down system design and efficient use of anesthetics, conservation of humidity and heat, closed loop operation and reduced emission of waste anesthetics, e.g., the experimental

University of Florida GRADS (Gainesville Recirculating Anesthesia Delivery System; to be described later in this and following chapters).

4.2 Design Considerations and Constraints

National, e.g, the US (ANSI 1979) and European, and international (ISO) standards for anesthesia delivery systems can, in some instances, serve as guidelines and objectives to system design.   However, more often, they mandate what is not permissible, act as recommendations and minimum performance requirements and do not specify how those minimum requirements are to be attained generally. Where applicable, national and international standards must be used as design specifications and constraints. These standards are subject to periodic revision and the design checklist should be updated whenever the standards are revised.

This section on design considerations and constraints will be divided into three sections: guidelines, objectives and options. The procedure for establishing the design guidelines, objectives and options was as follows:

1.   List all design considerations in a single, comprehensive list

2.   Sort the design parameters under three categories: guidelines, objectives and options

3.   Group the entries within each category under general headings

4.   Prioritize the general headings under each category

5.   Prioritize the entries under each general heading

6.   Repeat steps 3, 4 and 5 for sub-headings to as many levels as required

The resulting complete list (the intermediate steps leading to it are not shown) with its numerous levels of subheadings and prioritization forms a comprehensive design checklist. The entries within each subgroup do not necessarily relate directly to another entry in another subgroup (e.g., entry 4 under heading 3 in not necessarily of higher priority than entry 1 under heading 4 in the same category). The grouping scheme adopted in the design checklist allows reprioritization of the design considerations according to the designer's judgement and the desired emphasis of the end-product, while providing a checklist to ensure that all design parameters are systematically considered. The numbering scheme, although slightly unwieldy as the levels get lower, provides a concise means of documenting the "genealogy" of a design characteristic or feature.

Solution examples are differentiated from the design specification from which they derive by having a letter added to the specification number. For example, if there are 3 possible solutions for design objective 1.2.3, then the 3 possible solutions will be numbered 1.2.3a, 1.2.3b and 1.2.3c.

Prioritization inevitably brings subjectiveness and contention to an engineering design exercise. It cannot be avoided because eventually design involves compromises and priorities must be established before compromises can be judiciously made. Obviously, the prioritization is not cast in stone and must be trimmed or reevaluated according to the designer's judgement, new clinical data and the desired end-product characteristics. The main thrust of the checklist is to provide a comprehensive and well-organized checklist which is applicable to the design of all anesthesia delivery systems, whereas prioritization is end-product specific, and in the final analysis, subjective. The

design for an anesthesia delivery system that results from the methodology described in this chapter is based on the full design checklist. The experimental prototype described in chapter 6 implements in hardware the design features that are of highest priority in establishing the feasibility of the design: the <u>ventilation and life-support component</u>.

Some control engineering concepts will be used in their abbreviated form in the design checklist. SSE is the steady state error (desired value - steady state value), RT is the rise time in seconds to 90% of the target value for a step input, ST is the settling time in seconds to within 5% of the steady state value and OS is the overshoot at the first oscillation above the desired value for a positive step input while US is the undershoot at the first oscillation below the desired value for a negative step input (Ogata 1970). Jitter is the seemingly random variation in the controlled value that is most evident when pulse width modulation of a binary (on/off) actuator is used to control plant behavior.

4.2.1 Design Guidelines

Due to the extent of the design checklist, its contents are first outlined as a convenience to the reader.

Contents of the design guidelines section:

1   Patient Safety
    1.1   Reliability
    1.2   Failsafe mode
    1.3   Control accuracy
    1.4   Fast response
    1.5   Human error prevention
    1.6   Flexibility
    1.7   Materials compatibility

1.8   Open information architecture
1.9   Electrical hazards and safety
1.10 Simplicity in design and module interaction

2   Operator safety/liability
    2.1   Reduction of spilled anesthetic gases into OR
    2.2   Medico-legal considerations
    2.3   Electromagnetic radiation
    2.4   Environmental pollution
    2.5   Electrical hazards and safety

3   Cost containment
    3.1   Operating costs
    3.2   Capital costs

4   Human factors
    4.1   Ease of use
    4.2   Low noise levels
    4.3   Structural and mechanical considerations

A detailed list of the design guidelines follows:

1 Patient Safety

1.1 Reliability (no failures)

1.1.1 Control robustness (e.g., insensitivity of the control software and hardware

to common anesthesia or surgical events like O_2 flushes, preoxygenation, temporary

ET tube disconnects for aspiration, X-ray imaging, electro-cautery, etc) that occur

randomly (not clinically, but in the engineering sense that they can occur at any

point in time during the anesthetic)

1.1.1.1 Information sharing

1.1.1.1.1 Control software must be informed of operator-initiated internal

events like O_2 flushes or changes in ventilation mode

1.1.1.1.1a Decouple the O_2 flush button from the O_2 flush valve via the computer for increased patient safety. For example, assuming the system is computer-controlled, then manually depressing the O_2 flush button simply creates a request for an O_2 flush which will get serviced (i.e., the computer opens the O_2 flush valve) if and only if the computer and a simple rule-based expert system decide that it is safe to flush O_2

1.1.1.1.1b Electro-pneumatic rather than purely pneumatic valves for operator-initiated events like an O_2 flush. The binary nature of a solenoid valve (energized or de-energized) can then be used to set a data bit which indicates that an O_2 flush is indeed in progress

1.1.1.1.1c Microswitch on a manually-actuated pneumatic valve is used to determine if an O_2 flush is in progress. A less desirable option since malfunctions at the interface between the valve pushbutton and the microswitch create a potential for error

1.1.1.1.2 Control software must know that a multiple-event anesthetic procedure like preoxygenation or suctioning is occurring

1.1.1.1.2a Operator entry of events like preoxygenation by pressing a corresponding pushbutton on front panel

1.1.1.1.2b Make events like preoxygenation become known by providing a pushbutton that will set the anesthesia delivery system in a preoxygenation configuration, for example

1.1.1.1.2c Deduce that the system is, for example, in preoxygenation mode by comparing the settings chosen by the operator to a template

1.1.1.1.2c.1 Electronically controlled flowmeters facilitate sensing of events like preoxygenation

1.1.1.1.2d Pause/resume button for control software to cope with events like suctioning that also introduce a large, temporary leak in the system

1.1.1.2 Immunity of hardware and software to electromagnetic interference (EMI) from, e.g., electrocautery, microwave blood warmers, X-ray equipment

1.1.1.3 Absence of ground loops from the system wiring scheme

1.1.1.4 Anti-disconnect devices on breathing hoses

1.1.1.5 Guaranteed minimum FiO_2

1.1.1.6 Guaranteed maximum inspired anesthetic concentration to prevent accidental overdose

1.1.2 Longevity and durability of component parts

1.1.3 Predictability of mean time between failure (MTBF) of components

1.2 Failsafe mode (if failures occur, they are graceful, i.e., not catastrophic)

1.2.1 Redundancy

1.2.1.1 Ability to ventilate in case of loss of central gas supply with electrical power available, i.e., back-up gas supply like E-cylinders

1.2.1.2 Ability to deliver O_2 and ventilate in case of electrical power failure (e.g, ball-in-tube O_2 flowmeter directly piped to the common manifold shared by the central and back-up gas supplies connected to a manual resuscitator bag)

1.2.1.3 Ability to deliver O_2 in case of failure or suspected malfunction of anesthesia circuit (e.g., a back-up breathing circuit like a manual resuscitator bag. The back-up breathing circuit should preferably be "self-inflating" like a manual resuscitation bag rather than requiring high pressure O_2 to function properly like a Mapleson D breathing circuit in case of simultaneous failure of both the circuit and the gas supply (Good, Blaschke & Lampotang 1992)

1.2.1.4 Ability to ventilate with room air in case of loss of both central and back-up gas supplies with electrical power available, e.g., a centrifugal blower or a compressor with its inlet aspirating room air

1.2.1.5 Backup electrical supply (e.g., Uninterruptible Power Supply (UPS))

1.2.1.6 Must work in the event of total power failure with no back-up power supply

1.2.1.7 Duplicate microcontrollers

1.2.2 Software crash detection and recovery or switch to backup microcontroller

1.2.2.1 Watchdog timer

1.2.2.2 Failsafe default status of actuators in case of software crash

1.2.2.3 Defined software crash recovery states and reinitialization

1.2.2.4 Smooth transition between the mains power supply and the UPS in case of power failure

1.2.2.5 Defined procedure for reinitializing after a power outage

1.3 Control accuracy

1.3.1 FiO_2

1.3.2　End-tidal (or inspired) anesthetic agent vapor concentration

1.3.3　N_2O (or Xe if implemented)

1.3.4　CO_2 if deliberate rebreathing of CO_2 is implemented

1.3.5　Specific humidity of inspired gases

1.3.6　Temperature

1.3.7　Tidal volume

　　1.3.7.1　If the breathing circuit is compliant and the PIP is high, the amount of gas "absorbed" by the compliance of the circuit should not be included in the measurement of the exhaled tidal volume delivered to the patient.

　　1.3.7.2　FGF should not augment VT during mechanical inspiration

1.3.8　Respiratory rate

1.3.9　Positive end expiratory pressure (PEEP)

1.4　Fast response

　1.4.1　FiO_2

　1.4.2　End-tidal anesthetic, i.e., "square wave" anesthesia

　1.4.3　N_2O (xenon if implemented)

　1.4.4　Small circuit volume to promote fast response since the composition of the circuit gases can be changed faster as the breathing circuit becomes smaller

1.5　Human error prevention

　1.5.1　Slip (correct intention, wrong execution (Gaba 1989)) prevention. Slips are primarily prevented by sound engineering design, e.g., the DISS (diameter indexed safety system) that prevents inadvertent connection of an O_2 hose to a N_2O outlet

1.5.2 Mistake prevention (wrong action resulting from incorrect training or poor judgement (Gaba 1989)). Mistakes are primarily prevented by enhanced medical training, e.g., with anesthesia simulators. However, in some limited and well-defined situations, mistakes can be prevented by proper engineering and software design, e.g., an instruction to deliver 5% isoflurane during maintenance would not be executed and the operator informed of the mistake and asked to enter another value. Or, flushing of the O_2 valve during laser microsurgery can be prevented by designing an interface link whereby the laser surgery unit is disabled whenever an O_2 flush occurs.

1.6 Flexibility

1.6.1 Can ventilate different patient sizes with different compliances and airway resistances

1.6.2 Can provide anesthesia for different procedures, both surgical and non-surgical

1.6.3 Can ventilate patients with markedly different lung time constants (see chapter 5)

1.7 Materials compatibility

1.7.1 Absence of chemical reactivity between circuit materials and gases that may form toxic or undesirable products

1.7.2 Resistance to chemical attack from the volatile anesthetics, O_2 or N_2O, especially for the valve seal materials (e.g., Viton, Teflon)

1.7.3 Material/gas partition coefficient of circuit materials should be low

1.7.4   Gases do not form toxic compounds when reacting with CO_2 absorbent. Trichloroethylene, an anesthetic used in the 1940's in the US, decomposes into neurotoxic compounds (phosgene) in the presence of alkali and heat which are the conditions existing in a CO_2 absorber.   Although trichloroethylene is no longer used in the US because it was implicated in a number of patient fatalities, it is still used in other countries on occasion (Orkin 1986, 124)

1.7.5   Materials, especially metals, do not catalyze a degradation reaction of anesthetics into toxic compounds, at high temperatures

1.7.6   If the circuit is to be reusable, the materials should not be affected by sterilization, e.g., ethylene oxide, ultraviolet radiation

1.7.7   Materials and components must be compatible with 100% O_2 without risk of explosion. For example, valves must be rated "O_2 clean", i.e., no hydrocarbon residue that can start a spontaneous fire with high pressure O_2 and compressors must be of the non-lubricated type

1.8   Open information architecture through monitorability of machine functions (e.g., ventilation settings) facilitated by electronic operation and electro-pneumatic and electromechanical components. For example, the control system does not have to "guess" or determine through smart algorithms if a premature cessation of mechanical inspiration has occurred when the PIP exceeds the set limit. The control algorithm is informed about these events and can therefore accommodate them without unnecessary alarms or disruption

1.8.1 Adherence to proposed Medical Information Bus (MIB; IEEE P1073 standard) for data communication between modules when it is finalized

1.8.1.1 Internal events available to external systems, e.g., while an O_2 flush in progress warning is active, a laser surgery unit is locally disabled

1.8.1.2 Two-way communication: external events are communicated to internal control software and act as a redundant safety net, e.g., when the laser surgery unit is activated, the circuit that activates the O_2 flush valve is disabled

1.9 Electrical hazards and safety

1.9.1 Patient electrocution hazard

1.9.2 Static electricity

1.9.3 Electrical grounding

1.9.4 Prevention of electrical sparking in the presence of an oxygen rich atmosphere, e.g., isolation of electrical sparks from oxygen-rich atmosphere by enclosure in an air-tight casing

1.10 Simplicity in design and module interaction to reduce the risk of system accidents (Gaba & DeAnda 1987)

1.10.1 Explicit, intended interactions between functional modules

1.10.2 Absence of unintended interactions between functional modules (e.g., the insidious augmentation of tidal volume by FGF in present systems (Gravenstein, Banner, McLaughlin 1987))

2 Operator safety/liability

  2.1 Reduction or elimination of anesthetic gases spilled into OR

  2.2 Medico-legal considerations for the operator, medical institution, manufacturer and insurance company

    2.2.1 Access to an automated record-keeper: the anesthesia equivalent of the aviation "black box", which is also used during the anesthetic case

      2.2.1.1 Adherence to existing or proposed data transfer standards

  2.3 Absence of harmful electromagnetic radiation (microwave, etc)

  2.4 Reduced emission of anesthetics into atmosphere (ozone layer depletion)

  2.5 Operator electrocution hazard prevention

3 Cost containment

  3.1 Operating costs

    3.1.1 Efficiency of anesthetic gas use / low operating costs

    3.1.2 Flexibility (one system can perform many different anesthetic procedures)

    3.1.3 Durability / physical robustness

    3.1.4 Ease and cost of sterilization

      3.1.4.1 Cost of disposable option

    3.1.5 Ease and cost of maintenance

      3.1.5.1 Modularity of subsystems and software

    3.1.6 Ease and cost of upgrade / delayed obsolescence

      3.1.6.1 Modularity of functional subsystems and software

3.2 Capital costs

3.2.1 Low manufacturing costs

3.2.1.1 Off-the-shelf component selection where justifiable

3.2.1.2 Compatibility with existing and proposed standards (facilitates incorporation or retrofit of competitive third-party modules)

3.2.2 Ease of manufacture

3.2.2.1 Modular manufacturing units

4 Human factors

4.1 Ease of use ("user friendliness")

4.1.1 Ease and speed of pre-use check

4.1.1a Automated or semi-automated pre-use check (facilitated by a design where the mechanical components are fully integrated with the electronics)

4.1.2 Control settings

4.1.2.1 Prevention of human error (slip)

4.1.2.2 Prevention of human error (mistake) in well-defined situations (e.g, by a rule-based expert system that will, for example, obey a command to give 5% isoflurane during induction but will not execute the same instruction during maintenance and will instead prompt the user for another entry)

4.1.2.3 Location of control settings

4.1.2.4 Inspired gas (O_2, N_2O, He, Xe)

4.1.2.5 Volatile anesthetics

4.1.2.6 Ventilation

4.1.2.7 Inspired gas temperature

4.1.3 Alarm settings

4.1.4 Data presentation

4.1.4.1 Location of data presentation modules

4.1.5 Data interpretation

4.1.5.1 Data condensation to manage information explosion

4.1.6 Alarm interpretation

4.1.6.1 Absence of false alarms (intelligent alarms)

4.2 Low noise levels

4.3 Structural and mechanical considerations

4.3.1 Mechanical stability / resistance to tipping / low center of gravity

4.3.2 Mechanical strength

4.3.3 Ease of moving the system

4.3.4 Compact design (OR space at a premium)

4.3.5 No sharp edges

4.3.6 No mechanical vibration

4.3.7 Ease of cleaning and disinfecting work surfaces and control panels

4.2.2 Design Objectives

Here again, due to the extent of the design objectives list, a list of contents is included

for the convenience of the reader.

Contents of the design objectives section:

1 Life support capability
   1.1   Guaranteed minimum FiO_2
   1.2   Precise control of FiO_2
   1.3   Fast control of FiO_2
   1.4   Automated mechanical ventilation capability
   1.5   Capability to deliver O_2 to patient even with a total loss of gas supply
   1.6   PEEP capability
   1.7   Flexibility
   1.8   Capability to ventilate with room air in case of total loss of gas supply

2 Anesthesia delivery capability
   2.1   Precise and fast control of end-tidal anesthetic concentration
   2.2   "Overpressure" induction capability
   2.3   Ability to deliver different carrier/anesthetic gases
   2.4   Precise N_2O concentration control
   2.5   Fast N_2O control (30 s RT, 45 s ST)
   2.6   Ability to provide real-time feedback control of anesthetic ET concentration
   2.7   Automated closed-circuit anesthesia delivery without constant user supervision
   2.8   Ability to deliver desflurane
   2.9   Ability to deliver xenon gas efficiently
   2.10 Monitorability

3 OR personnel safety
   3.1   Reduced anesthetic emissions into the OR environment
   3.2   No explosion hazard
   3.3   Low acoustic noise emission
   3.4   Low electromagnetic radiation

4 CO_2 rebreathing control
   4.1   Minimal equipment deadspace
   4.2 CO_2 absorption
   4.3   Unidirectional gas flow

5 Human error prevention
   5.1   Slip prevention
   5.2   Mistake prevention
   5.3   Ease and speed of pre-use check

6 Humidity control
   6.1   Maintenance of humidity at optimum level

6.2 Maintain pressure rise across a forced recirculation or recompression device to below 2 psig for minimal water condensation

7 Temperature control
7.1 Maintain optimum inspired gas temperature of 32°C
7.2 Allow user adjustment of gas temperature delivered to patient to facilitate warming

8 Spontaneous work of breathing (WOB) minimization
8.1 Minimal equipment flow resistance
8.2 Spontaneous breathing assistance

9 Scavenging system
9.1 Control <u>pressure</u> in the scavenging system manifold with a pressure control device
9.2 Isolation of pressure or vacuum buildup in the scavenging system manifold from the breathing circuit and the patient
9.3 Scavenging system should not require any operator input
9.4 Scavenging system should only spill gases into OR as a last resort
9.5 Scavenging system operation should be unaffected by fluctuations in central hospital vacuum

10 User psychology
10.1 Retention of familiar features
10.2 Project the perception that the system is safe and simple in design and to use

A detailed listing of the design objectives follows. Whenever specific official standards or recommendations exist, they have been used and acknowledged as a reference next to the quantitative design objective. In the absence of a formal reference in the listing below, no established recommendations were available and the quantitative design specifications are the result of the author's assessment from technical discussions with clinicians.

1 Life support capability: Above any other considerations, an anesthesia machine is a life-support system. More critical incidents in anesthesia are related to the life support component (e.g., airway disconnects during mechanical ventilation, ventilator malfunction, esophageal intubation, accidental extubation, loss of gas supply: 260 out of 507 reported critical incidents) compared to the anesthesia delivery component (e.g., vaporizer malfunction: 20 out of 507 reported critical incidents) (Cooper, Newbower & Kitz 1984).

   1.1 Guaranteed minimum FiO_2 of 21%

   1.2 Precise control of FiO_2 ($\pm$2% absolute SSE, 5% absolute US, jitter 1%)

   1.3 Fast control of FiO_2 (30 s RT, 45 s ST to a step change)

      1.3.1 Small circuit volume for small ST (time constant = volume/inflow rate)

      1.3.2 O_2 flush capability to rapidly change the FiO_2 to 1.0

   1.4 Automated mechanical ventilation capability

      1.4.1 Automatically ventilate the complete range of patient sizes from a neonate to an obese adult: 3 - 400 lbs body weight, 0.01 - 0.1 l/cm H_2O compliance and 1.5 - 19.2 cm H_2O/l/s airway resistance.

VT (ml)	RR (/min)	PIP (cm H_2O)	I:E_{max}
1000-1500	5-10	40	1:3
400-999	6-20	60	1:3
150-399	10-40	40	1:4
15-149	20-60	40	1:4
1-14	60-800	10	1:6

1.4.2 Deliver constant minute ventilation against PIPs from 20 to 100 cm H_2O

  1.4.2.1 Feedback control of inspiratory flowrate into patient

  1.4.2.1.1 Accuracy of flowrate sensor independent of gas composition

  1.4.2.1.2 Accuracy of flowrate sensor of ± 20 ml/s

  1.4.2.2 Eliminate, reduce or take into account loss of tidal volume due to circuit compliance

1.4.3 Automatic limitation of airway pressure to user-adjusted level (10-100 cm H_2O in steps of 5 cm H_2O)

1.4.4 Inherent limitation of the PIP to a default value of 20 cm H_2O (e.g., make it physically impossible to accidentally generate pressures that can rupture a human lung, for example, in the unfortunate event that a scavenging line gets accidentally kinked or plugged, by limiting the absolute pressures in the system to an absolute minimum)

1.4.5 Inspiratory pause capability to improve the distribution of ventilation for patients with unequal lung time constants (different compliances (C) and airway resistances (R) where the product of R and C is the time constant, $\tau = RC$)

1.4.6 Inspiratory waveform shaping for minimizing maldistribution of ventilation

1.4.7 Airway disconnection alarm

1.4.8 Automatic abortion of mechanical inspiration in the event of an O_2 flush

1.4.9 VT delivery must not be affected (increased or decreased) by FGF or T_i

1.4.10 The ventilator must not need compressed gases for its own operation. Loss of gas supply will render the ventilator useless even if electrical power is available

1.5 Capability of oxygen delivery to patient without electrical power or backup power supply (e.g, ball-in-tube O_2 flowmeter and manual resuscitator bag)

1.6 PEEP capability (2-30 cm H_2O in steps of 2 with a 1 cm H_2O accuracy)

1.6.1 It should not be possible to insert the PEEP valve backwards such that the patient is breathing against a closed valve (e.g., a bi-directional PEEP valve that works equally well with gas flowing through it in either direction).

1.7 Flexibility, i.e., capability to operate in open, semi-open, semi-closed and high-frequency ventilation modes on top of closed-circuit mode. There is a reluctance of the market to purchase an anesthesia delivery system that will operate in only one mode, especially if it is a closed circuit (e.g., the Physioflex system).

1.8 Capability to ventilate with room air in case of total loss of gas supplies (central and back-up). This simultaneous occurrence of two failures can happen as reported by Good, Blaschke and Lampotang (1992).

2 Anesthesia delivery capability

2.1 Precise and fast control of end-tidal concentration for volatile anesthetics

Agent	Target	RT (s)	OS (%)	ST (s)	SSE (%)	Jitter (%)
Isoflurane	1.0	15	1.5	30	0.25	±0.1
Enflurane	2.0	15	2.0	30	0.5	±0.2
Halothane	1.0	15	1.0	30	0.25	±0.1
Desflurane	6.0	15	2.0	30	1.0	±0.4

2.1.1 Fast, multi-agent capable, volatile anesthetic analyzer for real-time control (≤ 500 ms response time, 0.1% resolution)

2.2 "Overpressure" induction capability

RC = rate of climb of inspired anesthetic concentration (%/s)

RE = ramp error (%)

Agent	Target (%)	RC (%/s)	S.T. (s)	OS (%)	RE (%)
Isoflurane	2.5	0.0833	30	1	0.75
Enflurane	3.5	0.1167	30	2	1.25
Halothane	2.0	0.0667	30	1	0.75
Desflurane	6.0	0.2	30	3	2.0

2.2.1 Rate of anesthetic delivery independent of metabolic O_2 consumption or gas inflow rate (e.g., FGF) into anesthesia circuit

2.3 Ability to deliver different carrier/anesthetic gases: O_2, N_2O, He, Xe (impacts flowrate measurement methods)

2.3.1 Ability to monitor O_2, N_2O, He and Xe concentration

2.4 Precise N_2O concentration control (70% target concentration, 10% overshoot, 2% SSE, jitter 1%)

2.5 Fast N_2O control (30 s RT, 45 s ST)

2.6 Ability to provide feedback control of anesthetic ET concentration

2.7 Automated closed-circuit anesthesia delivery without constant user supervision

2.7.1 CO_2 removal capability

2.7.2 Automatically maintain a constant circuit volume to compensate for consumption, small leaks and non-returned sampled gases

2.7.2.1 If O_2 inflow into circuit to maintain circuit volume is 25% above metabolic rate for body weight and normal body temperature, raise an alarm flag (malignant hyperthermia or leak)

2.7.3 Efficient use of the volatile anesthetics

2.7.4 Purging capability to remove N_2, CO and CH_4 accumulated during closed circuit operation (maximum allowable N_2 concentration 5% so that FiO_2 or N_2O concentration does not decrease significantly because of the presence of N_2; maximum CO concentration 0.003% because of the high affinity of CO for blood hemoglobin (Strauß et al. 1991); maximum CH_4 concentration 2% because lower limit of flammability is 6.5% with O_2 and 4% with N_2O (Macintosh, Mushin & Epstein 1963))

2.7.5 Purging capability to remove N_2O from circuit when a reduction in N_2O concentration is required

2.7.6 Remove volatile anesthetics quickly from the circuit for fast emergence

2.7.6.1 Ability to cut a charcoal canister into the breathing circuit

2.7.6.1.1 Ability to cut CO_2 absorber out of the circuit with charcoal canister cut in. Deliberate hyperventilation thus removes anesthetic without excessively dropping $ETCO_2$

2.7.6.1.2 Addition of CO_2 to the circuit. If the patient was already hyperventilated or has a low CO_2 production, then simply removing the CO_2

absorber out of the circuit may not raise the CO_2 level to the desired level within a given time.

2.7.6.2 Purging capability to reduce volatile anesthetic quickly in case of charcoal canister failure

2.8 Ability to deliver desflurane, with its high vapor pressure at room temperature, efficiently

2.8.1 Ability to monitor desflurane concentration

2.9 Ability to deliver xenon gas efficiently

2.9.1 Ability to monitor xenon concentration

2.10 Monitorability (facilitated by electronic operation). For safety reasons, and in accordance with proposed European standards, transducers used for control purposes must not be the same as those used for front-end monitoring purposes

3 OR personnel safety

3.1 Reduced anesthetic emissions into the OR environment (meet or exceed NIOSH standards: < 30 ppm N_2O on average, < 0.5 ppm halothane, enflurane, isoflurane or desflurane (NIOSH 1975))

3.2 No explosion hazard

3.3 Low acoustic noise emission ($\leq$ 55 dB (A), background "white noise" level, at 3 m from front of system)

3.3.1 Low acoustical energy emission, e.g., ultrasound

3.4 Electromagnetic radiation (X-ray, alpha, beta and gamma radiation, microwave, infrared, ultraviolet) to meet relevant standards

4 CO_2 rebreathing control

4.1 Minimal equipment deadspace wherever bidirectional gas flow occurs like at the ETT or face mask

4.2 CO_2 absorption capability to handle CO_2 production rates as high as 600 ml/min (malignant hyperthermia scenario where the human metabolism goes into overdrive as a reaction to volatile anesthetics)

4.3 Maintain unidirectional gas flow (e.g., with check valves or forced recirculation)

4.3.1 Maintain unidirectional flow without check valves because they can get stuck open or closed when wet and can also impose additional WOB on the spontaneously breathing patient

5 Human error prevention

5.1 Slip (correct intention, wrong execution (Gaba 1989)) prevention

5.1.1 Pin indexed cylinder yokes

5.1.2 Diameter indexed safety system to prevent connection of wrong gas supply hose to anesthesia delivery system inlet

5.2 Mistake prevention (wrong action resulting from incorrect training or poor judgement (Gaba 1989))

5.2.1 Minimum guaranteed FiO_2 (21%)

5.2.1.1 Cessation of non-oxygen gas delivery in the absence of oxygen supply and triggering of alarms

5.2.2 Pipeline supply override of cylinder backup supply so that pipeline gas is preferentially used if cylinder is not closed after pre-use check

5.2.2.1 Cylinder gas supplies cut in via electropneumatic valves controlled by back-lit switches on front panel increase monitorability (e.g, if the cylinders are left on after the pre-use check, the user is warned that the cylinder supply is being depleted. Also enables the possibility of partially automating the pre-use check of the cylinder pressure.

5.3 Ease and speed of clinical pre-use check

6 Humidity control

6.1 Maintenance of specific humidity of inspired gases at optimum level (optimum 32 mg H_2O/l carrier gas at 32°C (Kleemann 1989))

6.1.1 If water vapor is added to the circuit to obtain the desired specific humidity of the inspired gases, the added water must be maintained sterile.

6.1.2 If only the exhaled moisture from the patient is used to humidify the inspired gases, then sterility of the water is not a concern.

6.2 If recirculation or recompression of the circuit gases is used, the maximum pressure that the recirculating gas ever attains at 32°C must not exceed 2 psig (approx. 140 cm H_2O) to prevent rainout of the exhaled moisture and subsequent decrease of the specific humidity below the optimum

7 Temperature control

7.1 Inspired gas temperature is kept at an optimum of 32°C (Kleemann 1989)

7.2 Temperature of gas delivered to patient adjustable to facilitate warming or cooling of patient (e.g. in case of malignant hyperthermia)

8 Spontaneous work of breathing (WOB) minimization

8.1 Minimal equipment flow resistance

8.2 Spontaneous breathing assistance

8.2.1 Sampling of airway pressure at distal tip of ETT

9 Scavenging system

9.1 Control pressure in the scavenging system manifold directly using for example a back pressure regulator (Tescom 1989). Do not use a needle valve which is inherently a flowrate control device rather than a pressure control device because the needle valve approach assumes that the central hospital vacuum level is constant. In reality, the central vacuum level fluctuates because of varying user loads and poorly fitted, leaking connections which overload the scavenging system

9.2 Isolation of pressure or vacuum buildup in the scavenging system from the breathing circuit and the patient (ANSI 1982)

9.2.1 Electronically-controlled combined pressure/vacuum relief valve opens if scavenging manifold pressure diverges from ambient by more than 10 cm H_2O

9.2.1.1 Differential pressure transducer to monitor scavenging manifold pressure and refer it to ambient independent of altitude or ambient pressure

9.3 Scavenging system should not require operator input. Experience with existing designs which require user adjustments show that they are rarely adjusted and therefore rarely properly set. The pressure in the scavenging manifold should always be controlled at ambient pressure thus effectively providing the same outlet conditions to the anesthesia circuit as if there were no scavenging system present

9.4 Scavenging system should only spill gases into, or draw gas from the OR, as a last resort

9.4.1 Ability to accept expected peak flowrates of 60 l/min for 15 seconds without spilling gas into OR environment (O_2 flush in progress)

9.4.2 Operator must be warned when the relief valve opens the scavenging manifold to the OR environment, i.e., gas is being spilled into or sucked from the OR. In current designs, overloading or incorrect setting of the scavenger system results in insidious spillage of anesthetic gases of which the anesthesiologist is totally unaware

9.5 Operation of scavenging system should not be affected by fluctuations in central hospital vacuum

9.5.1 Regulation of pressure in scavenging manifold rather than flowrate by using pressure control devices rather than flowrate devices (like needle valves) for pressure control

10 User psychology

10.1 Retention of familiar feel and features for user acceptance, e.g., circle breathing circuit hoses, Y-piece gas analysis algorithms, breathing bag, APL valve, O_2 flush. A good example is fly-by-wire airplanes where the designers included dashpots and springs on the electronic joystick to reproduce the familiar feel of conventional joysticks in airplanes where the control surfaces are hydraulically controlled.

10.1.1 Changes in the internal mechanisms of a new design do not need to be transparent to the user who is usually aware of the user interface only, which should be made as familiar and reassuring as possible. For example, the change in the function of the O_2 flush pushbutton from actually triggering an O_2 flush to generating a request for an O_2 flush (design solution 1.1.1.1.1a)

10.2 Project a perception that the system is safe because it is simple in concept and simple to use, e.g., a single switch to change between ventilation modes

10.2.1 Project a perception of safety by catering to the perception of the user. For example, it has been stated that anesthesiologists perceive high FGF rates to provide a higher margin of safety (Cohen et al. 1974, 338) while there is no margin for error in closed circuit anesthesia. Thus, an emphasis on the high effective recirculation flowrate of gas around the circuit which is in many ways equivalent to the FGF may assuage some of the possible concerns of potential users about closed circuit anesthesia. The possibility of using modes other than closed-circuit ventilation (flexibility; design objective 1.7), unlike the Physioflex system, should also reassure the user because there are other modes to choose as backups.

4.2.3 Design Options

1 Single switch to change ventilation mode (e.g., spontaneous to mechanical ventilation) compared to existing designs where the anesthesiologist has to perform as much as three separate actions when switching from mechanical to manual ventilation

2 Manual ventilation and tactile evaluation of lung clinical characteristics through the bag possible during spontaneous and assisted ventilation or non-inspiratory phase of mechanical ventilation

3 Active control of airway pressure from ETT tip for minimal spontaneous work of breathing (inspiratory and expiratory)

4 If a proportional inspiratory flow control valve is used, then the ratio of the supply pressure to the back pressure (P_s/P_b) needed for choked flow across it should be minimal because of the desirable operating characteristics that VT delivery is independent of PIP together with the need for as low a pressure rise across the recompression or forced recirculation device as possible for minimal water condensation

5 Xenon anesthesia delivery and control during closed circuit anesthesia

6 Automatic disable of a laser microsurgery unit on O_2 flush

7 Ability to cut in reserve gas cylinders from the front control panel without having to leave the patient's side

8 Preoxygenation from an auxiliary O_2 ball-in-tube flowmeter with the outlet connected to a face mask

9 For induction by insufflation, the output from an auxiliary flow-over halothane (least pungent) vaporizer could be combined with the output from the auxiliary ball-in-tube O_2

flowmeter. Due to the small size of their veins, it is hard to insert an intravenous needle to give intravenous premedication to sedate pediatric patients prior to anesthesia. The insufflation technique is especially useful in these situations as it allows sedation without need for intravenous access. However, insufflation is an inherently open anesthesia circuit technique, usually of short duration.

10 Obstructed airway contingency: delivery of 100% O_2 at 50 psig (to overcome flow resistance of cricothyrotomy needle with approximately an i.d. of 2 mm and a length of 10 cm) to patient during cricothyrotomy

11 Ability to preoxygenate with the main anesthesia circuit

12 Cooling of the patient during malignant hyperthermia by cooling the inspired gases. Adult lungs provide approximately 85 m^2 of heat transfer area (West 1974). Cooling of the circuit gases will return dry, cool gases to the patient's respiratory system where they become saturated with moisture. The cooling effect on the patient is provided by the latent heat of vaporization of water which the patient supplies.

13 Shaping of inspiratory flowrate during mechanical ventilation

14 Shaping of inspiratory pressure during mechanical ventilation

15 Automated determination of lung compliance

16 Ability to use insufflation with the main anesthesia circuit (as opposed to the auxiliary circuit), which will require a robust control software and interface.

The preceding design checklist is intended to be comprehensive and results from an extensive literature survey as well as the experience gained in designing, building and testing three different recirculating anesthesia circuit prototypes. Using the checklist to implement an actual design will help to avoid mistakes and prevent relevant parameters like humidity from being overlooked. The checklist can be updated, adapted or trimmed to the desired end-product (e.g., a third world anesthesia delivery system without compressed gases) by deliberately and judiciously disregarding certain design parameters. The design checklist may also help the customer (hospital equipment purchaser or administrator) in methodically evaluating and comparing the technical merits of different anesthesia delivery systems.

Current anesthesia delivery systems do not meet many of the design requirements enumerated in the checklist. For example, the Ohmeda and Dräger line of anesthesia machines which currently comprise almost 100% of the North American market (a) require constant user supervision during closed circuit anesthesia (design objective 2.7), (b) deliver volatile anesthetics inefficiently (design objective 2.7.3), (c) allow insidious augmentation of VT with FGF during mechanical inspiration (Ohmeda 1990) (design objective 1.4.9), (d) generally measure exhaled VT falsely high due to the volume "absorbed" by the breathing circuit compliance (Ohmeda 1990) (design objective 1.4.2.2), (e) allow an O_2 flush during mechanical inspiration with the attendant risk of barotrauma (design objective 1.4.8), (f) cannot mechanically ventilate a patient with room air in the event of total loss of gas supply (design objective 1.8) and (g) their ventilators will not work without a supply of a compressed gases (design objective 1.4.10).

More recent systems like the Physioflex (section 3.2.13) meet the requirements of better efficiency of anesthetic usage and improved retention of humidity. However, the Physioflex does not have an O_2 flush capability (design objective 1.3.2) which is a serious drawback that could adversely affect patient safety. Further, the Physioflex is inflexible and can only be used in closed circuit mode (design objective 1.7). It is impossible to mechanically ventilate the patient with room air in case of total loss of gas supply (design objective 1.8) and the Physioflex does not sample airway pressure at the ETT tip to reduce the spontaneous work of breathing (design objective 8.2.1). The Physioflex depends on the availability of both a gas and a vacuum supply for its ventilator to work properly (the vacuum supply is used to assist spontaneous exhalation).

4.3 Design Path

In this section, the path taken to arrive at the design implemented in chapter 6 is documented. A certain amount of heuristic input is always present in any design exercise and this work is no exception, especially since a complete system is being designed and interactions between components and subsystems are generally not formalized. This section attempts to structure the heuristic component of the design process into an engineering design methodology. Rather than simply describing the proposed solution, the alternatives for implementing each design objective are listed whenever possible and the chosen solution is justified on the basis of the criteria enumerated in the checklist.

4.3.1 Assumptions

Before starting with the design process, the assumptions that will be used to simplify the design process are justified and their limits are specified.

4.3.1.1 Incompressible flow regime

The maximum absolute pressure in the recirculating circuit will be 16.7 psia (2.0 psig), by design and the Mach number of the internal flows will never exceed 0.2 at all possible and clinically realistic ventilation modes and settings in any part of the anesthesia circuit (see appendix B). Consequently, an incompressible flow regime is assumed for the entire anesthesia circuit (Shapiro 1953, 48). The assumption of incompressible flow will start breaking down at Mach numbers greater than 0.2.

4.3.1.2 Perfect gas mixture

A thermally perfect gas obeys the equation of state: $p = \rho RT$ where p is pressure, ρ is the density, R is the gas constant of the particular gas or gas mixture and T is the absolute temperature. The perfect gas assumption is justified if the temperature of the gas is high compared to the critical temperature and pressure is low to moderate. The critical temperatures and pressures for the various gases that are used in anesthesia are listed in table 3.

The expected temperature range of the gas or gas mixture in the anesthesia circuit (298K - 313K) is high compared to the critical temperatures of the gas or constituent gas that will be used except for N_2O, CO_2 and Xe. However, the pressure range at which

the gases will be employed (14.7 - 16.7 psia) is low compared to the critical pressure of N_2O, CO_2 and Xe. Therefore the assumption that the mixture of real gases will behave as a thermally perfect gas is warranted (Shapiro 1953, 41).

Table 3. The critical pressures and temperatures of gases commonly used in anesthesia.

	air	CO_2	He	N_2	N_2O	O_2	Xe
P_{cr} (psia)	546	1,072	33	492	1,053	730	847
T_{cr} (K)	133	304	5.4	126	310	154	290

Source: Hawkins 1978, Chemical Rubber Company 1990

A calorically perfect gas has constant C_p and C_v, the specific heats at constant pressure and volume respectively. Real gases however have specific heats (C_p and C_v) that are dependent on temperature. The assumption of a calorically perfect gas mixture is still valid if the temperature at which the real gases will be used does not vary significantly like in our application where the temperature range will be extremely tight (15 K; from 298 K to 313 K). Therefore, we can assume that the real gases in the anesthesia circuit will behave as a perfect gas, both calorically and thermally (Shapiro 1953, 42).

4.3.1.3 One-dimensional flow

One-dimensional (1-D) flow enables a simplified analysis which leads to rapid calculations for a varied range of practical engineering problems. Three conditions are

required before a 1-D flow analysis can be applied to the anesthesia circuit (Shapiro 1953, 73):

(a) The fractional rate of change of flow area with respect to distance along the anesthesia circuit axis is negligible (dA/A dx ≪ 1).

(b) The radius of curvature of the anesthesia circuit axis is large compared to the diameter of the flow area.

(c) The shapes of the velocity and temperature profiles are approximately unchanged from section to section along the axis of the anesthesia circuit, i.e., the flow is fully-developed

The anesthesia circuit will mainly consist of standard 22 mm i.d., circular cross-section, corrugated, PVC breathing hose. The corrugations are regularly spaced at approximately 3.32 mm peak to peak longitudinally (i.e., along the hose axis) and are 1.8 mm deep radially (peak to trough). The corrugations are small compared to the main flow area of the tube and the breathing hose can therefore reasonably be treated as a uniform cross-section duct, thus satisfying condition (a) for 1-D flow.

The breathing hose is corrugated to prevent accidental kinking of the breathing circuit hose. Consequently, the radius of curvature of the breathing hose axis will be large compared to the diameter of the hose and condition (b) for 1-D flow will also be met. Finally, in a recirculating flow circuit at steady state, the volumetric flowrate will be constant. Because (a) the breathing circuit hose is of approximately constant cross-sectional area, (b) the flow paths are long, and (c) there is no large heat source or sink

in the circuit, the velocity and temperature profiles will remain approximately unchanged thus satisfying the last condition for a 1-D flow analysis.

4.3.2 Initiating the Design Process

Since the design checklist is comprehensive and generic in nature, features of the design to be emphasized or omitted (if any) must first be selected. In our case, the main objective is to improve the efficiency of anesthetic usage while attaining the other basic objectives of an anesthesia delivery system. A first pass is then made through the modified design guidelines and objectives lists.

4.3.2.1 Efficient anesthetic usage

For efficient anesthetic usage, unused anesthetics (i.e., anesthetics not absorbed by the patient) should be recycled and reused, thus reducing both anesthetic cost and emissions. There are two possible approaches to anesthetic recycling: in-circuit, real-time recycling or out-of-circuit, off-line collection and recycling.

4.3.2.1.1 In-circuit anesthetic recycling

In-circuit recycling would necessarily have to be done in real time. The exhaled gases would be recirculated in a closed circuit and gases or vapors would only be added to maintain a desired concentration (inspiratory or end-tidal). The in-circuit approach requires no centralized collection apparatus and has the same benefits (cost savings, humidity and heat conservation, knowledge of O_2 consumption and faster detection of

circuit leaks like an airway disconnection) and drawbacks (requires the anesthesiologist to constantly adjust the gas and vapor inflow rates) as closed circuit anesthesia. However, with existing fast-response multi-gas analyzers, the task of adjusting the gas and vapor inflow rates can be readily automated under feedback control.

4.3.2.1.2 Out-of-circuit anesthetic recycling

In out-of-circuit recycling of volatile anesthetics, the exhaled gases coming out of the scavenging system of an anesthesia delivery system must be collected. Oxygen and nitrous oxide must be removed and the resulting mixture compressed, cooled and shipped in special containers to a central recycling facility. The volatile anesthetics then have to be separated, purified, sterilized, tested, rebottled and shipped back to the user. While out-of-circuit recycling allows existing delivery systems to remain in use without any modification, it requires more steps and handling than the in-circuit approach and questions still remain about its medico-legal implications.

A group of researchers from Germany has recently described a method of recycling the volatile anesthetics coming out of the scavenging system of an anesthesia machine by absorption with charcoal filters (Groß-Alltag, Marx & Friesdorf 1992). When the charcoal filters were heated to 220°C, about 60% of the volatile anesthetics supplied during anesthesia were recovered. The charcoal filters are reusable at least five times. The purity of the recycled enflurane and isoflurane was identical to that initially delivered while the recycled halothane was contaminated with known metabolites. The charcoal filters absorbed more than 95% of the volatile anesthetics passing through at the

standard flowrate and concentration, as long as they were not saturated (Groß-Alltag, Marx & Friesdorf 1992).

In spite of their technical successes, the authors admit that they still have to address the problems of (a) separating different anesthetics collected in the same charcoal filter, (b) the possibility of cross-contamination of patients and (c) legal restrictions. The authors also investigated the efficiency of a hospital-wide system where the volatile anesthetics would be absorbed at the central exhaust of the hospital scavenging system and "found such an approach not adequate" (Groß-Alltag, Marx & Friesdorf 1992). Therefore, in-circuit anesthetic recycling appears to be a simpler proposition given the current state of the technology, at this point in time.

4.3.2.2 Topological configuration of anesthesia circuit
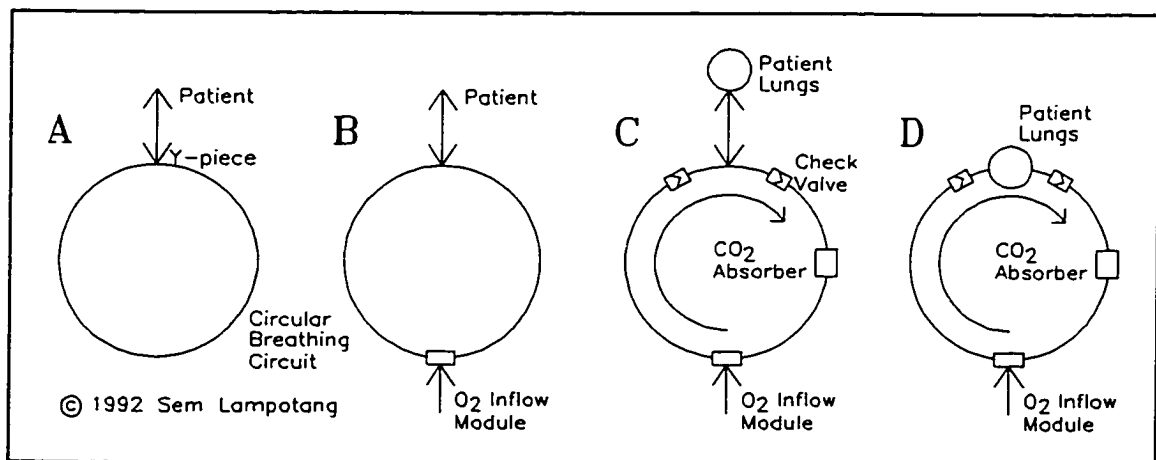
Figure 19. The initial topological design configurations for an anesthesia circuit

If anesthetics are to be recycled within the anesthesia circuit, then the anesthetics have to be recirculated and the circuit configuration has to be "circular" in the topological sense, i.e., a complete loop because the recycled exhaled anesthetics need to be routed back to the patient. A circle forms the simplest loop and is therefore the initial breathing circuit configuration. The circular layout of the existing circle breathing circuit is therefore retained as a familiar feature in a new design (design objective 10.1) (figure 19A).

4.3.2.3 Reduced anesthetics emission

To meet the requirement of reduced anesthetics emissions, the circuit must normally be of a "closed" nature and run in closed-circuit mode except when (1) denitrogenation (preoxygenation) is occurring, (2) "insufflation" is taking place, (3) accumulated N_2, CO (from smokers) or CH_4 (from the intestinal tract) need to be purged, (4) the O_2 flush is used, (5) a drop or rise in inspired concentration of a constituent gas is desired in a shorter time span than the system can achieve while running in closed mode so that the circuit needs to be purged, (6) a temporary disconnection is performed during suctioning of the trachea, (7) there are leaks in the circuit and (8) gases sampled by side-stream gas analyzers are not returned to the circuit. The closed circuit requirement would also have the bonus of conserving humidity and heat within the anesthesia circuit.

4.3.2.4 Metabolic oxygen requirement

As a reminder from section 2.5.1.4, even a truly "closed" anesthesia circuit is not a closed system in the engineering sense because of the minimum inflow rate of metabolic O_2 into the control volume defined by the patient's lungs and the circuit. Therefore, an O_2 inflow module is needed to supply the metabolic O_2 requirement of the patient (figure 19B).

4.3.2.5 CO$_2$ absorption

In a recirculating closed system, CO_2 exhaled by the patient must be removed, if intentional rebreathing of CO_2 is not desired. Thus, a CO_2 absorber is required.

4.3.2.6 Unidirectional gas flow

To prevent CO_2 rebreathing in a closed circuit with a circular topology (i.e., excluding the Waters canister specifically), gas flow around the closed circular circuit must be unidirectional. A pair of low cracking pressure check valves imposes unidirectionality on the gas flow. At this stage we have a normally closed, unidirectional, circular circuit including a CO_2 absorber, two check valves and a gas inflow module connected to a spontaneously breathing patient. This system is sufficient to keep a spontaneously breathing person alive (figure 19C). The system cannot mechanically ventilate or deliver anesthetics yet. However, provision has already been made during the critical initial steps of the design process, that will heavily influence the final design, for reduced anesthetic emissions when anesthetic delivery is implemented.

4.3.2.7 Patient-circuit interface
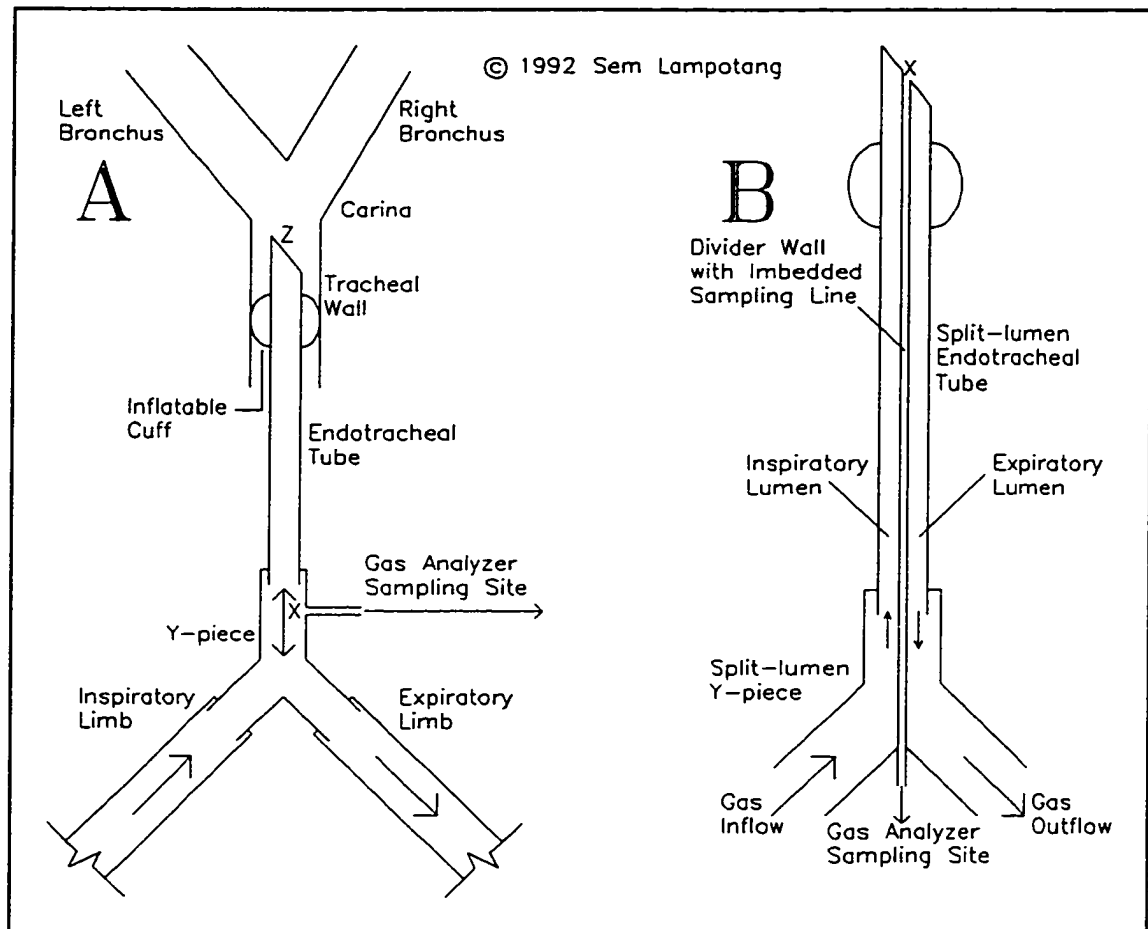
Figure 20. Two possible endotracheal tube (ETT) configurations. A) The conventional ETT; B) The split-lumen ETT

Due to the deadend configuration of the lungs, they cannot be in-line (figure 19D) with the circular breathing circuit and are instead attached as a side connection (figure 19C). The interface can be either a conventional endotracheal tube (ETT, figure 20A) or an ETT with a split lumen (i.e., a divider wall, with an imbedded gas sampling line,

runs down the length of the ETT and flow is unidirectional but in opposite directions in each lumen, see figure 20B).

A conventional ETT has tidal (bi-directional) flow in it and therefore contributes to mechanical deadspace (section 2.3.1) while reducing anatomical deadspace (section 2.3.1) because the mouth, nose and pharynx are bypassed by the ETT. A split lumen ETT eliminates the mechanical deadspace contributed by a conventional ETT because flow in the ETT is no longer tidal but unidirectional. The maximum outside diameter (o.d.) of an ETT is constrained by the internal diameter (i.d.) of the trachea. For a given o.d. and assuming that the inspiratory and expiratory bores are identical, the flow areas are more than halved, creating more flow resistance, i.e., pressure drop during both inspiration and expiration, which is a drawback during spontaneous breathing due to the resulting increase in WOB for the patient.

The ETT configuration also impacts the gas sampling site location. As explained in section 2.2, valuable clinical data ($PaCO_2$, arterial anesthetic concentration) are inferred from end-tidal (ET) gas concentrations that are usually sampled at the ETT-breathing circuit connection (Y-piece for a circle system). The full potential of fast, multi-gas analyzers can only be realized if the sampling site is exposed to both inspiratory and expiratory gases. With a conventional ETT, a convenient and accessible sampling point that meets this criterion is the Y-piece. With a split lumen, the point where the two lumens join, i.e., the distal tip of the ET tube, X, is the only location that is exposed to both inspired and exhaled gas concentrations.

However, if there is forced recirculation of the gases in the circuit, the ET gas values measured at the tip of a split lumen ETT (point X in figure 20B) will be diluted by the recirculating flow, causing artificially low gas concentration measurements. On the other hand, forced recirculation will not dilute the ET values with a conventional ETT if the sampling point is moved from the Y-piece to the ETT distal tip (point Z in figure 20A).

A split-lumen ETT conflicts with forced recirculation as a design option and has the drawback of increased flow resistance. Therefore, a conventional ETT is retained as the interface between the patient and the anesthesia circuit.

4.3.3 Spontaneous Work of Breathing

During spontaneous breathing, inspiratory pressures lower than 8 cm H_2O below ambient pressure, or the set baseline airway pressure level if PEEP (section 2.3.2) is being used, are not recommended (Johannigman et al. 1990). Ideally, the airway pressure should not dip more than 5 cm H_2O below baseline during spontaneous inspiration, with 8 cm H_2O being the absolute limit. A larger dip in airway pressure results in a wider pressure-volume loop for a given spontaneous tidal volume which translates into increased spontaneous WOB for the patient.

The closed nature of the anesthesia circuit will cause the spontaneously breathing patient to generate inspiratory pressures lower than ambient and thus increase the work of breathing (WOB) required to spontaneously draw gases into the lungs.

Five possible solutions for reducing the WOB while keeping the system closed are: (1) an increase in the size of the anesthesia circuit, i.e., the gas volume contained in the anesthesia circuit, (2) an increase in compliance of the anesthesia circuit (see equation 4.2), (3) an increase in the flow areas channelling gas to the patient, (4) a demand flow system that directs recompressed high-pressure ($\geq$ 50 psig requirement for commercially available designs) gas to the patient on the basis of either the inspiratory flowrate at the patient's airway or the dip in airway pressure (2-5 cm H_2O) below a set baseline pressure, e.g., demand valve CPAP systems similar in design to scuba mouthpieces (Banner, Lampotang & Blanch 1992) or (5) a high recirculating flowrate of gas ($\geq$ 25 l/min) past the airway that the patient can divert into his lungs by generating a pressure of about 2-5 cm H_2O below the set baseline pressure, as in continuous flow CPAP systems commonly used in ICU ventilators (Banner, Lampotang & Blanch 1992).

4.3.3.1 Increased circuit volume

An increase in the ratio of the anesthesia circuit volume to the spontaneous tidal volume (V_{circ}/VT) will reduce the maximum pressure drop that the patient's diaphragm (ΔP_{lung}) has to generate and hence the area of the pressure/volume loop representing the WOB required to inhale a given tidal volume into the lungs. The dependence of the spontaneous WOB on breathing circuit size will be analyzed by taking two extreme cases. In both cases, we assume that the circuit is airtight and that the FGF and the PEEP are both zero, for simplicity.

If V_{circ} is 100 m³ (roughly the size of a room) at one extreme, then the drop in pressure in the circuit (ΔP_{circ}) will be negligible as the spontaneous breath of about 700 ml is inspired. Therefore, the respiratory muscles need only generate an intra-pulmonary pressure below ambient (pressure in the circuit will remain approximately ambient because $VT/V_{circ} \ll 1$) that will provide the pressure differential to propel the desired gas flowrate across the ETT and upper airway flow resistances (ΔP_{ett}).

On the other hand, if $VT/V_{circ} = 1$, then the pressure in the circuit will drop markedly as the breath is initiated. The patient's intra-pulmonary pressure will thus have to drop by the same amount as the breathing circuit pressure drop in addition to the drop required to generate the pressure differential across the ETT and upper airways flow resistances that will provide the desired spontaneous inspiratory flowrate. Consequently, spontaneous WOB will decrease with a larger V_{circ}.

However, the circuit volume also influences the time constant of the breathing circuit when inspired gas concentrations need to be changed ($\tau_{washout}$). The washout time constant is a function of the circuit volume and the net inflow rate of fresh gas into the circuit:

$$\tau_{washout} = \frac{V_{circ}}{FGF} \qquad 4.1$$

Consequently, an increase in V_{circ} will cause an undesirable lag in the response time of the system when a change in inspired gas concentrations is desired. Furthermore, space is at a premium in the OR and a bulky breathing circuit would be impractical.

The example above also suggests that if a feedback control loop of airway pressure is implemented such that pressure is maintained at a set reference level (ambient or PEEP) during spontaneous breathing, then the benefit ($\Delta P_{circ} \approx 0$) of a large ($VT/V_{circ} \gg 1$) circuit volume may be attained without the attendant drawbacks.

4.3.3.2 Increased anesthesia circuit compliance

By increasing the ratio V_{circ}/VT, in the previous section, we were increasing what is commonly called in anesthesia circles, the "compliance" of the gas in the circuit. The compliance of the anesthesia circuit itself, C_{circ}, can be increased by addition to the anesthesia circuit of components with large compliance (e.g., a 3 l breathing bag or bellows) or by using materials or designs for the breathing hoses that are compliant (either by being highly elastic or easily deformed or collapsed).

The definition for the compliance of a container (the anesthesia circuit) is:

$$C = \frac{\Delta V}{\Delta P} \qquad\qquad \textbf{4.2}$$

$$C_{circ} = \frac{\Delta V}{\Delta P_{circ}}$$

$$\Delta P_{circ} = \frac{\Delta V}{C_{circ}} \qquad\qquad \textbf{4.3}$$

The above equation predicts that an increase in C_{circ} will reduce ΔP_{circ}, thus reducing the spontaneous WOB.

However, a highly compliant circuit also has drawbacks. Some of the components that increase the compliance of an anesthesia circuit (e.g., bellows and breathing bags) also increase its volume resulting in an undesirable increase in $\tau_{washout}$. A circuit of elastic material and with a design that increases compliance (e.g., concertina-type, "corrugated", breathing hoses or bellows and breathing bags) will absorb significant proportions of the tidal volume intended for the patient during mechanical ventilation of a patient with stiff lungs (high PIPs). The dependence of tidal volume delivery on the various parameters affecting it is described by the equation below for the most general case.

$$VT_{delivered} = VT_{set} + FGF * T_i - ((PIP - PEEP) * (C_{circ} + C_{gas})) \qquad \textbf{4.4}$$

VT_{set} is the set tidal volume that is output by the ventilator outlet port into the anesthesia circuit. $VT_{delivered}$ is the volume of gas that actually reaches the patient's respiratory system. T_i is the inspiratory time. If no PEEP is used, a value of zero is entered for PEEP in the generalized equation. Similarly, if the gas volume is small, then C_{gas} may be neglected. The larger the total compliance of the circuit (sum of the circuit compliance, C_{circ} and the circuit gas compliance, C_{gas}) or the larger the PIP, the larger will be the volume of gas that will be delivered from an open-loop (usually time triggered) mechanical ventilator and yet not ventilate the patient. Consequently, a compliant breathing circuit is not indicated for systems with open-loop ventilation control or systems where a fast $\tau_{washout}$ is required if the increase in circuit compliance is obtained via components that increase V_{circ}.

4.3.3.3 Increased flow areas

The breathing hoses in an anesthesia circuit have circular flow areas of 22 mm internal diameter. The i.d. of an adult ETT is typically 5-9.5 mm and drops down to about 2.5-5.0 mm for a pediatric ETT (Portex 1990). Therefore, the majority of the equipment flow resistance presented to a spontaneously breathing patient comes from the ETT resistance, R_{ett} (Bersten et al. 1989; Bolder et al. 1986; Hatch 1978).

$$\Delta P_{ett} = R_{ett} \cdot \frac{\Delta V}{\Delta t} \qquad \qquad 4.5$$

An increase in the flow area of the ETT will decrease R_{ett} and thus ΔP_{ett}, the pressure difference relative to the pressure in the anesthesia circuit that the patient has to generate across the ETT to inhale an incremental volume ΔV in a time increment Δt. An increase in the flow area of the ETT will thus decrease the WOB because the dip in lung pressure during spontaneous inspiration will be reduced resulting in a smaller pressure - volume loop. However, the flow area of the ETT is physically constrained by the size of the patient's trachea and this design option is therefore not available.

4.3.3.4 Demand flow systems

Demand flow systems can be demand valves or of the positive displacement type. Commercially-available demand valves currently used in life-support systems like ICU ventilators and scuba gear, whether pneumatically or electronically triggered, require a high supply pressure for proper operation ($\geq$ 30 psig). All or part of the recirculating

gases must be recompressed to 30 psig to provide an adequate supply pressure to the

demand valve which increases the partial pressure of water leading to rainout.
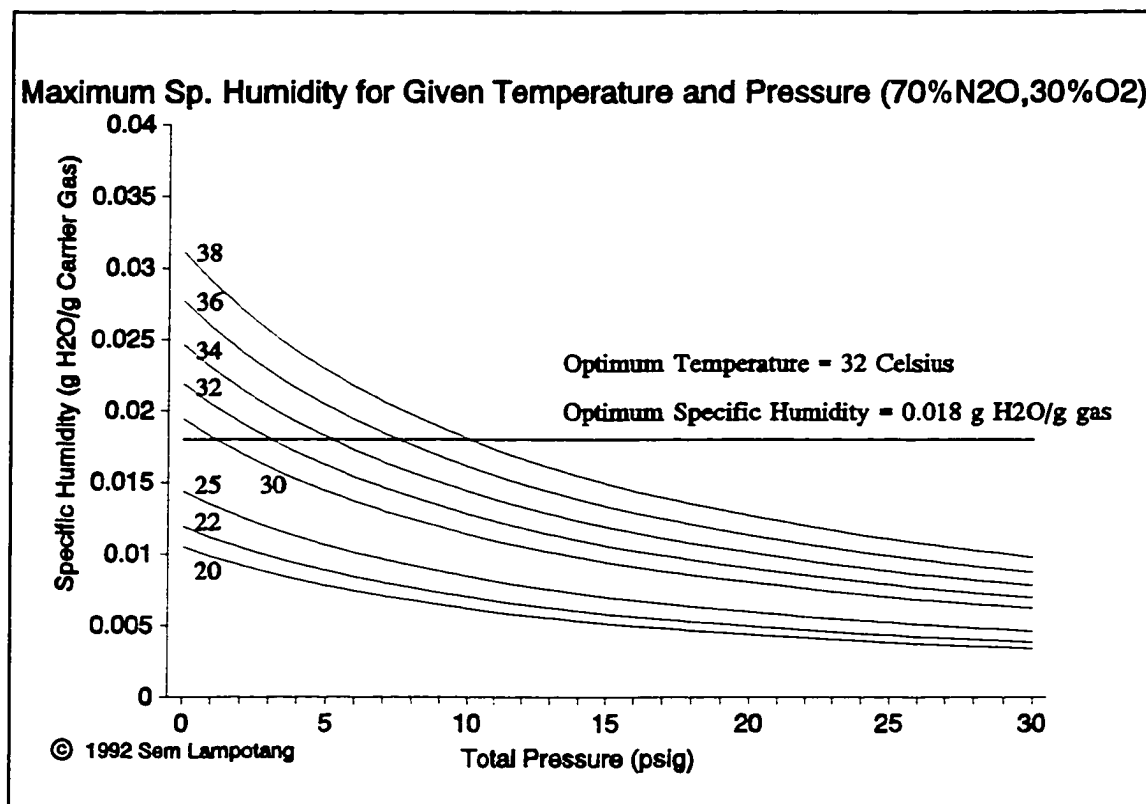
Figure 21. The maximum specific humidity possible for given temperatures and pressures with a gas mixture of 70% N_2O and 30% O_2.

Based on the rainout of humidity experienced during evaluation of the prototype

preceding the GRADS design (section 6.2.5), a program based on the steam tables

(Mayhew & Rogers 1977) was written in Turbo C++ v2.0 (Borland International Inc.,

Scotts Valley, CA) to calculate the maximum specific humidities for a range of total

pressures and temperatures. The results are graphically displayed in figure 21. The

maximum specific humidity possible at 30 psig and 32°C was calculated to be roughly

0.006 g H_2O/g carrier gas (70% N_2O, 30% O_2); this is 3 times lower than the optimum specific humidity of 0.018 g H_2O/g carrier gas at 32°C (Kleemann 1989) (figure 21). Exhaled moisture from the patient will therefore rain out (condensation) on the discharge side of the gas compression device used to recompress the gas back to at least 30 psig. Thus, current commercially-available demand valves are not indicated as a design solution because the advantage of humidity conservation during closed circuit anesthesia is lost. Although the humidity lost from rainout during the compression process could be added back with the help of humidifiers, the design philosophy here is to try to prevent the problem of moisture rainout from occurring in the first place by using lower pressures (< 2 psig; see figure 21) rather than addressing the problem caused by the rainout. The unreliable and poor performance of current humidifier designs and the risk of introducing complications (like stuck valve leaflets) when using existing humidifiers (section 2.5.6) also speaks in favor of the approach of preventing the rainout in the first place.

4.3.3.5 Positive displacement demand systems

A positive displacement demand system has a pneumatically or mechanically actuated, airtight, moving surface(s) that is a part of the control volume boundary of the closed system just like the patient's lungs also form part of the boundary. When a positive displacement demand system is triggered, the moving surface undergoes an excursion that shifts gas volume from the breathing circuit to the patient's lungs in response to the patient's spontaneous breathing demand. The concertina bellows

commonly used in anesthesia machines meets the airtight, moving surface requirements but its large compliance is undesirable because it diverts ("steals") a significant amount of the tidal volume intended for the patient, especially during mechanical ventilation at high PIPs.

An implementation with lower compliance consists of a thin, flat, stiff and circular metal diaphragm with a concentric band of elastic material attached to its edge. The elastic material maintains the airtightness of the system while allowing a limited axial excursion of the diaphragm, e.g., the Physioflex diaphragm (Physio Medical Systems 1990; section 3.2.13). Another variation of the airtight moving surface is the "rolling seal" piston to prevent blow-by past the piston rings (Erdmann, Prakash & Schepp 1984; Schepp et al. 1985). The rolling seal is used in the prototype Narcocon system from Mijnhardt-Hellige of the Netherlands (Erdmann, Veeger & Verkaaik 1989). Conceptually, the rolling seal piston is simply the metal diaphragm in the Physioflex replaced by a piston with a wider concentric band of elastic material to accommodate the longer travel of the piston.

Unlike demand valves, positive displacement demand systems only generate as much pressure rise as is required to drive gas into the patient's lungs. Humidity rainout due to pressure rise is minimal and exhaled moisture is therefore conserved. However, a compromise has to be struck between the amount of travel and the compliance of the moving surface which both depend on the width of the concentric elastic band.

In the Physioflex system, compliance is kept at a low level by reducing the width of the concentric elastic band and therefore the travel. Consequently, to meet the volume

excursion required for an adult patient, four identical metal diaphragms need to be installed in parallel in the Physioflex system adding to system complexity and the need for numerous additional valves. Only one diaphragm is used with a neonate while two and four diaphragms are used with a pediatric and adult patient respectively (figure 18).

An apparent alternative to 4 diaphragms is to use a single diaphragm with the same travel but with twice the diameter such that its area is the same as the total area of the 4 diaphragms. However, the motion of the metal diaphragms is also transduced capacitively in the Physioflex system to measure exhaled volume and the volume measurement resolution would therefore be degraded by a factor of four.

The metal diaphragm positive displacement demand system is a viable solution to reduction of spontaneous WOB in a closed circuit as demonstrated by the Physioflex system. However, a simpler design solution capable of ventilating patients of all sizes would be an improvement.

4.3.3.6 High flowrate systems

In the ICU, a high flowrate of gas ($\geq$ 25 l/min) past the Y-piece, ideally meeting or exceeding the expected peak spontaneous inspiratory flowrate of the patient, is commonly used in open (non-rebreathing), continuous flow CPAP (continuous positive airway pressure) circuits as a means of reducing spontaneous WOB (Banner, Lampotang & Blanch 1992). The net gas consumption rate of these high-flowrate, open circuits is large ($\geq$ 25 l/min) but affordable since the gas is usually O_2 which is inexpensive. In a closed system, this large constant flowrate past the Y-piece can be obtained by forced

recirculation within the circuit which influences the gas sampling site. To prevent dilution of the ET gas samples by the recirculating gas flow, the sampling location must be moved from the Y-piece to the ETT tip.

4.3.4 Forced Recirculation

A recirculating device will mix the gases, thus providing more homogeneous gas composition within the circuit. Furthermore, a recirculator provides the pressure head necessary to overcome pressure losses in the breathing circuit so that the pressure drop across a breathing circuit component due to its flow resistance becomes a less critical design parameter, providing more freedom of choice to the designer. For example, the pore size or length of a bacterial filter can be made as small or large as it needs to be without too much concern about the effect on the flow resistance of the filter. Finally, a recirculating device also acts as a valve by imposing unidirectional flow in the circular circuit, thus making check valves unnecessary. Check valves impose additional work of spontaneous breathing on a patient, add a little PEEP on expiration and may also become stuck open or closed; thus the ability to obtain unidirectional flow without check valves is a design bonus.

Ideally, the recirculating device should generate sufficient pressure rise to meet the specified PIP capability (100 cm H_2O) while minimizing rainout of exhaled moisture by keeping the absolute pressure rise to a minimum. Another critical parameter of the recirculator from the point of view of patient safety is the shut-off pressure. The shut-off pressure is the maximum outlet pressure achievable, for a given rotational speed and gas

composition, when the recirculator is delivering into a closed ended vessel (the lungs in this case), i.e., when there is no flow at the outlet (hence the term "shut-off") (Lapina 1982).

In other words, if by accident, the patient's lungs are directly connected to the outlet of the recirculator in such a way that gas cannot escape and the pressure cannot be relieved, pressure will keep on building in the lungs until the shut-off pressure is reached. Once the shut-off pressure is attained, the pressure cannot rise further and no more gas will flow into the lungs (shut-off condition). This operating characteristic can be exploited into an inherent safety feature by choosing or designing a recirculator such that the shut-off pressure is below the level at which a normal lung will rupture (60 cm H_2O).

Forced recirculation can be accomplished by a fan (output pressure $\leq$ 1 psig), blower (output $\leq$ 40 psig) or compressor (output > 40 psig) (White 1979).

4.3.4.1 Positive displacement compressors

All positive displacement compressors (e.g., reciprocating piston and diaphragm) have pulsatile outputs because of the repeated sequence in which the cavity volume aspirates, traps and squeezes the gas. Large plenums are therefore required to smooth the pressure pulsations and prevent their transmission to the patient's airway, although it could be argued that the pulsations could be advantageously used as form of high frequency ventilation superimposed on conventional ventilation. More importantly, however, the pressure pulsations will cause havoc with any flowmetering device like

electronic flow control valves whose proper operation depends on a constant supply pressure. Large plenums increase the circuit volume, V_{circ} and therefore the circuit washout time constant and are undesirable.

Reciprocating piston compressors also suffer from blow-by past the piston rings which over time accumulates to significant gas and anesthetic losses. Condensation of the exhaled moisture will occur inside the piston; the liquid water may interfere with the operation of the inlet and outlet valves and may even blow-by the piston rings and cause further problems due to water ingress into the sump.

Furthermore, reciprocating piston compressors usually need lubrication which is not acceptable for use with 100% O_2. The lubrication problem can be overcome by using Teflon rings. Non-lubricated carbon rings are not as indicated since the carbon rings wear out and the carbon dust may be deposited into the patient's lungs.

Diaphragm pumps on the other hand do not suffer from blow-by, do not need lubrication and are also less noisy. Diaphragm pumps can be designed to deliver small (≤ 2 psig) pressure rises, e.g., aquarium pumps, so that there is reduced rainout of the exhaled moisture. However, the output of a diaphragm compressor will still be pulsatile. Furthermore, being a positive displacement machine, the shut-off pressure of a diaphragm compressor can be in excess of 100 psig (White 1979, figure 11.2), well beyond the pressure that will rupture human lungs. Consequently, positive displacement compressors are not indicated as recirculating devices because of their pulsatile output and high shut-off pressure.

4.3.4.2 Fans
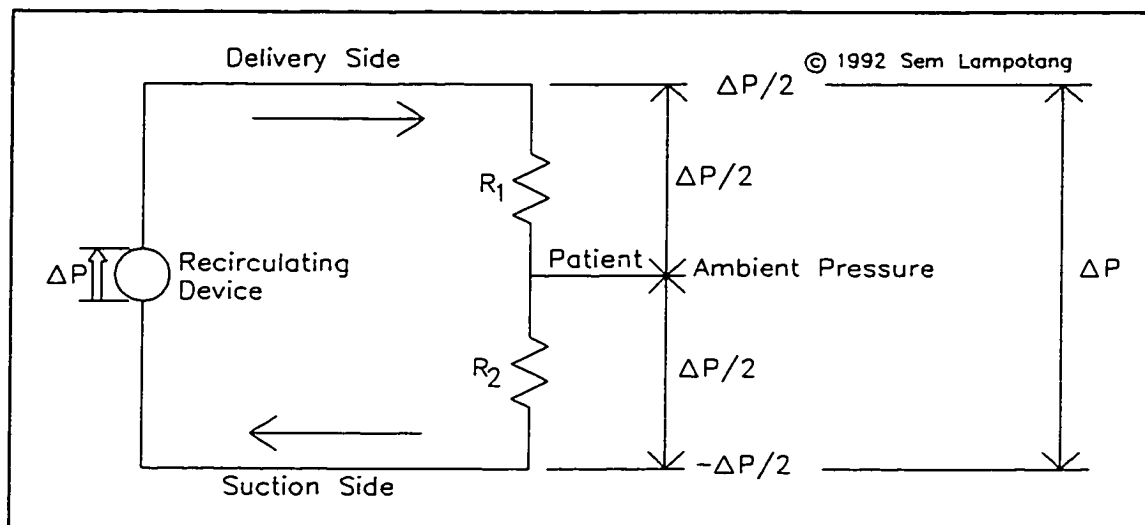
Figure 22. The ideal pressure distribution across a closed circular circuit with a forced recirculation device, at equilibrium

Axial-flow fans typically produce less than 1 psi (70 cm H_2O) of pressure rise from the inlet to the outlet. With specially-constructed ducted fans, it may be possible to increase the pressure rise to up to 2 psi. However, in keeping with the objective of using off the shelf components whenever possible (design guideline 3.2.1.1), we will discuss only common fans. This pressure rise capability is not sufficient to produce PIPs of 100 cm H_2O or even 40 cm H_2O because the closed and circular nature of the breathing circuit requires that the pressure rise across the recirculation device be at least twice the required PIP above atmospheric pressure. In other words, a pressure rise of 60 cm H_2O across a recirculation device in a closed, circular circuit will ideally be distributed such that the outlet pressure is 30 cm H_2O above atmospheric pressure whereas the inlet pressure will be 30 cm H_2O below atmospheric pressure and the

pressure at the Y-piece will be at atmospheric pressure (midway between the inlet and outlet pressure, figure 22). This also implies that, at equilibrium and at the design flow rate, the flow resistances R_1 and R_2 are identical and balanced.

Note that the pressure at the Y-piece will also be a function of the volume of gas in the circuit, i.e., the priming volume. As the priming volume increases for a given circuit size, the pressure head distribution along the recirculating circuit will get shifted up on a distance/pressure curve.

Fans are quiet, have a non-pulsatile output and a low shut-off pressure (< 1 psig) and would be ideal recirculation devices if the pressure rise capability was not marginal.

4.3.4.3 Blowers

Blowers are also sometimes known as radial fans or centrifugal blowers. The output is non-pulsatile and the pressure range can be as high as 40 psig with multistage compression (White 1979). The discharge pressure is a function of the square of the blade tip speed. The shut-off pressure can be designed to be as low as required so that if a shut-off condition occurs with the patient connected to the discharge side of the blower, the patient's lungs will not be ruptured.

Furthermore, due to the physical configuration of the blower (and also the fan), the patient will still be able to breathe through the blower in the event that the blower stops circulating the gases in the circuit because of electrical power failure. The absence of valves in the blower allows gas to move through a stationary blower. On the other hand, a positive displacement compressor, like a reciprocating piston compressor or

diaphragm compressor, will not allow gases to flow through it when it is stopped. Therefore, a centrifugal blower is the preferred choice for the recirculating device.

Only three commonly available and inexpensive recirculating devices were considered as design alternatives. Other non-positive displacement type recirculating devices can be considered if they meet the design criteria described above and as long as they have ducted inlets and outlets or can be easily shrouded.

4.3.5 Relative Positioning

Our evolving system configuration now includes a centrifugal blower. The CO_2 absorber can be placed either on the suction or the delivery side of the blower. The chemical reaction of absorption of CO_2 by the CO_2 absorbent results in a reduction in gaseous volume (section 2.5.4). Therefore, according to Le Chatelier's principle (Petrucci 1989, 584), higher pressures will favor the forward reaction, i.e., CO_2 absorption, which is desirable since smaller volumes of CO_2 absorbent can be used, thus reducing circuit volume. Consequently, the CO_2 absorber is preferably placed on the delivery side of the blower where pressure is higher.

Other considerations in the placement of the CO_2 absorber are the unwelcome possibility of blowing CO_2 absorbent dust into the lungs of the patient and the wear on the rapidly-spinning blower blades (up to 15,000 rpm) from the abrasive CO_2 absorbent dust. Because the gases are being continuously recirculated, once the CO_2 absorbent dust is picked up in the airstream it will eventually get into the patient's lungs. Therefore, a filter is needed to trap the CO_2 absorbent particles and remove them from the

recirculating airstream. The only location where the filter protects both the lungs and the blower blades from CO_2 absorbent dust is between the CO_2 absorber and the patient (figure 23).
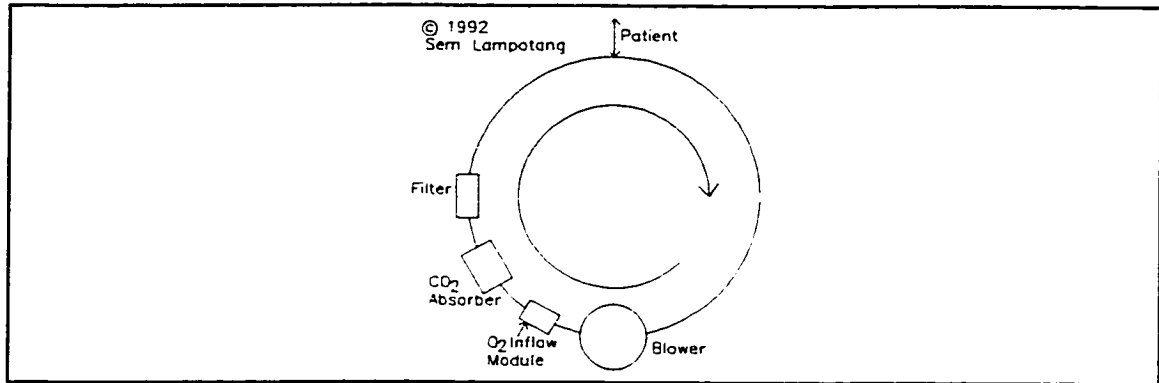
Figure 23. Optimized location for the CO_2 absorber, blower, filter and lungs

4.3.6 CO₂ Absorption

The time of residence of the CO_2-laden gases in the CO_2 absorber is decreased because the gases flow through the absorber faster. However, the gases also make more passes per unit time through the CO_2 absorber because of the circular nature of the design. A simplified analysis indicates that the shortened residence time should be exactly compensated by the increased number of passes.

Let V_{abs} be the volume of the CO_2 absorber, t_{res} the residence time of the recirculating gases in the CO_2 absorber, Q_{recirc} the recirculation flowrate around the circuit, V_{circ} the circuit volume, N the number of passes of the recirculating gases through the CO_2 absorber per unit time and $t_{res, total}$ the total residence time per unit time. The simplified analysis shows that the total residence time per unit time of the recirculating

gases in the CO_2 absorber is independent of Q_{recirc}. This prediction is validated by the experimental results obtained with the Revell circulator where no increase in inspired CO_2 was detected with a forced recirculation flowrate of approximately 60 l/min through a closed, circle breathing circuit (Revell 1959).

$$t_{res} = \frac{V_{abs}}{Q_{recirc}}$$ **4.6**

$$N = \frac{Q_{recirc}}{V_{circ}}$$ **4.7**

$$t_{res\,.\,total} = t_{res} \cdot N = \frac{V_{abs}}{Q_{recirc}} \cdot \frac{Q_{recirc}}{V_{circ}} = \frac{V_{abs}}{V_{circ}}$$ **4.8**

4.3.7 Mechanical Ventilation

The evolving system configuration (figure 23) cannot mechanically ventilate a paralyzed patient (design objective 1.4). Furthermore, although there is a high flowrate of gas at the Y-piece in the circuit configuration depicted in figure 23, the spontaneously breathing patient would have to compete with the suction of the blower to draw part of the recirculating gases into the lungs, due to the closed and circular nature of the circuit. Therefore, a means of shunting a variable proportion of the recirculating gas flow to the patient's lungs would assist in reducing spontaneous WOB. This proportional flow shunting capability would concurrently enable automated mechanical ventilation of the patient's lungs, PEEP delivery by trapping an amount of gas in the lungs at end expiration and shaping of the inspiratory flowrate or pressure during mechanical

ventilation. Another way to look at the proportional flow control valve is to consider it as a means of modifying the pressure distribution across the recirculating circuit and more specifically, the pressure at the tip of the endotracheal tube, i.e., at the patient's lungs.

In present anesthesia delivery systems (including the Physioflex; section 3.2.13), the anesthesia ventilator will not function without a supply of compressed gases (O_2 in the Ohmeda and Dräger line of anesthesia ventilators) and generally consumes O_2 at a faster rate (typically the minute ventilation which for an adult will be about 7 - 10 l/min) than the FGF (typically 3 - 5 l/min).

Consequently, in the event of a loss of central gas supply with electrical power and back-up gas supply (E-cylinder of O_2; 625 l of O_2 when full) available, the clinician is taught to manually ventilate the patient to conserve the limited back-up supply of O_2 and make it last as long as possible while help is on the way (Lampotang et al. 1992b). Thus, during a minor emergency like loss of central gas supply, the design of present systems burdens the user with an additional task, i.e., manual ventilation of the patient.

Therefore, at this point in the design path, we preferably seek a means of mechanically ventilating the patient which requires only electrical power for its proper operation without the need for compressed gases (design objective 1.4.10).

4.3.7.1 Flapper valve
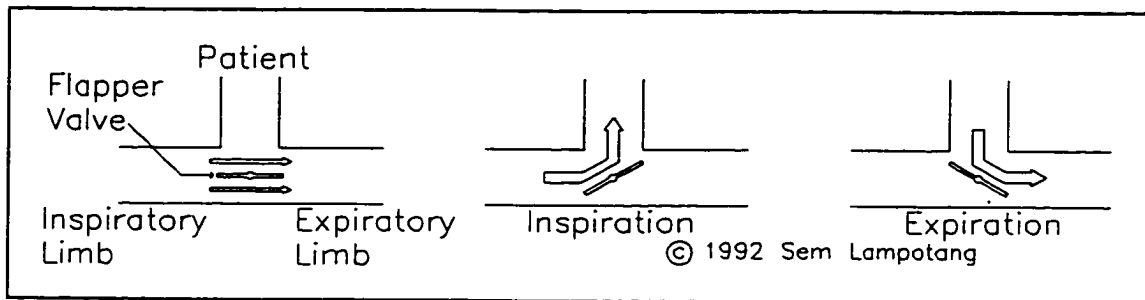
Figure 24. Shunting of gas flow at the T-piece with a flapper valve

A flapper valve at the T-piece that diverts gas flow into or away from the lungs could be the proportional flow shunting device (figure 24). This solution allows the use of a single actuator to control inspiration and expiration, during both spontaneous and mechanical ventilation. However, a stepper motor or proportional actuating device needs to be present on the T-piece. This is not ideal since the weight of the actuator will tend to pull the ETT out of the trachea, increasing the risk of accidental extubation. Although a mechanical structure could be used to support the weight of the actuator, it would also clutter the operating field which is undesirable, especially if the surgeons are working in the vicinity of the head. The breathing circuit also becomes less disposable because the flapper valve has to be built into the circuit. However, remotely actuating the flapper valve, e.g. with a push-pull lightweight cable may eliminate the primary disadvantage of this approach, if the cable does not degrade the frequency response of the actuator.

4.3.7.2 Proportional flow control valve

Another way to shunt the recirculating flow from the breathing circuit into the lungs of the patient is to use a large bore (2.54 cm (1") diameter), low flow resistance (1 cm H_2O pressure drop at 60 l/min air with valve fully open) variable orifice flow control valve as a proportional flow restrictor. The restrictor cannot be upstream of the patient connection to the anesthesia circuit (figure 25A) because there would be no control of the vacuum generated at the patient's lungs when the restrictor is fully closed (predisposes to excessive suction on the lungs) and poor control of the tidal volume delivered to the patient's lungs when the restrictor is opened.
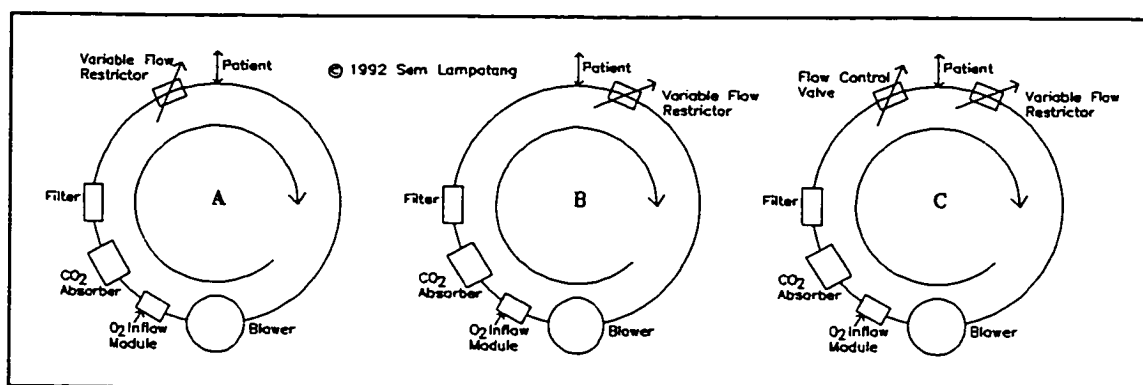
Figure 25. The possible flow shunting configurations. A) Single proportional flow control valve upstream of patient; B) Single proportional flow control valve downstream of patient; C) Dual proportional flow control valves configuration

Therefore, the restrictor is preferentially placed downstream of the patient connection to the circuit (figure 25B). This configuration allows the level of vacuum at the Y-piece to be limited as well as controlling the tidal volume. However, there is no inherent means of assisting exhalation from the patient, i.e., reducing the flowrate

arriving at the Y-piece from the blower outlet so that more gas is suctioned from the lungs thus assisting the exhalation of the patient.

A proportional flow control valve upstream of the T-piece (figure 25C) will permit assistance of spontaneous exhalation. However, a situation where two independent actuators (the flow control valves upstream and downstream of the T-piece) control one variable (pressure at the ETT tip or gas flowrate at the ETT) renders the control algorithm more complicated. A change in the controlled variable resulting from an action of actuator A will cause actuator B to respond to it thus setting up a situation where the two actuators are constantly correcting each other. (A dual proportional flow control valve was actually implemented in the second prototype that used a diaphragm compressor and the two actuators (a high pressure inspiratory proportional flow control valve and a low pressure exhalation proportional flow control valve) were observed to work against each other instead of complementing each other. Lung inflation was erratic and unpredictable with violent oscillations.)

Therefore, the proportional flow shunting should preferably be accomplished with only one actuator. If all the resistance producing components (e.g., filter, CO_2 absorbent, O_2 inflow module) except for the proportional flow control valve, are placed between the blower outlet and the patient Y-piece, their constant flow resistance (R_{BP}) will favor the suctioning of the gases from the lungs whenever the variable resistance is lower than the equilibrium setting (figure 25B). At a given recirculation flowrate, equilibrium occurs when no flow is being forced in or out of the lungs because the flow resistance of the proportional flow control valve is identical to the constant flow

resistance R_{BP} and the pressure at the T-piece is therefore ambient. The equilibrium setting of the variable resistor should correspond to its midrange so that there is an equal amount of adjustment of the flow resistance up or down, to produce flow shunting into and out of the lungs respectively.

The range of flow resistances of the variable resistor should be wide. At the high end, it must be able to completely occlude flow through it by creating an air-tight seal and shunt gas into the lungs and deliver the correct VT against PIPs of up to 100 cm H_2O (present US-made anesthesia ventilators cannot ventilate patients with stiff lungs (Gravenstein & Lampotang 1990)). At the low end, the resistance must be lower than the fixed flow resistance between the blower outlet and the patient so that gas is preferentially suctioned from the patient's lungs.

It should be noted that poorly controlled active suctioning of the gases to assist exhalation can cause collapse of the small airways and atelectasis. Therefore, the controller for assisting exhalation will provide active suctioning with the objective of maintaining ambient pressure at the ETT tip, thus providing to the patient the same effect as if he was not intubated and was exhaling freely into the ambient atmosphere. However, because of the pressure drop across the ETT during exhalation, pressure at the Y-piece will be sub-ambient during active exhalation assistance although the pressure in the lungs themselves will be ambient or slightly above ambient (the controller should be biased to err on the high side to prevent accidental atelectasis). It is anticipated that there will be a need for user education before this approach to assisting exhalation can be accepted in clinical practice. A clinician who is not forewarned, will incorrectly

conclude that airway collapse is occurring if pressure at the Y-piece is sub-ambient even though pressure in the lungs (as inferred from pressure at the ETT tip) will be ambient.

4.3.8 Collapsible Volume on Sub-ambient Suction Side

We now determine the volume of gas that would be required on the suction side of the blower (between the blower inlet and the proportional flow control valve) if the circuit compliance (both on the suction and delivery sides) was zero (infinitely stiff). For the analysis, assume that in addition to the gas mixture being a perfect gas, the conditions are isothermal so that the equation of state (section 4.3.1.2) is transformed into the familiar expression:

$$pv = constant$$
$$p_1 v_1 = p_2 v_2$$

4.9

where p is the absolute pressure and v is the specific volume.

Assume that the proportional flow control valve gives an airtight seal when fully closed and that at the given constant rotational speed the maximum sub-ambient blower inlet pressure is 35 cm H_2O (-0.5 psig; 14.2 psia) at a no-flow condition at the blower inlet. Also assume that when the proportional flow control valve is fully open and for the given priming volume of gas in the circuit, the pressure at the suction side of the blower is ambient (14.7 psia). Therefore, when the proportional flow control valve is completely closed after being fully open, the amount of gas that will be shifted into the patient's lungs from the suction side is going to be a function of the no-flow suction head, p_2 and the volume of gas initially present at the suction side, V_s.

$$p_1v_s = p_2v_2$$

$$\frac{v_2}{v_s} = \frac{p_1}{p_2} = \frac{14.7}{14.2} = 1.0352$$

$$VT = v_2 - v_s = v_s(1.0352 - 1) = 0.0352\ v_s \qquad \textbf{4.10}$$

$$if\ VT = 1000\ ml$$

$$then\ v_s = \frac{1000}{0.0352} = 28,410\ ml$$

Thus, the gas volume required at the suction side for the transfer of a VT of 1,000 ml, assuming an infinitely stiff breathing circuit, is in excess of 25 l since the simplified analysis above was for a PIP of 0 cm H_2O (for convenience of calculation). In practice, a PIP as high as 100 cm H_2O (≈ 1.5 psig) will be used. A volume of 25 l on the suction side conflicts with the guidelines for a small circuit volume to shorten response time for changes in gas concentration (design guideline 1.4.4) and the need to have a compact machine because space is at a premium in the OR (design guideline 4.3.4).

Consequently, since depending on only the "compliance" of the gas on the sub-ambient side of the circuit to provide the tidal volume renders the system too bulky and degrades the washout time constant of the system, the compliance of the anesthesia circuit at the suction side is made more compliant by using a hanging bellows (figure 26). The bellows is weighted so that it will remain seated (bottomed out in its casing that is open to atmospheric pressure) at sub-ambient pressures up to 10 cm H_2O.
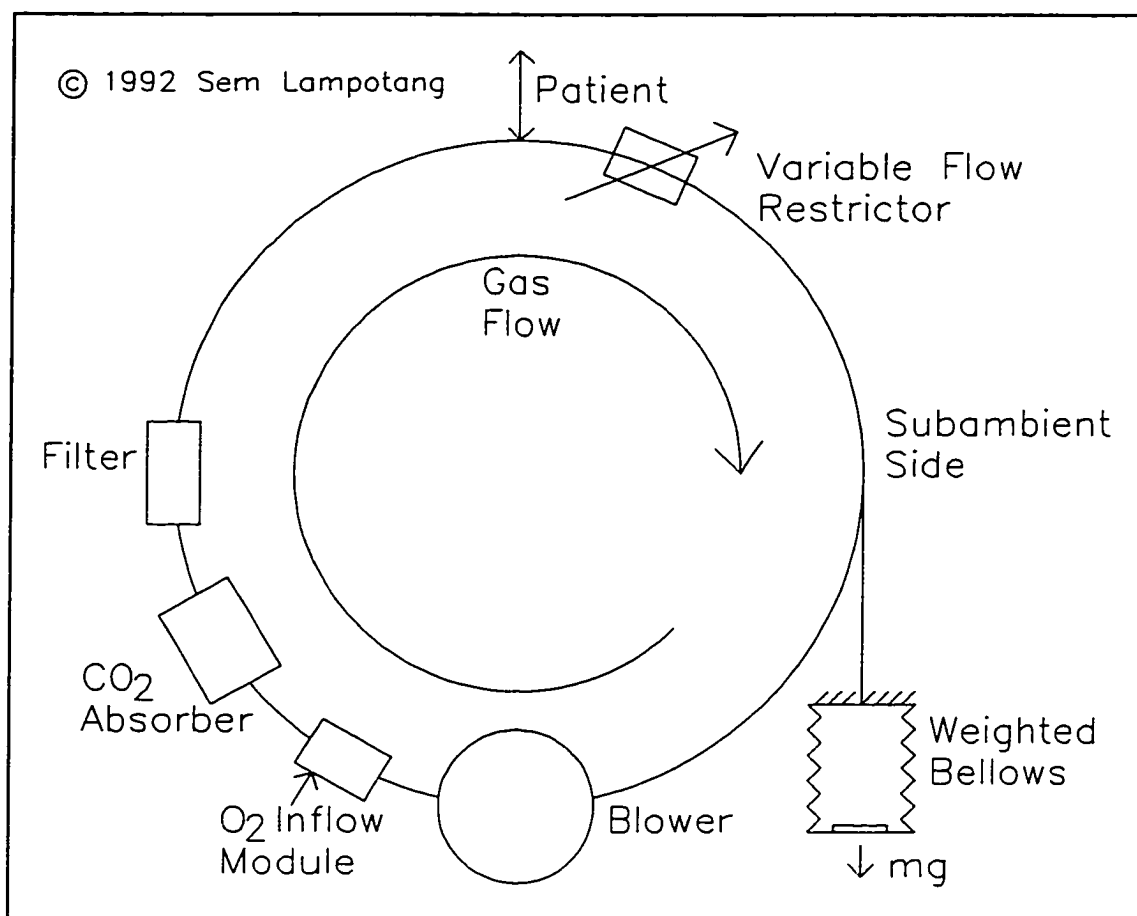
Figure 26. The addition of a weighted bellows to increase the compliance of the suction side of the circuit

4.3.9 Airway Pressure Measurement

A pressure transducer is required to ensure that airway pressure limits are not being exceeded. The pressure transducer should have a range of at least -20 to 100 cm H_2O and a linear voltage output for ease of analog-to-digital (A/D) conversion. Airway pressure is sampled at the ETT distal tip via a pressure sampling lumen embedded in the wall of the ETT so that the flow resistance of the ETT, R_{ett}, does not distort the measurement of lung pressure, as would happen if pressure is sampled at the Y-piece.

4.3.9.1 Airway pressure sampling site

Another pressure transducer functions as the control and feedback sensor for reducing spontaneous WOB (because the control and monitoring transducers should provide independent confirmation of each other; see section 2.5.7). The control pressure transducer also samples airway pressure at the ETT distal tip to reduce the work of spontaneous breathing (design objective 8.2.1).

The flow resistance of ETTs is orders of magnitude higher than that of the breathing circuit (Bersten et al. 1989). Conventionally, the airway pressure is sampled at the CO_2 absorber or the breathing circuit or the Y-piece. The location of the airway pressure sampling site is especially important during spontaneous ventilation. The interposed flow resistance of the ETT causes the pressure at the Y-piece to be higher, and lower, than the actual lung pressure during spontaneous inspiration and expiration respectively. Consequently, pressure sampled at the ETT tip is a more accurate representation of lung pressure.

4.3.9.2 Pressure feedback control of spontaneous breathing

The airway pressure sampling site becomes a significant factor if spontaneous breathing is assisted with the objective of reducing WOB. As the airway pressure dips below a set baseline, indicating spontaneous inspiration, the proportional flow control valve would shunt flow into the lungs to minimize the dip in airway pressure according to a digital proportional-integral-derivative (PID) algorithm set to maintain the airway pressure at a reference level, e.g., ambient or the desired PEEP level. Conversely,

during spontaneous exhalation, gas would be suctioned to minimize the overshoot past the baseline reference pressure, thus reducing the expiratory WOB.

The objective of the PID controller in simple terms is to reproduce the pressure/flowrate conditions at the upper airway for an unintubated healthy person breathing spontaneously; the pressure fluctuations are insignificant because the upper airway is in free and direct communication with the supply of room air. Thus, the PID controller attempts to reproduce normal unintubated spontaneous breathing conditions for an intubated patient by minimizing the flow resistance effects of the ETT.

With an ideal controller, the pressure volume loop would be reduced to a line with zero area and therefore zero WOB. In practice, the PID algorithm is driven by the pressure error signal and the pressure volume loop will not be a line but a narrow loop; the WOB will never be zero but will be lower than if there was no assistance via the PID controller. However, if the feedback pressure signal for the closed loop pressure controller is sampled at the Y-piece, the "airway" pressure signal is distorted by the flow resistance of the ETT and the flowrate of gas through the ETT and a wider pressure-volume loop (implying more WOB) is obtained compared to pressure sampling at the ETT distal tip.

4.3.9.3 Other advantages of ETT distal tip pressure sampling

There are other advantages to sampling pressure at the ETT distal tip. Cases have been reported where a partial disconnection occurred at the connection between the Y-piece and the ETT. The flow resistance at the leak generated a pressure rise at the Y-

piece and in the breathing circuit during mechanical inspiration so that pressure sampled at the breathing circuit or Y-piece cycled as expected and no alarm was raised. On the other hand, pressure sampling at the ETT distal tip will detect a leak between the Y-piece and ETT because pressure will not cycle in the lungs because of the leak. Similarly, a kinked ETT will generate the expected pressure fluctuations at the Y-piece and breathing circuit during mechanical ventilation even though the patient's ventilation is being compromised. Here again, the pressure at the ETT distal tip will not cycle and the kinked ETT condition will be readily detected by an alarm algorithm that looks at expected pressure fluctuations during mechanical ventilation.

By providing a more accurate measurement of the actual lung pressure, the ETT distal tip pressure will allow measurement of true dynamic lung compliance, C_D, by delivery of a calibration flowrate for a given time and monitoring the rise in the actual pressure in the airway to obtain C_D. Pressure sampled at the ETT tip in combination with a flowrate transducer as in figure 27B will confirm proper operation of each other and can also warn of developing incidents like a progressing ETT cuff leak. The flowmeter will measure that the correct tidal volume is being delivered and will also detect the reduced exhaled volume due to the ETT cuff leak. A lower pressure at the ETT distal tip will thus confirm the diagnosis by the flowmeter that an ETT cuff leak is developing, assuming that C_D remains constant.

4.3.9.4 Hazards of ETT distal tip pressure sampling and proposed solutions

There are valid practical concerns about sampling pressure at the ETT tip, namely the danger that the pressure sampling line port at the tip of the ETT might become occluded with secretions or moisture from the patient which would cause the system to behave unpredictably and possibly harm the patient. One of the objectives of the prototype is to establish the benefits of sampling pressure at the ETT distal tip and thus make a compelling case for further research into ways of obtaining those benefits safely.

Three possible solutions that are worth investigating are (a) an intermittent purge flow of gas through the pressure sampling line which is intended to blow away any secretions before they can dry and obstruct the pressure sampling port, (b) hydrophobic materials that could be coated on the tip of the ETT and would repel moisture and secretions which are mostly water-based and (c) a different pressure sampling port configuration with multiple pressure sampling holes connected to the imbedded pressure sampling lumen rather than a single pressure sampling port. Thus, obstruction of one of many sampling holes would not prevent accurate sampling of the pressure at the ETT distal tip. Obviously, the three alternatives could be combined to arrive at a safe pressure sampling configuration.

4.3.10 Flowrate Measurement

Technically, the pressure transducer could also be used as the feedback sensor for mechanical ventilation. Assuming a constant dynamic lung compliance (C_D), the rise in pressure in the lungs (ΔP) could be directly correlated to the volume in the lungs above

FRC (ΔV) by the equation $\Delta P = \Delta V/C_D$. However, in some clinical situations, e.g., open heart surgery, the dynamic compliance of the lungs will change markedly when the surgeon opens the pleural cavity. Furthermore, anesthesiologists are accustomed to using respiratory rate and tidal volume to titrate ventilation. Therefore, to maintain ease of use and familiar concepts, we choose to control the inspiratory flowrate during mechanical ventilation. Consequently, a flowrate transducer that measures the flowrate of gas into the lungs is needed for feedback control of inspiratory flowrate in mechanical ventilation.

Ideally, the accuracy of the flowrate transducer will be independent of gas composition, or only marginally affected across the full range of gas mixtures typically used in anesthesia. Additionally, components like elbows, tees, sharp bends and valves introduce flow disturbances which can affect the accuracy of a flowmeter downstream of them by up to 15%. These flow disturbances disappear if there is a minimum length of straight conduit downstream of the component or if straightening vanes are introduced upstream of the flowmeter to smooth the flow (Doebelin 1990; Fox & McDonald 1978). Ideally, the flowmeter should not require a long upstream straight length of tubing for accurate measurement.

4.3.10.1 Flowrate measurement configuration

The flowrate measurement configuration must be selected first because it is a higher level design decision which will affect the type of flowrate transducer. The desired attributes for the configuration are: (1) primarily, the location must allow measurement of the inspired flowrate for closed loop control of mechanical inspiration,

(2) the volume of gas absorbed by the compliance of the circuit should not be measured as part of the tidal volume received by the patient's lungs, (3) the location should have no or an absolute minimum number of potential leak or disconnection locations between it and the lungs (measure as close to the destination of the gas, i.e., the lungs, as possible) and (4) the location also allows measurement of exhaled volume as a safety measure (if the exhaled volume is smaller than the inspired volume, a leak is present downstream of the flowrate transducer; bidirectional flow measurement capability is required if the flowrate transducer is placed at the ETT).
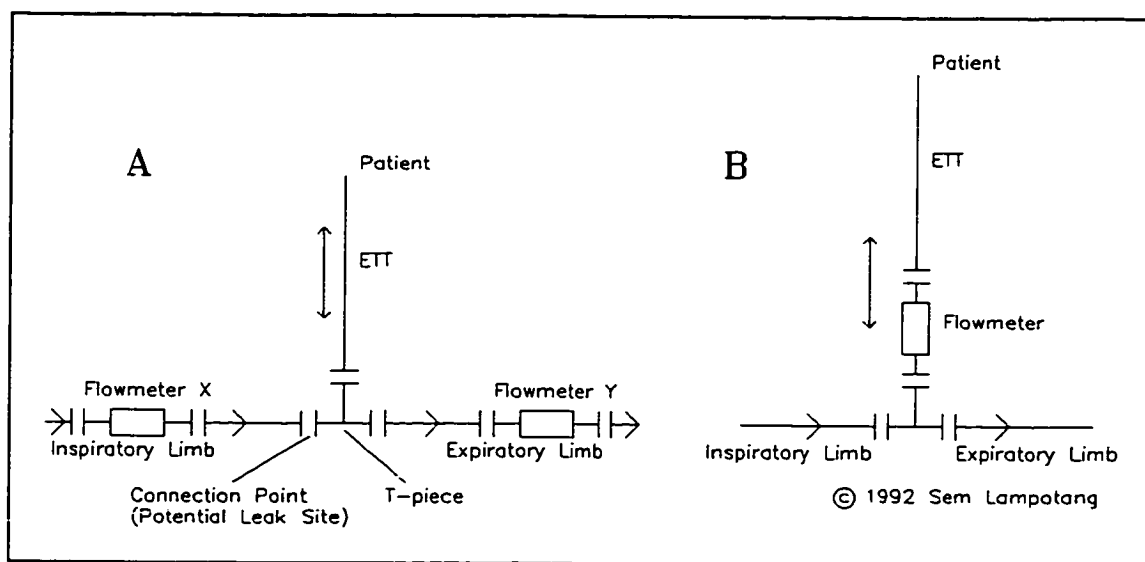
Figure 27. Two possible flowrate measurement configurations. A) Dual flowmeter arrangement; B) Single flowmeter at the endotracheal tube

Two possible configurations for flow measurement, with the proportional flow control valve at the exhalation limb, are shown in figures 27A and 27B. With configuration 27A, the flowrate into or out of the lungs is obtained from the difference between the readings of the X and Y flowmeters. If there is a leak between the 2

flowmeters, the deduced inspiratory flowrate to the patient will be smaller than what the feedback control system measures as being delivered. However, the leak can be detected during the following exhalation because the exhaled volume will be smaller than the apparent inspired volume. The flowmeters used in configuration 27A do not need to have bidirectional flow measurement capability and the configuration allows longer upstream straight conduit sections. A disconnection between the Y-piece and the ETT (a relatively common occurrence (Cooper, Newbower & Kitz 1984)) is easily detected (exhaled volume < delivered volume).

The drawbacks are: (1) the volume "absorbed" by the compliance of that part of the breathing circuit between flowmeters X and Y will be incorrectly included as part of the volume delivered to the patient's lungs, (2) two flowmeters and two data acquisition channels or a subtraction interface circuit and one data acquisition channel are required, (3) more real-time computation may be required to obtain the inspiratory flowrate, (4) the inaccuracy of the measurement is doubled with two flowmeters compared to a single flowmeter configuration, (5) the risk of failure of the flowmetering system is also doubled compared to a single flowmeter configuration and (6) the number of potential disconnection sites is increased compared to a single flowmeter configuration.

Configuration 27B possesses all the desirable attributes listed above. However, a flowmeter with bidirectional flow measurement capability is required if leaks between it and the lungs are to be detected. The compliance of the breathing circuit does not steal a portion of the tidal volume intended for the patient (existing compliant corrugated tubing can be used) because the flow is being measured at the ETT which is a relatively

stiff tube. The drawbacks are: (1) to minimize deadspace, restrictions must be placed on the upstream straight conduit length requirements of the flowmeter (equipment deadspace; section 2.3.1), (2) the flowmeter must have bidirectional flow measurement capability if exhaled volume is to be measured, (3) the flowrate transducer itself must be compact to reduce deadspace and (4) the flowrate transducer must be light so that it does not increase the risk of accidental extubation or kinking of the ETT. Configuration 27B is the preferred choice because it is a simpler, safer and more accurate approach. It will have the drawbacks of requiring cleaning and sterilization of the flowmeter probe between patients and increasing the equipment deadspace by an amount equal to the volume of the flowmeter probe.

An alternative to measuring exhaled volume for leak detection with configuration 27B is to monitor the pressure rise in the lungs in response to inspiratory flowrate. However, this scheme, while removing the need for bidirectional flow measurement capability, is less foolproof than direct measurement of exhaled tidal volume. A sudden increase in compliance of the lungs will cause a lower rise in pressure for the same tidal volume and might trigger a false leak alarm. Or a leaky cuff combined with a kinked ETT and airway pressure measurement at the Y-piece will fool the system into believing that an adequate amount of ventilation is being delivered, because of the apparent pressure rise in the lungs due to the kinked ETT.

4.3.11 Flowrate Transducer Selection Criteria

The conventional method of controlling tidal volume delivery by adjusting inspiratory flowrate to a constant level (for a "square" inspiratory flowrate) or according to a predetermined time-varying flowrate input (for accelerating, decelerating and sinusoidal flowrate waveforms; section 2.3.4) over the inspiratory time determined by the operator-selected respiratory rate and I:E ratio will be used. Thus, the flowmeter will be evaluated with that mode of application in mind.

4.3.11.1 Accuracy

The accuracy requirements for a flowmeter that controls inspiratory flowrate and thus tidal volume are not stringent because, in clinical practice, the anesthesiologist makes a rough estimate of the required tidal volume based on the patient's size, gender and weight. The tidal volume is then manually adjusted by the operator, using the $ETCO_2$ level as an inversely proportional indicator of adequacy of ventilation (typically, the anesthesiologist tries to obtain an $ETCO_2$ value of 35-40 mm Hg).

A flowmeter accuracy of $\pm 10\%$ will therefore contribute an error of $\pm 10\%$ to VT delivery, for a constant ("square") inspiratory flowrate wave shape. Over the range of VTs listed in design objective 1.4.1, 1 - 1500 ml, a $\pm 10\%$ accuracy will cause errors of 150 ml to 0.1 ml. These errors in VT are not clinically significant especially in view of the way in which the anesthesiologist uses the $ETCO_2$ values to evaluate and adjust the minute ventilation.

4.3.11.2 Gas composition

The accuracy of the flowmeter must not be significantly affected by the composition of the gas mixture, because during a typical anesthetic, gas composition varies considerably. These gas mixture density variations will be even more pronounced when gases like xenon (density: 5.85 kg/m^3) and helium (density: 0.1663 kg/m^3) are used. Furthermore, ventilation with anesthetic gases is always dosed on a volumetric basis rather than a mass basis. Because the accuracy of a volumetric flow transducer is insensitive to gas composition, it is the preferred method.

4.3.11.3 Flow steps

The accuracy of the flowmeter should not be affected by abrupt enlargements and constrictions because the i.d. of the ETTs will range from 2.5 to 10 mm.

4.3.11.4 Response time

If the flowmeter has bidirectional flow measurement capability, it must have a frequency response of at least twice the highest harmonic (Nyquist sampling criterion) for a given flowrate shape at fundamental frequencies of up to 150 breaths/min (HFV).

4.3.11.5 Output format

For a computer controlled system, transducers that readily provide an electrical voltage or electrical pulses are preferred for ease of interfacing.

4.3.11.6 Turn-down ratio

The turn-down ratio is the ratio of the upper flowrate limit to the lower flowrate limit of the measurement range where the desired accuracy can be maintained (Stoecker & Stoecker 1989, 87). From the table for the different ranges of ventilatory parameters specified in design objective 1.4.1, the required flowrate measurement range for the flowmeter in configuration 27B is calculated for a constant inspiratory flowrate and assuming a minimum I:E of 1:1. The maximum flowrate, Q_{max}, is calculated from the equation

$$Q_{max} = VT_{max}*(60/RR_{max})/(1+I:E_{max}) \qquad \textbf{4.11}$$

and the minimum flowrate (Q_{min}) is obtained from

$$Q_{min} = VT_{min}*(60/RR_{min})/2 \qquad \textbf{4.12}$$

These 2 equations give the following table:

VT (ml)	RR (/min)	I:E_{max}	Q_{max} (l/s)	Q_{min} (l/s)
1000-1500	5-10	1:3	1.0	0.167
400-999	6-20	1:3	1.33	0.08
150-399	10-40	1:4	1.33	0.05
15-149	20-60	1:4	0.75	0.01
1-14	60-800	1:6	1.4	0.002

The desired turn-down ratio for the flowrate transducer is 1.4/0.002 = 700. This turndown ratio is extremely high and some compromises will have to be made to relax this design requirement. For example, the $\pm 10\%$ accuracy specification will widen the turn-down ratio for most flowrate transducers.

4.3.12 Flowrate Transducer Selection

With the flow measurement configuration already selected, the actual type of the flowrate transducer can now be considered. The characteristics of the orifice plate, venturi, vortex shedder and turbine flowmeters (Stoecker & Stoecker 1989, Cheremisinoff & Cheremisinoff 1988) were compared to the desired application (configuration in figure 27B).

4.3.12.1 Orifice plate

The orifice plate was discarded because of its high pressure loss characteristics, i.e., there is a large pressure drop across it which would make assistance of spontaneous inspiration and expiration mandatory rather than a design option. Also, the orifice plate works better with higher pressures, larger pipe diameters (> 5.08 cm (2")) and requires a straight upstream tubing length of at least 5 diameters (Doebelin 1990, 568) and up to 40 diameters (Fox & McDonald 1978). The straight upstream tubing length requirement becomes a significant design impediment because it would introduce significant equipment deadspace.

4.3.12.2 Venturi

The venturi flowmeter has a lower pressure loss than the orifice plate. However, the venturi meter is a unidirectional measuring device. Furthermore, the venturi meter is an "obstruction" meter just like the orifice plate. Therefore, volumetric flowrate is directly proportional to the square root of the pressure difference between the region

upstream of and the throat of the venturi, and inversely proportional to the square root of the gas mixture density (Holman 1985) over the flow measurement range for which the venturi meter is calibrated. Assuming that the calibration gas mixture is 50% O_2 and 50% N_2O, there will be a 68% overestimation error with a 70% Xe, 30% O_2 gas mixture and a 43% underestimation error with a 70% He, 30% O_2 gas mixture (see appendix C). The magnitude of the errors with these gas mixtures that will be commonly encountered during anesthesia is larger than the 10-15% desired flowrate measurement accuracy. The dependence of obstruction meters on the density of the gas mixture makes them unsuitable for applications where the density varies significantly like in anesthesia.

The argument could be made that if a fast multi-gas analyzer is already available in the system, then the output of the venturi meter could be corrected for the different gas densities so that accurate flow measurement would be achieved independent of the gas mixture density. However, there are two disadvantages to this approach. The flowmeter and gas analyzer will have to be synchronized if they have different response times because the flowrate and the gas composition data must represent samples from the same point in time, especially if the rate of change of flowrate or gas composition is fast. Further, failure or inaccuracies of the multi-gas analyzer will also affect the flowrate transducer. This dependency of one monitor on another is unacceptable in a life support system.

4.3.12.3 Vortex shedding flowmeter

In this fairly recent flowrate measurement method, a blunt object in the middle of a steady flow stream creates downstream vortices that are shed alternately on either side of the object (Stoecker & Stoecker 1989, 87). The volumetric flowrate is proportional to the rate of vortex passage and is independent of gas density or viscosity. The rate of vortex passage is sensed either by a sensitive pressure pickup (e.g., a microphone) downstream of the blunt object or by sensing the force impulses imparted to the blunt object by each vortex over a fixed time interval. The nominal turn-down ratio is 15 (Stoecker & Stoecker 1989, 87; Doebelin 1990, 594)), twice that for an orifice plate or venturi (7) and may be increased to 200, in some cases (Doebelin 1990).

The dimensionless Strouhal number ($St = fD/V$ where f = frequency of vortices (/s), D = diameter of blunt object (m), V = velocity of the fluid (m/s)) is approximately a constant (e.g., 0.21 for a cylinder (White 1979, 278)) independent of gas viscosity and density for internal flows within a fixed range of Reynolds numbers, only. This Reynolds number range where accurate flow measurement can be performed is dependent on the cross-sectional shape of the blunt body. For example, for a circular cross-section, i.e., a cylinder, the range in which vortex shedding occurs is $10^2 < Re < 10^7$ (White 1979, 278) and the portion of that range that can be reliably used for flow measurement is $10^3 < Re < 10^5$ (Stoecker & Stoecker 1989, 88; White 1979, 278). For a trapezoidal cross-section with the longer parallel side facing upstream or a variation of that basic shape, the reliable measurement range is $10^4 < Re < 10^5$ (Cheremisinoff & Cheremisinoff 1988, 283-289; Doebelin 1990, 594).

$$fD/V = St = \text{constant for } 10^4 \leq Re \leq 10^5 \text{ ONLY}$$

$$f = (St/D)V = \text{constant} \cdot V \qquad\qquad \textbf{4.13}$$

$$f \propto V$$

For a trapezoidal blunt body and a Reynolds numbers less than 10,000, the proportionality between volumetric flowrate and vortex frequency and the independence from density and viscosity no longer apply. The flowmeter can still operate, albeit in a non-linear mode, in the flow regime defined by $3,000 \leq Re \leq 10,000$ and is inoperable in the region defined by $Re \leq 3,000$ (Stoecker & Stoecker 1989, 289).

Response time is adequate but velocity dependent, i.e, the vortex frequency responds to changing flowrate within about 1 cycle. Response time is therefore faster at higher flowrates which is desirable. Unlike the ultrasonic flowmeter which is designed mostly for use with liquids, the vortex shedder flowmeter can be used with a wide variety of liquids, gases or steam. Accuracy is high (about 1%) and gas velocities of up to 183 m/s (600 ft/s) can be measured. The meter has no moving parts; reliability, stability and repeatability for control purposes are good and maintenance requirements are minimal.

The vortex shedding flowmeter appears to be an ideal candidate for the application depicted in figure 27B. However, the minimum internal Reynolds numbers for 100% O_2 and the lowest minimum inspiratory flowrate, Q_{min}, must first be calculated to verify if it will exceed 10,000. The calculations are carried out in appendix D. The resulting Reynolds number of 311 is smaller than the minimum requirement of 10,000. Therefore,

the flowmeter readings will be inaccurate during operating conditions that are commonly encountered during anesthesia.

Furthermore, the vortex shedder flowmeter is generally configured as a unidirectional flowrate measurement device. However, the flowmeter could conceptually be converted for bidirectional flow measurement by having a sensitive pressure pickup on either side of the blunt object. Although the vortex flowmeter has many desirable qualities, it fails to meet the design specification for the minimum Reynolds number and cannot be used for configuration 27B. The possibility of reducing the minimum Reynolds number requirement for the vortex shedder flowmeter with new blunt body shapes and converting it for bidirectional flow measurement deserves to be investigated further because of its many inherent qualities that are desirable for flowrate measurement in anesthesia.

4.3.12.4 Turbine flowmeter

In these devices originally developed for critical and precise flowrate measurements in jet, rocket and missile engines, the rate of revolution of the turbine is proportional to the volumetric flowrate of fluid passing by its blades. The turbine meter can measure both liquids and gases, is highly linear (as good as 0.05% in larger sizes (Doebelin 1990, 580)), has a wide linear range (turn-down ratios of 200 (BOC Health Care 1984, 6) are possible), has high repeatability ($\pm$0.02% of reading or better (Cheremisinoff & Cheremisinoff 1988, 302)), is highly accurate ($\pm$0.25% of true flowrate with liquids in the linear measurement range (Cheremisinoff & Cheremisinoff

1988, 302)), has fast response time (typically, 2-3 ms (Cheremisinoff & Cheremisinoff 1988, 302)) and can be used in pulsating flows (Holman 1985, 253).

Standard units have diameters ranging from 1.9 - 7.62 cm (0.75 - 3"). Pressure drop across the meter varies with the square of the volumetric flowrate, Q (Doebelin 1990, 580). For accurate and linear flowrate measurement, the dimensionless constant Q/nD^3 must be a constant where n is the turbine rotor angular velocity, D is the turbine meter bore and ν is the kinematic viscosity. Q/nD^3 is a constant (approximately 2) for the flow regime where $nD^2/\nu > 900$ for a typical turbine meter (Doebelin 1990, 580). Although the upper end of the measurement range is usually set at $nD^2/\nu < 10,000$, it can be easily extended with resulting improvement in linearity but at the cost of increased pressure loss and reduced bearing life. However, short bursts of up to 100% flowrate overranging can be tolerated, without permanent damage (Doebelin 1990, 580). Turbine meters are factory calibrated to have a uniform Q/nD^3 to eliminate the need for recalibration when internal parts are replaced (e.g., for routine maintenance or sterility between patients).

In early meters, the rate of revolution of the turbine was measured by the rate of passage of a single permanent magnet mounted on the turbine past a reluctance pickup mounted on the turbine housing (Stoecker & Stoecker 1989). However, this configuration sometimes caused the turbine to lock up at very low flowrates, i.e., the magnetic force was larger than the impulse imparted by the fluid flow on the turbine blades. Newer configurations use optical means to detect the number of interruptions of a light beam by each blade as it spins (BOC Health Care 1984). If two emitter-detector

pairs are used, the direction of rotation can also be sensed by looking at the order in which the emitter-detector pairs are being interrupted. The optical detection of blade revolution eliminates the magnetic lock up condition at low flowrates and also increases the resolution by a factor equal to the number of blades in the turbine if the counter can keep up with the faster rate of interrupts.

If condensate or contaminants from the patient interfere with transmission of the light beams between the emitter-detector pairs, the sensor might not work. Active warming by an electrical filament of the turbine meter housing to slightly above body temperature will prevent condensation of the exhaled moisture on the emitter and detector surfaces (BOC Health Care 1984).

The turbine meter has its own flow straightening vanes inbuilt in the transducer and should therefore be less affected by sharp flow disturbances like tees and bends. The requirement for a straight length of pipe upstream of the turbine meter was not specified in the references consulted (Stoecker & Stoecker 1989; Cheremisinoff & Cheremisinoff 1988; Doebelin 1990, Fox & McDonald 1978; BOC Health Care 1984).

In view of its inherent advantages for the flow measurement configuration depicted in figure 27B, the turbine flowmeter is selected for the desired application. The vortex shedder flowmeter was a close second and deserves to be investigated further, especially for cross-sectional shapes that will shed vortices reliably at Reynolds numbers as low as 50.

4.3.13 O_2 Flush Valve

In clinical practice, the three main purposes of the O_2 flush valve are: (a) to compensate for a large leak in the system, (b) to quickly flush away (wash out) anesthetics from the breathing circuit and (c) to rapidly change the FiO_2 to 1.0. The washout time constant when the O_2 flush is used should not exceed 10 seconds. Assuming a circuit volume of 10 l, an O_2 flush flowrate of 60 l/min will therefore be adequate.

The O_2 flush valve should be positioned such that it actually flushes as much of the anesthesia circuit as possible. Thus, its placement has to be considered relative to the purge valve (to be described in the next section).

An O_2 flush is a random but deterministic event which is also highly disruptive, e.g., for an intelligent alarm expert system shell. Its possible detrimental consequences during laser microsurgery of the airway (airway fire: sections 2.5.6 and 4.2.3; design option 6) and mechanical inspiration (barotrauma: section 4.2.3; design objective 1.4.8) have already been described. By changing the function of the O_2 flush pushbutton from valve activation to an O_2 flush request via a microcontroller and supporting software (design solution 1.1.1.1.1a), the randomness of the O_2 flush event is controlled. Thus, an O_2 flush becomes a predictable, expected and safe event for all subsystems (internal and external to the anesthesia delivery system) that will be affected by it because these systems will have been forewarned of the impending O_2 flush.

The O_2 flush valve is opened by the microcontroller after an O_2 flush request if and only if it is safe to do so. The user will in general not be aware of this subtle but

fundamental change in the function of the O_2 flush valve because the microcontroller runs at 12 MHz and executes an instruction in about 1 microsecond on average. Therefore, the delay while the microcontroller is checking and configuring the system in preparation for an O_2 flush will at most be of the order of a millisecond which is below the temporal resolution of humans. In other words, the user will not notice that the function of the O_2 flush valve has been changed.

Consequently, a wide-bore ($\geq$ 0.16 cm (1/16") orifice size) electromechanical valve supplied with 50 psig O_2 that can be readily interfaced and controlled by a microcontroller is required as the O_2 flush valve. This choice allows automatic disabling of a laser microsurgery unit during an O_2 flush, automatic abortion of mechanical inspiration during an O_2 flush and communication of the occurrence of an O2 flush to an alarm expert system shell.

4.3.14 Purge Valve

In a closed breathing circuit, a purge valve is required for many reasons. During an O_2 flush, when O_2 is being flushed into the system at a flowrate of 60 l/min, undesirably high pressures will be obtained in a very short time if a purge valve with low flow resistance (≤ 1 cm H_2O pressure drop at a 60 l/min 100% O_2 flowrate) and fast response time ($\leq$ 20 ms) is not opened before the O_2 flush valve is energized. The purge valve also allows the gas mixture existing in the circuit prior to the O_2 flush event to be flushed out.

During closed circuit operation, the rate of change in inspired gas concentration will be determined by the time constant of the breathing circuit. In the event, that a rate of change in inspired concentration faster than that possible with closed circuit operation is desired, then the purge valve allows the system to be opened and will thus allow that faster rate of change of inspired gas concentration to be attained, albeit at the cost of higher anesthetic and gas consumption rate.

Finally, when the breathing system is operating in steady state in a closed circuit mode, the pressure distribution along the circuit will be mainly determined by three factors: (a) the setting of the proportional flow control valve, (b) the blower speed and (c) the volume of gas in the circuit. Situations will arise (to be described later) where to obtain the desired pressure distribution the volume in the circuit will have to be reduced. The purge valve also serves this function by opening and dumping the excess gas volume into a scavenging system.

The location of the purge valve is decided primarily on the basis of its function as the outlet port for the pre-existing circuit gases during an O_2 flush. Thus, the purge valve should be located such that the breathing circuit is between it and the O_2 flush valve to ensure that all pre-existing gases are washed away during an O_2 flush. Furthermore, in the event that the proportional flow control valve fails in the completely shut position and the purge valve is "downstream" of the proportional flow control valve, there will be a rapid buildup of pressure in the circuit that will rupture the patient's lungs, during an O_2 flush. Consequently, the O_2 flush valve is placed at the blower outlet and the purge valve is placed at the connection between the exhalation hose and

the proportional flow control valve, i.e., "upstream" of the proportional flow control valve (figure 28).

4.3.15 Gas Make-Up Valves

Gas make-up valves are required to inject O_2 and other carrier and anesthetic gases like air, N_2O, He and Xe into the circuit to maintain the desired FiO2 and also to maintain the circuit volume at a desired level. The gas make-up valves are preferably binary on/off valves because they are inexpensive ($17) compared to proportional flow control valves (approximately $400) and reliable (in excess of 10^9 cycles MTBF (Clippard 1981)). Pulse width modulation (PWM) is not used with the binary valves because past experience with similar binary valves has shown that the transient response of the valve (approximately 10 ms) will affect the volume output by the valve, especially as the pulse width approaches the response time of the valve. Thus, with PWM, the volume output of the valve will not be a linear function of the pulse width duration, especially when the pulse width approaches the response time of the valve. Consequently, frequency modulation (FM) of the valves at a constant pulse width (50 ms) is used instead.

Furthermore, past experience in a similar application has also shown that the valves must operate in the choked flow regime so that the volume of gas output for each pulse is solely dependent on the supply stagnation pressure and the pulse width duration and independent of the pressure in the breathing circuit which will approach PIPs of up to 100 cm H_2O (≈ 1.5 psig). Choked flow operation is ensured by reducing the flow

resistance between the valve outlet and the breathing circuit by placing the lightweight valves (~ 100 g) directly on 15 mm i.d. plastic connectors (a standard in breathing circuit equipment) that are then interposed into the breathing circuit.
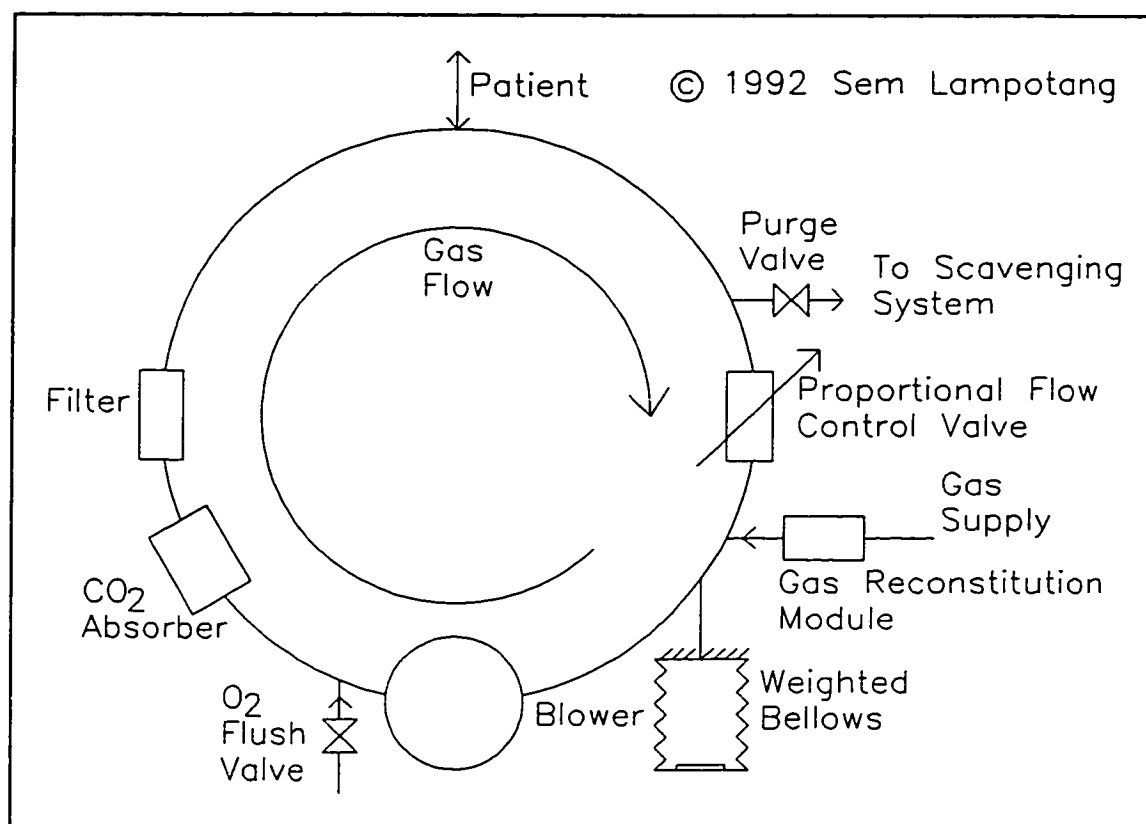
Figure 28. The evolving circuit configuration with an O_2 flush valve, a purge valve and a gas reconstitution module

Thus the gas reconstitution module will consist of a battery of binary valves each independently controlled by an input/output (I/O) line from the microcontroller and the opening and closing of the valve controlling each make-up gas will be decided according to the control software. To promote choked flow, the highest pressure difference possible across the valves for a given supply pressure is desirable. Consequently, the gas

reconstitution module is placed at one of the lowest pressure points in the circuit, i.e., near the blower inlet at the bellows (figure 28).

4.3.16 Manual Ventilation and Breathing Bag

Manual ventilation is an intrinsic and necessary part of any anesthesia delivery system and depending on personal preference and national practices, the breathing bag for manual ventilation can be an important aspect of the system design (Boquet, Bushman & Davenport 1980; section 3.2.12). The presence of a breathing bag in the anesthesia circuit allows the anesthesiologist to ventilate the patient's lungs manually, by periodically squeezing the bag and also to obtain a tactile feel for the compliance and resistance of the patient's respiratory system. Collapse of the bag when the patient takes spontaneous breaths as the anesthetic wears off and the patient starts waking up also helps the anesthesiologist to detect inadvertent light anesthesia or confirms the onset of emergence. The breathing bag also acts as a buffer and collapses to provide gas flow to a spontaneously breathing patient if the spontaneous inspiratory flowrate demand exceeds the flowrate at the ETT, thus helping to reduce the inspiratory pressure dip during spontaneous inspiration and therefore the WOB.

However, the bag is also a nuisance during mechanical ventilation because its compliance then diverts part of the set tidal volume away for the patient (section 4.3.3.2). An analysis of the ways in which the bag is used reveals that its behavior is desirable and useful when it can collapse (i.e., it can be easily squeezed for manual ventilation and it freely collapses when the patient takes a spontaneous breath) and is

detrimental when it can easily expand and divert part of the mechanical tidal volume intended for the patient. Traditional anesthesia circuit designs deal with this schizoid nature of the breathing bag by isolating it from the breathing circuit during mechanical ventilation, by forcing the user to flip a ventilation mode selector knob and turn on the mechanical ventilator. This is not an optimal solution because it requires the anesthesiologist to remember to perform multiple actions when switching from one ventilation mode to another.

Consequently, the concept of a "unidirectionally" compliant breathing bag is proposed. The ideal "unidirectional" bag would collapse easily but would have infinite stiffness in the other direction, i.e., inflation past its normal filled shape. This "unidirectional" compliance would allow the breathing bag to remain in the circuit at all modes of ventilation so that manual ventilation can be delivered and the patient's inspiratory efforts, compliance and resistance characteristics can be felt at all times without having to pay the price in loss of mechanical tidal volume. A possible way of obtaining this "unidirectional" compliance is to have a mesh of fine, high tensile strength nylon preformed into the full shape of the bag, imbedded in the rubber side wall of the breathing bag during manufacture.

4.3.17 FiO₂ Control

The control of the inspired O_2 concentration is obviously important. For ease of closed circuit operation, it is desirable that the user simply enters the desired inspired O_2 concentration and not have to adjust the flow settings anymore thereafter. For this

capability to be realized, independent of the ventilation mode and settings, a feedback control loop is required for the inspired O_2 fraction. The FiO_2 feedback control loop must be supplied with real time measurement of the FiO_2. In practice this is most likely to be accomplished by readily-available multi-gas analyzer benches which can measure O_2, N_2O, CO_2 and anesthetic agents (Ohmeda 1990a).

Depending on the error in FiO_2, the control software would then frequency modulate the O_2 make-up valve at a fixed pulse width to obtain the desired FiO_2.

4.3.18 Isovolumetric Operation and Anesthetic/Carrier Gas Control

During anesthesia, a mixture of more than two gases (excluding the volatile anesthetic which is differentiated as being a "vapor" in anesthesia circles) is rarely used. Typical mixtures are 70% N_2O, 30% O_2; 50% O_2, 50% N_2O; 70% He, 30% O_2. One of the gases must always be O_2 and the other can be either an anesthetic gas (like N_2O or Xe) or a carrier gas (like He or air). Consequently, the control of the second, non-O_2, gas in the anesthetic mixture can be accomplished indirectly by maintaining a constant circuit volume (isovolumetric operation)

If the desired gas mixture is 30% O_2 and 70% N_2O and the control loop for FiO_2 (which takes precedence over the isovolumetric control loop) has achieved its goal of maintaining the FiO_2 at 30%, then by definition the desired N_2O concentration (70%) has also been reached. Thus once the desired FiO_2 is attained, all that is required to maintain isovolumetric operation (to compensate for the gas consumption of the patient)

<u>and</u> the desired gas concentration is to inject gas into the circuit at the desired ratio (70% N_2O and 30% O_2 in this example) until the circuit volume is restored.

Thus, a transducer that will give a measurement or indication of the circuit volume is required for the isovolumetric control loop. The weighted bellows will be seated (bottomed out) if the circuit volume is maintained. On the other hand, the bellows will not bottom out but will instead keep on rising if volume is not maintained, i.e., the priming volume decreases and for a given blower speed and proportional flow control valve setting the pressure distribution will alter and become lower at the bellows. Thus, instead of the weight of the weighted bellows being balanced by the sub-ambient pressure inside the bellows, it is overcome by the increased sub-ambient pressure resulting from the decrease in priming volume.

Consequently, a simple electromechanical switch or an optical emitter-detector pair at the bottom of the bellows case can act as the constant volume sensor. The optical approach has the advantage of requiring no triggering force while the electromechanical switch is insensitive to ambient lighting. Other more involved and expensive systems include a slide potentiometer with the wiper attached to the bottom of the bellows or an ultrasonic proximity sensor which gives an analog reading from waves bounced off the bottom of the bellows.

4.3.18.1 Flow resistor between blower inlet and bellows

In the evolving system configuration in figure 28, the seating of the bellows will be tightly coupled to the speed of the blower because the blower inlet pressure will

become more sub-ambient as the blower speed increases for a constant circuit volume and the bellows is in direct communication with the blower inlet. This tight coupling is relaxed by inserting a flow resistor between the blower inlet and the bellows to force a pressure drop between the bellows and the blower inlet. The flow resistor allows the bellows to stay seated at a wider range of blower speeds for a given priming volume and proportional flow control valve setting.

4.3.19 Gas Sampling Site

It is assumed that a multi-gas analysis bench will be used for determining the inspired and expired gas and vapor concentrations. Because a multi-gas analyzer is used, all the gases are sampled from the same point. If the gases were conventionally sampled at the Y-piece, the measurements, especially for end-tidal values, would be diluted by the recirculating flow of gas. For gases like CO_2 where the end-tidal value is normally more important clinically than the inspired concentration, such a dilution would be unacceptable. Therefore, the gas sampling point is moved to the distal tip of the ETT to prevent dilution of the gas samples by the recirculating flow. For true closed circuit operation, the sampled gases should be returned to the breathing circuit after analysis. A suitable site would preferably be the sub-ambient side of the circuit to prevent inadvertent back pressure that may affect the operation of the multi-gas analysis bench.

Gas sampling at the ETT brings the interesting possibility of "software" reduction in deadspace since rebreathed CO_2 contributed by the ETT mechanical deadspace will be

apparent and can therefore be compensated by increased minute ventilation if there is a

feedback loop for end-tidal CO_2 ($ETCO_2$) also.

4.4 Implemented Prototype

Airway Pressure Sampling

Patient

© 1992 Sem Lampotang

Endotracheal Tube

Multigas Analysis Sampling

Flowmeter

Purge Valve

To Scavenging System

Gas Flow

Filter

Unidirectionally Compliant Bag

Proportional Flow Control Valve

Gas Supply

CO_2 Absorber

Gas Flow

Flow Resistor

Gas Reconstitution Module

O_2 Flush Valve

Blower

Weighted Bellows

Bellows Sensor
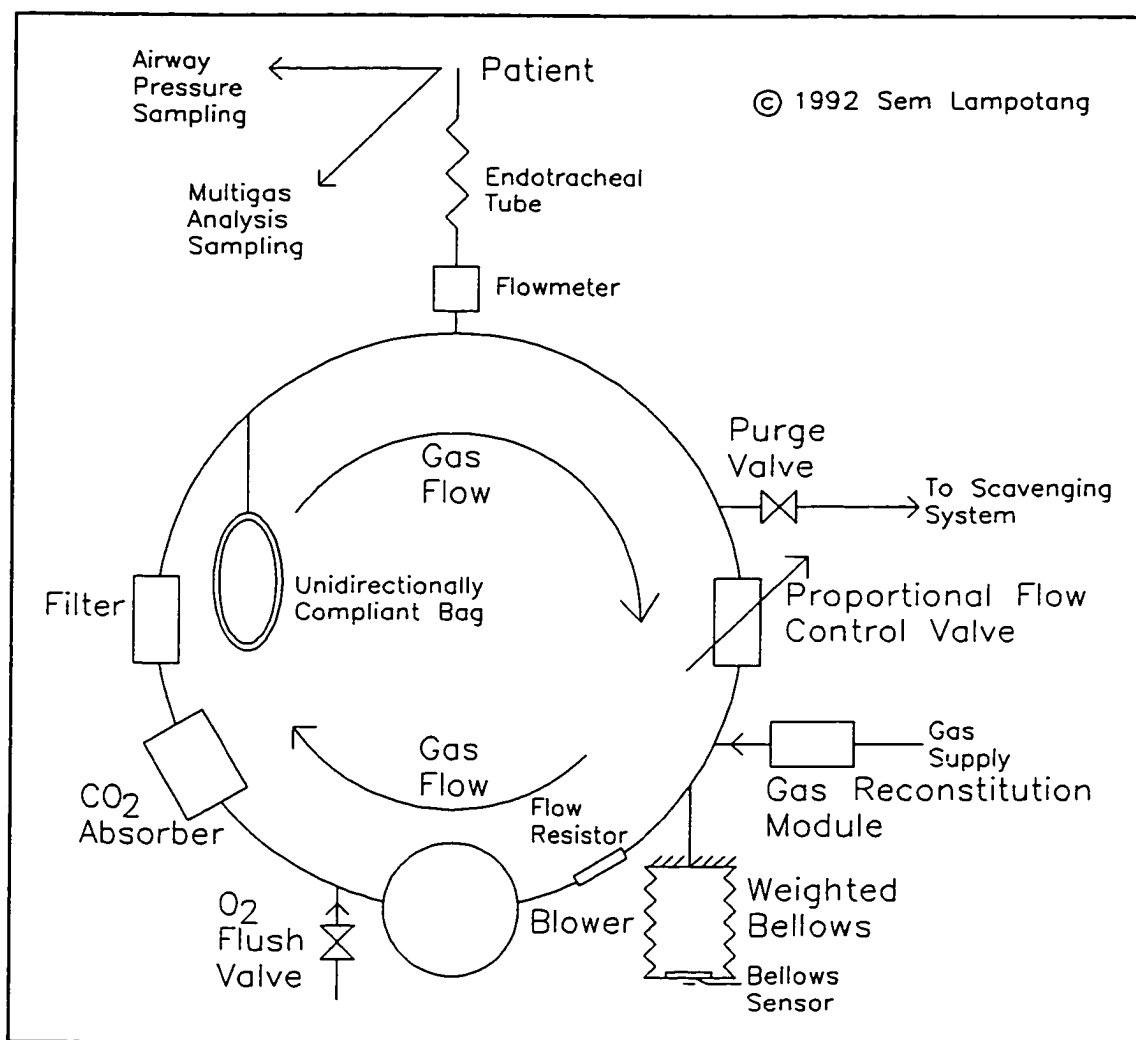
Figure 29. The conceptual representation of the part of the anesthesia delivery system that was fabricated and evaluated

The present point in the design path of the conceptual system is depicted in figure 29 and is representative of that part of the anesthesia delivery system that was actually fabricated and evaluated as part of this study. The closing sections of this chapter describes the features that will need to be added for anesthetic delivery and control. Further, advantageous design options are also proposed and the issue of sterility is addressed to round off the design.

4.5 Anesthetic Delivery and Control

Although we have chosen to concentrate on the life support component of the anesthesia delivery system in this chapter, the ultimate purpose of the prototype system is to deliver anesthesia. The design is now completed with the addition of volatile anesthetics to the circuit under feedback control. The distinction should be made here between feedback control of the concentration of volatile anesthetics (inspired or end-tidal) and automated (also called closed-loop) anesthesia. The design for the anesthetic delivery system that is described in the next sections is for feedback control of the anesthetic concentration according to a desired end-tidal anesthetic concentration that is chosen by the anesthesiologist.

In other words, instead of turning the concentration control knob on the anesthetic vaporizer as is currently done, the anesthesiologist will dial the desired anesthetic concentration on the front control panel. This new entry will then become the target concentration that the feedback control loop of anesthetic concentration will attempt to achieve. In automated or closed-loop anesthesia, the controller determines what

anesthetic concentration to deliver independent of the anesthesiologist. Feedback control of user selected anesthetic concentrations was chosen over closed-loop anesthesia because it was felt that the feedback approach will be more familiar to the anesthesiologist and there will be user resistance to a system that relegates the user to observer status. Furthermore, closed-loop anesthesia delivery is still at an experimental stage.

In the absence of an unequivocal and measurable parameter for quantifying depth of anesthesia, control of end-tidal anesthetic concentration is acceptable and the preferred method, even though this method relies on many assumptions (section 2.2). At this point, it is worth mentioning that it simplified the design process to be able to more or less design the life support component of the anesthesia delivery system relatively independently of the anesthesia delivery component. This considerable design benefit was obtained because it was decided at the critical, initial stages of the methodology of the design process, i.e., when laying out the design specifications for the system and subsystems (see figure 37), that the anesthetic introduction device would be independent of the FGF, e.g., a liquid anesthetic injector.

4.5.1 Computer-Controlled, Motorized, Anesthetic Syringe

Existing flow-over vaporizers (section 2.5.3.2) are limited in the amount of vapor that they can deliver because they are dependent on the FGF to pick up the anesthetic vapor as it passes through the vaporizer. Consequently, during closed-circuit anesthesia where low FGFs are used, the desired anesthetic consumption rate of the patient might not be met leading to light anesthesia or the need to supplement the volatile anesthetics

with intravenous anesthetics or forcing the anesthesiologist to use higher FGFs which result in more waste and pollution and a higher hospital bill for the patient.

Furthermore, current flow-over vaporizer designs suffer from the pumping and pressure effects, which are caused by pressure fluctuations in the anesthesia circuit, especially during mechanical inspiration (section 2.5.3.2).

Thus a strong case is made for making the output of the device for introduction of volatile anesthetics into the breathing circuit independent of FGF (design objective 2.2.1) or pressure conditions in the anesthesia circuit. A motorized, computer-controlled syringe that squirts liquid anesthetic into the anesthesia circuit (similar to the one used in the Harrow I system; section 3.2.4) meets those two specifications above. The rate of injection of liquid anesthetic can then be controlled by a digital controller (e,g, PID or adaptive) that obtains its feedback from a multi-gas analyzer that can measure anesthetic agent concentration (not the same one that is used for monitoring purposes by the anesthesiologist).

4.5.1.1 Hazards of liquid anesthetic injection and proposed solutions

The location of the anesthetic syringe outlet into the anesthesia circuit will be decided on the criteria of preventing (a) unvaporized volatile anesthetic (i.e., liquid anesthetic) from entering the patient's respiratory system which is harmful to the patient and (b) uncontrolled vaporization of the liquid anesthetic into the anesthesia circuit, i.e., anesthetic entering the circuit through vaporization rather than because it is being squirted out by the syringe.

To prevent liquid anesthetic from reaching the lungs, the liquid anesthetic introduction site should be as far away as possible from the patient. This gives any liquid anesthetic drop that is injected by the syringe as long a path as possible to the patient's respiratory system, thus increasing the likelihood that all liquid anesthetic drops will be vaporized by the time they arrive at the respiratory system.

To prevent unwanted and uncontrolled vaporization the liquid anesthetic in the syringe is "pressurized" by using very high flow resistance, narrow bore (0.1 mm) needles and tubing to create a large back pressure on the syringe. The narrow bore of the needle also presents a lower area for evaporation of the liquid anesthetic at the needle tip. To further reduce uncontrolled vaporization, the needle is located at the highest pressure point in the circuit, the blower outlet. Finally, as a last protection layer, the bacterial filter is placed downstream of the liquid anesthetic injection site and upstream of the patient, i.e., between the patient and the anesthetic injection site (figure 30). Liquid anesthetic drops larger than the pore size of the filter will thus get trapped on the filter material and eventually vaporize.

Air bubbles might be present in the liquid anesthetic syringe and would cause the anesthetic concentration feedback loop to malfunction because air would be squirted out instead of liquid anesthetic when the bubbles reach the needle tip. The risk of injecting air is diminished by orienting the syringe such that the needle is at a lower point than the plunger so that the air bubbles will rise and collect against the syringe plunger and will thus be injected only after all the liquid anesthetic has been injected. Similarly, the syringe must be placed at a lower elevation than the point in the circuit where liquid

anesthetic is introduced. The anesthetic introduction point in turn must be lower in elevation than the Y-piece and ETT to prevent the possibility of gravity feed of liquid anesthetic into the patient's lungs in case of catastrophic failure of the system (figure 30).
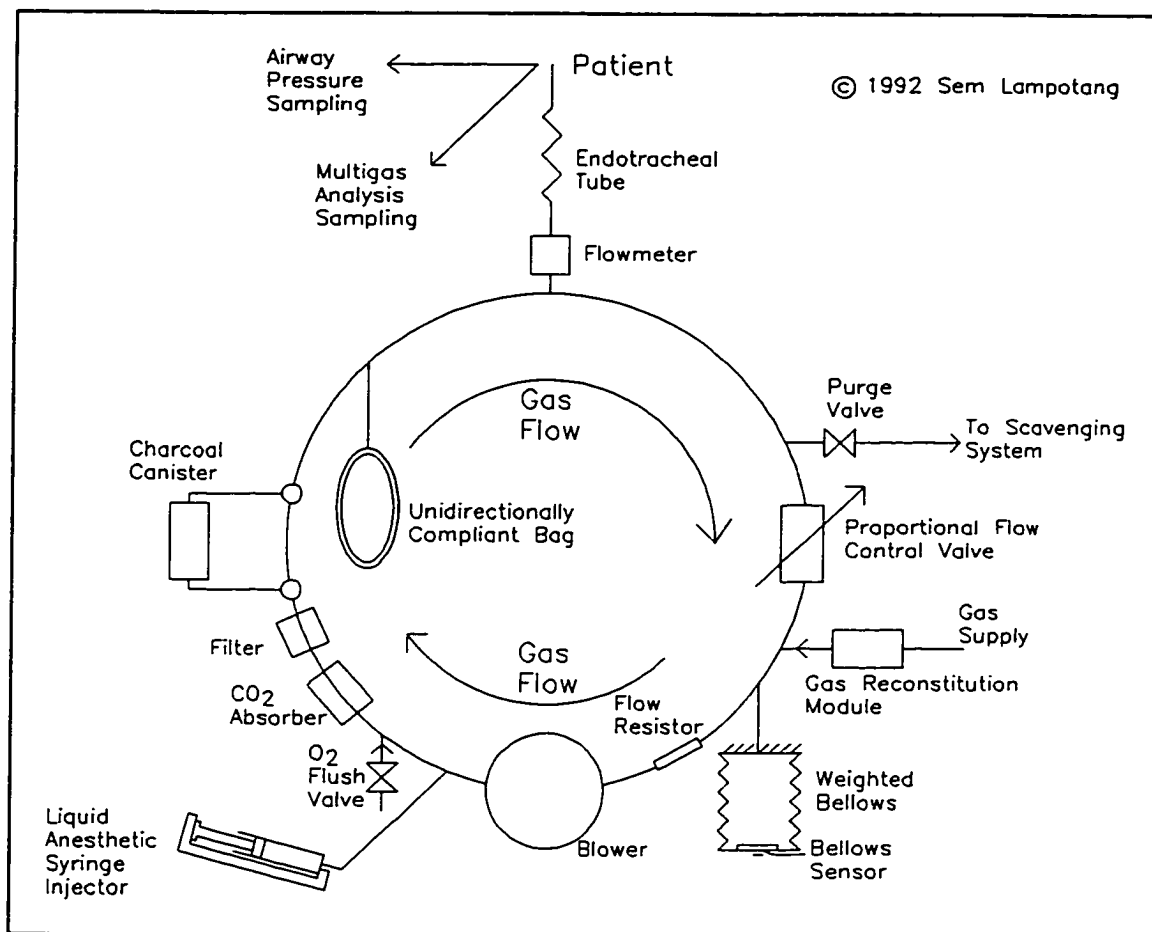
Figure 30. The incorporation of volatile anesthetic delivery and control features to the anesthesia delivery system

4.5.2 Anesthetic Gas Sampling Site

With a multi-gas analyzer capable of measuring volatile anesthetic, the anesthetic gas sampling site will be at the ETT distal tip, by default (section 4.3.19). If a multi-gas

analyzer is not used, the anesthetic gas sampling site should still be at the ETT distal tip to prevent dilution of the end-tidal anesthetic concentration by the recirculating gas flow.

4.5.3 Charcoal Canister

As already discussed, the purge valve can be used to allow the system to run in open circuit mode so that changes in gas or anesthetic concentrations can be effected more quickly than when the system is running in closed circuit mode, at the cost of increased waste of anesthetic gases and vapors. Thus, in cases where a fast rate of change of anesthetic concentration is not required, it would be less wasteful to be able to control (especially reduce) the anesthetic concentration while keeping the circuit closed. A charcoal canister allows reduction, of the anesthetic concentration in the anesthesia circuit while maintaining the system in a closed state. Thus, a charcoal canister that can be switched in or out of the circuit by both the user and the microcontroller is a desirable feature of anesthetic control (figure 30).

4.5.4 Risk of Volatile Anesthetic Liquefaction

The possibility that the pressure rise across the blower will liquefy the volatile anesthetics must be investigated because liquid anesthetics in the circuit would hurt the patient if they get into the lungs and will also lead to unpredictable volatile anesthetic concentrations if and when they evaporate again in an uncontrolled fashion. The risk of liquefaction of volatile anesthetic within the circuit can be assessed by examining the vapor pressure for each volatile anesthetic.
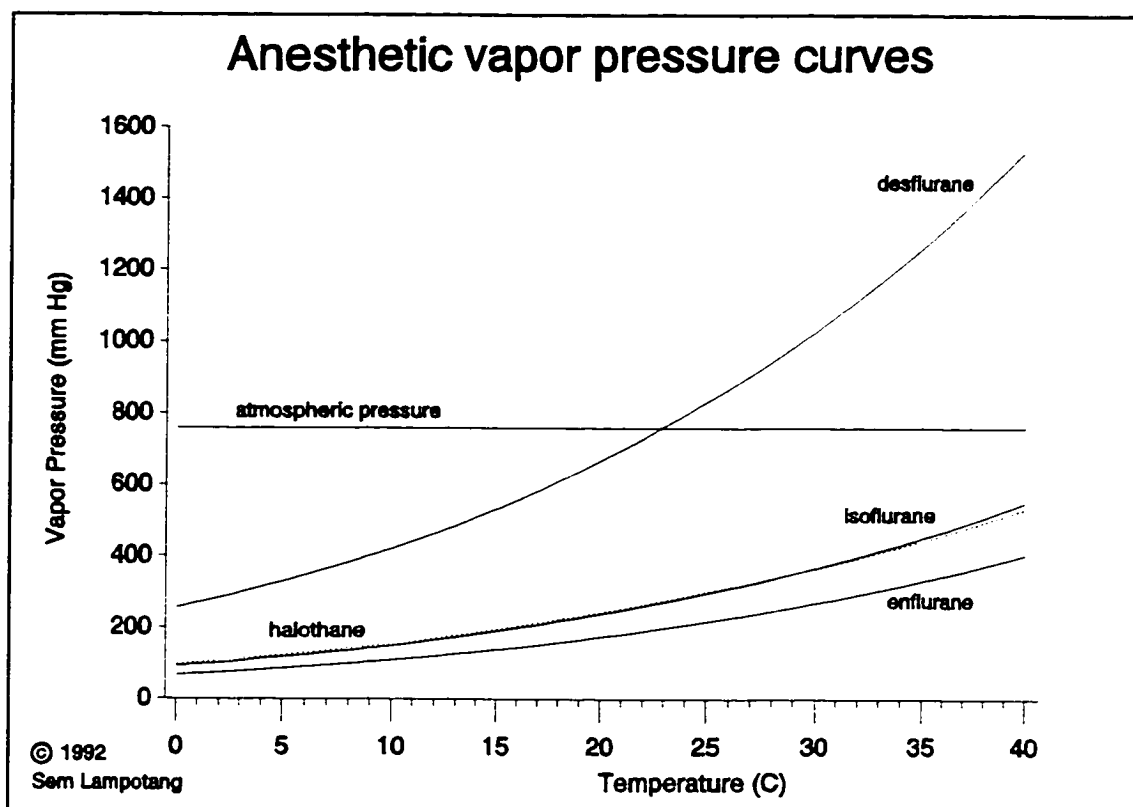
Figure 31. The vapor pressure curves of different volatile anesthetics.

The vapor pressure curves for different volatile anesthetics are shown in figure 31. The curves were obtained using a program written in Turbo C++ (Borland International Inc., Scotts Valley, CA) and using the physical properties data supplied by Anaquest, a manufacturer of volatile anesthetics and a paper by Rodgers and Hill (1978). The experimental Antoine coefficients (C1, C2 and C3) and the semi-empirical equation (see below) for the desflurane vapor pressure curve shown in figure 31 were obtained by contacting the manufacturer, Anaquest, directly.

$$\ln P_{vap} = C1 + \frac{C2}{T} + C3 \ln T \qquad\qquad \textbf{4.14}$$

where P_{vap} is the vapor pressure in atmospheres and T is the temperature in Kelvin and

$C1 = 18.8682;$ $\qquad C2 = -4086.9756$ $\qquad C3 = -0.8897$

The vapor pressure curve of desflurane should thus be used with caution as it has not yet been confirmed by independent studies. However, a check was made of the accuracy of the vapor pressure equation by inserting the known boiling point of desflurane at 760 mm Hg (22.8°C) into the vapor pressure equation. A vapor pressure of 759.6 mm Hg was obtained, as expected. From figure 31, it can be seen that desflurane has the highest vapor pressure at any given temperature among the 4 anesthetics.

However, it is not easy to predict from figure 31 whether anesthetic liquefaction will occur at the maximum envisaged design pressure in the system (2 psig) and the minimum design temperature (35°C; see section 4.6.1 on temperature control). Therefore, the vapor pressures for the different volatile anesthetics were expressed as an equivalent volumetric concentrations (%) for a total pressure of 2 psig, the maximum design pressure. The maximum volumetric concentration that is ever clinically used (including "overpressure" induction) for each anesthetic is generously set at 5% for isoflurane and halothane, 7% for enflurane and 12% for desflurane as shown in figure 32. The volumetric concentration curves were obtained by modifying the program used to obtain figure 31.
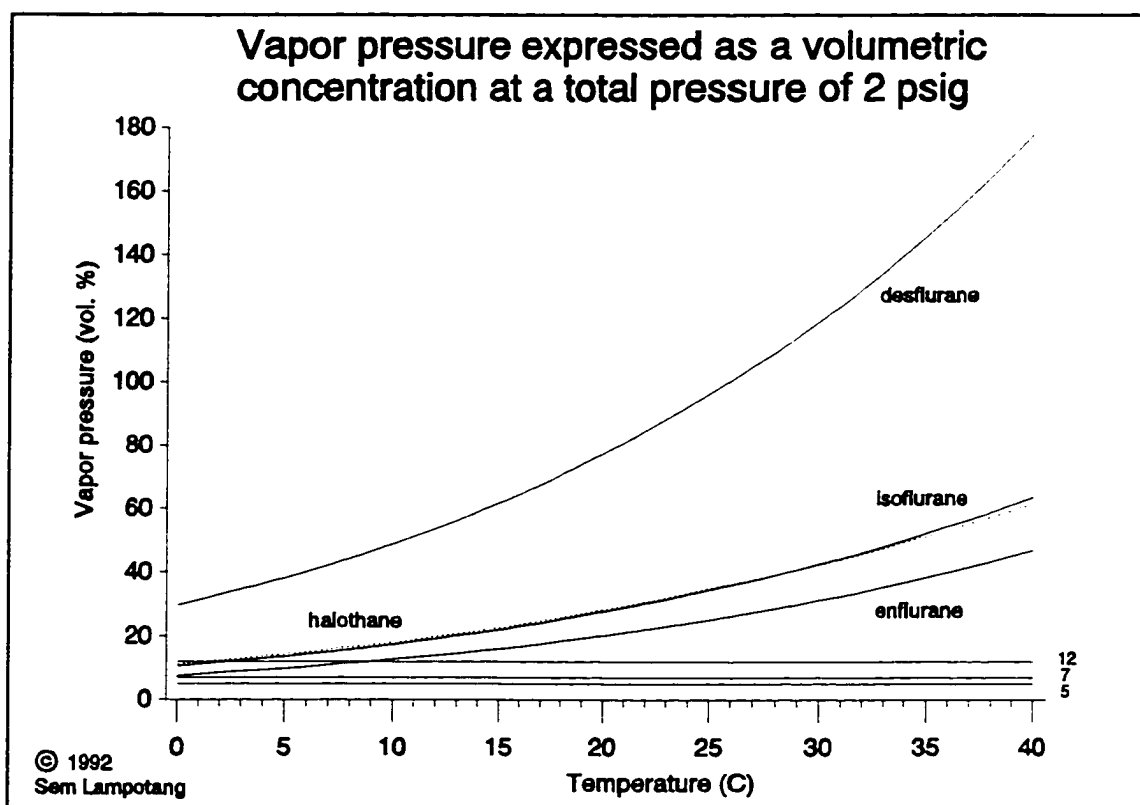
Figure 32. The maximum volumetric concentration for volatile anesthetics before liquefaction starts at a total pressure of 2 psig

Thus, if the vapor pressure curve is lower than the corresponding maximum expected volumetric concentration, there will be a risk of anesthetic liquefaction. It can be seen from figure 32 that, at the minimum temperature of 35°C for the gases in the circuit (assuming that the gases will be maintained at a constant temperature of 38°C with a ±3°C control accuracy by a heat exchanger that will be described in section 4.6.1) and at the maximum design pressure of 2 psig (greater than the maximum PIP of 100 cm H_2O (≈ 1.5 psig) because of the pressure drop from the blower outlet to the patient), there will be no liquefaction of halothane, enflurane, isoflurane or desflurane.

4.6 Desirable Design Options

In a breathing circuit where the gases circulate passively, there is no forced recirculation and no device like a blower to impart head to the gases to overcome the pressure drop through add-on devices like filters and humidifiers. Thus, the designer is constrained in the selection and amount of devices that can be added to the circuit because the spontaneous WOB will increase as the flow resistance of the add-on components increases. For example, wet bacterial filters will increase the spontaneous WOB of the patient.

In a breathing circuit with forced recirculation, the head producing ability of the recirculator, e.g., a blower, provides the designer with an increased choice of add-on devices that can be incorporated into the circuit without too much concern for the pressure drop that these devices will cause as long as the blower can generate enough head to compensate for the pressure drop of the add-on devices. Consequently, a list of desirable add-on devices is suggested for the breathing circuit.

4.6.1 Heater/Cooler

A benefit of closed circuit anesthesia is that humidity and heat are better conserved compared to semi-open or open circuit anesthesia. However, there will still be heat loss through the circuit material which is exposed to ambient temperature (25°C). The cooling of the circuit gases from 38°C leads to condensation which implies that the gases returning to the patient during closed circuit ventilation carry less water than the exhaled gases. Thus, in restoring the relative humidity of the returning gases back to

100% at 38°C, the patient's respiratory system will have to supply the latent heat of vaporization of water, resulting in undesirable cooling of the patient.

A small finned radiator/heater made of copper or another good conductor like aluminum, similar to the ones used in car interior heaters could maintain the temperature of the gases in the circuit at a constant level when controlled as part of a feedback loop. The heating power could be supplied with thermo-electric (Peltier) modules which have the peculiar property that if the direction of current flow through the modules is changed, then the heating side of the module becomes the cooling side and vice-versa (figure 33).
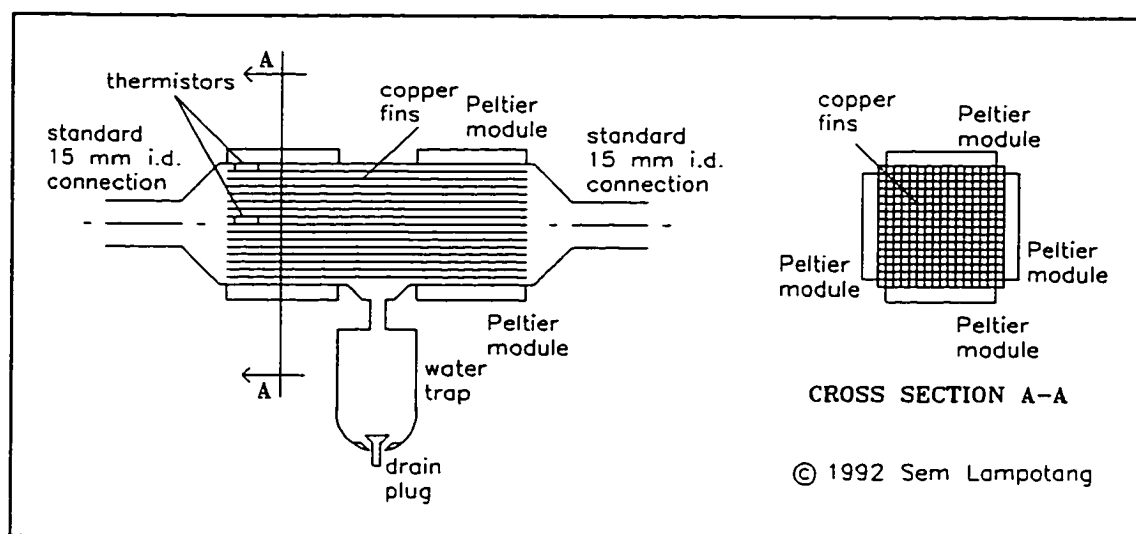
Figure 33. A schematic representation of the proposed heater/cooler for the recirculating anesthesia delivery system

This bidirectional heat transfer capability can be exploited for active cooling of the breathing circuit gases with the purpose of cooling the patient during malignant hyperthermia (MH). The large surface area of the lungs combined with the resulting latent heat of condensation will result in effective lowering of the core temperature of the

patient, especially since the patient can now be cooled from both inside (by the cooled dry gases) and outside (by ice packs which are part of the standard clinical protocol for treating MH). The heat exchanger should have a water trap to collect and remove the water that will condense when it is used as a cooler.

A temperature measurement scheme will be needed to maintain the gases at a fixed temperature. Thermistors could be used to measure the temperature of the surfaces in the heat exchanger. Due to the fact that the temperature in the heat exchanger will not be uniform (hotter during heating near the exterior surfaces which will be closer to the Peltier modules), more than one thermistor will be used (figure 33). A weighted average of the temperatures can thus be computed in real time and used to provide feedback to the heat exchanger control loop that maintains the fins and thus the circuit gases at a fixed temperature.

If one considers the heater as a hot wire meter, it could also work as a detector for confirmation of MH because the circuit gases will be warmer during MH and all other parameters remaining constant, the control loop will need to put less or no current into the heater or even reverse the current flow to maintain the desired circuit gas temperature.

The large wetted area of the finned radiator will cause a pressure drop as the gases flow through it. That pressure drop is not of as much concern as it would be in a system without forced recirculation because the head loss at the heater will be compensated by the blower.

4.6.2 CO₂ Absorber Bypass

In cases where it is desired to wash away the volatile anesthetic rapidly while maintaining a closed circuit, the charcoal canister would be switched into the circuit and the patient would be hyperventilated. However, hyperventilation will also decrease the CO_2 level in the lungs to the point that the pH of the patient's blood will become higher (more alkaline) with undesirable consequences. Consequently, the ability to bypass the CO_2 absorber in this circumstance is a desirable design feature (figure 34).

4.6.2.1 CO₂ injection

As an extension of the situation above, a situation could exist where the CO_2 production rate of the patient is low and even with the CO_2 bypass implemented in a closed circuit, the patient's blood remains too alkaline. In that situation, the ability to add CO_2 to the breathing circuit gases would be a design bonus. This could be readily accomplished by adding a binary valve for controlling CO_2 injection rate to the battery of binary valves in the gas reconstitution module (figure 34).

4.6.3 Open Circuit, Room Air Operation

In the event of total loss of gas supply (i.e., both central and back-up) with electrical power available, the proposed design will still be able to provide mechanical ventilation because (a) the mechanical ventilator (proportional flow control valve) does not need compressed gases (only electrical power) to operate and (b) the blower can entrain room air and mechanically ventilate the patient at an FiO_2 of 0.21. The system

could be readily transformed for room air, open circuit operation at the flip of the ventilation mode selector knob by appropriate valving, e.g. a large bore (25 mm i.d. orifice) at the blower inlet that is normally closed and lets the blower aspirate room air when energized and a similarly configured valve at the outlet of the proportional flow control valve for exhausting the blower recirculated room air to atmosphere (figure 34).
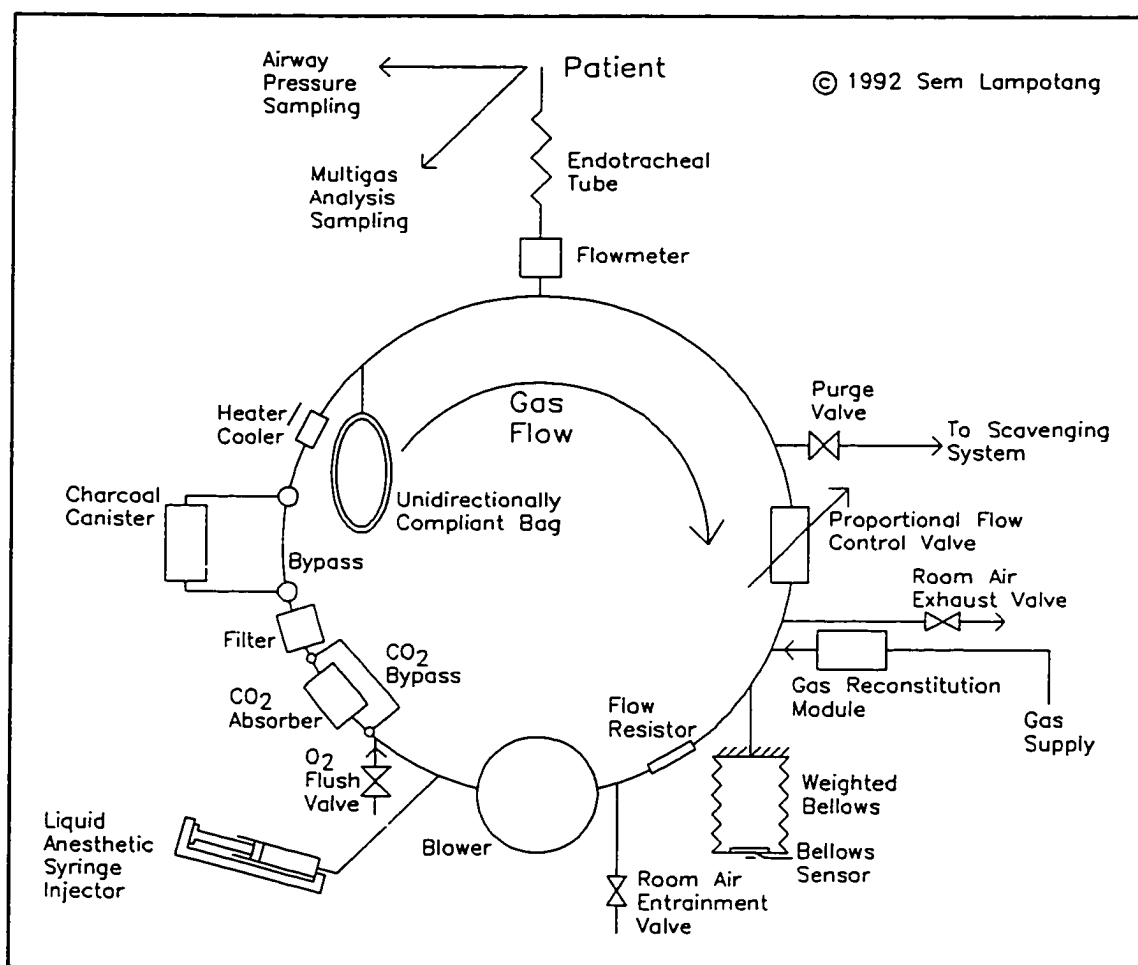
Figure 34. The GRADS system with a CO_2 bypass, a thermo-electric module heater/cooler and valving for open-circuit, room air operation

4.6.4 A Proposed Integrated Scavenging System
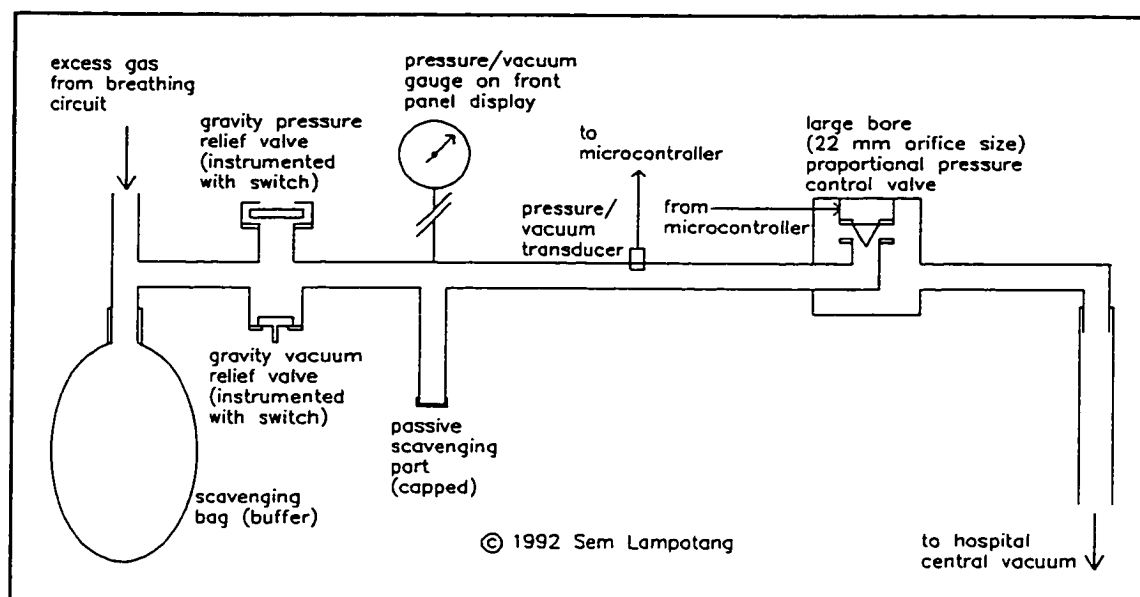
Figure 35. A proposed integrated scavenging system design with an improved user interface

The scavenging system can be simplified (i.e., no user input (design objective 9.3) and operation independent of central vacuum level (design objective 9.5)) by the addition of a simple pressure control loop that maintains pressure in the scavenging manifold at ambient pressure for gas inflow rates of up to 60 l/min for durations of 15 seconds (design objective 9.4.1). A differential pressure transducer referenced to ambient pressure would serve as the feedback sensor. A large bore (22 mm i.d.), low flow resistance (≤ 1 cm H_2O pressure drop at 60 l/min O_2) proportional pressure control valve would serve as a back pressure regulator when working in combination with the differential pressure transducer to control pressure in the scavenging manifold at ambient pressure within ± 5 cm H_2O. The gases exhausted from the proportional pressure control

valve would enter the central hospital scavenging system. A conventional scavenging bag is retained to buffer sudden large flowrates of gas from the breathing circuit into the scavenging manifold (figure 35).

If the pressure in the scavenging system diverts from ambient (either above or below) by more than 10 cm H_2O, (i.e., the scavenging system is being overloaded or has malfunctioned), this situation will be detected by the differential pressure transducer which will generate an internal (to the alarm algorithm, i.e., not communicated to the user) warning status. The corresponding switch-instrumented, gravity-operated relief valve would lift up, opening the scavenging manifold to atmosphere, if the situation persists. If the switch on the appropriate gravity-operated relief valve is still triggered after a delay of 0.5 second after the internal warning status was triggered, then the user is alerted that gas is either being spilled into the OR or excessive vacuum was present in the scavenging manifold (design objective 9.4.2). The 0.5 second delay in the control software is to prevent transient pressure swings from causing too frequent alarms. The proposed system will not need any user input or adjustment and can thus be left in its traditional place on the anesthesia machine where it is out of sight of the user.

The pressure conditions in the scavenging manifold are also monitored by an analog pressure gauge (e.g., a Bourdon tube gauge), preferably placed on the front control panel of the system so that the user can conveniently check the state of the scavenging system, at all times. A scavenging pressure gauge on the front control panel will remind the user that the scavenging system is an integral part of the anesthesia delivery system that is necessary for proper and safe function of the total system,

something which present anesthesia delivery front control panels fail to do. The Bourdon gauge should not be placed on the scavenging system manifold itself because the manifold is usually out of the line of sight of the user and thus hard to check.

If no central vacuum is available, a passive (see section 2.5.5) scavenging system can still be implemented by connecting the passive scavenging port to a window or a non-recirculating air conditioning system exhaust grille via a hose.

The position of the proportional pressure control valve can be used to infer the flowrate through the scavenging system during normal operation. Thus, the flowrate through the scavenging system should be nearly equal to the inflow of fresh gases into the circuit (which is known because the microcontroller controls the inflow of gases into the system and thus can keep track of it) minus any consumption by the patient and small acceptable leaks (50 - 100 ml/min). Consequently, a massive leak in the system (or an inadvertent obstruction of gas flow between the breathing circuit and the scavenging system) could also be detected or confirmed by the scavenging system by comparing the fresh gas inflow rate to the outflow rate (inferred from the proportional pressure control valve position). Thus, the scavenging system is converted into a monitor of the status of the anesthesia delivery system.

4.6.5 Continuous Flow Apneic Ventilation (CFAV)

As discussed in section 2.3.2, CFAV would be ideal for procedures in which the respiratory motion of organs (e.g., kidney. liver, lungs, etc.) should be zero. CFAV becomes a practical possibility with the proposed GRADS circuit design. Up to now,

CFAV has not become an established technique because of its high (28 - 100 l/min; Smith et al. 1984) FGF requirement of heated and humidified gases which overstretch the limit of present day heaters and humidifiers and would also be extremely wasteful of anesthetics with an open circuit technique.
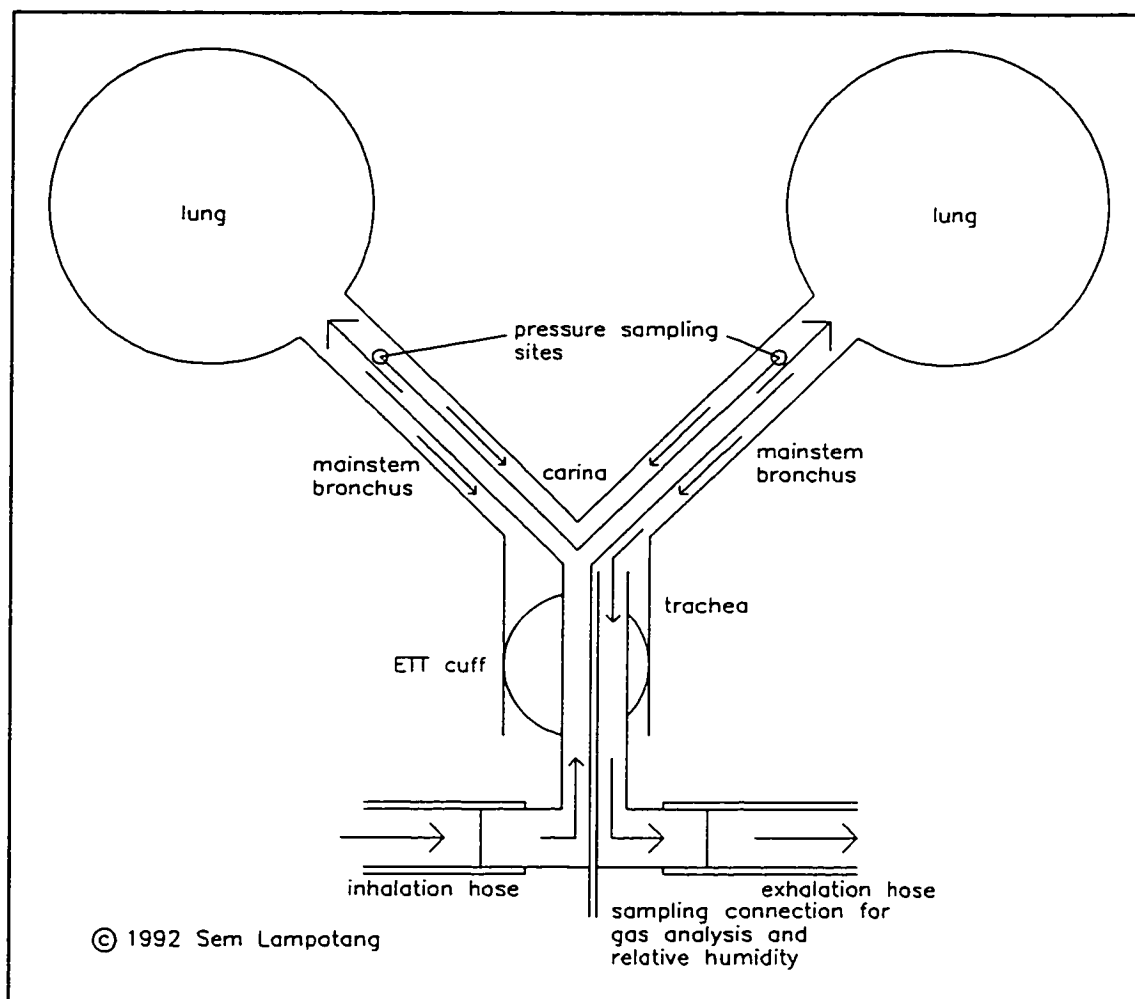
Figure 36. The envisaged interface between the patient and the breathing circuit for CFAV on GRADS

These requirements are readily addressed by the proposed GRADS design while still using anesthetics efficiently. A special endotracheal tube will need to be used so that

each mainstem bronchus can be cannulated and the pressure should be sampled at each bronchus for added safety (figure 36). The concept of end-tidal concentrations does not apply during CFAV since a constant and steady flow of gas will be washing out the CO_2 produced by the lungs and bringing in O_2 and volatile anesthetics. The possibility of using CFAV on the proposed system increases its flexibility.

4.6.6 Cross-Contamination Between Patients

The issue of sterilization of the circuit between patients is always a concern even though there is no conclusive scientific evidence of cross-contamination when patients are anesthetized on the same circuit without sterilization of the circuit between patients (section 2.5.1.4). It is also interesting to note that in present anesthesia delivery systems, the breathing circuit hoses are changed between each patient while leaving in the CO_2 absorber, ventilator bellows, inspiratory and expiratory valves and other assorted tubing, piping and devices which have come into direct contact with the patient's exhaled gases.

However, although there is still debate about the issue of cross-contamination, there is no doubt that in extreme cases like tuberculosis and acquired immuno deficiency syndrome (AIDS), the circuit will need to be thoroughly sterilized after use or a disposable circuit that can be discarded after the case is required. Thus, the designer of an anesthesia delivery system must keep in mind the need for sterilization or a disposable option if the system is to be truly flexible (i.e., it can be used on all patients, including infectious ones).

4.6.6.1 Sterilization between patients

Because of the environmental and cost impact of the disposable option (20,000,000 disposable breathing circuits per year in the US alone will quickly overflow a landfill and represent a waste of oil-derived plastics), sterilization of a reusable circuit is first considered.

4.6.6.1.1 The NASA circulating ETO sterilization method

Researchers at the National Aeronautics and Space Administration (NASA) have recently described a method of circulating a sterilizing gas containing ethylene oxide (ETO) and a chlorofluorocarbon through laboratory and medical equipment (Lyndon B Johnson Space Center 1991). The researchers claim that the method is suitable for sterilization of bioreactors, heart/lung machines, dialyzers and other equipment with complicated internal tubing or piping. The sterilizing gas is only circulated through the parts to be treated. Claimed advantages are: (a) exposure of personnel to ethylene oxide which is toxic is minimized, (b) it maintains a sterilizing concentration of gas in restricted places and cavities (e.g., a valve manifold) where the volume/surface area ratio is small; in a conventional method without circulation of the sterilizing gas, the concentration of the sterilizing gas will decrease over time in cavities with low volume/surface area ratios and thus not all microbes and viruses might be killed and (c) equipment that does not need to be treated like the exterior surfaces of the anesthesia circuit which have not been in direct contact with the patient's exhaled gases are not

subjected to the unwanted side effects of ethylene oxide or the products of its decomposition.

On close examination, the main novel feature of the NASA sterilization approach is the recirculation of the sterilizing gases through the internal surfaces of the equipment to be treated during the ETO process which is a well established process that requires both warming and humidification. Thus it becomes apparent that the blower in the GRADS design can be used to circulate the sterilizing gas.

Unfortunately, the ETO process requires a long aeration period (conservatively set to at least 24 hours) after exposure to the ETO to ensure that all toxic ETO absorbed by the circuit materials are desorbed before the circuit is reused on a patient. Thus, it would not be economically practical to have an anesthesia delivery system be unavailable for 24 hours after every use of about 1 - 6 hours. Assuming a daily case load of 3 per OR, every OR would require at least 3 anesthesia machines which would be expensive.

4.6.6.1.2 Concept of the breathing circuit module

Consequently, the concept of a plug-in anesthesia breathing circuit module suggests itself as a possible solution. The complete breathing circuit (including CO_2 absorber, heater/cooler, bellows, manual breathing bag, hoses, proportional flow control valve, etc.) could be contained within a module that fits into a rack in the anesthesia delivery system chassis with appropriate snap-on connections for gases (O_2, N_2O, air, He, Xe, CO_2), vacuum and electrical power and input and output signals. Thus, after each case, the breathing circuit module would be removed from its rack and sent to be

sterilized. A clean module would replace the used one and the new case would be ready to start with a completely clean system, including new CO_2 absorbent, with minimum downtime. The breathing circuit module approach should also allay the concerns of those physicians who wonder if the bellows and CO_2 absorber in an anesthesia circuit should also be changed between patients.

The centrifugal blower could be designed to be easily separated in a similar fashion to a kitchen blender where the base contains the drive mechanism and the top holds the spinning blades. The blower blades would then be part of the breathing circuit module while the variable speed drive motor and controls would stay with the anesthesia machine chassis. Thus, the sterilizing machine would have an identical drive mechanism for the blower blades and use the blower blades in the breathing circuit module to circulate the gases during the modified ETO process. A closed loop control system would maintain the desired ETO concentration in the circuit during sterilization. The ETO would be introduced via the snap-on gas connections in the module.

The breathing circuit module concept has other advantages. It allows modular manufacture of the breathing circuit. It could also potentially be used as a transport ventilation system when the patient is moved from the OR to the recovery room. However, if the transport ventilator option is to be implemented, the material/gas partition coefficient of the circuit materials must be extremely low so that they do not store volatile anesthetics which are then released after the operation is over, which would prolong the emergence period for the patient and cause possibly lethal consequences in the recovery room.

4.6.6.2 The disposable option

The disposable option could be implemented by simply discarding the breathing circuit module described in the previous section. Obviously, the design for a disposable breathing circuit module would use different materials and lifetime specifications with the objective of minimizing cost.

4.7 Flowchart of the Design Methodology

The design methodology that was taken to arrive at the design for GRADS is formalized into the flowchart of figure 37. First of all, the design objectives to be emphasized were chosen. In the case of GRADS, the primary objectives were efficient use and reduced emissions of volatile anesthetics and a flexible and safe life support system geared for the needs of anesthesia.

The system design process was then made manageable by splitting the system into as many independent subsystems as possible. The subsystems specifications were then set and each subsystem designed, one at a time. Each subsystem design was then checked for possible undesirable interactions with other subsystems (existing or envisaged). If a conflict or undesirable interaction existed, other design alternatives were considered until there was no unwanted interaction between each subsystem. Each subsystem design was then checked to see if it met the subsystem design specifications, with the possibility of altering the subsystem specifications if they cannot be met by any of the design alternatives. When all subsystems have been designed, the entire system is evaluated and the whole process is repeated if the system specifications have not been

achieved. The evaluation of the subsystem and system design is accomplished at two

different levels as shown in the flowchart.
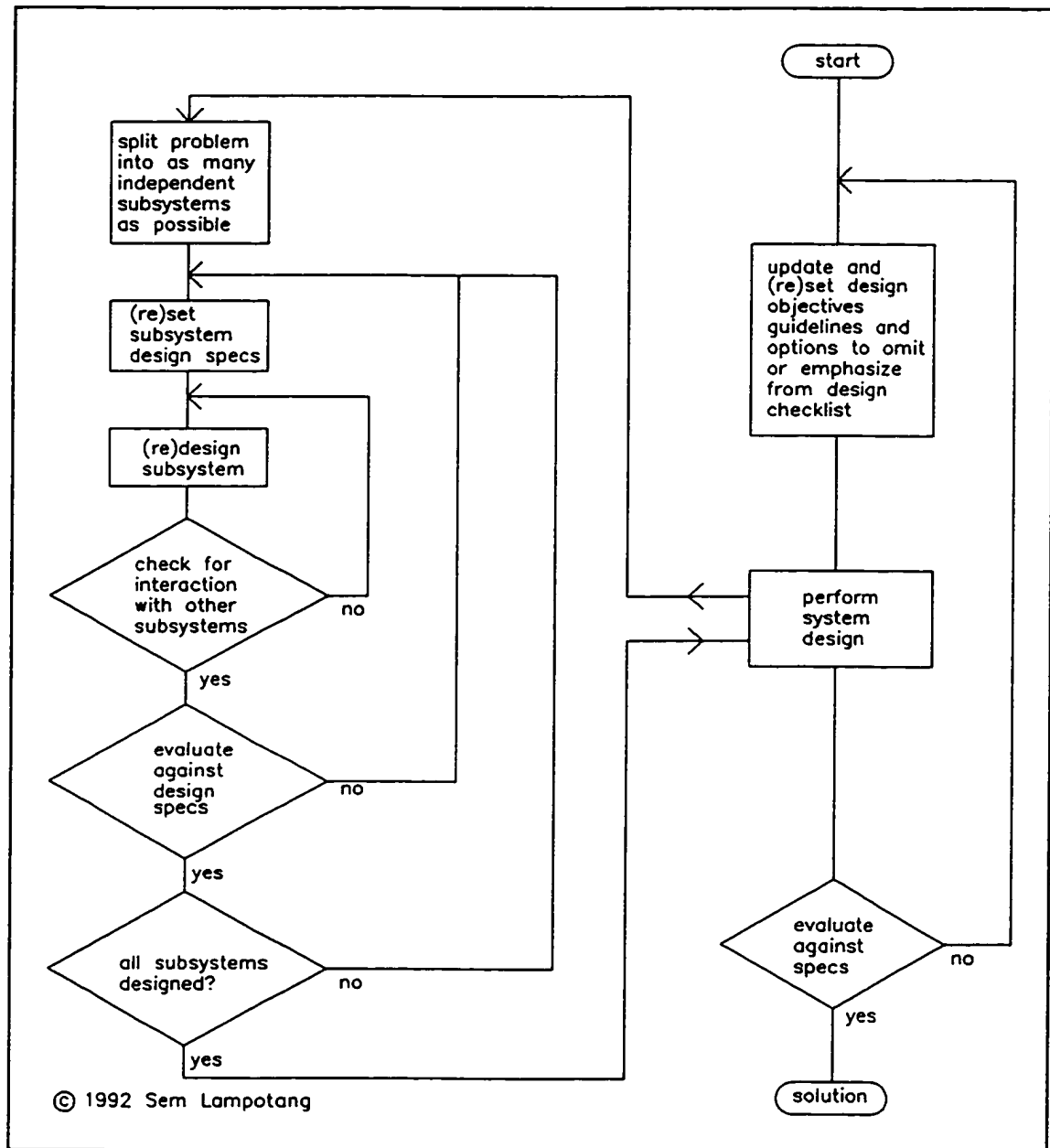
Figure 37. The flowchart of the design methodology that was used to arrive at the proposed anesthesia delivery system design

4.8 Summary

A design methodology for an anesthesia delivery system based on a comprehensive design checklist has been established and documented. A conceptual design exercise for a new anesthesia delivery system platform was carried out using the proposed design methodology.

The expected advantages of the system are (a) reduced operational costs through more efficient use of expensive anesthetics, (b) inherently safer operation (inherent limitation of PIP via default blower speed, ability to mechanically ventilate without compressed O_2, ability to mechanically ventilate with room air, automatic abortion of mechanical inspiration during an O_2 flush, reduced risk of an airway fire during an O_2 flush, ability to generate PIPs up to 100 cm H_2O), (c) reduced spontaneous work of breathing, (d) improved user interface (single ventilation mode selector switch, manual bag connected into the circuit at all times, closed circuit anesthesia with minimal user input or supervision, no insidious augmentation of VT with FGF), (e) improved real world interface (ease of communication to an expert system shell or performing a semi-automated pre-use check), (f) flexibility (closed circuit, open circuit, HFV and CFAV ventilation) and (g) reduced anesthetics emission through efficient use of volatile anesthetics.

Some general design philosophies solidified themselves during the design process and are worth mentioning at this point. These are: (a) go to the source, i.e., if the purpose is to measure the airway pressure in the lungs, then measure the pressure at the lungs or if that is not physically possible, then get as close to the source as possible, i.e.,

the ETT distal tip, (b) adopt the WYSSIWYG (what you set and sample is what you get) design philosophy. In other words, it is not acceptable that VT delivery is affected by FGF, T_i and breathing circuit compliance and PIP. The user should get what is set, (c) as an extension of (b), the user should make the decisions for the settings of the feedback control loops and (d) always warn the user if a safety measure has been activated (e.g., anesthetic gases being spilled by an overloaded or malfunctioning scavenging system).

The next chapter will focus solely on a theoretical analysis of the interactions of inspiratory waveform shape and other ventilatory parameters like inspiratory time and inspiratory pause on distribution of ventilation and mean lung pressure during mechanical ventilation.

CHAPTER 5
THEORETICAL ANALYSIS OF MECHANICAL INSPIRATION:
PROPOSED HYPOTHESIS, LUNG CLASSIFICATION,
WAVEFORMS AND CLASS IDENTIFICATION ALGORITHMS

This chapter is the result of an investigative analysis during the design process for the GRADS system of the benefits of inspiratory waveform shaping during mechanical ventilation (section 2.3.4), in anesthesia. Incorporating the latter feature in an anesthesia ventilator (which is offered by ICU ventilators but not by anesthesia ventilators at the time of writing) was being considered and would have been a novelty in itself. But the fundamental question remained to be answered whether the expense and effort of adding inspiratory waveform shaping would be justified by its scientific merit or whether it would be just a marketing gimmick.

An extensive survey of the current literature and state of the art was inconclusive, with conflicting conclusions drawn by different researchers about the benefits of inspiratory waveform shaping. Consequently, a computer model was written to specifically analyze the benefits of inspiratory waveform shaping. The computer analysis generated interesting data from which new concepts, physical and mathematical insight, inspiratory waveforms and algorithms were derived, to the point that it became necessary to allocate a complete chapter to the issues of inspiratory waveform shaping.

Thus, this chapter departs from the previous format of the dissertation in the sense that it is self-contained and has its own literature review and results section. In this chapter, the theoretical clinical relevance and constraints of inspiratory waveform shaping during mechanical ventilation are first described in more depth than section 2.3.4 covered. The current state of the literature on distribution of ventilation in lungs of unequal time constants during the inspiratory phase of mechanical ventilation is then reviewed. A theoretical analysis of the dynamic response of lungs with unequal time constants to inspiratory waveform inputs (both pressure and flowrate) follows, based on the assumptions of linear lung-thorax compliances and linear flow resistances of the respiratory pathways.

The lung-thorax compliance curve is actually sigmoidal in shape on a pressure-volume plot (see figure 39) while the flow resistance curve is really curvilinear on a flowrate-pressure plot. When assuming a linear compliance, a straight line is fitted to the linear portion of the sigmoidal compliance curve. For a linear flow resistance assumption, a straight line is fitted to the curvilinear resistance curve over the expected flowrate range. The consequences and justification of the assumptions of linear compliance and resistance are described in more detail in section 5.4.1.

The results of the analysis using a computer model suggest that a lung classification scheme based on lung configuration would be clinically relevant if ventilatory therapy procedures and parameters like inspiratory pause (IP), inspiratory time (T_i) and inspiratory flowrate waveform (IFW) are not to be applied indiscriminately, in everyday clinical practice.

The computer modelling gave more insight into the physical problem and led to a mathematical analysis in the time domain which produced exact solutions, based on the assumptions of linear compliances and resistances, that corroborated the results of the computer model, for specific cases. A consistent, unified and global picture began to crystallize which was confirmed when the existing literature was then reviewed again in the light of the results from the computer and mathematical analysis.

A unifying hypothesis based on the proposed lung classification scheme is presented that reconciles the conflicting results obtained by different researchers. A new class of time-dependent, inspiratory waveforms is identified which, according to the hypothesis, should improve the distribution of ventilation and hence the delivery of anesthetics and ventilation, for a given lung class. Finally, software algorithms for systematic identification of the lung class, using the ventilator as a respiratory diagnosis platform are presented as a tool to help the clinician choose the best course of ventilatory therapy for the given lung class of the patient.

5.1 Terminology

Before we start we set some standard engineering conventions and terminology which are explained here for the benefit of the non-engineering, medical readers. The 'r' and 'l' suffixes will be consistently used to denote the right and left part of the respiratory system (see figure 38; p208). Thus, the volume in the right lung will be denoted by $V_r(t)$ where the (t) indicates that the volume in the right lung is a function of time (t), i.e., changes with time. Similarly, the volume in the left lung is $V_l(t)$. The

volume in the right lung at the end of inspiration ($t=T_i$) will be denoted as $V_r(t=T_i)$ or simply $V_r(T_i)$. The flow resistances will be denoted by R_r and R_l and the compliances by C_r and C_l. The ventilation distribution ratio is denoted as $R_v(t)$ and is defined arbitrarily as $V_r(t)/V_l(t)$. The pressure at the Y-piece is $P_y(t)$ and at the carina is $P_c(t)$. The flowrate at the Y-piece, ETT and carina is $Q_{ca}(t)$ since, assuming no fistula (leak) and compression and through the continuity equation, the flowrates will be identical at those three points in the respiratory network of figure 38. The pressures and volumes in the right and left lungs are $P_r(t)$ and $P_l(t)$ and $V_r(t)$ and $V_l(t)$ respectively. The flowrates in the right and left bronchi are $Q_r(t)$ and $Q_l(t)$ respectively (see figure 38).

The time constant for the right and left respiratory pathway are denoted as τ_r and τ_l respectively, where $\tau_r = R_r C_r$ and $\tau_l = R_l C_l$. The effective flow resistance and compliance of the parallel network, i.e., the entire respiratory system, represented in figure 38 are symbolized by $R_e(\omega)$ and $C_e(\omega)$ where the 'e' subscript implies effective and the (ω) signifies that R_e and C_e are functions of the frequency (ω) of the forcing function at the carina or Y-piece, i.e., the respiratory rate. In general, R_e and C_e will be functions of the forcing input frequency, unless $\tau_r = \tau_l$ (Otis et al. 1956).

There is a term existing in the current literature called the mean airway pressure (MAP) which is implied to be the time average of the pressure in the airway. The MAP is supposed to be an indication of the average pressure in the lungs. A high MAP (>15 cm H_2O) is clinically not recommended because of its undesirable effect on venous return, cardiac filling and cardiac output, in general, since the heart and the lungs share the same cavity, i.e., the thorax and can mechanically compress each other. In current

anesthesia and ICU ventilators, the "airway" pressure is measured at the Y-piece or even inside the ventilator. Thus, the MAP is not only a function of the pressure in the lungs but also of the flow resistance of the ETT and the flowrate passing through the ETT.

The time averaged pressure in the trachea sampled at the ETT distal tip provides a better indication of the mean pressure in the lungs compared to the conventional MAP incorrectly sampled at the Y-piece or breathing circuit because the resistance of the ETT is bypassed and the flowrate at the ETT is no longer an artifact. To differentiate between those two pressures, we introduce the term mean intratracheal pressure, MITP(t), which is simply the time average of the pressure in the trachea which is itself a function of time (figure 38). In actual clinical practice, the mean lung pressure, MLP(t), is not available and is inferred from MITP(t) sampled at the ETT distal tip. Finally, for convenience, an equal compliance, unequal resistance lung configuration will be abbreviated to ECUR and an unequal compliance, equal resistance lung configuration is denoted as UCER.

5.2 Introduction

From an engineering point of view, the purpose of inspiratory flowrate waveform shaping in lungs of unequal time constant (section 2.3.4) is to match the ventilation (gas "flowrate") to the perfusion (blood flowrate) in the lungs with the objective of improving the mass transfer rate and efficiency in either direction (i.e., removal of CO_2 and anesthetics; inflow of O_2 and anesthetics) at the blood/gas interface.

Mechanical factors like compliance and flow resistance affect the distribution of pulmonary ventilation (Otis et al. 1956; Lyager 1968; Banner & Lampotang 1988). In disease or injury, the lungs of a patient may have markedly different compliances or flow resistances. For example, one bronchus may have more flow resistance due to swelling of its mucous membrane that constricts its flow area or one lung could be less[1] compliant due to trauma or aspiration of gastric acid from the stomach. A lung with a shorter time constant, τ (lower resistance and/or lower compliance since $\tau = RC$) will build up pressure at a faster rate than a longer time constant lung when both are exposed to a common pressure or flowrate input at the trachea or carina (the Y-shaped location where the bronchi join with the trachea, figure 38).

Consequently, the distribution of ventilation in the lungs can become unequal, i.e., the volume in the right lung at the end of inspiration, $V_r(T_i)$, may not be equal to the volume in the left lung, $V_l(T_i)$, where the sum of $V_r(T_i)$ and $V_l(T_i)$ is the tidal volume (VT). In a normal, healthy individual where the flow resistances of the respiratory pathways and the compliances of the lungs are similar, the ventilation distribution ratio $R_v(t) = V_r(t)/V_l(t)$ approximates unity at all times during inspiration (Otis et al. 1956).

---

[1] Essentially, the surfactant normally present in a healthy lung, with a surface tension lower than water, is washed away by water resulting from the edema that accompanies trauma to the lung. The Laplace equation for a bubble is adapted to a liquid-lined spherical alveolus ($P = 2T/r$ where $P =$ pressure inside the bubble, $T =$ surface tension and $r =$ alveolar radius (West 1974, 94); the constant in the numerator is 2 instead of 4 as in the original Laplace equation because only one surface is involved). The increase in surface tension causes the pressure inside the alveoli to increase so that gas then flows from the alveoli at higher pressure to those at lower pressure. This causes the alveolar radius to decrease which in turn causes the pressure inside the alveoli to increase further leading to reduced compliance. Only in the case of a large tear with a significant leak will the lung compliance appear to "increase".

If both lungs receive similar blood perfusion rates, i.e., the same proportion of the cardiac output (the volume of blood pumped by the heart per unit time: about 5 l/min in an adult) but different gas volume rates (ventilation), there is an undesirable ventilation/perfusion ratio mismatch. If one considers the lungs as a mass exchanger, this mismatch degrades mass transfer rate (gas exchange) and efficiency. Less CO_2 (and gaseous and volatile anesthetics during emergence) come out of solution from the blood and less O_2 (and gaseous and volatile anesthetics during anesthesia) dissolve into the blood per unit time. Although the body's compensatory mechanisms will shunt the perfusion to favor the better-ventilated lung, there is a limit to that self-regulatory action which is depressed by some anesthetics. Improvement of the distribution of ventilation towards an $R_v(T_i)$ of 1.0 by mechanical means, e.g., inspiratory waveform shaping during mechanical ventilation, is therefore desirable.

Another parameter that must be considered during mechanical ventilation is the mean pressure in the lungs over time. Higher mean lung pressures, MLP(t), during mechanical ventilation reduce the cardiac output by interfering with the filling and emptying of the heart (Nunn 1987, 374) and should therefore be minimized during mechanical ventilation (Kirby et al. 1975). Thus, the engineering design objective can be concisely stated as: equalize the distribution of ventilation in lungs of unequal time constants while minimizing the mean lung pressure.

5.3 Literature Review

Numerous studies have been performed on the effectiveness of inspiratory waveform shaping as a means of reducing maldistribution of ventilation. The studies include theoretical analyses using phasor theory (Otis et al. 1956), Laplace transforms (Baker & Hahn 1974) and Fourier analysis (Bergman 1984). Other researchers relied on experimentation with mechanical analogues (Otis et al. 1956; Herzog & Norlander 1968; Lyager 1968; Hedenstierna & Johansson 1973; Sullivan, Saklad & Demers 1977; Dammann & McAslan 1977; Banner & Lampotang 1988), analog computer models (Baker & Hahn 1974), digital computer models (Jansson & Jonson 1972); animals (Baker, Wilson & Hahn 1974; Baker et al. 1977a, Baker, Colliss & Cowie 1977); healthy human volunteers (Rehder at al. 1981) and patients (Otis et al. 1956; Johansson & Löfström 1975; Fuleihan, Wilson & Pontoppidan 1976; Dammann, McAslan & Maffeo 1978; Al-Saady & Bennett 1985).

The different papers will be grouped under five main sections according to the method used: mechanical models, mathematical and computer models, animals, volunteers, and patient data. Within each section, the studies are chronologically arranged, with the oldest appearing first. Where applicable, the lung configuration in each work (e.g., equal compliance, unequal resistance (ECUR); unequal compliance, equal resistance (UCER); etc.) will be emphasized since it will have a major bearing on each set of results. As each work is reviewed, it is critiqued in light of the computer model analysis that will be described in section 5.4 so that a global and unified picture of the pre-existing work can emerge as we proceed with the literature review.

5.3.1 Pioneering Work

Otis et al. (1956) laid the foundation for understanding the effect of mechanical parameters like compliance and flow resistance on the distribution of pulmonary ventilation during mechanical ventilation. The work of Otis et al. is among the earliest papers on the subject and is the most commonly cited work in the field. The authors were extremely thorough and developed first a mathematical model based on an electrical analogy, then verified the predictions of the mathematical model against a double-compartment mechanical model and finally performed experiments on human subjects.

The mathematical analysis of Otis et al. rested entirely on the assumption of linear compliances and resistances which allowed an electrical analogy to be used for deriving the equations governing the dynamic response and mechanical characteristics of the system (figure 38). After laying out the electrical analogy to the physical problem, Otis et al. (1956, 428) stated that " ... if the pattern of applied pressure is known, it is not possible in general to construct the associated pattern of volume change ... in any simple fashion ...". Thus the researchers chose to limit themselves to a sinusoidal pressure pattern because it would allow them to readily apply the electrical phasor theory to obtain equations that describe the behavior of the analogous electrical network.

It turns out that Otis et al. did not pursue the mathematical analysis far enough. If the problem is cast as an initial value problem for a first order linear ordinary differential equation and the integrating factor method is used, exact analytical solutions for pressure waveform inputs other than the sinusoid are readily obtained which enhance

the understanding of the dynamic response of a parallel network with unequal time constant respiratory pathways. These will be described in section 5.6.

Using the phasor theory for analyzing alternating current electrical networks (Laycock 1976; Johnson et al. 1986), the equivalent or effective compliance (C_e) and resistance (R_e) for two pulmonary pathways (with dissimilar and frequency-invariant resistances and compliances) connected in parallel and sharing a common sinusoidal forcing function (figure 38) were obtained. R_e and C_e were observed to be dependent on the frequency of the sinusoidal forcing function if the time constants of the individual pathways were unequal.

Otis et al. validated their own mathematical analysis with a mechanical model consisting of a pair of rubber bellows encased in a rigid box that simulated the common intrapleural space. The bellows were connected in parallel like in figure 38 via flow resistances made by mounting discs of sintered bronze or of wire gauze in the lumen of 2.38 cm (15/16") i.d. brass tube. The forcing function was a sinusoidal pressure waveform imposed indirectly by a compressor connected to the rigid box enclosure. It was observed that the separate flowrates in each "bronchus" were in phase with each other and with the combined flowrate in the "trachea" when the time constants were equal. The phenomenon of pendelluft was also observed, i.e., gas flows from one compartment to another because a pressure differential exists between the two compartments. The effective compliance and resistance of the mechanical model, i.e., the parallel pathway network, diminished with increasing frequency of the forcing

sinusoidal function from the compressor, thus confirming the researchers' own initial

mathematical predictions.
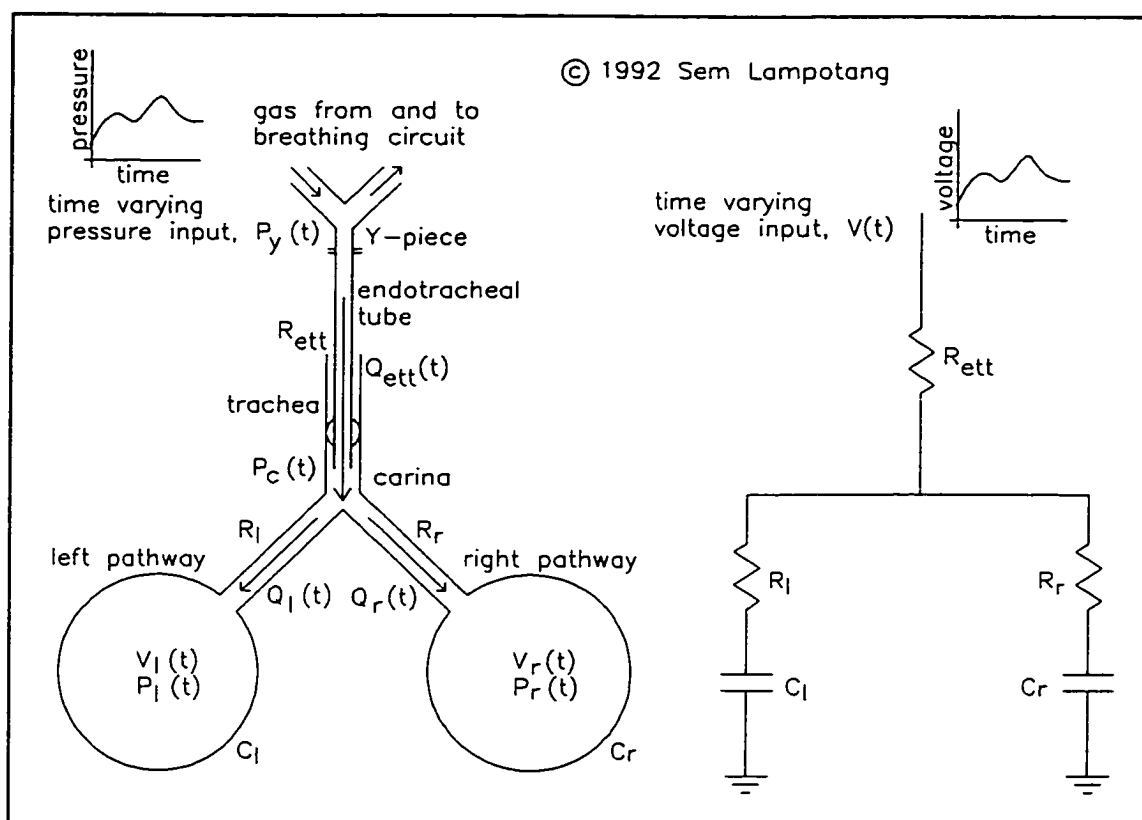
Figure 38. The electrical analogy employed by Otis et al. (1956) for analyzing the behavior of two pulmonary pathways connected in parallel, extended for the computer and mathematical analysis

Finally, Otis et al. tested their theory on patients. After inserting a flow

resistance in the left bronchus of a patient, a phase difference in the separate flowrates

in each bronchus was observed which was qualitatively similar to the predictions of the

theoretical analysis and the mechanical lung model. Next, the authors demonstrated that

there was no significant change in compliance with increasing frequency (2 - 100 breaths

per minute) for normal healthy adults with lungs of similar time constants. The normal subjects then inhaled a 3% histamine (bronchoconstrictor) aerosol dose sufficient to produce a two- to threefold increase in resistance as measured during quiet breathing. As a result, and in accordance with the theory, a definite and progressive fall in pulmonary compliance was observed as the rate of breathing increased.

Similarly, a patient with bronchial asthma and a patient with advanced pulmonary emphysema both exhibited decreased compliance at higher respiratory frequencies. The investigators concluded their tests with patients by looking at the fall in compliance with increasing frequency in an asthmatic patient before and after administration of a bronchodilator (1:100 adrenaline aerosol). As predicted by theory and the mechanical model, the fall in compliance with increasing frequency after administration of the bronchodilator became less steep.

5.3.2 Mechanical Models

5.3.2.1 Herzog and Norlander (1968)

A mechanical model consisting of two 50-liter glass bottles, each filled with water to obtain a compliance of 0.025 l/cm H_2O, was connected in a parallel network that included flow resistors similar to figure 38. The model also used a piece of plastic tubing called a shunt tube to connect the two glass bottles directly to each other, i.e., the shunt tube was in parallel to the path formed by the "bronchi". The authors stated that the shunt tube creates conditions similar to a local decrease in lung compliance with uneven ventilation.

The compliances were equal at 0.025 l/cm H_2O but the flow resistances were set at 2 and 20 cm $H_2O/l/s$ so that the time constant of one respiratory pathway was ten times that of the other (if one ignores the controversial shunt tubing that was used). The authors claim that with this equal compliance, unequal resistance (ECUR) configuration, an increasing flowrate waveform with an inspiratory pause gave equal distribution of ventilation, i.e., $R_v(T_i) = 1.0$ whereas the constant ("square") flowrate waveform gave an $R_v(T_i)$ of 1.65, 1.75 and 2.0 at constant flowrates of 0.475, 0.8 and 0.950 l/s.

The experimental protocol of Herzog and Norlander was controversial from the start because of the use of the shunt tube and the lack of rigor. The authors' justification for the shunt tube is vague but appears to imply that without the shunt tube, each glass bottle would fill independently whereas in real life, the faster filling lung will cause a decrease in compliance by mechanically compressing the slower filling lung because both share the same body cavity, i.e., the thorax. The addition of an inspiratory pause to the increasing flowrate waveform when comparing it with the constant flowrate waveform is confusing because it makes it impossible to pinpoint whether the more equal distribution was due to the inspiratory pause or the increasing flowrate waveform. Furthermore, the total inspiratory time for the increasing flowrate waveform with pause was 1 second with an increasing flowrate for 0.5 second followed by an inspiratory pause with zero flowrate at the ETT for the remaining 0.5 second. For the constant flowrate waveform, the inspiratory times varied at 0.96, 0.69 and 0.57 seconds for constant flowrates of 0.475, 0.8 and 0.95 l/s respectively. Thus, the T_is were not the same within a group and between groups which was another confounding influence.

The authors incorrectly concluded that an increasing flowrate waveform provided better distribution of ventilation ($R_v(T_i)$ closer to 1.0) than a constant flowrate waveform. Actually an increasing flowrate waveform provides an $R_v(T_i)$ further from 1.0 (i.e., more unequal distribution) than a constant flowrate waveform for an ECUR lung. This latter statement was proven by the later work of Hedenstierna and Johansson (1973; section 5.3.2.3) who repeated Herzog and Norlander's work but without the shunt tube and will also be confirmed by the computer model analysis later in this chapter (section 5.4).

The authors did make the correct observation with their mechanical model that the supposedly high "airway" pressures with an increasing flowrate waveform are actually not transmitted to the alveoli, thus disproving the hypothesis held at that time that an increasing flowrate waveform was more prone to cause ruptures and lesions of the alveoli compared to a constant flowrate waveform. What the authors failed to explain is that the higher peak pressures seen with an increasing flowrate waveform are actually caused by the resistance of the ETT (figure 38) and the higher flowrates that are delivered towards the end of the inspiratory period for a constant VT and T_i, compared to a constant flowrate waveform (see figure 2). As can be seen from figure 2, the peak flowrate, Q_{max}, for an increasing flowrate waveform will be twice that of the constant flowrate waveform, all other factors being kept constant.

As will be proven later, the increasing flowrate waveform generates the lowest mean lung pressure, $MLP(T_i)$, during the inspiratory period among the 4 basic flowrate waveforms shown in figure 2, although if pressure is sampled at the Y-piece or in the ventilator, it will appear that the increasing flowrate waveform has the highest "MAP".

This pressure measuring artifact through the interaction between the inspiratory flowrate at the ETT and the flow resistance of the ETT also speaks in favor of pressure sampling at the ETT distal tip (section 4.3.9.1) which will eliminate the artifact.

5.3.2.2 Lyager (1968)

Instead of using glass bottles and relying on the compliance of a large volume of air, Lyager (1968) made his lungs out of two concertina bellows with identical mechanical properties housed in an airtight box. The compliance of the concertina bellows was independently modified by changing the external linear spring that compressed the corresponding concertina bellows. The flow resistances in the mainstem bronchi were independently adjusted by inserting shutters of different sizes into them. The experimental set up was geometrically similar to figure 38.

From the experimental results, the author concluded that for an ECUR lung configuration, the distribution of ventilation ($R_v(T_i)$) is more uneven for an increasing flowrate waveform compared to a constant flowrate waveform; this result is in contradiction with the results obtained by Herzog and Norlander (1968) but consistent with the computer analysis of section 5.4.

The author's conclusions that (a) with an UCER lung configuration, an increasing flowrate provides better distribution than a constant flowrate waveform and an inspiratory pause is to be avoided and (b) with an ECUR lung configuration, a constant rather than an increasing flowrate and an inspiratory pause will both favor better distribution are consistent with the predictions of the computer analysis in section 5.4.

5.3.2.3 Hedenstierna and Johansson (1973)

A mechanical model similar to that used by Herzog and Norlander (1968; section 5.2.3.1) was used without a shunt tube. Two 60 l glass bottles were partly filled with water to obtain a compliance of 0.025 l/cm H_2O in each bottle and the "bronchial" flow resistances were 2 and 40 cm $H_2O/l/s$ such that the time constant of one respiratory pathway was 20 times that of the other. The flow resistance of the trachea was set at either 15 or 35 cm $H_2O/l/s$. Thus the lung configuration was similar to the one used by Herzog and Norlander (1968): equal compliances, unequal resistances (ECUR). As in the case of Herzog and Norlander (1968), the authors were depending on the "compliance" of the air to modulate compliance. Because of the stiff walls of the glass bottles, the volume introduced into each "lung" could be determined from the pressure rise.

The authors used three different inspiratory flowrate waveforms: increasing, decreasing and constant maintained at 25% of the respiratory cycle as well as an inspiratory pause of 10% of the respiratory cycle. In a first series of experiments, the minute ventilation was kept constant at 12 l/min. The decreasing flowrate waveform had an $R_v(T_i)$ closest to 1.0 followed by the constant and the increasing flowrate waveforms, both before and after an inspiratory pause for breathing frequencies of 12, 18 and 24 breaths per minute and at both tracheal flow resistances. The results of Hedenstierna and Johansson are consistent with the work of Lyager (1968) and the predictions of the computer analysis performed in section 5.4 of this chapter.

5.3.2.4 Dammann and McAslan (1977)

The mechanical model was geometrically similar to figure 38 and was set up as an ECUR lung configuration. The interesting feature of the study was that the distribution of ventilation was inferred from the washout rate of nitrogen from each lung using two separate mass spectrometers.

A comparison was performed of the washout rate with an increasing and a constant flowrate waveform where the inspiratory time was 25% of the respiratory period and an inspiratory pause of 10% followed both waveforms; no significant difference was observed in the washout rate of nitrogen. From this experiment, the authors incorrectly concluded that the shape of the flowrate waveform does not affect the distribution of ventilation. The investigators missed the point (that they themselves make later on) that an inspiratory pause will improve distribution of ventilation.

Consequently, it is likely that the inspiratory pause compensated for the differences in distribution of ventilation between each waveform and made $R_v(T_i)$ become unity (1.0) for both waveforms, which would explain why the washout rate was the same for each waveform. According to the results of Lyager (1968), Hedenstierna and Johansson (1973) and the computer analysis in section 5.4, if the authors had used no inspiratory pause after each waveform, they would have obtained a faster washout rate with a constant flowrate waveform compared to the increasing flowrate waveform.

An inspiratory pause improved the rate of washout, i.e., the distribution of ventilation and the washout rate became steeper as the duration of the inspiratory pause lengthened. The authors were bold enough to identify an "optimal" flowrate pattern

(increasing flowrate with a 10% or more inspiratory pause where the total inspiratory time is kept at less than 33% of the respiratory period) from their experiments with a mechanical lung model set in only one configuration: ECUR. As will be shown in the computer analysis of section 5.4, this advice is too sweeping and clinically incorrect because an increasing flowrate waveform will actually provide worse distribution of ventilation with an ECUR lung configuration. Furthermore, as already shown by Lyager (1968) and as is corroborated by the computer simulation of section 5.4, an inspiratory pause degrades the distribution of ventilation for an UCER lung configuration and would definitely not be indicated for such a patient.

5.3.2.5 Sullivan, Saklad and Demers (1977)

The lung model was geometrically similar to figure 38. The lungs consisted of metal chambers with an ECUR lung configuration. Three flowrate waveforms were used: constant without an inspiratory pause, increasing with an inspiratory pause and half-sine $(0-\pi)$ without an inspiratory pause. The presence of the inspiratory pause precludes any meaningful comparison between the results from the increasing waveform and the other two waveforms. The most significant finding of the study was that an increased respiratory frequency, while keeping VT fixed, will make the distribution of ventilation worse in an ECUR lung configuration. This observation can be explained by the fact that T_i decreases with increasing breathing rate and is consistent with the predictions of the computer analysis in section 5.4.

5.3.2.6 Banner and Lampotang (1988)

The experiments were performed with a mechanical lung model modified to "produce" CO_2 and with independently adjustable compliances and flow resistances (Lampotang et al. 1986). $ETCO_2$ was used as a measure of the distribution of ventilation, with a 100 ml/min inflow rate of CO_2 into each lung representing the equal "blood perfusion" rate of each lung. A higher $ETCO_2$ implied more unequal distribution of ventilation when all other parameters were kept constant.

The experimental data indicated that a decreasing inspiratory flowrate waveform provided the most equal ventilation distribution with an equal compliance, unequal resistance (ECUR) lung configuration when all other parameters were kept constant. The decreasing flowrate waveform gave the lowest $ETCO_2$, followed by the constant and half-sine $(0-\pi)$ (no significant difference between the constant and half-sine $(0-\pi)$ flowrate waveforms if one takes into account the standard deviations on the $ETCO_2$ readings). The increasing flowrate waveform gave the highest $ETCO_2$. These results are in agreement with the work of Hedenstierna and Johansson (1973) and the computer analysis of section 5.4.

PIPs measured at the Y-piece were from lowest to highest in the following order: decreasing, half-sine $(0-\pi)$, constant and increasing which was also consistent with the computer analysis of section 5.4.

This completes the literature review on the mechanical models. As can be seen, a unifying picture is developing as the contradictory results from different researchers are consistently explained within the framework of the computer analysis of section 5.4.

5.3.3 Mathematical and Computer Models

5.3.3.1 Jansson and Jonson (1972)

A digital computer was used to model the equations describing a pulmonary network similar to figure 38. The lungs were contained within a thoracic cage with a compliance denoted by C_{th}. It is interesting to note that the computer model used resistance values which were dependent on flowrate and volume in the lung, i.e., $R_r(V_r(t), Q_r(t))$ and compliance values which were dependent on the volume in the lung, i.e., $C_r(V_r(t))$. Thus, the resistance and compliance values were indirectly time-dependent too since volume and flowrate change with time. The time step size for the calculations was 0.01 seconds.

The computer simulation confirmed the results obtained by Lyager (1968) with a mechanical model and the predictions of the computer analysis in section 5.4. For example, with an ECUR lung configuration, a low flow rate, a long T_i and an inspiratory pause promote more even distribution of ventilation whereas these same features actually cause more uneven distribution of ventilation with an UCER lung configuration. It was also observed that for an ECUR lung configuration, a better $R_v(T_i)$ is obtained by adding an inspiratory pause rather than by increasing the T_i by the time period of the inspiratory pause or by using a decreasing flowrate waveform. Both observations are consistent with the computer analysis in this chapter. Further, it was observed that the lowest mean lung pressures were obtained with an increasing flowrate waveform, which is also in agreement with the results from the computer model in section 5.4.

5.3.3.2 Bergman (1984)

Bergman (1984, 174) introduced his fairly recent work with one sentence that is an accurate description of the state of confusion in the area of inspiratory waveform shaping: "The potential for the shape or pattern of the respiratory waveform to influence the efficiency of pulmonary gas exchange during artificial ventilation lingers as an unresolved problem in clinical respiratory physiology." Bergman used the same electrical analogy as Otis et al. (1956; figure 38). Using a program written in BASIC computer language and implemented on a DEC PDP-11 computer, Bergman employed Fourier analysis to decompose each of 4 pressure waveforms (constant, half-sine (0-π), increasing, decreasing) into a Fourier series of 10 harmonics. The individual responses of the electrical circuit analogue to each of the 10 harmonics of a given waveform were then added to obtain the total dynamic response.

Bergman also analyzed two other waveforms but used an inspiratory pause in one and shortened T_i in the other so that they cannot be really used for any meaningful comparison of the effect of inspiratory waveform on distribution of ventilation. It is likely that Bergman chose to use a pressure (voltage) waveform rather than a flowrate (current) waveform because flowrate shaping is more involved to program as is explained in section 5.4.4 which describes the computer modelling.

Bergman found that with an ECUR lung configuration, the $R_v(T_i)$ for different waveforms in the order of closest to 1.0 (most even) to furthest from 1.0 (most uneven) was: square, decreasing, half-sine (0-π) and increasing. Using computer simulations, the decreasing and half-sine (0-π) inspiratory pressure waveforms were shown to be

impractical as mechanical ventilation waveshapes because pressure tails off to ambient towards the end of the inspiratory period whereas the pressures in the lungs will be greater than ambient from the inflow of gas into them during the previous portion of the inspiratory period. Thus, with a half-sine $(0-\pi)$ and a decreasing pressure inspiratory waveform, the computer model in this chapter predicts that gas will actually flow <u>out</u> of the lungs into the breathing circuit towards the latter part of the inspiratory period when the pressure in the lungs will be higher than the pressure in the circuit. Thus, the half-sine $(0-\pi)$ and decreasing pressure waveforms will not be discussed here.

The outflow of gas from the lungs to the breathing circuit during the latter part of the inspiratory period with a decreasing pressure waveform (predicted by the computer model in this chapter) is confirmed by the observation of Bergman that a decreasing pressure waveform delivers the lowest tidal volume of all 4 pressure waveforms for a fixed peak inspiratory pressure (1.93 kPa) and T_i (2 seconds) for both an ECUR lung configuration and an UCER lung configuration.

Furthermore, the more even distribution of ventilation observed by Bergman with the constant compared to the increasing pressure waveforms for an ECUR lung configuration is in agreement with the computer model results of this chapter. However, with an UCER lung configuration, Bergman concluded that the ventilation distribution ratio $(R_v(T_i))$ would be independent of the pressure waveform and would be only dependent on and directly proportional to the ratio of the compliances (C_c/C_i).

Bergman's conclusion is in disagreement with the computer model of section 5.4 which indicates that an increasing pressure waveform will deliver more even distribution

of ventilation than a constant pressure waveform with an UCER lung configuration. Upon closer examination of the raw data plotted by Bergman, it is seen that the increasing pressure waveform data points are consistently closer to an $R_v(T_i)$) of 1.0 compared to the constant pressure waveform data points, for an UCER lung configuration. Thus, although the data points for the different waveforms are clustered close to each other for the UCER lung configurations (which led Bergman to incorrectly conclude that pressure waveform does not affect $R_v(T_i)$ for an UCER lung configuration), the raw data from Bergman support the prediction of the computer model.

We conclude this section on mathematical and computer models by looking back at the work performed with models (theoretical, computer, electrical and mechanical). It is seen that the results are mostly consistent if one discards the work of Herzog and Norlander (1968) which unfortunately was one of the earlier papers and had a lasting confounding influence, especially with their use of a shunt tube. Other apparent discrepancies between the results from different researchers can be readily explained through poor design of the experimental protocol (most commonly, changing more than one parameter at a time during comparative tests). Another confounding influence was the tendency to think only in terms of time constant inequality between the respiratory pathways when the lung configuration through which the time constant inequality is obtained also matters (section 5.4).

Thus, as will be proposed with the computer analysis of section 5.4 and the subsequent mathematical analysis, the results of all previous work with models reviewed up to now, have been unified into a consistent and therefore clearer framework. All the

models used either the mechanical model of Otis et al. (1956) or the electrical analogy of Otis et al. (1956) or some variation of the two. The accuracy of the models as representations of the human lung is another issue which will be addressed in the following sections.

5.3.4 Animal Experiments

Due to the multitude of uncontrolled parameters in an animal experiment, it will not always be possible to directly compare the experimental observations with the results of the computer analysis of section 5.4. The discussion will be brief, with emphasis on the results.

5.3.4.1 Baker, Wilson and Hahn (1974)

Using dogs, the researchers set out to validate the prediction of an electrical analog model (Baker & Hahn 1971) that a step input in pressure or flowrate at the trachea would result in a instantaneous pressure rise in the lungs at the alveolar and pleural levels. At the time of the experiment, it was believed that alveolar pressure changes smoothly during mechanical inspiration, independently of the pressure waveform applied at the breathing circuit.

The authors were able to demonstrate that the esophageal pressure, from which they inferred the alveolar pressure, exhibited a discontinuity (step rise) which was in phase with the applied pressure step at the tracheal pressure. This result is consistent

with the computer model simulation of section 5.4. Thus, the hypothesis that alveolar pressure will always rise smoothly was disproved.

5.3.4.2 Baker, Colliss and Cowie (1977)

Dogs were used to demonstrate the effect of varying inspiratory flowrate waveforms and times on various physiological variables during intermittent positive pressure ventilation while keeping VT and RR constant. Cardiac output and mean airway and intrathoracic pressures were among the physiological variables studied. The airway pressure was sampled at the carina while the intrathoracic pressure was inferred from esophageal pressure sampled by an esophageal catheter probe. It was experimentally observed that an increase in T_i led to an increase in the airway and intrathoracic pressures. The flowrate waveforms studied gave different mean airway pressures with all other parameters kept constant. In order of lowest to highest mean airway pressure, the ranking of the flowrate waveforms was: increasing, half-sine (0-π), constant, and decreasing. This ranking is in agreement with the computer model analysis of section 5.4 although there was no significant difference between the MLP(T_i) of the half-sine (0-π) and constant flowrate waveforms in the computer analysis.

An extremely interesting result was that an increase in mean "airway" pressure measured at the carina, MITP(T_i), caused by an increase in T_i did not decrease cardiac output. But an increase in MITP(T_i) caused by a change in inspiratory flowrate waveform decreased cardiac output. Thus, the influence of the flowrate or more generally the inspiratory waveform on cardiac output via the mean lung pressure

(measured at the carina which provides a more accurate representation of the lung pressure (section 4.3.9.1)) is confirmed with these animal experiments.

5.3.5 Volunteers

Rehder et al. (1981) used the clearance rate of radioactive xenon, ^{133}Xe, after previous equilibration in <u>healthy</u> male volunteers in the right lateral decubitus position to study distribution of ventilation. The latter position was chosen because the authors had "previously observed for this position the most dramatic alteration in gas distribution with induction of anesthesia-paralysis". The volunteers were divided into 2 groups: 5 awake and spontaneously breathing and 5 anesthetized-paralyzed and mechanically ventilated with a constant flowrate waveform at 12 bpm and approximately the same nominal tidal volume as for the spontaneously breathing volunteers (0.7 l).

Three inspiratory flowrates were used on the awake volunteers who were experienced in performing respiratory maneuvers: 0.3-0.5, 0.5-0.8 and 1.0-1.1 l/s. Four inspiratory flowrates were used in the mechanically ventilated volunteers: 0.2, 0.4-0.6, 1.0-1.2 and 1.5-1.8 l/s. Scintillation detectors (four) were mounted on the apical and basal regions of the dependent and non-dependent lungs of each volunteer. The rate of drop of counts on each scintillation detector was fitted to an exponential decay curve. A faster rate of decay of the scintillation counts was taken as better ventilation. The uniformity of ventilation between any two regions is compared by taking the ratio of the cumulative ventilation volume required for the ^{133}Xe to reach 50% of its initial concentration in each region.

Distribution of ventilation was significantly more uniform (p < 0.001) among the dependent/non-dependent lung regions in anesthetized-paralyzed, mechanically-ventilated volunteers than in awake, spontaneously-breathing volunteers. No difference in distribution of ventilation was apparent at the different inspiratory flowrates in either anesthetized or awake volunteers. The authors concluded that "manipulating inspiratory flow during anesthesia-paralysis and mechanical ventilation is not a useful clinical tool to improve pulmonary gas exchange, at least in patients with healthy respiratory systems".

The data were obtained from healthy volunteers who presumably had similar time constants for all lung regions. Therefore, here again, the investigators came to an equivocal conclusion while their experimental data actually support the computer analysis of section 5.4 (table 4) which indicates that for healthy lungs with equal time constants, inspiratory waveform has no influence on $R_v(T_i)$ which is always 1.0.

5.3.6 Patient Data

This is the ultimate test of the validity of all the models described in the previous sections. As with animal experiments, there are always many uncontrolled parameters and thus, a comparative analysis becomes harder to pin down because one cannot always be sure that all other parameters were kept constant.

5.3.6.1 Johansson and Löfström (1975)

The researchers set out to prove that results from an ECUR mechanical model (Hedenstierna & Johansson 1973) could also be demonstrated in patients. Ten supine patients without known cardiac or respiratory abnormalities (i.e., presumably with equal time constant lungs) were studied during intravenous anesthesia and artificial ventilation with three different flowrate waveforms (increasing, constant and decreasing). Breathing rate was set at 24/min with the inspiratory period set at 25% of the respiratory cycle, i.e., the I:E ratio was 1:3. No inspiratory pause or PEEP was used. Lung pressure measurements were correctly made at the trachea by inserting a thin catheter with side holes through the ETT connection.

A paired differences statistical analysis was performed on the experimental results. The authors extrapolated heavily on the results to conclude that an apparent increase in compliance with a decreasing flowrate compared to an increasing flowrate implied better distribution of ventilation. However, according to the computer model of section 5.4, if the time constants of both parallel pathways are identical, then the $R_v(T_i)$ will always be 1.0 irrespective of the inspiratory waveform shape. It is difficult to draw too many conclusions from the work of Johansson and Löfström because the lung configuration is unknown. If the authors had used patients with known respiratory abnormalities like a tumor in the mainstem bronchus that creates a flow constriction, more direct comparison to the ECUR lung configuration used by Hedenstierna and Johansson (1973) could have been performed. The objective of the authors was to identify one optimal waveform for all lung configurations and their closing discussion

suffers from that attempt. Nowhere is the relevance of the lung configuration mentioned even though the avowed objective of the study was to reproduce the results obtained with an ECUR lung model configuration.

5.3.6.2 Fuleihan, Wilson and Pontoppidan (1976)

The effects of an inspiratory pause at the end of mechanical inspiration were investigated with 10 adult patients with "acute respiratory insufficiency". The patients suffered from different respiratory diseases (multiple fractures with left lower lobe atelectasis, Guillain-Barré, chronic obstructive pulmonary disease (COPD), etc.) such that they did not belong to any specific lung configuration. In all the series of tests on one patient, VT, RR, FiO_2 and end expiratory pressure (EEP) were kept constant. PEEP needed to be used in 4 patients such that EEP was not zero. An inspiratory pause of either 0.6 or 1.2 seconds was added to the end of mechanical inspiration.

The statistical analysis of the results was done with Student's t-test for paired data. Cardiac output decreased with EIP as a result of the increased mean airway pressure. The ratio of dead space (V_D) to tidal volume (VT) is an indication of the efficiency of ventilation. A higher V_D/VT indicates worse ventilation. In the patients studied, the V_D/VT ratio and the $PaCO_2$ (partial pressure of CO_2 in arterial blood) decreased in proportion with the duration of the inspiratory pause. However, the efficiency of oxygenation was not improved with an inspiratory pause. The study would have had more scientific value if the investigators had been more selective in their choice of patients.

5.3.6.3 Dammann, McAslan and Maffeo (1978)

Four series of experiments were performed on four groups of patients. The patients were divided into groups according to age and the kind of respiratory disease they had (acute respiratory insufficiency vs. chronic lung disease). In the first series, a half-sine (0-π) flowrate waveform was compared to a constant flowrate waveform while in the second series an inspiratory pause was added to both waveforms of the first series. In the third series, the half-sine (0-π) flowrate waveform was compared to itself but with an inspiratory pause added and in the last series, a half-sine (0-π) flowrate waveform with a long inspiratory pause was compared to one with a shorter inspiratory pause. The rate of washout of argon measured at the airway and in arterial blood was used to assess the efficiency of ventilation and by inference, the evenness of ventilation distribution.

The experimental results were analyzed with a non-parametric statistical test called the Walsh test. The results from the first series indicate that a half-sine (0-π) flowrate waveform provides better distribution of ventilation compared to the constant flowrate waveform which is consistent with the prediction of the computer model of section 5.4 for an ECUR lung configuration. The results from the experiments in the second series show that the inspiratory pause tends to obliterate any effect of the half-sine (0-π) or constant flowrate waveform on distribution of ventilation. Here again, this observation is supported by the predictions of the computer model for an ECUR and an UCER lung configurations (tables 5 and 6).

The investigators observed an improvement in distribution of ventilation with an increased inspiratory pause in the experiments of the third and fourth series. In their

conclusions, the investigators proposed a half-sine $(0-\pi)$ flowrate waveform with an inspiratory pause as the "optimal waveform especially for diseased lungs".

Here again, as with Fuleihan, Wilson and Pontoppidan (1976), the authors never attempted to sort the patients according to their different lung configurations and were trying to identify the "best" waveform for all lung configurations. The patients were selected at random and thus can be assumed to have had random lung configurations too. Consequently, when the data were lumped together for the statistical analysis, the results were to a large extent dependent on the random representation of different lung configurations in that patient sample and therefore random themselves.

5.3.6.4 Al-Saady and Bennett (1985)

Fourteen supine patients were selected on the basis of sex (7 males and 7 females), age (20 - 71 years) and dependence on intermittent positive pressure ventilation to form a representative sample of the patient population, with no regard for the lung configuration, thus unfortunately rendering this study also of limited value as a validation for the predictions of the mechanical inspiration hypothesis. VT, T_i, I:E ratio and RR were kept constant in the study. A decreasing and a constant flowrate waveform were used.

Statistical analysis of the experimental results was done using paired Student's T-test. The decreasing flowrate waveform provided better distribution of ventilation and improved the partial pressure of O_2 in arterial blood. Like their predecessors, the researchers were trying to pinpoint the "optimal" waveform for all lung configurations

and recommended that a decreasing flowrate waveform should be "more generally" employed with patients on mechanical ventilation.

To conclude this section on clinical experiments with human patients, it is unfortunate that all four groups of investigators reviewed were determined to find the one magic waveform that would work for all patients, irrespective of lung configuration. Thus, no attempt was ever made in any of the four clinical studies to select the lung configuration of the patients. This omission is in itself sufficient to explain the conflicting recommendations of Al-Saady and Bennett (1985) and Dammann, McAslan and Maffeo (1978). The results of each study were totally dependent on the representation of different lung configurations which was truly random in the patient samples studied. Thus, the clinical data are of limited value for validation of the mechanical inspiration hypothesis that was developed with the lung models.

This concludes our literature survey of past research into the effect of inspiratory waveform shape on the distribution of ventilation. Numerous other papers exist which were not reviewed because they were not readily available. The papers that were readily available at the Health Center library are assumed to be a representative sample of papers on the subject and have all been reviewed in this section and a cohesive picture has emerged as a result of this undertaking especially in the light of the computer analysis of the following section.

5.4 Computer Model and Analysis

A computer model was written in C++ (Turbo C++ 2.0, Borland International, Inc., Scotts Valley, CA) to simulate and analyze the effects of inspiratory waveform shape, inspiratory time (T_i), inspiratory pause and tidal volume (VT) during mechanical ventilation on any user-selected configuration of lung mechanical parameters. The mathematical model on which the computer modelling is based is similar to that used by Otis et al. (1956) and assumes that compliances and flow resistances are linear and is recommended for situations where the total lung volume is less than 2.0 l above FRC and the inspiratory flowrates are less than 80 l/min.

The computer model was verified to be accurate and consistent with its mathematical model by comparing its results against special cases where exact analytical solutions were readily derivable. To a large extent, the model also agrees qualitatively with experimental and theoretical data existing in the literature.

The computer model runs on an IBM-PC compatible personal computer and outputs graphical displays and numerical values of the pressures, volumes and flowrates in the lungs, bronchi, carina, trachea and Y-piece during mechanical inspiration. The interactive interface and graphical outputs of the computer model make it adaptable as a teaching tool to help medical personnel visualize and understand the complex effects of uneven mechanical parameters on the inflation characteristics of sick lungs.

5.4.1 Assumptions

The flow resistances of the pathways in each lung are lumped into one constant value (i.e., flow is assumed to be laminar with a linear flow resistance curve). Similarly, the compliances of the alveoli in each lung are lumped into a constant; each lung is assumed to be an elastic bladder with a linear volume-pressure plot and a resting (or equilibrium) volume which is defined as the functional residual capacity (FRC). These two starting assumptions allow the classical electrical analogy employed by Otis et al. (1956) (compliance $\equiv$ capacitance, flow resistance $\equiv$ electrical resistance) to be used to set up the mathematical model on which the computer model is based.

The assumptions of linear compliances and resistances introduce limitations which must be analyzed and defined before results obtained with the model can be used with confidence. The lung compliance curve for a healthy, anesthetized patient in the supine position is actually a highly skewed sigmoid with a wide linearly sloping portion that flattens out at the top of the curve as the elastic limit of the lung is approached (Nunn 1987, 38) (figure 39). The inflection point where the compliance curve departs from linearity is approximately at the (30 cm H_2O, 2.5 l above FRC) coordinate for healthy, anesthetized patients in the supine position (Nunn 1987, 38).

The assumption of linear compliance is therefore valid in a healthy anesthetized patient in the supine position, for tidal volumes not exceeding 2.0 l. This conclusion based on analysis of the compliance curves from Nunn (1987), is supported by the observation of Lyager (1968, 204) that "the volume-pressure curve may be regarded as linear when there is a reasonable proportion between the tidal volume and the functional

residual capacity" (which is typically 2.3 1 in an adult (Guyton 1986)). Since, in clinical

practice, tidal volumes during mechanical ventilation rarely exceed 1.0 1, the limitation

of the computer model to total lung inflation volumes below 2.0 1 for healthy adult

patients is not overly restrictive.
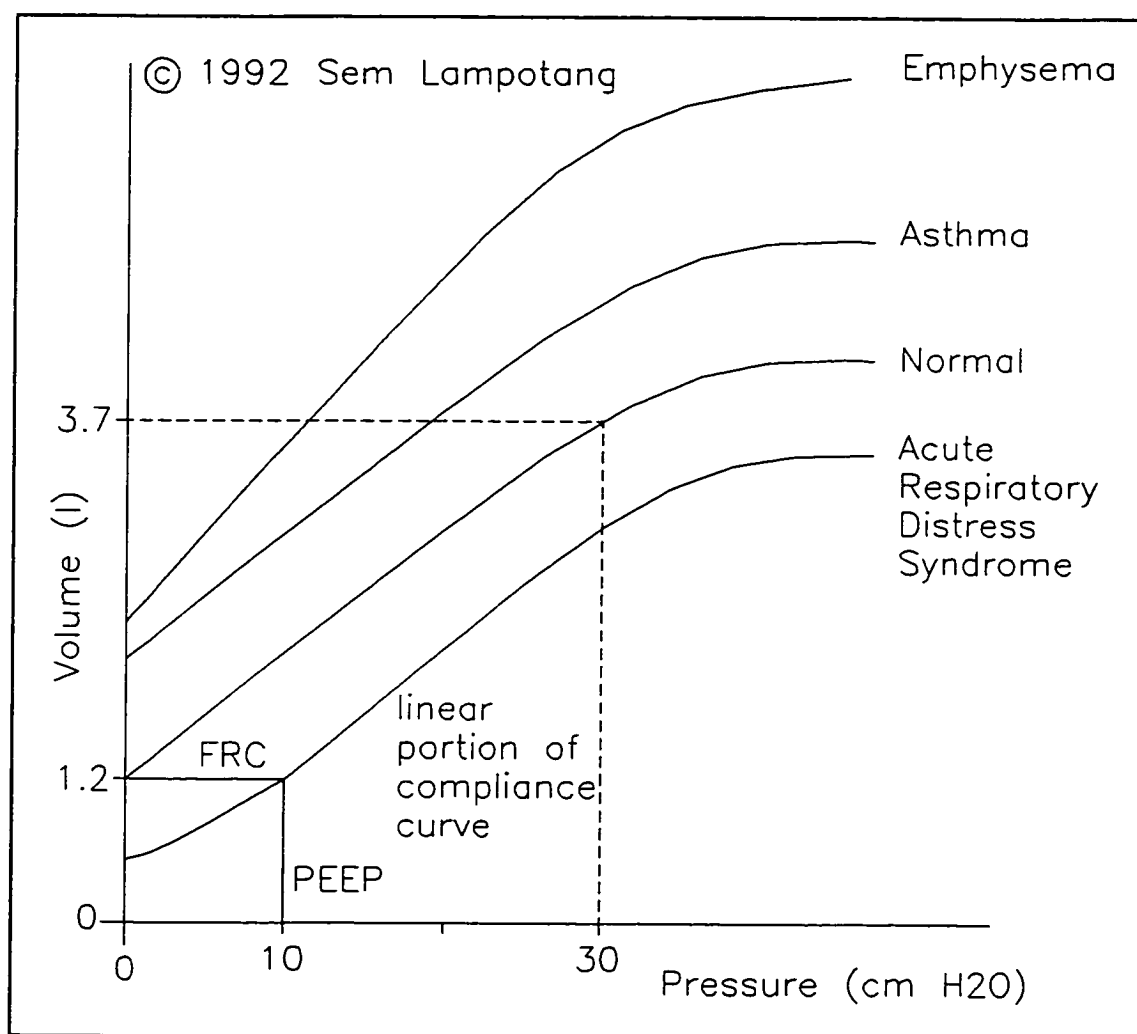
Figure 39. The compliance curves for normal and diseased lungs. FRC is the functional residual capacity and PEEP is positive end expiratory pressure.

However, we are trying to model the behavior of sick or injured lungs with uneven mechanical parameters. From examination of volume vs. pressure plots (Nunn 1987, 40; Cameron & Skofronick 1978, 142) where the compliance curves of an emphysematic patient (high compliance), adult respiratory distress syndrome (ARDS) patient (low compliance), asthmatic in bronchospasm (high resistance, normal compliance) and a healthy patient are superimposed (figure 39), it can be observed that the compliance curves still retain their skewed sigmoidal shape although the scale and the degree of skew (the slope, i.e., the compliance) are different. Therefore, the same reasoning used above for healthy lungs (the assumption of a linear compliance is practically useful and valid if the volume of the lung is below the inflection point) can also be applied to sick lungs.

It can be observed that the inflection points of the compliance curves for different lung pathologies follow a roughly diagonal locus that runs from the upper left to the bottom right of the volume-pressure plot. From a practical standpoint, the inflection point locus implies that a less compliant lung will top its curve at a lower volume above FRC compared to a normal lung. Because it is less compliant, the stiffer lung will generally receive less volume than a more compliant lung in proportion to the ratio of the compliances between the two lungs. Consequently, the very nature of the less compliant lung tends to prevent it from topping its curve and thus stay within the linear compliance region. Conversely, the more compliant lung accepts more volume but also tops its curve at a higher volume above FRC and will thus stay within the linear portion of its compliance curve for a larger volume range.

During exhalation, the lung compliance curve displays hysteresis. The curvature of the exhalation component of the compliance curve becomes more pronounced, accentuating the hysteresis, as tidal volume increases (Nunn 1987, 31). Clearly, the assumption of a linear compliance curve is not justified during exhalation. However, we are only interested in the inspiratory part of the compliance curve which is highly linear below the inflection point and coincident for different tidal volumes (Nunn 1987, 31). Consequently, the hysteresis and pronounced curvature of the compliance curve during exhalation can be ignored for the computer modelling as long as we limit ourselves to modelling inspiration.

While the compliance curve contains an inflection point, the flow resistance curve has a monotonically increasing curvilinear shape with no inflection points (Nunn 1987, 363). The curvature of the pulmonary resistance plot is slight (Nunn 1987, 363); the slope of the tangent to the resistance curve at the 1 l/s point (3.6 cm H_2O/l/s) can therefore be taken as the constant linearized flow resistance. This approximation fits well with the flowrate range of 0 to 80 l/min (Nunn 1987, 363) which is the portion of the curve where the inspiratory flowrate most commonly resides during mechanical inspiration. The error introduced by linearizing the resistance curve is about 2.1 cm H_2O/l/s (5.7 cm H_2O/l/s at 100 l/min) at a flowrate of 100 l/min. Consequently, if the total inspiratory flowrates do not exceed 80 l/min, a linear flow resistance can be assumed and the results obtained from the computer model can be of practical utility.

Furthermore, the good agreement obtained by Otis et al. (1956) between a linearized mathematical model and both a mechanical bellows model and human subjects

supports our hypothesis that a mathematical lung model which assumes linear compliances and resistances gives useful predictions of the dynamic behavior of the lungs, within a defined operational range which is not so constrained that it is of impractical value.

The flow resistance of an endotracheal tube (ETT) (6.6 cm $H_2O/l/s$ at 1.0 l/s for a 9 mm i.d. ETT (Nunn 1987, 363)) is larger than the flow resistance of the lungs (3.6 - 4.9 cm $H_2O/l/s$ at 1.0 l/s (Nunn 1987, 363) and is also curvilinear. The flow resistances for the ETTs were also linearized by fitting a line passing through the origin on the curvilinear plot such that equal areas are bounded by the straight line and the curvilinear plot on either side of the straight line. The linearized flow resistances of the ETTs were used to demonstrate the disparity between "airway" pressure measured at the Y-piece and the ETT distal tip and its dependence on flowrate at the ETT (Q_{ett}) and the resistance of the ETT (R_{ett}).

5.4.2 Mathematical Model

Having defined the limits of the validity of linearized resistances ($\leq$ 80 l/min total inspiratory flowrate) and compliances ($\leq$ 1.0 l for a single, healthy lung), the mathematical model on which the computer simulation will be based can now be developed. Some conventions must first be established: all pressures and volumes in the lungs are measured relative to the baseline or resting values (FRC per lung for volumes and baseline ambient pressure or PEEP level for pressures). Referencing to baseline values simplifies mathematical manipulation by allowing the direct use of the

compliance term in the equations involved. The formal definition of lung compliance is $C = \Delta V/\Delta P$. By referencing all volumes and pressures to the baseline values, the definition of compliance can be simplified to $C = V/P$. Flowrate into a lung is defined as positive whereas flowrate out of a lung is considered "negative". Since low pressures (≤ 60 cm H_2O; ≈ 0.85 psig) and gas velocities less than Mach 0.2 are involved, an incompressible flow regime is assumed for the entire analysis.

We start by considering only the right half of the respiratory system in figure 38. Because the layout is symmetrical and because both limbs are driven by a common pressure input, $P_c(t)$, (and therefore a common flowrate, $Q_{ca}(t)$, also) at the carina, the analysis derived for one limb or pathway will be directly applicable to the other. As we develop the mathematical model, it is important to understand the cause/effect relationship between pressure and flowrate. In the respiratory network of figure 38, it is pressure that generates flowrate; in other words, pressure difference is the cause and flowrate of gas in the direction of the pressure differential is the effect.

The flowrate of gas into one limb when subjected to a time-varying pressure input at the carina, $P_c(t)$, can be defined as (figure 38):

$$\frac{dV_r(t)}{dt} = \frac{P_c(t) - P_r(t)}{R_r} = \frac{P_c(t)}{R_r} - \frac{(V_r(t)/C_r)}{R_r} \qquad \textbf{5.1}$$

where $P_r(t)$ is the time-varying pressure in the right lung and $V_r(t)$ is the time dependent volume of the right lung. From the definition of compliance, the pressure in the right lung can be expressed as $P_r(t) = V_r(t)/C_r$. By further manipulation, we can express equation 5.1 for inflation of the right lung as a linear first-order differential equation:

$$\frac{dV_r(t)}{dt} + \frac{1}{R_r C_r} V_r(t) = \frac{P_c(t)}{R_r} \qquad 5.2$$

Equation 5.2 has been cast into a standard form which can be readily solved by the method of integrating factors (Spiegel, 1968) yielding the expression:

$$V_r(t) \cdot e^{\int \frac{1}{R_r C_r} dt} = \int_{t=0}^{t=T_i} \frac{P_c(t)}{R_r} \cdot e^{\int \frac{1}{R_r C_r} dt} dt \qquad 5.3$$

where T_i is the inspiratory time in seconds. If we assume that $P_c(t)$ is a pressure step input ($P_c(t<0) = 0$; $P_c(t \geq 0) = P_c$) and apply the initial condition that at $t = 0$ (the beginning of inflation) the volume in the right lung is at its resting volume ($V_r(t=0) = 0$), we arrive at equation 5.4 for the volume of the right lung during mechanical inflation with a pressure step input. Equation 5.5 for the volume of the left lung during mechanical inflation with a pressure step input is similar to that for the right lung except that all 'r' subscripts are replaced by 'l' subscripts.

$$V_r(t) = P_c \cdot C_r (1-e^{-\frac{t}{R_r C_r}}) \qquad 5.4$$

$$V_l(t) = P_c \cdot C_l (1-e^{-\frac{t}{R_l C_l}}) \qquad 5.5$$

An exact analytical solution for the ventilation distribution ratio $R_v(t) = V_r(t)/V_l(t)$ is therefore available for the case of inflation with a pressure step input of <u>any</u> specified time duration. This exact analytical solution is obtained by dividing equation 5.4 by equation 5.5 and will subsequently be used to test the accuracy of the finite difference scheme and to select the time step size for the numerical simulation.

By taking the derivative with respect to time of equations 5.4 and 5.5, we obtain

an expression for the flowrate into each lung in response to a pressure step input.

$$Q_r(t) = \frac{dV_r(t)}{dt} = \frac{P_c}{R_r} \cdot e^{-\frac{t}{R_rC_r}} \qquad 5.6$$

$$Q_l(t) = \frac{dV_l(t)}{dt} = \frac{P_c}{R_l} \cdot e^{-\frac{t}{R_lC_l}} \qquad 5.7$$

The total flowrate at the trachea for a pressure step input is obtained by adding the

flowrates into each lung, i.e., by summing equations 5.6 and 5.7.

$$Q_{ea}(t) = Q_r(t) + Q_l(t) = \frac{P_c}{R_r} \cdot e^{-\frac{t}{R_rC_r}} + \frac{P_c}{R_l} \cdot e^{-\frac{t}{R_lC_l}} \qquad 5.8$$

τ is the effective time constant of the entire respiratory system. Equation 5.8 defines the

time course of the total flowrate at the trachea during inflation with a pressure step input

and describes an exponential wash-in curve (Nunn 1987, 525) from which the time

constant of the total respiratory system during inflation can be determined. Equation 5.8

is a generalized equation where the time constant of the left and right respiratory

pathways are unequal. Equation 5.9 represents a special case of equation 5.8 when the

two pathways have equal time constants.

$$Q_{ea}(t) = \frac{R_r + R_l}{R_r R_l} P_c \, e^{-\frac{t}{R_rC_r}} = \frac{R_r + R_l}{R_r R_l} P_c \, e^{-\frac{t}{\tau}} = constant \; e^{-\frac{t}{\tau}} \qquad 5.9$$

When the time constants of the two pathways are unequal, the expression for the

effective compliance and resistance of the total system is complex and breathing

frequency dependent (Otis et al. 1956; Bhansali et al. 1983) and can be derived from the

electrical phasor theory used to analyze alternating current networks if the forcing function is sinusoidal. On the other hand, effective compliance and resistance are not breathing frequency dependent when the time constants of the parallel pathways are identical. In the latter case, direct current theory can be applied to obtain the effective compliance and resistance of the network: the effective compliance is simply the addition of the separate compliances while the effective resistance is obtained by applying the formula for adding two electrical resistances in parallel. The effective time constant of the two pathway network when the individual time constants are equal has the same value as the time constant of either of the pathways as shown in equation 5.9.

In the computer model, the individual compliances and resistances are always known since the user is asked to enter them because these values are necessary to drive the simulation. Consequently, the effective time constant of the system can be hand calculated for cases where the time constants of the individual pathways are identical. This special case is also used to verify the accuracy of the computer model by comparing the exact hand-calculated total respiratory system time constant against that derived by a subroutine in the program which performs feature analysis of the tracheal flowrate wash-in exponential curve in response to a pressure step input.

The other equations in addition to equation 5.1 that are used to simulate the flowrates, pressures and volumes in each lung are:

$$\frac{dV_r(t)}{dt} = Q_r(t) \qquad\qquad 5.10$$

$$\frac{dV_l(t)}{dt} = Q_l(t)$$ 5.11

$$P_r(t) = \frac{V_r(t)}{C_r}$$ 5.12

$$P_l(t) = \frac{V_l(t)}{C_l}$$ 5.13

5.4.3 Numerical Method

The finite difference scheme for the computer model is based on Euler's method (Hornbeck 1975). A forward-difference representation is used to solve the first-order, initial value problems that define the inflation of each lung. A characteristic of the Euler method is that stability improves as the time step size decreases. However, in this application, the speed of the simulation is not critical. A time step size of 0.001 s was selected by comparing the accuracy of the simulation at various time step sizes against an exact analytical solution which will be described in the model verification section.

The finite difference representations of equations 5.1, 5.10 and 5.12 are respectively:

$$Q_{r,t} = \frac{P_t - P_{r,t}}{R_r}$$ 5.14

$$V_{r,t+1} = V_{r,t} + Q_{r,t} \cdot DT$$ 5.15

$$P_{r, t+1} = \frac{V_{r, t+1}}{C_r}$$ **5.16**

where the subscript 'r,t' means relating to the right lung at the present time step and the subscript 'r,t+1' means relating to the right lung at the next time step and DT is the time step size. Equations similar to 5.14, 5.15 and 5.16 (except that the 'r' subscripts are replaced by 'l' subscripts) are used for the finite difference representation of the dynamic response of the left lung.

5.4.3.1 Verification of the computer model

As mentioned earlier, verification of the accuracy of the computer model was performed against special cases where exact analytical solutions could be readily derived. The computer model gave a ventilation distribution ratio, $R_v(T_i)$, of 1.001256 at the end of a pressure step input lasting 2.0 seconds on a lung configuration where $C_r = C_l = 0.05$ l/cm H_2O and $R_r = 2$ cm $H_2O/l/s$ and $R_l = 6$ cm $H_2O/l/s$. The exact analytical solution obtained by dividing equation 5.4 by equation 5.5 and plugging the corresponding values into the resulting expression is $R_v(T_i) = 1.001274$ giving an accuracy of 0.002% which is sufficient for the intended use of the model.

Similarly, the subroutine for analysis of the tracheal flowrate response, $Q_{tr}(t)$, to a pressure step input determined that the time constant of the entire respiratory system was 0.150 seconds for 2 lung configurations where the time constants of the individual pathways were equal (0.15 s for both pathways in both lung configurations).

(a) $C_r = C_l = 0.025$ l/cm H_2O; $R_r = R_l = 6$ cm $H_2O/l/s$

(b) $C_r = 0.025$ l/cm H_2O, $C_l = 0.0125$ l/cm H_2O;

$R_r = 6$ cm $H_2O/l/s$, $R_l = 12$ cm $H_2O/l/s$

For lung configuration (a), the time constant of each limb is $0.025 \times 6 = 0.150$ s. The effective respiratory system compliance, C_e, is $0.025 + 0.025 = 0.05$ l/cm H_2O. The calculated effective respiratory system resistance, R_e, is 3.0 cm $H_2O/l/s$:

$$\frac{1}{R_s} = \frac{1}{R_r} + \frac{1}{R_l} = \frac{1}{6} + \frac{1}{6} = \frac{1}{3}$$

The system time constant is the product of R_e and C_e ($3 \times 0.05 = 0.150$ s) which matches perfectly with the time constant derived from the computer model.

Similarly, for lung configuration (b), $C_e = 0.025 + 0.0125 = 0.0375$ l/cm H_2O and $R_e = 4.0$ cm $H_2O/l/s$:

$$\frac{1}{R_s} = \frac{1}{R_r} + \frac{1}{R_l} = \frac{1}{6} + \frac{1}{12} = \frac{2+1}{12} = \frac{1}{4}$$

The product of the effective resistance and compliance is $0.0375 \times 4.0 = 0.150$ s which again matches exactly the result from the computer model.

From the results of the above comparisons, it is concluded that the computer model has been verified to be accurate and consistent with its mathematical model for the special case of a step input in pressure.

5.4.4 Inspiratory Flowrate Shaping

Up to this point, we have only discussed pressure inputs to the carina in the computer model. However, what we want to simulate is the shaping of the flowrate waveform during mechanical inflation of the lungs. Since the mathematical model and the finite-difference representation are pressure-driven (pressure at the Y-piece drives flowrate through the ETT into the lungs), the pressure that is required to drive the desired flowrate waveform through the ETT must be calculated. The fact that the operator of an ICU ventilator can select inspiratory flowrate shapes can be confounding since it appears to be in conflict with the previous statement that flowrate is the effect of pressure.
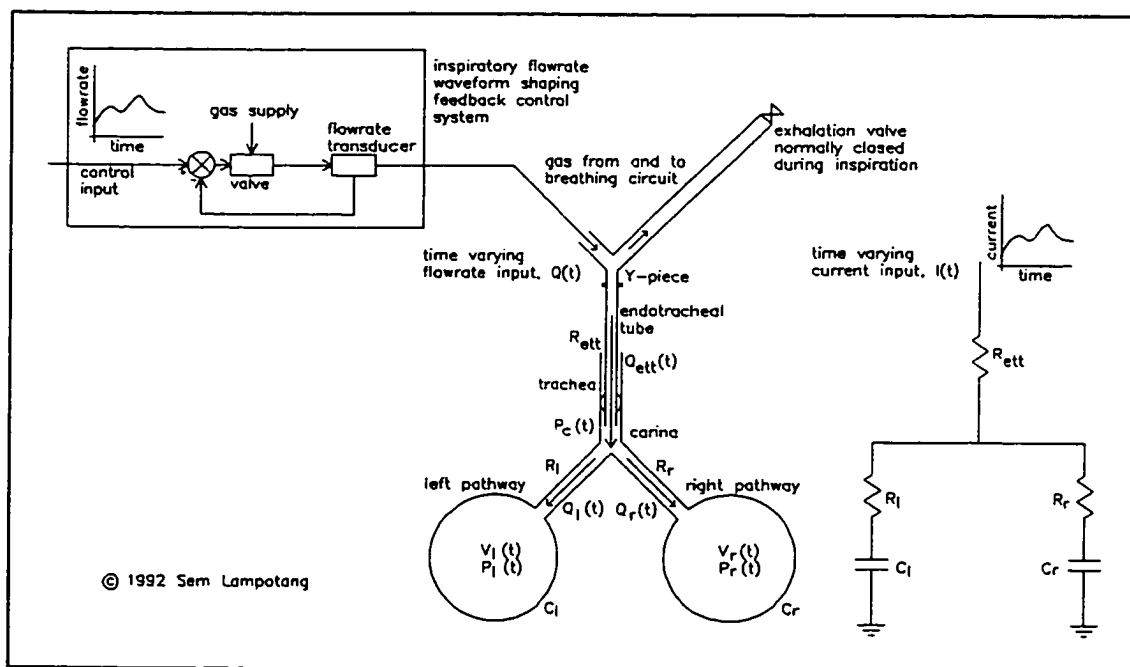
Figure 40. The simplified model of the respiratory system and its equivalent electrical analog. The inspiratory flowrate shaping control system is also sketched.

Although it would be semantically correct to state that the drive input into the lungs is the flowrate during inspiratory flowrate shaping selection, one has to realize that there is a feedback control loop internal to the ventilator (Hamilton Medical 1988; Puritan-Bennett 1984)), which is not apparent to the user, that is modulating the driving input (pressure) necessary to produce the user selected flowrate waveshape during mechanical inflation (Lampotang, 1990a) (figure 40). Therefore, even though the flowrate shaping feedback control system confuses the issue, the cause and effect relationship between pressure and flowrate is still valid. Consequently, we model the physical reality of the feedback control loop by back-calculating the pressure required to obtain the desired flowrate waveshape, $Q_{ea}(t)$, while implicitly assuming a perfect inspiratory flowrate feedback control loop. The required drive pressure, $P_c(t)$, at the carina for flowrate shaping is derived below.

$$Q_{ea}(t) = Q_r(t) + Q_l(t) = \frac{P_c(t) - P_r(t)}{R_r} + \frac{P_c(t) - P_l(t)}{R_l} \qquad 5.17$$

$$Q_{ea}(t) = \frac{P_c(t)}{R_r} - \frac{(V_r(t)/C_r)}{R_r} + \frac{P_c(t)}{R_l} - \frac{(V_l(t)/C_l)}{R_l}$$

$$Q_{ea}(t) = P_c(t) \left[\frac{1}{R_r} + \frac{1}{R_l} \right] - \left[\frac{V_r(t)}{R_r C_r} + \frac{V_l(t)}{R_l C_l} \right]$$

$$Q_{ea}(t) = P_c(t) \left[\frac{R_r + R_l}{R_r R_l} \right] - \left[\frac{V_r(t)}{R_r C_r} + \frac{V_l(t)}{R_l C_l} \right]$$

$$P_c(t) = \frac{R_r R_l}{R_r + R_l} \left[Q_{ea}(t) + \frac{V_r(t)}{R_r C_r} + \frac{V_l(t)}{R_l C_l} \right] \qquad 5.18$$

The four flowrate shapes presently used are all described by mathematical functions of time (see equations 5.23). Therefore, in equation 5.18, where $P_c(t)$ is an explicit function of $Q_{ett}(t)$, the required $P_c(t)$ for a given $Q_{ett}(t)$ is readily computed. The ability to describe every single waveshape in terms of explicit mathematical functions simplifies the task of updating the total inspiratory flowrate during the course of inflation. New waveshapes other than the four standard patterns presently used (figure 2) can thus also be conveniently included in the computer simulation, the only limitation being the imagination of the investigator. Consequently, the program was structured in a modular fashion that facilitated the addition of new inspiratory flowrate shapes (see equations 5.24) and modes apart from the four existing ones.

5.4.5 Modeling of the Inspiratory Pause

The inspiratory pause is modeled by imposing its defining condition, i.e., flowrate in the ETT is zero. The model assumes that the flow resistances in each respiratory pathway have the same value whether gas is flowing into or out of the lung; i.e., the flow resistance values are not direction dependent. Flowrate in the bronchi during the pause is also zero if the lungs are at the same pressure. If, on the other hand, the pressures in the lungs at the end of the active inflation period (just prior to the onset of the inspiratory pause) are unequal, the difference in pressure will cause gas to flow from the higher pressure lung to the lower pressure lung (pendelluft).

$$Q_{ca}(t) = Q_r(t) + Q_l(t) = 0 \qquad \textbf{5.19}$$

$$Q_r(t) = - Q_l(t) \qquad \textbf{5.20}$$

$$Q_r(t) = \frac{P_l(t) - P_r(t)}{R_r + R_l} \qquad \textbf{5.21}$$

During pendelluft, the previously established sign convention for flowrate ensures that the flow of gas is always physically correct, i.e., flowing from the higher pressure region to the lower pressure region. The equation governing pendelluft is arbitrarily set up as if gas is flowing into the right lung from the left lung. Inspection of equation 5.21 shows that if pressure in the right lung is actually higher than pressure in the left lung (gas is flowing out of the right lung instead of into it), the numerator of the right hand side (RHS) of the equation becomes negative thus giving a "negative" value to $Q_r(t)$, indicating that flowrate is out of the right lung which is physically correct. Throughout pendelluft, the flowrates in the bronchi have the same magnitude but different signs. During pendelluft, the resistances in each lung are added in series as shown by the denominator of the RHS of equation 5.21.

During the inspiratory pause, we assume (a) that the system is closed because total inspiratory flowrate, $Q_{ca}(t)$, is zero, (b) that the compliance of the trachea is zero so that none of the gas being redistributed goes into the trachea and (c) that as the equilibrating flowrate between the two lungs negotiates the acute angle at the carina, there is no appreciable pressure drop. With those assumptions, the pressure at the carina

during the inspiratory pause is determined solely by the flowrate of gas moving from one lung to the other and the resistances of each lung according to equation 5.22. Although the equation is set up as if gas is moving into right lung, the sign for flowrate at the right bronchus, $Q_r(t)$, ensures that the pressure at the carina, $P_c(t)$, will be physically correct whether gas is moving into or out of the right lung.

$$P_c(t) = P_r(t) + Q_r(t) \, R_r \qquad\qquad \textbf{5.22}$$

5.4.6 Statistics Monitoring

In addition to the ventilation distribution ratio ($R_v(T_i)$), the model also outputs the peak pressure at the Y-piece (PIP), the time-averaged mean pressure at the Y-piece (MAP), the peak pressures in each lung as well as the instantaneous mean lung pressure, IMLP(t). The IMLP(t) is taken as the arithmetic mean of the pressures in each lung (IMLP(t) = ½[$P_r(t)$ + $P_l(t)$]). The IMLP(t) is time averaged over the duration of the inspiratory period (T_i) to obtain MLP(T_i). It should be noted that in the computer model the actual MLP(t) is obtained because the pressures in each lung, $P_r(t)$ and $P_l(t)$, are available. In actual clinical practice, MLP(t) would be inferred from the mean intratracheal pressure sampled at the distal tip of the ETT, MITP(t).

5.4.7 New Waveforms

As the four standard waveforms were being tested, different patterns in the dynamic response of different lung configurations began to emerge and based on these observations and an undeniable amount of heuristic intuition, new waveforms were

designed and tested. These additional inspiratory waveforms are: the quarter sine flowrate ($\pi/2$ to π), the trapezoid flowrate, decaying exponential flowrate, the shifted quarter sine flowrate (π to $3\pi/2$), and increasing exponential flowrate.

Each of the inspiratory waveforms is defined by a characteristic parameter (usually the peak pressure or peak flowrate) and an equation which is an explicit function of time and of the characteristic parameter such that the desired VT is delivered in the allotted T_i. For brevity, the mathematics leading to the defining equations will not be shown. Only the resulting describing equation is shown. The four presently implemented flowrate waveforms are described first.

$$
\begin{aligned}
\text{constant flowrate:} \quad & Q_{en}(t) = \frac{VT}{T_i} \\
\text{increasing flowrate:} \quad & Q_{en}(t) = \frac{2VT}{T_i^{\,2}} \cdot t \\
\text{decreasing flowrate:} \quad & Q_{en}(t) = -\frac{2VT}{T_i^{\,2}} \cdot t + 2\frac{VT}{T_i} \\
\text{half-sine (0-π) flowrate:} \quad & Q_{en}(t) = \frac{\pi VT}{2T_i} \cdot \sin\left[\frac{\pi}{T_i} \cdot t\right]
\end{aligned}
$$

$$5.23$$

Note that the existing waveforms were all described by a single mathematical function. There is nothing to prevent the use of piecewise functions, i.e., functions made up of more than one equation with each equation describing a particular portion of the inspiratory waveform, like the trapezoid which is described next. The new flowrate waveforms are described by the following equations:

$$\text{quarter sine } (\tfrac{\pi}{2}-\pi): \quad Q_{ea}(t) = \frac{\pi VT}{2T_i} \sin\left[\frac{\pi}{2} + \frac{\pi}{2T_i}\cdot t\right]$$

$$\text{sh. quarter sine } (\pi-3\tfrac{\pi}{2}): \quad Q_{ea}(t) = \frac{VT}{T_i\cdot(1-\frac{2}{\pi})}\left[1 + \sin(\pi + \frac{\pi}{2T_i}t)\right]$$

$$\text{trapezoid: } Q_{ea}(0\leq t<\tfrac{T_i}{2}) = \frac{4VT}{3T_i}$$

$$: \quad Q_{ea}(\tfrac{T_i}{2}\leq t\leq T_i) = -\frac{8VT}{3T_i^2}\cdot\left[t-\frac{T_i}{2}\right] + \frac{4VT}{3T_i}$$

$$\text{decaying exp. } (\tau=\tfrac{T_i}{5}): \quad Q_{ea}(t) = \frac{VT}{0.198652T_i} e^{-\frac{5t}{T_i}}$$

$$\text{rising exp. } (\tau=\tfrac{T_i}{5}): \quad Q_{ea}(t) = \frac{0.033918\ VT}{T_i} e^{\frac{5t}{T_i}} \qquad \textbf{5.24}$$

5.4.7.1 Derivation of the equation for a decaying exponential flowrate waveform

As an example, the equation for a decaying exponential inspiratory flowrate waveform will be derived in this section. The exponential decay will have a time constant, τ. Therefore, the equation for the decaying exponential flowrate is initially expressed as:

$$Q_{ea}(t) = Q_{max}\ e^{-\frac{t}{\tau}} \qquad \textbf{5.25}$$

where Q_{max} is the maximum initial flowrate which is a characteristic parameter of the flowrate waveform, i.e., $Q_{max} = Q_{ea}(t=0)$. For this particular flowrate waveform, it is desired that the flowrate, $Q_{ea}(t)$, is almost zero at the end of mechanical inspiration, i.e., $Q_{ea}(T_i)$ tends to zero. This is ensured by arbitrarily imposing that the time constant of the flowrate decay, τ, is equal to $T_i/5$ which will make $Q_{ea}(T_i) = Q_{max}\ e^{-5} = 0.0067\ Q_{max}$.

A tidal volume of VT ml must be delivered by the decaying exponential flowrate waveform in a time duration of T_i s. This can be expressed as:

$$VT = \int_{t=0}^{t=T_i} Q_{en}(t)\,dt = \int_{t=0}^{t=T_i} Q_{max}\, e^{-\frac{t}{\tau}}\,dt$$

$$VT = Q_{max} \int_{t=0}^{t=T_i} e^{-\frac{5t}{T_i}}\,dt \qquad\qquad \textbf{5.26}$$

$$VT = \frac{-Q_{max}\cdot T_i}{5}\left[e^{-\frac{5t}{T_i}}\right]_{t=0}^{t=T_i} = \frac{-Q_{max}\cdot T_i}{5}\left[e^{-5} - e^{0}\right]$$

$$VT = 0.198652\; Q_{max}\cdot T_i$$

Therefore, the characteristic parameter Q_{max} can be expressed as a function of VT and T_i which will be known since they are set by the user.

$$Q_{max} = \frac{VT}{0.198652\; T_i} \qquad\qquad \textbf{5.27}$$

By plugging equation 5.27 for Q_{max} into equation 5.25 for $Q_{en}(t)$ and setting τ at $T_i/5$, equation 5.28 for a decaying exponential flowrate mechanical inspiratory waveform which will deliver a tidal volume of VT in a time duration T_i is obtained.

$$Q_{en}(t) = \frac{VT}{0.198652\; T_i}\, e^{-\frac{5t}{T_i}} \qquad\qquad \textbf{5.28}$$

Obviously, there is nothing special about a τ of $T_i/5$. Other values like $\tau = T_i/n$ where n can be any number, within reason, can be used and should be tested using the same method of derivation illustrated above.

5.4.7.2 Inspiratory pressure waveform shaping

Since the computer model is pressure driven as described in section 5.4.4, it was straightforward to model new <u>pressure</u> inspiratory waveforms. However, if the same user interface is to be provided to the clinician who operates the ventilator, i.e., a choice of VT and respiratory rate to arrive at the minute ventilation, there is a slight problem with pressure waveform shaping. With a flowrate inspiratory waveform, the area under the waveform shape for $0 \leq t \leq T_i$ on a time-flowrate graph gives the tidal volume such that the characteristic parameter of the describing equation can be readily computed. This predetermined flowrate equation can then be used as the dynamic reference input for the flowrate feedback control loop like the one sketched in figure 40. In fact, this is the technique that was used to obtain the describing equations for the different new flowrate waveforms that were designed in section 5.4.7.

However, this technique is not applicable to a pressure inspiratory waveform. For simplicity, we examine the case of a constant pressure waveform. For a given peak pressure amplitude (the constant pressure step level) and T_i, the VT that will be delivered will be a function of the effective resistance (R_e) and effective compliance (C_e) of the patient's lungs. However, R_e and C_e are <u>not</u> constant among patients such that the peak pressure (the defining characteristic parameter of the pressure waveform) required to deliver the desired VT in the time period T_i cannot be predicted.

Therefore, in the computer model implementation, a VT feedback loop was implemented where the exhaled volume was monitored at the ETT. The error between the measured exhaled VT and the desired VT set by the clinician was used to "scale" the

pressure waveform, i.e., increase or decrease the peak pressure as required after each breath, until the error was less or equal to 1 ml, while maintaining the desired pressure waveform shape. The 1 ml target accuracy for VT in the computer model is overly stringent and in clinical practice, could be relaxed to about 10 - 50 ml for adults. However, this stringent VT error specification was used to test on the computer model how many iterations (i.e., breaths) it would take for the VT feedback control loop to zero in on the desired VT delivery. In the tests that were simulated with the computer model, the VT feedback controller was always able to zero in and lock onto the desired VT within 3 - 4 breaths (typically 12 - 30 seconds, tables 4-9). As a safety feature, the VT feedback control algorithm was deliberately biased to have an initial starting VT value that was lower than would be realistic, so that the danger of overinflation and consequent risk of barotrauma on the first inflation is reduced.

The tidal volume feedback control loop during pressure waveform shaping is implicitly based on the practical clinical reality that it is not critical if a patient is underventilated for 3 - 4 breaths only. The pressure waveform shaping control loop would be similar to the flowrate shaping control loop of figure 40, except that the feedback signal would be coming from the pressure sampled at the ETT distal tip instead of the turbine flowmeter at the ETT (figure 30) and the time-varying reference control signal would be a pressure input computed by the VT feedback control loop.

It is an advantage of the GRADS design that it allows the features of pressure and flowrate waveform shaping to be readily implemented on it without the need for hardware modifications because the feedback transducers required (flowrate sensor and

pressure transducer) are not only already present but they are also at the right location for the kind of waveform shaping that is discussed here. For example, shaping the pressure at the carina must be done by sampling pressure at the ETT distal tip while flowrate shaping requires a flowrate sensor at the ETT.

5.4.8 Possible Lung Configurations

The multitude of possible lung configurations creates confusion when trying to understand the different behavior of various lung configurations. Consequently, a systematic approach to testing was devised. All possible lung configurations were methodically listed by considering the compliances (C_r, C_l) and flow resistances (R_r, R_l) of each lung as independent variables. Borrowing from binary arithmetic, the normal state was assigned a '0' whereas the abnormal state was assigned a '1' irrespective of the degree or direction of abnormality. With 4 independent binary variables, $2^4 = 16$ combinations are possible. If we denote the normal compliance and resistance by C and R respectively, then the abnormal states are C/n and mR where n and m are typically (but not necessarily) greater than 1.0 since clinically, abnormalities normally manifest themselves as reduced compliance and increased resistance.

From the assumed symmetry of the set-up, position is not significant, i.e., if the compliances are similar but one flow resistance is twice the other, it does not matter if the higher resistance is at R_r (#9) or R_l (#3). Functionally, configurations #3 and #9 are similar. Because compliance and resistance are independent of each other, the actual magnitude of the compliance compared to the resistance is not significant and vice-versa.

Consequently, configurations #1, #6, #11 and #16 are similar. By invoking symmetry and independence of the parameters, the sixteen possible lung configurations can be reduced to 5 lung configuration types and 1 lung configuration type subset (type 5a).

#	R_r	C_r	R_l	C_l	R_r	C_r	R_l	C_l	type
1	0	0	0	0	R	C	R	C	1
2	0	0	0	1	R	C	R	C/n	2
3	0	0	1	0	R	C	mR	C	3
4	0	0	1	1	R	C	mR	C/n	5
5	0	1	0	0	R	C/n	R	C	2
6	0	1	0	1	R	C/n	R	C/n	1
7	0	1	1	0	R	C/n	mR	C	4
8	0	1	1	1	R	C/n	mR	C/n	3
9	1	0	0	0	mR	C	R	C	3
10	1	0	0	1	mR	C	R	C/n	4
11	1	0	1	0	mR	C	mR	C	1
12	1	0	1	1	mR	C	mR	C/n	2
13	1	1	0	0	mR	C/n	R	C	5
14	1	1	0	1	mR	C/n	R	C/n	3
15	1	1	1	0	mR	C/n	mR	C	2
16	1	1	1	1	mR	C/n	mR	C/n	1

Type	Example	Example	Example	Defining conditions
1.	$R_r = R_l$;	$C_r = C_l$;	$\tau_r = \tau_l$	$E\tau$ $(\tau_r = \tau_l)$
2.	$R_r = R_l$;	$C_r < C_l$;	$\tau_r < \tau_l$	UCER $(\tau_r \neq \tau_l)$
3.	$R_r < R_l$;	$C_r = C_l$;	$\tau_r < \tau_l$	ECUR $(\tau_r \neq \tau_l)$
4.	$R_r < R_l$;	$C_r < C_l$;	$\tau_r \lessgtr \tau_l$	UI $(\tau_r \ll \tau_l; \tau_r \gg \tau_l)$
5.	$R_r < R_l$;	$C_r > C_l$;	$\tau_r \neq \tau_l$ (in general)	BI $(\tau_r \neq \tau_l)$
5a.	$mR_r = R_l$	$C_r/n = C_l$	$\tau_r = \tau_l$ (m = n)	$E\tau$ $(\tau_r = \tau_l)$

A special case of configuration type 5 exists where R_r is less than R_l by the same proportion as C_l is less than C_r (i.e., $n = m$). In this special case of type 5, which we will call type 5a to make its association with type 5 explicit, $\tau_r = \tau_l$. Eτ stands for equal time constant. We differentiate for now between the cases where the inequalities in compliance and resistance are in the same direction (e.g., $R_r < R_l$ and $C_r < C_l$) which is denoted UI for unidirectional equality. When the inequalities are in opposite directions (e.g., $R_r < R_l$ and $C_r > C_l$), the type is BI for bidirectional inequality.

5.4.9 Method

The purpose of the comparative analysis using the computer model was to evaluate the effect of inspiratory waveform shape and mode, T_i and inspiratory pause on $R_v(T_i)$ and $MLP(T_i)$. The comparative analysis was performed by keeping all parameters, including R_r, C_r, R_l and C_l, constant over one set of computer simulation runs. For the comparative analysis, only one parameter was changed at a time from one simulation run to another, within a simulation set. Six sets of simulation runs were performed. Each computer simulation set corresponded to a lung type (1 - 5a) and is recapitulated in tables 4 - 9. The qualitative trends identified from tables 4 - 9 are condensed in table 10. For the simulations, the normal value of R_r, R_l, C_r, C_l for an anesthetized supine patient was 6 cm $H_2O/l/s$ and 0.025 l/cm H_2O respectively (Nunn 1987, 398-403).

A text-based screen allows the user to enter values for the right and left compliances and resistances, tidal volume, inspiratory time and to select the flowrate waveshape, an adjustable inspiratory pause and the ETT size. The graphical output

screen for a simulation run with R_r = 6 cm $H_2O/l/s$, C_r = 0.00625 l/cm H_2O, R_l = 18 cm $H_2O/l/s$, C_l = 0.05 l/cm H_2O, VT = 0.6 l, T_i = 4.0 seconds with a 25% inspiratory pause (3 s active inflation, 1 s pause) for an increasing flowrate waveform is displayed below (figure 41).

In figure 41, the two traces on the upper left volume-time plot are the volumes of each lung; addition of the end-point of the two traces gives the set tidal volume while division gives the distribution ratio, $R_v(T_i)$. The bottom left pressure-time graph plots the pressure inside each individual lung; the pressures in each lung are different at the end of the active inflation period (3 second line) and the equilibration of pressure between the two lungs during the inspiratory pause is clearly illustrated. On the top right hand corner, the total flowrate into the ETT is displayed and its appearance conforms to the selected shape (increasing flowrate waveform); note that the trace for total inspiratory flowrate disappears at the 3 s line since flowrate into the trachea is, by definition, zero during the inspiratory pause. The drive pressure at the carina (which would be available if "airway" pressure is monitored at the distal tip of the ETT) is displayed in the bottom right hand portion of the screen and the process of pressure equilibration is clearly evident during the inspiratory pause. The traces are color coded for ease of interpretation when the output is displayed on an EGA or VGA monitor.

When comparing the effect of waveform on $R_v(T_i)$ and $MLP(T_i)$, all other parameters like T_i and VT were kept constant at a given lung configuration type. Thus, tables 4-9 were generated, each corresponding to a different lung type (1,2,3,4,5 and 5a).
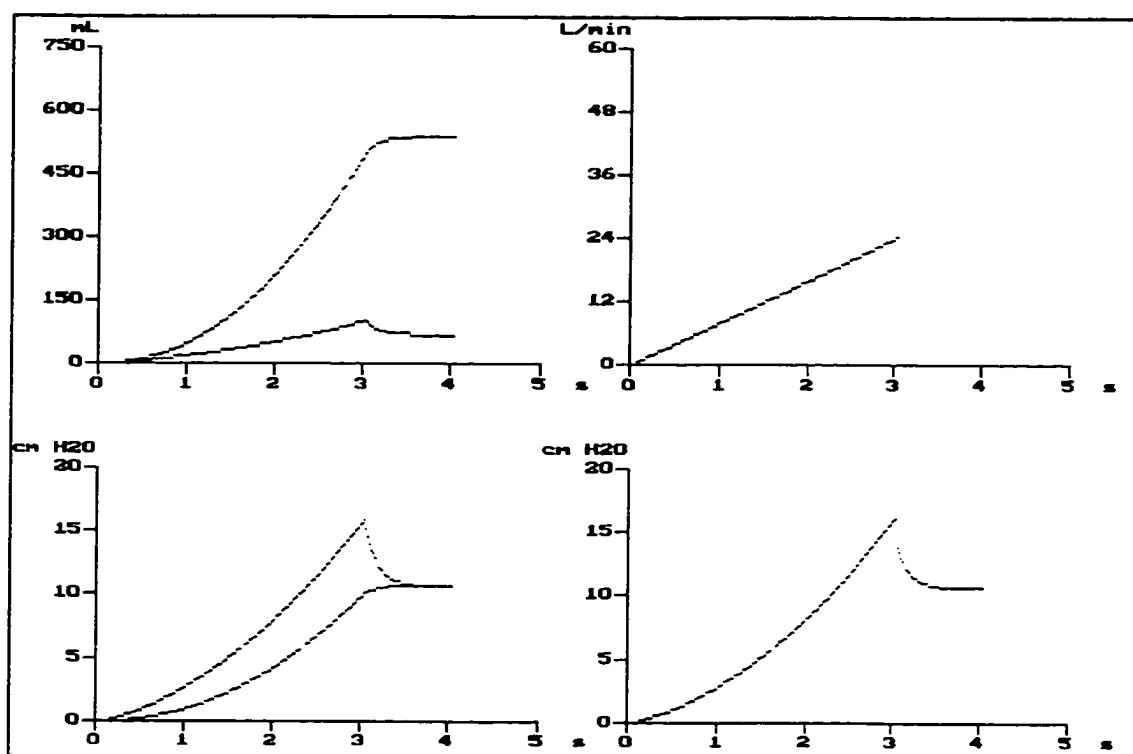
Figure 41. The graphical output screen for an increasing flowrate waveform. Top left plot: volumes in each lung; top right: flowrate at ETT; bottom left: pressures in each lung; bottom right: pressure at carina

5.4.10 Results

The results of the methodical computer analysis of all possible lung configuration types are tabulated in tables 4-9. Q_{max} in tables 4 - 9 stands for the maximum inspiratory flowrate required for the given inspiratory waveform pattern. 'Iter.' is the number of iterations (breaths) before the pressure waveform locks onto the desired VT.

Table 4. Computer simulation results with a type 1 (normal and healthy) lung configuration (R_r = 6 cm $H_2O/l/s$; C_r = 0.025 l/cm H_2O; R_l = 6 cm $H_2O/l/s$, C_l = 0.025 l/cm H_2O)

| | Ventilation Parameters | | | | Before Pause | | End of Inspiration | | | | | |
mode	shape	T_i (s)	VT (l)	pause (% T_i)	V_r/V_l	MLP (cm H_2O)	$R_v(T_r)$ V_r/V_l	MLP (cm H_2O)	PIP (cm H_2O)	Q_{max} (l/min)	system τ (s)	Iter.
flow	const	2.0	0.7	0	-	-	1.000	7.00	15.04	*21.0*	-	-
flow	const	*4.0*	0.7	0	-	-	1.000	7.00	14.52	10.5	-	-
flow	const	2.0	*1.0*	0	-	-	1.000	10.01	21.49	30.0	-	-
flow	const	2.0	0.7	*25*	1.000	7.00	1.000	8.75	15.39	28.0	-	-
flow	inc.	2.0	0.7	0	-	-	1.000	4.67	16.09	42.0	-	-
flow	dec.	2.0	0.7	0	-	-	1.000	9.34	14.08	42.0	-	-
flow	h-sin	2.0	0.7	0	-	-	1.000	7.00	14.19	33.0	-	-
flow	q-sin	2.0	0.7	0	-	-	1.000	8.92	14.10	33.0	-	-
flow	trap.	2.0	0.7	0	-	-	1.000	8.56	14.10	28.0	-	-
flow	d_exp	2.0	0.7	0	-	-	1.000	11.31	14.05	105.7	-	-
flow	sh-sin	2.0	0.7	0	-	-	1.000	10.36	14.04	57.8	-	-
flow	r_exp	2.0	0.7	0	-	-	1.000	*2.71*	*19.22*	105.4	-	-
press.	const	2.0	0.7	0	-	-	1.000	*12.96*	*14.00*	*280.0*	0.15	4
press.	inc.	2.0	0.7	0	-	-	1.000	6.52	15.13	22.7	-	4
press.	r_exp	2.0	0.7	0	-	-	1.000	2.78	19.20	104.8	-	4
flow	inc.	2.0	0.7	25	1.000	4.67	1.000	7.00	16.78	56.0	-	-
flow	dec.	2.0	0.7	25	1.000	9.34	1.000	10.50	14.14	56.0	-	-
flow	h-sin	2.0	0.7	25	1.000	7.00	1.000	8.75	14.34	44.0	-	-
flow	q-sin	2.0	0.7	25	1.000	8.92	1.000	10.19	14.18	44.0	-	-
flow	trap.	2.0	0.7	25	1.000	8.56	1.000	9.92	14.17	37.3	-	-
flow	d_exp	2.0	0.7	25	1.000	11.32	1.000	12.00	14.07	141.0	-	-
flow	sh-sin	2.0	0.7	25	1.000	10.36	1.000	11.28	14.08	77.1	-	-
flow	r_exp	2.0	0.7	25	1.000	2.71	1.000	5.52	20.95	140.5	-	-
press.	const	2.0	0.7	25	1.000	12.61	1.000	12.96	14.00	280.0	0.15	4
press.	inc.	2.0	0.7	25	1.000	6.38	1.000	8.29	15.54	31.1	-	3
press.	r_exp	2.0	0.7	25	1.000	2.78	1.000	5.58	20.94	139.8	-	4

Table 5. Computer simulation results with a type 2 lung configuration (R_r = 6 cm $H_2O/l/s$; C_r = 0.0125 l/cm H_2O; R_l = 6 cm $H_2O/l/s$; C_l = 0.025 l/cm H_2O)

		Ventilation Parameters			Before Pause		End of Inspiration					
mode	shape	T_i (s)	VT (l)	pause (% T_i)	V_r/V_i	MLP (cm H_2O)	$R_r(T_i)$ V_r/V_i	MLP (cm H_2O)	PIP (cm H_2O)	Q_{max} (l/min)	system τ (s)	Iter.
flow	const	2.0	0.7	0	-	-	0.519	9.45	19.82	21.0	-	-
flow	const	4.0	0.7	0	-	-	0.509	9.39	19.25	10.5	-	-
flow	const	2.0	1.0	0	-	-	0.519	13.50	28.32	30.0	-	-
flow	const	2.0	0.7	25	0.525	9.49	0.500	11.79	20.21	28.0	-	-
flow	inc.	2.0	0.7	0	-	-	0.537	6.33	20.97	42.0	-	-
flow	dec.	2.0	0.7	0	-	-	0.502	12.57	18.75	42.0	-	-
flow	h-sin	2.0	0.7	0	-	-	0.505	9.45	18.87	33.0	-	-
flow	q-sin	2.0	0.7	0	-	-	0.502	12.01	18.78	33.0	-	-
flow	trap.	2.0	0.7	0	-	-	0.502	11.53	18.77	28.0	-	-
flow	d_exp	2.0	0.7	0	-	-	0.501	15.20	18.73	105.7	-	-
flow	sh-sin	2.0	0.7	0	-	-	0.500	13.93	18.71	57.8	-	-
flow	r_exp	2.0	0.7	0	-	-	0.580	3.70	24.34	105.4	-	-
press.	const	2.0	0.7	0	-	-	0.500	17.63	18.67	373.3	0.106	4
press.	inc.	2.0	0.7	0	-	-	0.520	8.91	19.89	22.4	-	3
press.	r_exp	2.0	0.7	0	-	-	0.579	3.80	24.32	104.8	-	4
flow	inc.	2.0	0.7	25	0.548	6.37	0.500	9.46	21.73	56.0	-	-
flow	dec.	2.0	0.7	25	0.503	12.61	0.500	14.12	18.82	56.0	-	-
flow	h-sin	2.0	0.7	25	0.508	9.47	0.500	11.78	19.02	44.0	-	-
flow	q-sin	2.0	0.7	25	0.504	12.05	0.500	13.71	18.86	44.0	-	-
flow	trap.	2.0	0.7	25	0.504	11.56	0.500	13.34	18.85	37.3	-	-
flow	d_exp	2.0	0.7	25	0.501	15.25	0.500	16.11	18.75	141.0	-	-
flow	sh-sin	2.0	0.7	25	0.501	13.97	0.500	15.15	18.75	77.1	-	-
flow	r_exp	2.0	0.7	25	0.601	3.72	0.501	7.48	26.18	140.5	-	-
press.	const	2.0	0.7	25	0.500	17.27	0.500	17.61	18.65	373	0.106	3
press.	inc.	2.0	0.7	25	0.528	8.79	0.500	11.27	20.35	30.5	-	3
press.	r_exp	2.0	0.7	25	0.600	3.82	0.501	7.56	26.17	139.8	-	4

Table 6. Computer simulation results with a type 3 lung configuration (R_r = 6 cm $H_2O/l/s$; C_r = 0.025 l/cm H_2O; R_l = 12 cm $H_2O/l/s$; C_l = 0.025 l/cm H_2O)

mode	shape	Ventilation Parameters			Before Pause		End of Inspiration				system τ (s)	Iter.
		T_i (s)	VT (l)	pause (% T_i)	V_t/V_t	MLP (cm H_2O)	$R_t(T_i)$ V_t/V_t	MLP (cm H_2O)	PIP (cm H_2O)	Q_{max} (l/min)		
flow	const	2.0	0.7	0	-	-	1.078	7.00	15.57	21.0	-	-
flow	const	4.0	0.7	0	-	-	1.038	7.00	14.78	10.5	-	-
flow	const	2.0	1.0	0	-	-	1.078	10.01	22.24	30.0	-	-
flow	const	2.0	0.7	25	1.105	7.01	1.011	8.75	16.09	28.0	-	-
flow	inc.	2.0	0.7	0	-	-	1.143	4.67	17.10	42.0	-	-
flow	dec.	2.0	0.7	0	-	-	1.017	9.34	14.22	42.0	-	-
flow	h-sin	2.0	0.7	0	-	-	1.038	7.00	14.49	33.0	-	-
flow	q-sin	2.0	0.7	0	-	-	1.020	8.92	14.27	33.0	-	-
flow	trap.	2.0	0.7	0	-	-	1.022	8.56	14.28	28.0	-	-
flow	d_exp	2.0	0.7	0	-	-	1.006	11.31	14.08	105.7	-	-
flow	sh-sin	2.0	0.7	0	-	-	1.006	10.36	14.14	57.8	-	-
flow	r_exp	2.0	0.7	0	-	-	1.275	2.71	21.54	105.5	-	-
press.	const	2.0	0.7	0	-	-	1.001	12.43	14.00	210.0	0.188	4
press.	inc.	2.0	0.7	0	-	-	1.088	6.34	15.76	23.6	-	4
press.	r_exp	2.0	0.7	0	-	-	1.273	2.77	21.51	104.9	-	4
flow	inc.	2.0	0.7	25	1.186	4.67	1.019	7.00	18.11	56.0	-	-
flow	dec.	2.0	0.7	25	1.030	9.34	1.003	10.50	14.38	56.0	-	-
flow	h-sin	2.0	0.7	25	1.063	7.00	1.007	8.75	14.84	44.0	-	-
flow	q-sin	2.0	0.7	25	1.035	8.92	1.004	10.19	14.46	44.0	-	-
flow	trap.	2.0	0.7	25	1.039	8.56	1.004	9.92	14.49	37.3	-	-
flow	exp.	2.0	0.7	25	1.011	11.32	1.001	12.0	14.11	141.0	-	-
flow	sh-sin	2.0	0.7	25	1.014	10.36	1.002	11.28	14.31	77.1	-	-
flow	r_exp	2.0	0.7	25	1.336	2.71	1.032	5.52	23.96	140.5	-	-
press.	const	2.0	0.7	25	1.007	11.96	1.001	12.47	14.05	210.7	0.188	4
press.	inc.	2.0	0.7	25	1.123	6.18	1.013	8.13	16.44	32.8	-	3
press.	r_exp	2.0	0.7	25	1.334	2.77	1.031	5.58	23.93	139.7	-	3

Table 7. Computer simulation results with a type 4 lung configuration ($R_r = 6$ cm $H_2O/l/s$; $C_r = 0.0125$ l/cm H_2O; $R_l = 12$ cm $H_2O/l/s$; $C_l = 0.025$ l/cm H_2O)

mode	shape	T_i (s)	VT (l)	pause (% T_i)	V_r/V_i	MLP (cm H₂O)	R_x(T_i) V_r/V_i	MLP (cm H₂O)	PIP (cm H₂O)	Q_max (l/min)	system τ (s)	Iter.
flow	const	2.0	0.7	0	-	-	0.558	9.66	20.76	21.0	-	-
flow	const	4.0	0.7	0	-	-	0.529	9.50	19.71	10.5	-	-
flow	const	2.0	1.0	0	-	-	0.558	13.80	29.65	30.0	-	-
flow	const	2.0	0.7	25	0.579	9.76	0.503	12.02	21.45	28.0	-	-
flow	inc.	2.0	0.7	0	-	-	0.612	6.53	22.74	42.0	-	-
flow	dec.	2.0	0.7	0	-	-	0.508	12.80	19.01	42.0	-	-
flow	h-sin	2.0	0.7	0	-	-	0.520	9.67	19.44	33.0	-	-
flow	q-sin	2.0	0.7	0	-	-	0.510	12.24	19.09	33.0	-	-
flow	trap.	2.0	0.7	0	-	-	0.511	11.75	19.11	28.0	-	-
flow	d_exp	2.0	0.7	0	-	-	0.503	15.43	18.78	105.7	-	-
flow	sh-sin	2.0	0.7	0	-	-	0.502	14.16	18.90	57.8	-	-
flow	r_exp	2.0	0.7	0	-	-	0.739	3.86	28.18	105.5	-	-
press.	const	2.0	0.7	0	-	-	0.501	16.94	18.68	280.2	0.116	4
press.	inc.	2.0	0.7	0	-	-	0.566	8.80	21.01	23.6	-	3
press.	r_exp	2.0	0.7	0	-	-	0.737	3.96	28.22	104.9	-	4
flow	inc.	2.0	0.7	25	0.648	6.61	0.505	9.69	24.05	56.0	-	-
flow	dec.	2.0	0.7	25	0.515	12.91	0.501	14.35	19.27	56.0	-	-
flow	h-sin	2.0	0.7	25	0.534	9.78	0.501	12.02	19.98	44.0	-	-
flow	q-sin	2.0	0.7	25	0.518	12.35	0.501	13.94	19.40	44.0	-	-
flow	trap.	2.0	0.7	25	0.520	11.86	0.501	13.57	19.45	37.3	-	-
flow	d_exp	2.0	0.7	25	0.505	15.56	0.500	16.34	18.82	141.0	-	-
flow	sh-sin	2.0	0.7	25	0.505	14.28	0.500	14.28	19.19	77.1	-	-
flow	r_exp	2.0	0.7	25	0.803	3.92	0.509	7.71	31.06	140.5	-	-
press.	const	2.0	0.7	25	0.503	16.43	0.500	16.99	18.75	281.3	0.116	4
press.	inc.	2.0	0.7	25	0.593	8.70	0.503	11.23	21.92	32.7	-	3
press.	r_exp	2.0	0.7	25	0.800	4.01	0.509	7.79	31.03	139.8	-	3

Table 8. Computer simulation results with a type 5 lung configuration (R_r = 6 cm H_2O/l/s; C_r = 0.0375 l/cm H_2O; R_l = 12 cm H_2O/l/s; C_l = 0.0125 l/cm H_2O)

| | Ventilation Parameters | | | | Before Pause | | End of Inspiration | | | | | |
mode	shape	T_i (s)	VT (l)	pause (% T_i)	V_r/V_l	MLP (cm H_2O)	$R_v(T_i)$ V_r/V_l	MLP (cm H_2O)	PIP (cm H_2O)	Q_{max} (l/min)	system τ (s)	iter.
flow	const	2.0	0.7	0	-	-	2.891	7.12	15.44	21.0	-	-
flow	const	4.0	0.7	0	-	-	2.945	7.07	14.72	10.5	-	-
flow	const	2.0	1.0	0	-	-	2.891	10.18	22.05	30.0	-	-
flow	const	2.0	0.7	25	2.855	7.16	2.992	8.88	15.92	28.0	-	-
flow	inc.	2.0	0.7	0	-	-	2.804	4.78	16.87	42.0	-	-
flow	dec.	2.0	0.7	0	-	-	2.981	9.47	14.16	42.0	-	-
flow	h-sin	2.0	0.7	0	-	-	2.957	7.13	14.37	33.0	-	-
flow	q-sin	2.0	0.7	0	-	-	2.977	9.05	14.20	33.0	-	-
flow	trap.	2.0	0.7	0	-	-	2.975	8.69	14.20	28.0	-	-
flow	d_exp	2.0	0.7	0	-	-	2.993	11.44	14.07	105.7	-	-
flow	sh-sin	2.0	0.7	0	-	-	2.995	10.49	14.09	57.8	-	-
flow	r_exp	2.0	0.7	0	-	-	2.637	2.80	21.13	105.5	-	-
press.	const	2.0	0.7	0	-	-	3.000	12.69	14.00	209.9	0.197	4
press.	inc.	2.0	0.7	0	-	-	2.878	6.49	15.60	23.4	-	4
press.	r_exp	2.0	0.7	0	-	-	2.640	2.87	21.10	104.8	-	4
flow	inc.	2.0	0.7	25	2.750	4.81	2.986	7.13	17.82	56.0	-	-
flow	dec.	2.0	0.7	25	2.967	9.51	2.998	10.64	14.28	56.0	-	-
flow	h-sin	2.0	0.7	25	2.927	7.17	2.996	8.88	14.65	44.0	-	-
flow	q-sin	2.0	0.7	25	2.960	9.09	2.998	10.32	14.34	44.0	-	-
flow	trap.	2.0	0.7	25	2.956	8.73	2.998	10.05	14.36	37.3	-	-
flow	d_exp	2.0	0.7	25	2.989	11.49	3.000	12.13	14.09	141.0	-	-
flow	sh-sin	2.0	0.7	25	2.988	10.54	3.000	11.41	14.19	77.1	-	-
flow	r_exp	2.0	0.7	25	2.568	2.82	2.975	5.65	23.48	140.5	-	-
press.	const	2.0	0.7	25	2.996	12.27	3.000	12.70	14.01	210.2	0.197	4
press.	inc.	2.0	0.7	25	2.834	6.35	2.991	8.28	16.21	32.4	-	3
press.	r_exp	2.0	0.7	25	2.571	2.88	2.976	5.71	23.45	139.7	-	3

Table 9. Computer simulation results with a type 5a lung configuration (R_r = 6 cm $H_2O/l/s$; C_r = 0.025 l/cm H_2O; R_l = 12 cm $H_2O/l/s$; C_l = 0.0125 l/cm H_2O)

mode	shape	T_i (s)	VT (l)	pause (% T_i)	Before Pause		End of Inspiration				system τ (s)	Iter.
					V_r/V_t	MLP (cm H_2O)	$R_r(T_i)$ V_r/V_t	MLP (cm H_2O)	PIP (cm H_2O)	Q_{max} (l/min)		
flow	const	2.0	0.7	0	-	-	2.000	9.34	20.06	*21.0*	-	-
flow	const	*4.0*	0.7	0	-	-	2.000	9.34	19.36	10.5	-	-
flow	const	2.0	*1.0*	0	-	-	2.000	13.34	28.65	30.0	-	-
flow	const	2.0	0.7	*25*	2.000	9.34	2.000	11.67	20.52	28.0	-	-
flow	inc.	2.0	0.7	0	-	-	2.000	6.23	21.45	42.0	-	-
flow	dec.	2.0	0.7	0	-	-	2.000	12.44	18.77	42.0	-	-
flow	h-sin	2.0	0.7	0	-	-	2.000	9.33	18.92	33.0	-	-
flow	q-sin	2.0	0.7	0	-	-	2.000	11.89	18.80	33.0	-	-
flow	trap.	2.0	0.7	0	-	-	2.000	11.41	18.79	28.0	-	-
flow	d_exp	2.0	0.7	0	-	-	2.000	15.08	18.74	105.7	-	-
flow	sh-sin	2.0	0.7	0	-	-	2.000	13.81	18.71	57.8	-	-
flow	r_exp	2.0	0.7	0	-	-	2.000	*3.61*	*25.63*	105.5	-	-
press.	const	2.0	0.7	0	-	-	2.000	*17.28*	*18.67*	*280.0*	0.15	4
press.	inc.	2.0	0.7	0	-	-	2.000	8.70	20.17	22.7	-	4
press.	r_exp	2.0	0.7	0	-	-	2.000	*3.70*	*25.59*	104.8	-	4
flow	inc.	2.0	0.7	25	2.000	6.23	2.000	9.34	22.37	56.0	-	-
flow	dec.	2.0	0.7	25	2.000	12.45	2.000	14.00	18.85	56.0	-	-
flow	h-sin	2.0	0.7	25	2.000	9.33	2.000	11.67	19.11	44.0	-	-
flow	q-sin	2.0	0.7	25	2.000	11.89	2.000	13.59	18.90	44.0	-	-
flow	trap.	2.0	0.7	25	2.000	11.41	2.000	13.22	18.90	37.3	-	-
flow	d_exp	2.0	0.7	25	2.000	15.09	2.000	15.99	18.76	141.0	-	-
flow	sh-sin	2.0	0.7	25	2.000	13.82	2.000	15.04	18.77	77.1	-	-
flow	r_exp	2.0	0.7	25	2.000	3.61	2.000	7.36	27.94	140.5	-	-
press.	const	2.0	0.7	25	2.000	16.81	2.000	17.28	18.67	280.0	0.15	4
press.	inc.	2.0	0.7	25	2.000	8.51	2.000	11.05	20.72	31.1	-	3
press.	r_exp	2.0	0.7	25	2.000	3.70	2.000	7.44	27.92	139.8	-	4

266

Table 10. A condensed table of the results from the methodical computer simulation with emphasis on the qualitative trends and effects on different lung configuration types

	Type 1 $R_r = R_i$ $C_r = C_i$ $\tau_r = \tau_i$	Type 2 $R_r = R_i$ $C_r \neq C_i$ $\tau_r \neq \tau_i$	Type 3 $R_r \neq R_i$ $C_r = C_i$ $\tau_r \neq \tau_i$	Type 4 $R_r < R_i$ $C_r < C_i$ $\tau_r \neq \tau_i$	Type 5 $R_r < R_i$ $C_r > C_i$ $\tau_r \neq \tau_i$	Type 5a $R_r < R_i$ $C_r > C_i$ $\tau_r = \tau_i$
Influence of shape on R_v	none	yes	yes	yes	yes	none
Shape *without pause* with R_v closest to 1.0	all shapes: $R_v = 1.0$	inc. exp. flow/press.	const press.	inc. exp. flow/press.	inc. exp. flow/press.	all shapes: $R_v = C_r/C_i$
Shape *without pause* with R_v farthest from 1.0	$R_v = 1.0$ for all shapes	const press. sh-sin flow	inc. exp. flow/press.	const press. sh-sin flow	const press. sh-sin flow	$R_v = C_r/C_i$ for all shapes
Shape with lowest mean lung pressure over time	inc. exp. flow/press.	inc. exp. flow/press.	inc. exp. flow/press.	inc. exp. flow/press.	inc. exp. flow/press.	inc. exp. flow/press.
Shape with highest mean lung pressure over time	const press.	const press.	const press.	const press.	const press.	const press.
Effect of increased T_i on $R_v = V_r/V_i$	none for all shapes	worse or no improvement for all shapes	improved for all shapes	worse for all shapes	worse for all shapes	none for all shapes
Effect of increased T_i on MLP(T_i)	none for all flow shapes & r_exp, press.; ↑ for other press. shapes	↓ for all flow shapes and r_exp, press.; ↑ for other press. shapes;	none for all flow shapes & r_exp, press.; ↑ for other press. shapes	↓ for all flow shapes & r_exp, press; ↑ for other press. shapes	↓ for all flow shapes & r_exp, press; ↑ for other press. shapes	none for all flow shapes & r_exp, press; ↑ for other press. shapes
Effect of inspiratory pause on R_v	none for all shapes	worse or no improvement for all shapes	better for all shapes; const press. unchanged	worse for all shapes	worse for all shapes; const press. unchanged	none for all shapes
Effect of inspiratory pause on MLP(T_i)	↑ for all shapes; none for const press.	↑ for all shapes; none for const press.	↑ for all shapes; none for const press.	↑ for all shapes; none for const press.	↑ for all shapes; none for const press.	↑ for all shapes; none for const press.
Effect of increased VT with const flow shape	none on R_v, ↑ MLP, ↑ PIP	none on R_v, ↑ MLP, ↑ PIP	none on R_v, ↑ MLP, ↑ PIP	none on R_v, ↑ MLP, ↑ PIP	none on R_v, ↑ MLP, ↑ PIP	none on R_v, ↑ MLP, ↑ PIP
Lowest pressure at carina (PIP)	const press.	const press.	const press.	const press.	const press.	const press.
Highest pressure at carina (PIP)	inc. exp. flow/press.	inc. exp. flow/press.	inc. exp. flow/press.	inc. exp. press./flow	inc. exp. flow/press.	inc. exp. flow/press.

From the condensed results of table 10, a pattern in the response of the different lung types to different inspiratory waveforms becomes evident. The similarity of the response of lung configuration types 1 and 5a is striking and makes physical sense since the time constants for the parallel respiratory pathways are identical in both lung configuration types. Even more interesting is the similarity in the response of the lung types when the compliance is unequal (types 2,4 and 5). The type 3 lung (ECUR) is the odd man out and is, unfortunately, the one most studied with the mechanical lung models. The ECUR lung configuration's different response (sometimes exactly opposite) compared to the lung types where compliance is unequal (types 2,4 and 5) dramatically illustrates the danger of trying to obtain one best waveform for all lung configurations. Thus, table 10 explains why the tests performed on random samples of the patient population (section 5.3.6) were doomed to obtain conflicting and divisive results.

Another interesting result of the computer simulation is the prediction that the rising exponential flowrate or pressure waveform will generate both the lowest mean lung pressure and the most even $R_v(T_i)$ for all lung types except for an ECUR lung configuration. This observation that a new waveform was exhibiting promising properties was gratifying but also puzzling. A rigorous and scientific explanation for the superior properties of the rising exponential pressure waveform with non-ECUR lungs was sought so that other waveforms possessing the same characteristics that impart the desirable properties could be designed. This search using the computer model was unsuccessful and the answer did not become apparent until a mathematical analysis of the problem was performed (section 5.6).

5.5 A Proposed Lung Classification Scheme

Beyond the explanation of the inconclusive results of previous workers, the present hypothesis may have more immediate value in everyday clinical practice. The observation that in table 10, there are three distinct responses to different waveforms and ventilatory procedures like an inspiratory pause and an increased T_i makes it practical and worthwhile to propose that patients should be classified into three classes according to their lung configuration. The system is practical because the 16 different lung configurations have been effectively collapsed into 3 lung classes. Furthermore, if a patient's lung class is known, it is then straightforward to decide what kind of waveform to use and also what kind of waveform and ventilatory features should not be used.

The proposed lung classification scheme is:

Defining Conditions

Class I: types 1, 5a   equal individual time constants

Class II: types 2, 4, 5   unequal compliance, no restriction on resistance

Class III: type 3   equal compliance, unequal resistance

If it turns out in clinical practice that lung class II patients generally experience more severe respiratory insufficiency, the definitions of class II and III should be switched so that the numbering scheme also reflects the seriousness of the patient's respiratory condition with class I being the least serious. Normally, a class I patient would be a patient with a normal and healthy respiratory system since the type 5a lung configuration which also belongs to Class I is expected to be a statistically rare event.

5.6 The Mechanical Inspiration Hypothesis

A formal statement of the mechanical inspiration hypothesis and its definitions and corollaries that have been developed through the computer model is now presented:

<u>All lung configurations fit into 3 classes (I, II and III) with distinctive differences in their dynamic response to inspiratory waveform inputs of pressure or flowrate, to an inspiratory pause and to the time duration of inspiration during mechanical ventilation.</u>

Definitions:

1. A class I lung has equal time constants for all respiratory pathways.

2. A class II lung has unequal time constants and unequal compliances for the different respiratory pathways, with no restriction on the equality of flow resistances.

3. A class III lung has unequal time constants resulting from a difference in flow resistances in the respiratory pathways while the compliances are equal.

Corollaries:

1a. The distribution of ventilation, $R_v(T_i)$, in a class I lung is independent of the shape of the inspiratory waveform input (pressure or flowrate), duration of inspiration, T_i, or presence and duration of the inspiratory pause, IP, and is determined by the compliance ratio only.

1b.   Inspiratory waveforms (pressure P(t) or flowrate Q(t)) whose time derivatives are still strong functions of time, $dP(t)/dt = f(t)$ or $dQ(t)/dt = f(t)$, are recommended for reduced mean lung pressure, $MLP(T_i)$, for class I lungs.

1c. $MLP(T_i)$ in a class I lung is independent of T_i.

1d.   An inspiratory pause will increase $MLP(T_i)$ in a class I lung and is not recommended.

2a.   Inspiratory waveforms (pressure P(t) or flowrate Q(t)) whose time derivatives are still strong functions of time, $dP(t)/dt = f(t)$ or $dQ(t)/dt = f(t)$, are recommended for more even $R_v(T_i)$ and reduced $MLP(T_i)$ for class II lungs.

2b.   A shorter T_i produces more even $R_v(T_i)$ with class II lungs and is recommended.

2c.   An IP gives more uneven $R_v(T_i)$ with class II lungs and is not recommended.

2d.   An increase in T_i will marginally decrease $MLP(T_i)$ in class II lungs

2e.   An IP will increase $MLP(T_i)$ in a class II lung and is not recommended.

3a.   A constant pressure waveform will give the most even $R_v(T_i)$ for a class III lung.

3b.   An increase in T_i will make $R_v(T_i)$ more even in a class III lung and is recommended.

3c.   An IP will make $R_v(T_i)$ more equal in a class III lung and is strongly recommended.

3d. A constant pressure waveform will give the highest $MLP(T_i)$ for a class III lung and its $R_v(T_i)$ advantages should be weighed against the high $MLP(T_i)$ in the clinical setting.

3e. A rising exponential flowrate waveform will give the lowest $MLP(T_i)$ but also the most uneven $R_v(T_i)$ for a class III lung and its use also has to be decided in the clinical setting.

3f. An increase in T_i will give a lower $MLP(T_i)$ in a class III lung.

3g. An IP will give an increase of $MLP(T_i)$ with class III lungs.

5.7 Mathematical Analysis in the Time Domain

The results from the computer analysis gave more insight into the actual physical problem and a mathematical analysis was performed in the time domain. The actual mathematical derivations will not be shown for brevity. Only the results of the mathematical analysis which describe the relationship of $MLP(T_i)$ and $R_v(t)$, the two primary parameters of interest in this study, to the lung mechanical parameters (R_r, C_r, R_l, C_l) and ventilatory parameters (VT, T_i) for different inspiratory waveforms are shown.

The waveforms that were analyzed were the constant pressure, increasing pressure and the rising exponential pressure waveforms.

Constant Pressure Waveform at the carina (pressure waveform controlled from the ETT distal tip pressure sample:

$$P_c(t) = P_c$$

$$MLP(T_i) = \frac{P_c}{2T_i} \left(2T_i + R_r C_r(e^{-\frac{T_i}{R_r C_r}} - 1) + R_l C_l(e^{-\frac{T_i}{R_l C_l}} - 1)\right) \quad \textbf{5.29}$$

$$R_v(t) = \frac{C_r}{C_l} \cdot \left[\frac{1 - e^{-\frac{t}{R_r C_r}}}{1 - e^{-\frac{t}{R_l C_l}}}\right] \quad \textbf{5.30}$$

Increasing Pressure Waveform (ramp passing through origin) at the carina (pressure waveform controlled from the ETT distal tip pressure sample:

$$P_c(t) = mt \text{ where m is the ramp slope.}$$

$$MLP(T_i) = \frac{m}{2T_i} \cdot \left(T_i^2 - (R_r C_r + R_l C_l) T_i\right) -$$

$$\frac{m}{2T_i} \cdot \left[(R_r C_r)^2 (e^{-\frac{T_i}{R_r C_r}} - 1) - (R_l C_l)^2 (e^{-\frac{T_i}{R_l C_l}} - 1)\right] \quad \textbf{5.31}$$

$$R_v(t) = \frac{C_r}{C_l} \cdot \left[\frac{t + R_r C_r(e^{-\frac{t}{R_r C_r}} - 1)}{t + R_l C_l(e^{-\frac{t}{R_l C_l}} - 1)}\right] \quad \textbf{5.32}$$

$$R_v(T_i) = \frac{C_r}{C_l} \cdot \left[\frac{T_i + R_r C_r (e^{-\frac{T_i}{R_r C_r}} - 1)}{T_i + R_l C_l (e^{-\frac{T_i}{R_l C_l}} - 1)} \right]$$

$$5.33$$

Rising exponential pressure waveform ($P_c(t=0) \neq 0$) at the carina (pressure waveform controlled from the ETT distal tip pressure sample: $P_c(t) = P_o \exp(5t/T_i)$ where the time constant of the exponential was arbitrarily taken to be $T_i/5$. Thus at $t = T_i$, $\exp(5t/T_i)$ = $\exp(5)$. P_o is derived from the mechanical and ventilatory parameters:

$$P_c(t) = \left[\frac{VT}{C_r + C_l} + \left[\frac{R_r R_l}{R_r + R_l} \cdot \frac{VT}{T_i} \right] \right] \cdot e^{\frac{5t}{T_i}} = P_o \, e^{\frac{5t}{T_i}}$$

$$5.34$$

$$MLP(T_i) = \frac{P_o}{2} \left[\frac{1}{5R_r C_r + T_i} \cdot \left[\frac{T_i}{5} e^{\frac{5t}{T_i}} + R_r C_r \, e^{-\frac{t}{R_r C_r}} \right] \right] + $$
$$\frac{P_o}{2} \left[\frac{1}{5R_l C_l + T_i} \cdot \left[\frac{T_i}{5} e^{\frac{5t}{T_i}} + R_l C_l \, e^{-\frac{t}{R_l C_l}} \right] \right]$$

$$5.35$$

$$R_v(t) = \frac{C_r}{C_l} \cdot \left[\frac{5R_l C_l + T_i}{5R_r C_r + T_i} \right] \left[\frac{e^{\frac{5t}{T_i}} - e^{-\frac{t}{R_l C_l}}}{e^{\frac{5t}{T_i}} - e^{-\frac{t}{R_r C_r}}} \right]$$

$$5.36$$

Note that if $t \gg \tau_r$ and $t \gg \tau_l$, then the $\exp(-t/R_r C_r)$ and $\exp(-t/R_l C_l)$ terms in equation 5.36 for $R_v(t)$ reduce to zero such that the equation becomes:

$$R_v(t) = \frac{C_r}{C_l} \cdot \left[\frac{5R_lC_l + T_i}{5R_rC_r + T_i} \right]$$

<div align="right">5.37</div>

Thus, the rising exponential pressure waveform has the interesting peculiarity in its $R_v(t)$ expression that as t tends to T_i and if $T_i \gg \tau_r$ and $T_i \gg \tau_l$, then the transient response of $R_v(t)$ becomes independent of the mechanical parameters while the steady state response remains dependent on the mechanical parameters (equation 5.37). This behavior is depicted in figure 42 which was obtained by capturing the screen output of a modified version of the computer model.
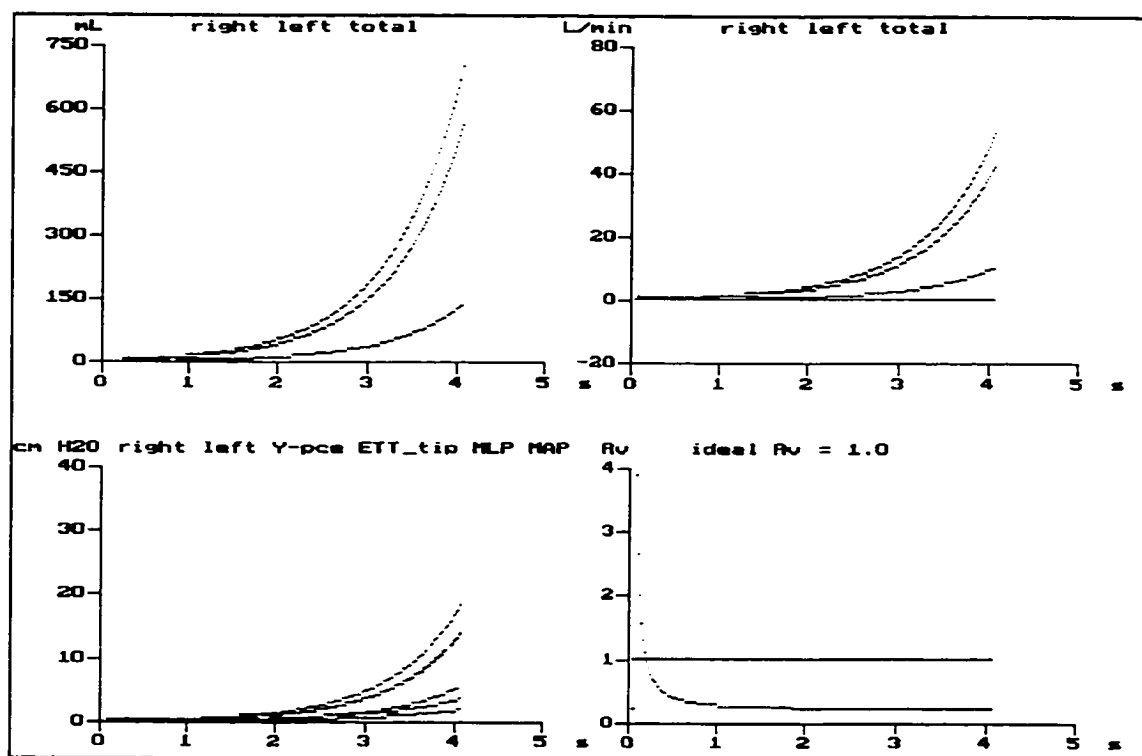
Figure 42. The rising exponential pressure waveform and the response of $R_v(t)$ (bottom right plot). Top left: volume vs. time; top right: flowrate vs. time; bottom left: pressures vs. time

In figure 42, the top left plot represents $V_r(t)$, $V_l(t)$ and $V_r(t) + V_l(t)$ as inspiration progresses. The top right plot shows the flowrates, $Q_r(t)$, $Q_l(t)$ and $Q_{ett}(t) = Q_r(t) + Q_l(t)$, over time. The bottom left graph shows the pressures and time-averaged pressures in the right and left lungs, at the Y-piece and at the ETT distal tip. The bottom right graph shows the evolution of $R_v(t)$ as inspiration progresses. The transient response of $R_v(t)$ to a rising exponential pressure waveform with a VT of 700 ml, T_i of 4 s, R_r of 2 cm $H_2O/l/s$, R_l of 12 cm $H_2O/l/s$, C_r of 0.01 l/cm H_2O and C_l of 0.1 l/cm H_2O and a 9 mm i.d. ETT is clearly seen in figure 42. The steady state response of $R_v(t)$ as t exceeds 2 s is also evident from figure 42. The behavior of $R_v(t)$ from the computer model (figure 42) corroborates the exact solution for $R_v(t)$ for a rising exponential pressure waveform (equations 5.36 and 5.37) obtained from the independent mathematical analysis in the time domain.

A close inspection of the equations for $R_v(t)$ and $MLP(T_i)$ for the constant pressure, increasing pressure and rising exponential pressure waveforms also reveals that the transient response of the first two is dominated by the individual time constants of the parallel pathways. While the transient response of the rising exponential does include the individual time constants, it also includes another term, $exp(5t/T_i)$, that exponentially increases with time and dominates the transient response as t tends to T_i while the contribution to the transient response from the individual time constants decays exponentially with time because their exponents are negative.

Therefore, from the mathematical viewpoint, we come to the conclusion that the rising exponential flowrate gives better distribution of ventilation because the derivative

with respect to time of the equation that defines the input waveform is still a strong (i.e., increasing) function of time. In other words, during the mathematical analysis, the equation of the input waveform, $P_c(t)$, has to be differentiated with respect to time to obtain the exact analytical solutions for $R_v(t)$ and $MLP(T_i)$. The term resulting from the differentiation, $dP_c(t)/dt$, is present in the transient response term of the analytical solutions.

The exact analytical solutions can be interpreted from a physical point of view that for the rising exponential pressure input, the influence of the input waveform shape persists (and actually grows stronger) in time as t tends to T_i during mechanical inflation of the patient's lungs because $dP_c(t)/dt$ is an increasing function of time. This explanation can be reinforced if we look at the constant pressure waveform and the increasing pressure waveform.

For the constant pressure waveform, $P_c(t) = P_c$. Therefore, $dP_c(t)/dt = 0$. Thus the influence of the input waveform shape on the transient response of any lung configuration is zero. The transient response is solely determined by the individual time constants.

For the increasing pressure waveform, $P_c(t) = mt$ where m is the ramp slope, a positive constant, $dP_c(t)/dt = m$ which is a constant and therefore not a function of time. Consequently, there again, the transient response is determined solely by the individual time constants of the parallel pulmonary pathways.

To verify the above hypothesis, two new waveshapes were added to the computer model after the mathematical analysis whose time derivatives are increasing functions of

time. These were the time squared: $P_c(t) = P_o(t/T_i)^2$ and time cubed: $P_c(t) = P_o(t/T_i)^3$

pressure waveforms where P_o is the same as in the equation for the rising exponential

pressure waveform. The time squared and the time cubed pressure waveforms both

produced more even $R_v(T_i)$ for a class II lung and lower MLP(T_i) for all lung classes (I,

II and III) compared to the constant or increasing pressure waveforms during the

computer simulation, as predicted by the mathematical analysis (table 11).

Table 11. A comparison of the time squared and time cubed pressure waveforms against other pressure waveforms for all 3 lung classes. T_i was set at 2 seconds and VT at 0.7 1 with no inspiratory pause.

Pressure waveform	CLASS I $R_r = 6, C_r = 0.025$ $R_l = 6, C_l = 0.025$		CLASS II $R_r = 6, C_r = 0.0125$ $R_l = 6, C_l = 0.025$		CLASS III $R_r = 6, C_r = 0.025$ $R_l = 12, C_l = 0.025$	
	$R_v(T_i)$	MLP(T_i)	$R_v(T_i)$	MLP(T_i)	$R_v(T_i)$	MLP(T_i)
constant	1.000	12.96	0.500	17.63	1.001	12.43
increasing	1.000	6.52	0.520	8.91	1.088	6.34
rising_exp.	1.000	2.78	0.579	3.80	1.273	2.77
time sq.	1.000	4.37	0.539	6.00	1.156	4.28
time cubed	1.000	3.29	0.555	4.53	1.213	3.23

Consequently, the analysis indicates that any waveform (pressure $P_c(t)$ or flowrate

$Q_{cn}(t)$) whose time derivative ($dP_c(t)/dt$ or $dQ_{cn}(t)/dt$) is a strong (i.e., increasing) function

of time will be beneficial to a class I or a class II lung, from the point of view of $R_v(T_i)$

and MLP(T_i).

The exact analytical solutions also present a reinforcing argument for ignoring the

direction of the inequalities in the parallel network that serves as our model. Terms that

include a difference between the compliances or resistances (C_r-C_l, R_r-R_l) are absent in the exact analytical solutions that describe the response and behavior of the model of the lungs to various inspiratory waveforms. If these terms had been present, then it would have meant that the direction of the inequality would affect the system behavior. Thus the argument that the direction of inequality can be ignored based on the physical symmetry of the parallel network model is supported by the exact analytical solutions.

5.8 Proposed Algorithms for Lung Class Identification and Respiratory Diagnosis

The lung classification scheme of section 5.5 would remain of purely academic interest and be of relatively little practical value if there was not a fast and convenient way of identifying the lung class of a patient in real time, during routine clinical practice. Having the patient tested in a respiratory function laboratory for lung class identification prior to anesthesia and/or mechanical ventilation would be impractical and costly in time and manpower, inconvenience the patient and be inapplicable when the patient is admitted on an emergency basis, e.g., following a car crash.

While using the computer simulation to collect the data in tables 4 - 11, a pattern in the dynamic response of the different lung classes to different inspiratory waveforms was observed. The dynamic response pattern suggests that the control software of a computer controlled ventilator, (especially the GRADS ventilator because it could be used without any hardware modification), could be modified to systematically identify the lung class of a given patient. Among the numerous possible ways of devising high level lung

class identification algorithms based on the lung classification scheme of section 5.5, three examples will be described for illustration purposes.

We are explicitly assuming in this section that real-time $ETCO_2$ values from breath to breath will be available to the ventilator control software. It is also assumed in these lung class identification algorithms that changing the pattern of the ventilation for 2 consecutive breaths will not disrupt the ventilation of the patient. Another assumption is that the lung CO_2 production will remain constant over the duration of 2 breaths (4 - 20 seconds) such that the $ETCO_2$ during the 2 breaths lung detection algorithm will be solely a function of the $R_v(T_i)$.

5.8.1 Increased Inspiratory Time

From table 10, it is evident that an increased T_i will improve $R_v(T_i)$ for a class III (type 3) lung while it will have no benefits for class I lungs or even make the $R_v(T_i)$ more uneven for class II lungs. For example, from table 6, with a constant flowrate waveform, lengthening T_i from 2.0 to 4.0 seconds, while keeping all other parameters constant results in an improvement of $R_v(T_i)$ from 1.078 to 1.038. Therefore, the ventilator control software could be programmed such that it, for example, increases the T_i while maintaining VT and inspiratory waveform between consecutive breaths.

An immediate decrease in end-tidal CO_2 ($ETCO_2$) should be apparent in the exhalation following the increased T_i inflation because of the better distribution of ventilation, $R_v(T_i)$, with a class III lung. The same T_i lengthening technique should yield

no significant change in $ETCO_2$ with a class I lung or even an increase in $ETCO_2$ with a class II lung. Thus, a class III lung would be positively identified.

5.8.2 Inspiratory Pause

It is also clear from table 10, that an inspiratory pause will also improve the $R_v(T_i)$ for a class III lung while having no effect on a class I lung or even deteriorating the $R_v(T_i)$ for a class II lung. Thus, here again, this distinguishing characteristic of the class III lung could be used to positively identify it. Looking at table 6 again, we choose the rising exponential flowrate inspiratory waveform which gives the most dramatic improvement of $R_v(T_i)$, 1.275 to 1.032, with an inspiratory pause for a class III lung. For example, the ventilator control software could be designed to follow a rising exponential flowrate waveform with a T_i of 2.0 seconds without pause with the same waveform but containing a 25% T_i inspiratory pause (1.5 seconds active inflation; 0.5 second pause) while keeping VT constant.

A class III lung will be positively identified by an immediate drop of $ETCO_2$ following the inflation with the inspiratory pause compared to the previous waveform without the inspiratory pause. No lowering of $ETCO_2$ will be seen with a class I lung or an increase or no change in $ETCO_2$ is expected with a class II lung.

For all practical purposes, the main requirement is really to identify the class III lung because promising new inspiratory patterns like the rising exponential flowrate or pressure waveforms are indicated for both class I and II lungs but not class III. In other words, there is no practical need to differentiate between a class I and a class II lung

while it is extremely important to be able to positively identify a class III lung so that, e.g., a rising exponential flowrate waveform is not used with a class III lung.

5.8.3 Consecutive Waveform Change

Finally, another way to achieve our priority of identification of lung class III is to change inspiratory waveforms between consecutive breaths. For example, table 10 indicates that if a constant pressure waveform is immediately followed by a rising exponential flowrate waveform of the same VT and T_i, a sudden rise of $ETCO_2$ will follow the inflation with the rising exponential flowrate waveform, for a class III lung. Obviously, the constant pressure waveform will need to be preceded by a few constant pressure breaths so that the VT feedback loop (section 5.4.7.2) can lock onto the desired pressure step size that will give the desired VT.

With the consecutive waveform change technique, a class I lung is expected to show no change in $ETCO_2$ while a class II lung is expected to produce a decrease in $ETCO_2$.

5.8.4 Pressure Monitoring at ETT Distal Tip During Inspiratory Pause

We now look at the problem of differentiating between a class I and a class II lung, which as stated before is not a practical necessity but is of academic interest since the solution will enhance our understanding of the dynamic behavior of a parallel lung network. It is assumed here that it has already been established through one of the above

algorithms that the lung is not class III and it is desired to positively identify a class I or class II lung.

A class I lung is characterized during the computer model simulations by the equality in pressure in each lung at all times during the inflation period, i.e., $P_r(t) = P_l(t); 0 \leq t \leq T_i$. Thus, if there is an inspiratory pause, there will be no gas redistribution (pendelluft) in a class I lung. Consequently, the pressure at the carina, measured at the ETT distal tip, will drop sharply during the inspiratory pause to a flat plateau.

With a non-class I lung, where the pressures are not generally equal in each lung at the end of active inflation, there will be gas redistribution during the inspiratory pause according to the pressure differential between the lungs. Thus the redistributing gas flow between the two lungs, via the carina, during the inspiratory pause, will cause the pressure at the carina, measured at the ETT distal tip, to decay in an exponential fashion to a plateau rather than falling steeply to a plateau (equations 5.22 and 5.38; figure 41). Thus, feature analysis of the carina pressure trace that focuses on the rate of drop of the pressure trace at the start of the inspiratory pause would be a way of differentiating between a class I and a class II or class III lung.

$$P_c(t) = \frac{R_r P_l(t) + R_l P_r(t)}{R_r + R_l} \qquad 5.38$$

Like for the inspiratory pause example above, the waveform could be chosen to emphasize the pressure differential at the end of the active inflation phase so that a pronounced equilibration gas flowrate between the lungs occurs during the inspiratory pause which will facilitate the feature analysis. The computer model predicts that all

lung classes can be positively identified by some simple identification algorithms that can be readily implemented on an integrated, computer controlled system like GRADS.

Knowledge of the lung class of the patient is critical to choosing the right waveform and T_i and whether to use an inspiratory pause or not. The automated lung class identification algorithm could warn the clinician if an inappropriate waveform is being used or it could change the waveform to a more indicated waveform and inform the clinician of its action (this latter feature would most likely be more acceptable in the ICU where patients are commonly left unattended on their ventilators than in the OR).

5.8.5 Determination of Effective Respiratory System Time Constant

According to the computer model of section 5.4, the use of a ventilator as a respiratory diagnosis tool could also be extended on the GRADS platform to determine the effective time constant, τ_e, of the respiratory system. τ_e can be determined from the flowrate response at the ETT, $Q_{ca}(t)$, to a pressure step (constant pressure waveform) at the carina delivered by a pressure control loop whose feedback signal is the pressure sampled from the ETT distal tip. $Q_{ca}(t)$ will decay exponentially in response to a pressure step with the maximum inspiratory flowrate, Q_{max} corresponding to the initial flowrate, $Q_{ca}(t=0)$. The point in time at which $Q_{ca}(t)$ decays to exp(-1) times Q_{max} (0.368 Q_{max}) corresponds to the time constant of the respiratory system, τ_e, and can be determined from monitoring the response of $Q_{ca}(t)$ to a pressure step input. The pressure step input does not need to be large to obtain τ_e. In fact, the pressure step should be low enough that Q_{max} is within the flowrate measurement range of the flowrate transducer.

The computer simulation is supported by the mathematical analysis which gave equation 5.39 below for $Q_{ea}(t)$ for a constant pressure waveform (see also equation 5.8):

$$Q_{ea}(t) = P_c \left[\frac{e^{-\frac{t}{R_rC_r}}}{R_r} + \frac{e^{-\frac{t}{R_lC_l}}}{R_l} \right]$$

5.39

The computer model indicates that τ_e could also be obtained from an increasing pressure waveform. For an increasing pressure waveform, $Q_{max} = Q_{ea}(T_i)$. The point in time when $Q_{ea}(t)$ reaches $(1-\exp(-1)) Q_{max} = (1 - 0.368) Q_{max} = 0.632 Q_{max}$ is the time constant of the respiratory system, τ_e, if T_i is large enough that $Q_{ea}(t)$ plateaus to an asymptote before $t = T_i$ (equation 5.40).

$$Q_{ea}(t) = m \left[C_r + C_l - C_r e^{-\frac{t}{R_rC_r}} - C_l e^{-\frac{t}{R_lC_l}} \right]$$

5.40

Knowledge of the respiratory system time constant, τ_e, will be useful in clinical practice because it has been shown with an ECUR (class III) mechanical lung model that if $T_i = 3\tau_e$, then there is an optimum compromise between $R_v(T_i)$ and duration of T_i (Banner & Lampotang 1988). T_i should not be too long since there will be less time remaining for the exhalation phase for a fixed respiratory frequency, which can cause problems like incomplete emptying of the lungs resulting in poorer ventilation, increased lung pressures and reduced cardiac output.

It should be noted that if the pressure step is controlled from a feedback signal sampled at the Y-piece, the time constant of the exponential decay of $Q_{ea}(t)$ will be heavily distorted by the flow resistance of the ETT, R_{ea}. Thus, pressure sampling at the Y-piece for the feedback signal would incorrectly give the time constant of the

respiratory system combined with the ETT resistance. Here again, the design advantages of the GRADS concept are demonstrated. The GRADS features of sampling pressure at the ETT distal tip and measuring flowrate at the ETT are essential to the lung class identification and respiratory time constant determination algorithms.

Before leaving the subject of pressure sampling location, the computer model also demonstrated clearly the enormous disparity between MAP determined from the Y-piece or breathing circuit and $MITP(T_i)$ determined from the ETT distal tip. The rising exponential waveform (flowrate or pressure) had the highest pressures measured at the Y-piece of all the waveforms while also having the lowest $MLP(T_i)$s. To the uninformed clinician, the high pressures in the breathing circuit with a rising exponential waveform will be alarming when it is actually the waveform that gives the lowest mean lung pressure and therefore with the least interference on cardiac output.

5.9 Conclusions and Recommendations

The design of GRADS fits well with the mechanical inspiration hypothesis derived in this chapter and many of its applications. For example, from tables 4 - 9, it can be seen that Q_{max}, the peak flowrate during inspiration can become quite high. The high effective recirculating flowrate while operating in a closed circuit in the GRADS design makes those high flowrates physically attainable first of all and secondly economically sustainable compared to conventional existing anesthesia delivery systems. Pressure sampling at the ETT distal tip will also allow the modulation through feedback control of pressure at the carina and also monitoring of pressure which is a more accurate

representation of the actual pressure in the lungs. The pressure sampling point used in conventional anesthesia delivery systems at the present time, will make pressure waveform shaping more complicated in those systems because the pressure in the circuit will be heavily influenced by the flowrate in the ETT and the flow resistance of the ETT itself.

The promising new waveshapes (rising exponential, time squared and time cubed) should be implemented in the GRADS system and tested on a test bench rig using a modified CO_2-producing, mechanical lung model (Lampotang et al. 1986) in open circuit ventilation. The $ETCO_2$, $MITP(T_i)$, PIP and MAP for the different waveshapes should be compared to validate the mathematical predictions. The same set of tests should then be repeated on the GRADS system while running in closed circuit ventilation mode.

The high level description of the algorithms for systematic lung class identification should be actually coded and tested on a double compartment mechanical lung model with independently adjustable compliances and resistances. Experiments to validate that the lung classification system is truly clinically relevant should be performed on the mechanical lung model first and then using live animals before finally going to clinical trials. Animal models will unfortunately be required as an intermediate step before going from the mechanical lung model to the human patient clinical trials because a valid argument can be made that the lungs are not a pair of parallel bellows but instead a branching network of myriad alveoli which are also subject to surface tension forces because of their small size (Laplace equation) and many other non-ideal effects.

With some careful consideration, the experimental protocol using anesthetized live animals could be designed such that they do not need to be sacrificed at the end of the tests. For example, unilateral changes in flow resistance of a respiratory pathway could be pharmacologically induced by local administration of bronchoconstrictors which wear out and cause no permanent physiological change or mechanically by lodging (e.g., by inflation of a cuff) a stint-like mechanical flow restriction of variable aperture into one mainstem bronchus of the animal which can be removed after the experiment.

Unilateral compliance changes might be induced mechanically by provoking a unilateral pneumothorax (ingress of air into the pleural cavity that separates the lungs and the chest wall causing a decrease in compliance because the affected lung collapses) in animal models that have separate pleural cavities (e.g., pigs but not dogs). Separate pleural cavities imply that a right lung pneumo- or hydrothorax will not cause the other (left) lung to collapse too. A hydrothorax (ingress of water into the pleural cavity) might be even preferable since sterile isotonic saline solution could be injected into the pleural cavity by a catheter thus allowing unilateral modulation of the compliance. The saline can be drawn out of the pleural cavity by aspirating on the catheter at the end of the experiment and any small amount of saline remaining in the pleural cavity will eventually get absorbed by the tissues of the test animal.

5.10 Summary

All possible different combinations and permutations of right and left compliances and right and left flow resistances have been cataloged and classified into three classes

according to their dynamic response to mechanical ventilation inspiratory waveform shape and ventilatory parameters like inspiratory time and inspiratory pause. Based on the proposed classification scheme, a mechanical inspiration hypothesis which reconciles the conflicting results of past studies on the effect of flowrate shaping on distribution of ventilation has been formulated. Using the new insight provided by the computer model and a mathematical analysis of the problem, new time-dependent inspiratory waveforms are proposed that promise to improve distribution of ventilation for a given lung class.

Finally, software algorithms that can be readily implemented on a ventilator platform and transform it into a respiratory diagnosis tool for systematic identification of lung class will be necessary if the different ventilatory parameters like inspiratory pause, time and waveform are not to be applied indiscriminately. These lung classification algorithms are described on a high level. The mechanical inspiration hypothesis and the hardware design of GRADS both predict that actual implementation on a ventilator of the lung class identification algorithms will be simple and straightforward.

A hypothesis which provides a consistent framework to interpret past work in the field of inspiratory waveform shaping has been formulated. Hopefully, the mechanical inspiration hypothesis will be validated by lung model experiments to be followed by animal and clinical experiments and will soon translate into improved and less expensive patient care.

The mechanical inspiration hypothesis is complementary and consistent with the GRADS design concepts, methodology and philosophy which was, in a nutshell, to

question and analyze all existing concepts and techniques related to an anesthesia delivery system with no preconceived notions and let engineering method and rigor determine the design. This chapter is an example of the power of the engineering design methodology described in chapter 4 and of the benefits to be derived when a thorough engineering approach is used when attacking a multidisciplinary problem. The mechanical inspiration hypothesis is likely to open the door for many clinical experiments and hardware applications that will benefit the patient. However, we must now return to the primary goal of this work, the GRADS system and its implementation and evaluation.

CHAPTER 6
FABRICATION OF PROTOTYPES AND REAL-TIME CONTROL SOFTWARE

This chapter documents the actual prototype implementation of the high level design and concepts embodied in figure 29 for an anesthesia ventilator that will be part of the anesthesia delivery system design depicted in figure 34. Beforehand, the two distinctive prototypes leading to the GRADS design, representing two system design iterations on the flowchart of figure 37, are also described.

The two distinctive prototypes preceding the GRADS design were part of the total engineering design methodology illustrated in the flowchart of figure 37. In fact, many entries in the design checklist of chapter 4 are a direct result of the lessons learned from the first two prototypes (#1 and #2). Part of the engineering design methodology consists of adding to or subtracting from the design checklist based on the lessons learned from the previous design exercise, during the design iteration loop as depicted in the flowchart of figure 37. For example, the importance of humidity conservation and the interaction between the pressure output of the forced recirculation device and the humidity of the circuit gases (design objective 6.2) became apparent during evaluation of prototype #2.

There were actually more than two design prototypes preceding the GRADS design in the sense that many slight variations based on the two initial prototypes described were tested. The two prototypes described below are distinctive and representative of the derivatives based on them.

290

The common feature shared by prototypes #1 and #2 and the GRADS system is a recirculating device (piston compressor, diaphragm compressor and centrifugal blower respectively) to provide a high recirculating flowrate ("FGF") while operating in a closed circuit for efficient anesthetic usage.

Prototype #1 (circa 1985) is characterized by the presence of ejectors and an absence of digital electronics, the control function being accomplished via pneumatic logic components and a minimal amount of analog electronics.

Prototype #2 (circa 1989) was in many ways an exercise with emphasis on interfacing electronics (both digital and analog) to the hardware components of an anesthesia machine for a mechanical engineer learning practical, hands-on, electronics and real-time digital control at the time. It was centered around a hand-built, wire-wrapped data acquisition and control system (DACS) board based on a Siemens 80535 microcontroller (Atwater & Good 1989) and was controlled in real-time using software written in C.

Prototype #3, the GRADS system (June 1991), is based on an improved understanding of the capabilities of microelectronics and microcontrollers and attempts to exploit them fully. It is centered around a printed circuit board DACS II microcontroller board. Familiarity with microelectronics and real-time control code written in C allowed the emphasis to be properly placed on the actual functions of the anesthesia delivery system and the establishment of a design methodology rather than being distracted by the actual implementation problems.

6.1 Prototype #1 (circa 1985)

The first prototype design (covered by US Patent 4,702,241 awarded on October 27, 1987) was based on a reciprocating, positive displacement piston compressor and was distinguished by the presence of a recirculating device (the compressor) as an integral part of the system, ejectors as unidirectional gas flow devices in the anesthesia circuit and an absence of check valves in the breathing circuit (design objective 4.3.1) (figure 43).
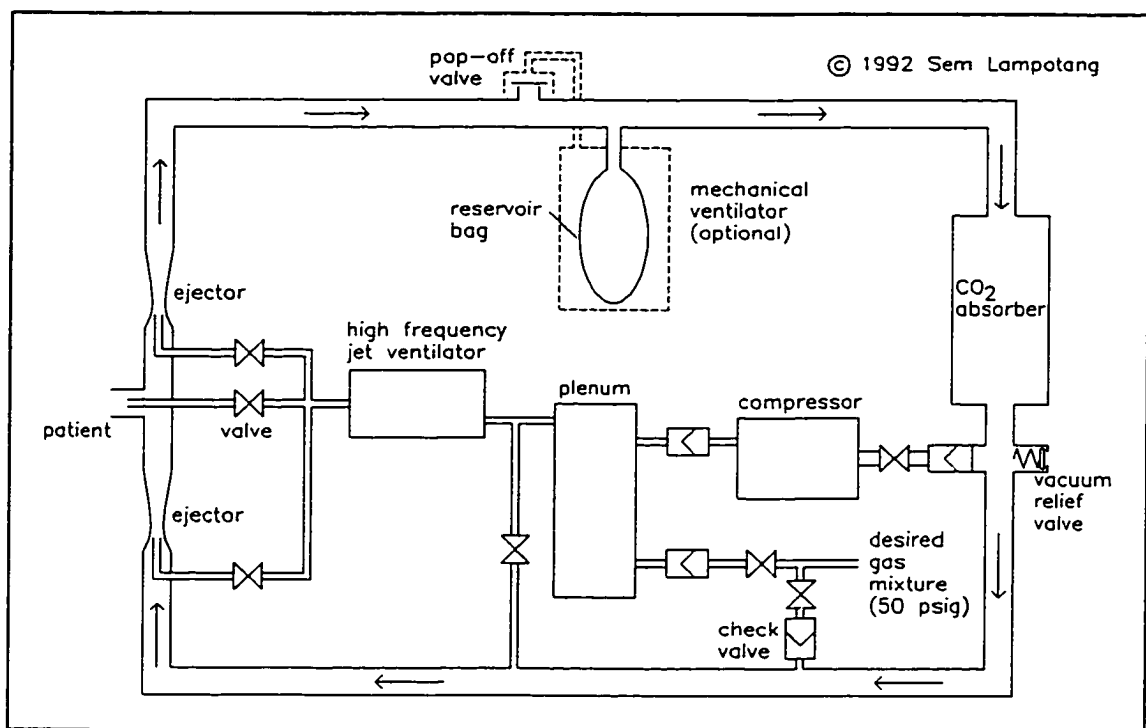
Figure 43. Prototype #1 (circa 1985) of the recirculating anesthesia delivery system concept, covered by US Patent 4,702,241.

In figure 43, the system is configured with two ejectors so that gas can be pushed into or pulled from the patient's lungs by changing the ratio of the primary flowrates to the ejectors during inspiration and expiration respectively. The primary flowrate of 50

psig O_2 that is directed to the nozzle of the ejector is metered via a pressure-compensated, O_2, ball-in-tube flowmeter (Puritan, Series A, calibrated at 21.1°C (70°F), 50 psig, 0-9 l/min range). In practice, it was difficult to manually balance the primary gas flowrate to the two ejectors in the circuit configuration depicted in figure 43 so that there was no net pressure buildup (primary flowrate at ejector upstream of patient higher than downstream ejector) or suction at the patient connection to the circuit. For that reason, the system was more often operated with a single ejector (figure 44).

6.1.1 Ejectors

The ejectors were commercially available (bird Corporation; P/N 2587), with nozzle orifice diameters of 0.038 and 0.152 cm (0.015" and 0.060") available. The ejector consisted of two plastic parts that screw on together: (a) the primary nozzle and entrainment port and (b) the venturi tube and the outlet port. Thus different nozzle sizes could be readily mated to different venturi tubes, in different combinations. The overall dimension of the ejector was 5.4 cm (2.125") long for the venturi tube with an outlet port of 1.08 cm (0.425") diameter and a throat diameter of 0.6 cm (0.236"). The entrainment port had a diameter of 1.52 cm (0.6"). The mixing chamber was 2.39 cm (0.94") long with a circular cross-section of 1.98 cm (0.78") diameter.

The entrainment ratio was approximately 5 with no back pressure ($P_b = 0$) on the ejector outlet. With a primary flowrate of 9 l/min into one ejector, a recirculating flowrate of about 54 l/min was obtained. During tests with the ejectors in the breathing circuit of prototype #1, there was flow reversal in the ejector whenever P_b exceeded 30

cm H_2O. This was not acceptable since bidirectional flow in a recirculating circuit will lead to rebreathing of CO_2 for the patient (design objective 4.3 requires unidirectional flow in a recirculating circuit).

With hindsight, the design of prototype #1 depended heavily on the ejectors to work as unidirectional flow devices, i.e., check valves. The ejectors failed in that function whenever $P_b \geq 30$ cm H_2O which was unacceptable. Design objective 1.4.2 requires that PIPs of up to 100 cm H_2O be possible for patients with very stiff compliances or high airway flow resistances and the PIP in the breathing circuit becomes the P_b of the ejector.

From a higher level design point of view, once the ejectors failed in their function as unidirectional flow devices for PIPs up to 100 cm H_2O, the ejectors were then solely working as flow recirculating devices when the compressor already present is itself a recirculating device. Thus, the ejectors became redundant and in conformance with a minimalist philosophy that promotes design simplicity, their use in a breathing circuit could no longer be justified.

6.1.2 Piston Compressor

The ejectors required high pressure gas to work properly (at least 30 psig and ideally 50 psig). A positive-displacement compressor was chosen to recompress part of the recirculating gases back to 50 psig (figures 43 and 44). Two other potential flow recirculating devices (blowers and fans) were considered at the time and were rejected because, for "available" units, their output did not meet the supply pressure requirements

of the ejectors. The compressor was an oil-less reciprocating compressor (ITT Pneumotive, Monroe, LA, Model # GH-3051 with a 1/4 HP, 115 V, 60 Hz, 7.4 A, single phase motor), with both the inlet and outlet ported so that the recirculating gases could be conveniently directed into and out of the compressor.
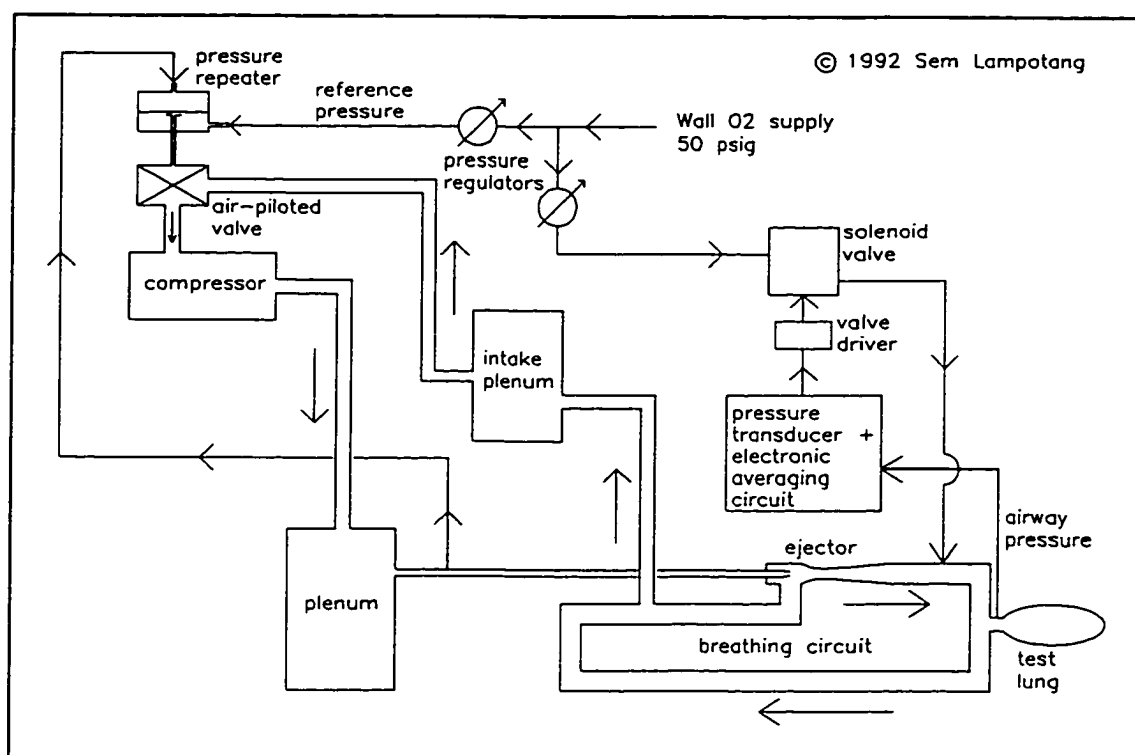
Figure 44. A single ejector configuration of prototype #1 with the pneumatic controller of plenum pressure and the electronic gas make-up circuit

The electric motor which drove the piston compressor had a rotational speed of 1725 rpm. The piston compressor thus imparted pressure pulsations to the breathing circuit. To prevent transmission of the pressure pulsations to the airway of the patient, they were damped with a plenum that was made of a cast iron E-size gas cylinder into which two holes were drilled, tapped and fitted with Diameter Indexed Safety System

(DISS) female O_2 fittings. Initially only one plenum was used on the outlet of the compressor (figure 43). In later versions of prototype #1, a plenum made of a large (40 l) plastic bell jar was added to the intake line of the compressor (figure 44).

The compressor was noisy and induced mechanical vibrations to the test bench on which it was placed. To reduce the noise and vibration, the compressor was enclosed in a recycled sound-proof enclosure for a printer (Radio Shack TRS-80 Acoustic Cover) on vibration dampening mounts made of rubber.

During tests, the piston compressor also suffered from blow-by of gases at the piston walls past the piston rings that caused a leakage of gas from the system which accumulated with time. The cumulative loss of gas caused the system to collapse if gas was not added to the system.

6.1.3 Gas Make-Up Electronic Circuit

The system collapsed if the gas leakage rate was higher than the inflow rate of gas in the circuit. Therefore, a gas make-up circuit was essential in maintaining the circuit volume and preventing circuit collapse (figure 44). The impending collapse of the circuit was detected via an electronic pressure transducer (Omega, P/N 162PC01G) with a range of 0 - 1.5 psig (0 - 100 cm H_2O). An averaging circuit was used to obtain a time average of the "airway" pressure at the Y-piece, in the circuit. Based on the relative value of the average pressure compared to an adjustable reference pressure, a solenoid-actuated valve was opened that added O_2 to the circuit. The electronics for the

gas make-up circuit performed well and reliably and were designed and built by Dr. H. Doddington, a member of the author's PhD committee.

6.1.4 Pneumatic Circuit for Control of Plenum Pressure

Pressure at the plenum had to be maintained at a constant level if the primary supply pressure and flowrate to the ejectors was to remain constant once set. The control of pressure at the plenum was performed with a binary (on/off or bang-bang) pneumatic logic control circuit. A "pressure repeater" (Clippard Instrument Laboratory, P/N 1043, 1981) was used as a pressure comparator. The adjustable reference pressure to the "pressure repeater" was obtained from a pressure regulator (C.A. Norgren Co., Littleton, CO, P/N R07-100-RNKA). The controlled pressure was sampled at the E-cylinder plenum. The pressure repeater was simply a diaphragm exposed to the controlled (plenum) pressure on one side and the reference (usually 50 psig) pressure on the other side. If the controlled pressure is lower than the reference pressure, the diaphragm moves accordingly and exposes the outlet port of the "repeater" to the pressure from the reference pressure source (see details of pressure repeater in figure 44).

The output of the pressure repeater triggers an air-piloted valve (Clippard Pow-R-Amp Valve, P/N 2012, 1981). Thus, if the pressure in the plenum is higher than the reference pressure, the output port of the pressure repeater is isolated from the reference pressure source. The air-piloted valve shuts closed because its trigger signal from the pressure repeater is no longer present. No more gas flows from the compressor to the plenum because the inlet to the compressor is blocked. The pressure in the plenum falls

because of the flow to the ejectors until it is eventually lower than the reference pressure. At this point, the pressure repeater output becomes "high" again and opens the air-piloted valve. The pneumatic on-off controller performed well and was consistently able to control the pressure at 50 psig $\pm$ 0.5 psig.

6.1.5 High Frequency Jet Ventilator

During the initial tests of the system, a commercially available high frequency jet ventilator (Healthdyne 300 model) was included in the circuit which always collapsed within 30 seconds of operation. A leak was suspected and was isolated to the HFJV unit by systematically removing each sub-component, one at a time, from the circuit, until the circuit did not collapse within 30 seconds. The leakage from the commercial HFJV unit was due to a Clippard 2013 "Electronic Fluidamp" valve which requires for proper operation a bleed flowrate to atmosphere of 2.8 l/min (0.1 cfm) at 100 psig supply pressure (Clippard 1981). Consequently, there was a flowrate deficit of about 1 - 2 l/min when the Healthdyne HFJV unit was in the circuit and supplied with the gases recompressed to 50 psig. Due to the leakage flowrate, less gas volume was returning to the compressor than was leaving the compressor per unit time so that the compressor made up for the deficit by aspirating gas from the circuit and collapsing it and the test lung (the "patient's" lungs) along with it.

At the time, another HFJV unit (Healthdyne, Impulse model) that also used the Clippard 2013 valve was being used daily during extra-corporeal shock wave lithotripsy (ESWL; section 2.3.2) with a mixture of 70% N_2O and 30% O_2. Upon discovery of the

leakage in the Healthdyne model 300 unit, a test was made of the ambient air in the ESWL room with an N_2O meter and the reading exceeded the full scale of the meter (250 ppm) when the maximum NIOSH recommended standard for N_2O in the work place is 25 ppm.

A high frequency ventilator that would not leak N_2O into the OR environment was not commercially available at the time. Consequently, a HFJV unit was designed and built from scratch so that HF jet ventilation could be delivered using the recirculating circuit of prototype #1 without circuit collapse. The HFJV unit was also initially intended for use on patients so that the fabrication specifications on it were more stringent than if the unit was only going to be used in prototype #1 on a test lung. As a result, the design and fabrication of the HFJV unit took 10 months. By that time a commercial manufacturer (Siemens) had introduced a ventilation system that would allow HF ventilation without a leak which was subsequently used in the ESWL room.

The prototype HFJV unit (circa 1985) used a Zilog Z-80 8-bit processor to perform the timing and alarm functions and performed well in service and is still functional at the time of writing, although it is being used in another function.

6.1.6 Results and Conclusions

The flow reversal through the ejectors at $P_b \geq 30$ cm H_2O was the major drawback of prototype #1. However, the noise, mechanical vibration and blow-by of the compressor were also of concern. The system was unstable and had a tendency to collapse during manual ventilation. In other words, the make-up gas module and the

plenum pressure control were usually able to maintain the system stable after manual adjustment of all parameters like the primary flowrate to the ejectors with no ventilation occurring. However, during manual bagging or when a conventional ventilator was used, an increase in the breathing rate or VT would result in a perturbation of the system which would sometimes lead to progressive loss of volume and eventual collapse of the test lung.

Prototype #1 identified the need for better and more robust control of the system and also demonstrated the advantage of electronics over pneumatics for feedback control. The pneumatic bang-bang controller for the plenum pressure control took about a month to implement and get to a stage where it was working reliably. The pneumatic control components were expensive and hard to obtain and had to be especially ordered compared to the electronic components which were readily available at local suppliers. In comparison, the electronically controlled make-up gas circuit was inexpensive to build and worked reliably.

6.2 Prototype #2 (circa 1990)

Prototype #2 was fabricated and tested during 1989 and the first half of 1990 (figure 45). Many of the concepts and features present in GRADS were first implemented and tested on prototype #2. These are (a) pressure sampling at the ETT distal tip, (b) the large orifice, low pressure loss proportional flow control valve that uses a woofer speaker as the linear motion actuator, (c) the DACS board, (d) the differential amplifiers and the pressure transducers, (e) an electro-mechanical, instead of a

conventional manually-actuated, O_2 flush valve, (f) the ventilation mode selector switch and (g) the ability to manually ventilate by squeezing the bag during all ventilation modes. Consequently, the description of the components and features in prototype #2 will be more detailed than for prototype #1 because many of these items are used unmodified as the building blocks of the GRADS prototype.
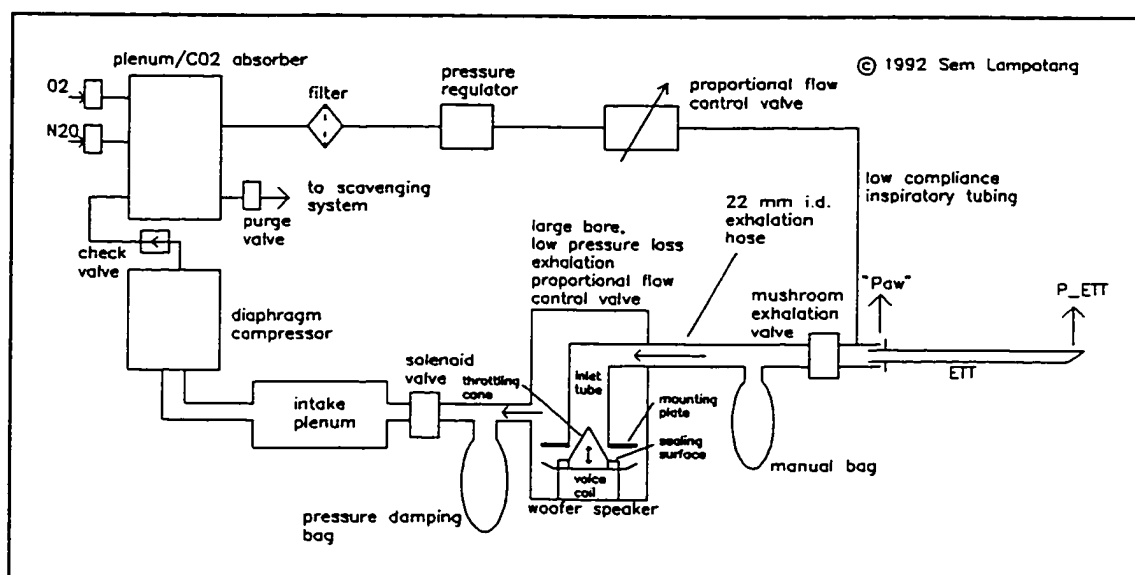
Figure 45. The design of prototype #2 (circa 1989) which had many of the features of GRADS already.

6.2.1 DACS Board

At the time of conception of prototype #2, the author was involved in another project, the Gainesville Anesthesia Simulator, GAS, (Lampotang 1992a, 1992b) which required inexpensive distributed processing power. The solution was a custom-designed data acquisition and control system (DACS) board (Atwater & Good 1989) based on a Siemens 80535 microcontroller.

The 80535 is a stand-alone, high-performance, single-chip microcontroller based on the generic 8051 microcontroller architecture. N-channel metal oxide semiconductor (NMOS) technology is used in the 80535. It has 3 16-bit timers/event counters, a 16-bit watchdog timer, 256 bytes of on-chip RAM, 8 multiplexed 8-bit A/D conversion channels, a full-duplex serial port and 48 I/O lines and can handle 12 interrupt sources at 4 priority levels (Advanced Micro Devices 1988). The 80535 can address 64 Kbytes of program memory (control logic code storage) and 64 Kbytes of data memory (storage of variables like pressure and proportional flow control valve setting being acquired or calculated and controlled).

One machine cycle consists of 12 oscillator periods and most instructions execute in 1 machine cycle, i.e., 1 microsecond with a 12 MHz oscillator circuit clocking the 80535 in the DACS board. The DACS board in prototype #2 was only the second one of its line and was entirely hand-built using wire-wrap assembly techniques.

6.2.2 Diaphragm Compressor

Compared to the piston compressor in prototype #1, the diaphragm compressor initially used in prototype #2 (Thomas Industries Inc., Model # 107CA18, 0.46 cm (0.180") stroke) did not suffer from blowby, was less noisy and required no acoustic cover but still delivered a pulsatile output. The compressor was driven by a 1/20 HP, 115 V, 60 Hz shaded pole motor. Both the inlet and outlet were ported (1/8" female NPT). The pressure and flowrate outputs were marginal with the 1/20 HP motor driving the system. Subsequently, a diaphragm compressor used in a suction apparatus (Air-

Shields, Dia-Pump Aspirator and Compressor, Model CA, SN 69180) for aspirating secretions from patients was modified for use in prototype #2. The Air-Shields compressor was driven by a General Electric motor (5XBF054D FKA) rated at 120V, 60 Hz, 3.2A and provided pressures up to 50 psig and flowrates in excess of 30 l/min.

Two intake plenums were required for damping the pressure oscillations from the compressor inlet. They were fabricated from 10.2 cm (4") i.d. PVC pipe with matching end-caps at both ends drilled, tapped and fitted in the center with DISS male O_2 fittings. Plenum sizing was done on a practical basis, using trial and error. The PVC pipe was 63.5 cm (25") long for each plenum giving a total volume of 5.2 l for each plenum. With the 2 intake and the high-pressure outlet (the modified E-cylinder from prototype #1) plenums in the system, no pressure oscillations were detected visually or with the pressure transducers. However, the volume added to the circuit by the three plenums was significant (approximately 15 l) compared to the size of a conventional breathing circuit (7-10 l).

With the Air-Shields diaphragm compressor, the danger of a positive displacement compressor as a recirculating device was dramatically demonstrated when the mushroom exhalation valve driver circuit malfunctioned during mechanical ventilation because of a loose control wire. A large volume of high pressure recompressed gas from the diaphragm compressor was injected into the test lung while the mushroom exhalation valve stayed closed over many breaths (figure 45). The resulting hyperinflation led to a deafening rupture as the rubber bellows in the test lung were ripped from the metal plates on which they were mounted.

This incident was a sobering illustration of the danger of using a positive displacement compressor in a recirculating anesthesia circuit to which a patient will be connected. If a malfunction occurs, the patient can become exposed to the shut-off pressure of the recirculating device. The incident provided the impetus to reconsider devices other than positive displacement compressors for recirculating gases around the system and to question the need or wisdom of having pressures much greater than the maximum foreseeable required PIPs in the circuit.

6.2.3 Pressure Sampling, Transducers and Differential Amplifiers

The airway pressure was sampled at the ETT distal tip instead of the Y-piece, through a 1.27 mm (0.05") i.d. lumen embedded in the wall of an ETT specially designed for delivering HF jet ventilation (National Catheter Co., Hi-Lo Jet, 8 mm (0.31") i.d.). The embedded lumen exits at the distal tip on the internal wall of the ETT. On the proximal end of the ETT, the lumen extends into an 21.6 cm (8.5") long, 0.25 cm (0.1") o.d. line that branches out of the ETT external wall, with an end connector to which the HFJV output line would be connected in normal use. The function of the embedded lumen was modified by attaching a pressure sensor to the proximal end connector of the lumen. Thus, the pressure sensor was sampling pressure at the carina of the patient even though it was itself physically outside of the lungs.

A pressure sensor at the conventional Y-piece site was also included as a design safety feature in the event that the ETT distal tip sampling point becomes occluded. "Airway" pressure control would then switch over to the Y-piece transducer in case of

suspected malfunction of the ETT tip transducer. The pressure transducers were from the Motorola MPX series (MPX10GP and MPX11GP) which have a 0 - 1.5 psi (0 - 105 cm H_2O) range (Motorola Publication No. DS2701, 1984). The pressure sensors were silicon piezoresistive devices incorporating a shear stress strain gage as part of a Wheatstone bridge arrangement (figure 46). Therefore, the output is a differential voltage proportional to the applied pressure which needs a differential amplifier for amplification and reference to electrical ground.
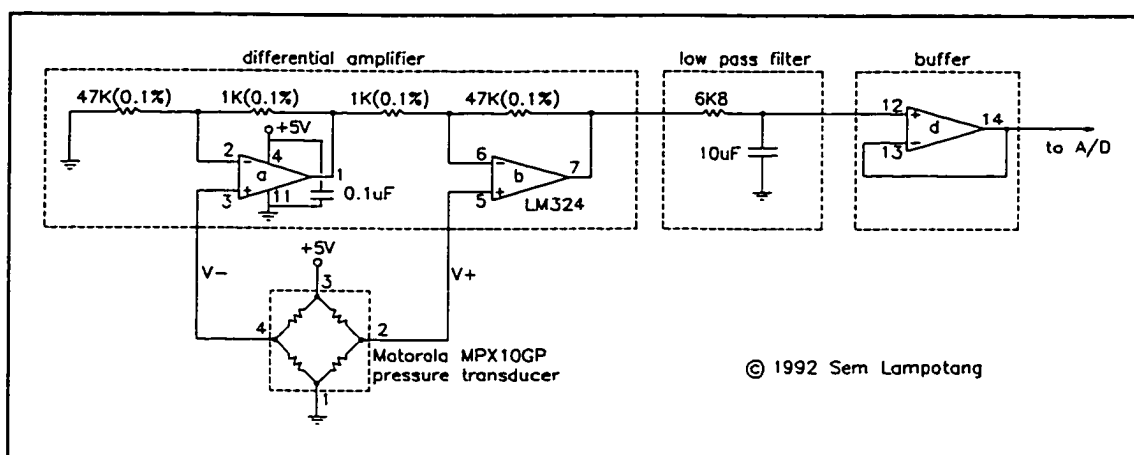
Figure 46. The interface circuit between the pressure transducers and the A/D line of the microcontroller board shown with an amplification factor of 47

The differential amplifiers were fabricated as shown in figure 46 with LM324 low power quad operational amplifiers ICs. A low pass filter was inserted at the output of the differential amplifier to attenuate noise from the pressure signal. The -3dB cutoff frequency, f_c, of 2.34 Hz (140 breaths per min) was calculated using the formula $f_c = 1/2\pi RC$. The selected -3dB cutoff frequency allows breathing rates of up to 140 breaths/min (HFV) to be transmitted with an attenuation not exceeding 0.707 (1/$\sqrt{2}$).

The performance of the low pass filter was also visually confirmed by probing its output during operation with a 100 MHz bandwidth oscilloscope (Tektronix Model 2235).

An output buffer is interposed between the low pass filter and the A/D line of the 80535. According to the specifications for the 80535 (Advanced Micro Devices 1988), the internal resistance of the analog source must be less than 10 KΩ to ensure full loading of the sample capacitance at sample time. The impedance of the output buffer is nearly zero thus guaranteeing full loading of the sample voltage (the pressure signal) into the A/D circuit.

The pressure transducers were calibrated over a range of 20 cm H_2O below ambient to 50 cm H_2O above ambient in steps of 5 cm H_2O using a water column manometer (Wescor Inc., Model AC-010, Logan, Utah). The upper limit of the calibration was set at 50 cm H_2O because that was the maximum calibration pressure attainable with the water column manometer. The lower limit of the pressure range was selected on the reasoning that a spontaneously breathing patient should never have to draw more than 20 cm H_2O below ambient on a well-designed system.

The A/D converter was observed to give errors of ± 4 LSB (least significant bits) when supplied with the same input voltage through the LM324 buffer. To compensate for the conversion errors of the A/D converter, the calibration was performed using raw A/D integer values rather than the analog voltage coming from the differential amplifier.

Prior to the calibration using raw A/D values, the analog voltage output range for the desired pressure measurement range was obtained with a digital voltmeter (DVM) (Fluke 75 Multimeter). With the analog voltage range from the pressure transduction

board determined, the input range of the A/D converter in the DACS board was set in software to bracket the analog voltage range as tightly as possible to obtain maximum resolution. For example, assume that the range of output voltage from the pressure transduction board was 1 - 3 volts for the desired pressure range of 20 cm H_2O below ambient to 50 cm H_2O above ambient. The A/D input range would then be set at 0.9375 - 3.125 V rather than the full 0 - 5 V capability of the A/D converter so that the 256 discrete values of the 8-bit A/D conversion are evenly spaced over the tighter range, giving better resolution of pressure measurement.

A linear regression of the calibration input pressures against the raw A/D integer values was performed on an IBM-compatible PC using a commercial package (Quattro, Borland International, Scotts Valley, CA). The output of the pressure transducer was highly linear to the calibration pressure input with an r^2 correlation factor of 0.999407 and 0.998523 for the Y-piece and ETT distal tip pressure transducers, respectively.

6.2.4 The Inspiratory Proportional Flow Control Valve (IPFCV)

A current-controlled proportional flow control valve (South Bend Controls, P/N 10019760, South Bend, IN) was recycled from an Ohmeda 7800 anesthesia ventilator prototype. The inspiratory proportional flow control valve (IPFCV) is driven by the voltage output of a demultiplexed D/A line from the DACS board via the voltage to current driver circuit shown in figure 47. A BUZ71 field effect transistor (FET) was used to modulate the current to the inspiratory valve coil.
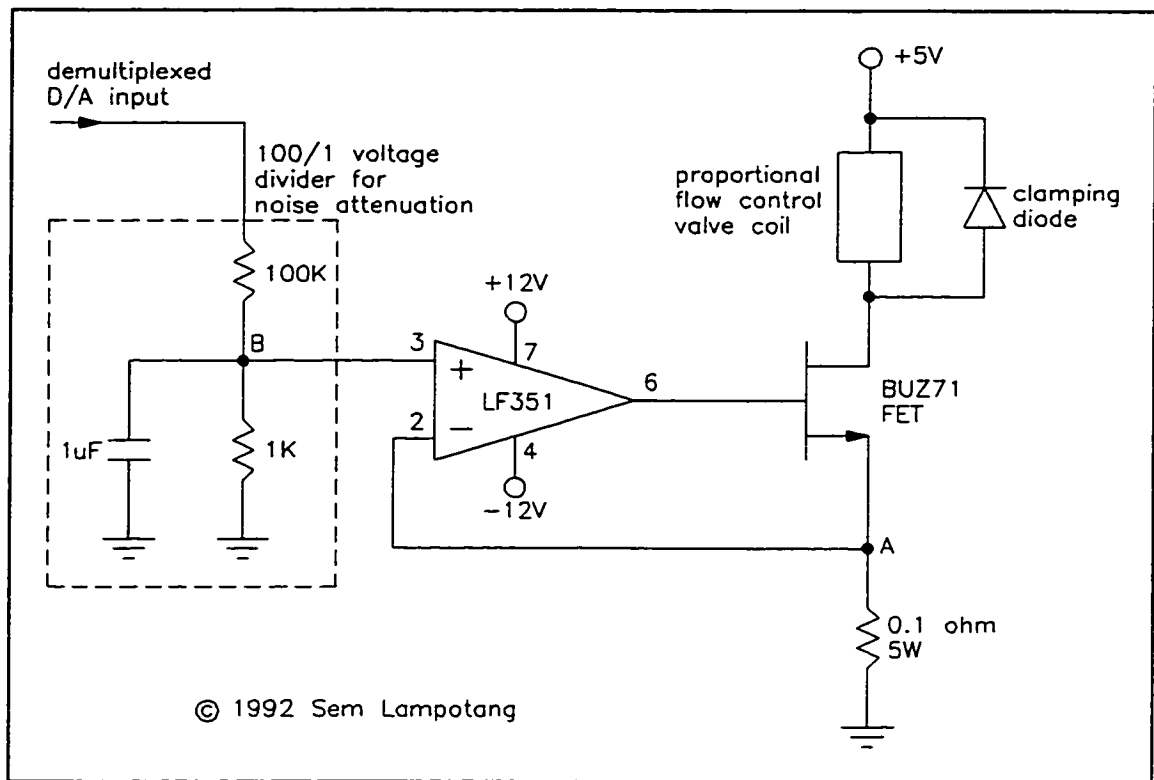
Figure 47. The voltage to current driver circuit for the inspiratory proportional flow control valve in prototype #2.

There was high frequency noise of about 40 MHz and 1 V peak to peak on the output line of the D/A (0-10 V output range) from the DACS board when it was probed with an oscilloscope (Tektronix 100 MHz Model 2235). This created concern that the electrical noise would cause the IPFCV to chatter and to have a reduced life span. The input current range for the IPFCV for a flowrate output range of 0 - 90 lpm when supplied with 35 psig air is 0 - 1.0 A, according to the manufacturer's calibration data. Consequently, a noise attenuation circuit was placed between the D/A output line and the voltage to current driver circuit which functioned in combination with the 0.1Ω resistor.

The 100/1 voltage divider caused the output range of the D/A to be scaled from 0 - 10 V to 0 - 0.1 V at point B. The function of the LF351 operational amplifier is to maintain the voltage at pins 2 (point A) and 3 (point B) identical. The current flowing through the coil of the IPFCV is the same as the current flowing through the FET and the 0.1Ω, 5W resistor. Thus, dividing the voltage range at point A (0 - 0.1 V) by the 0.1Ω resistor value gave the desired current range at point A (0 - 1.0 A) that would enable a 0 - 10 V output range from the D/A to modulate the current supply to the IPFCV across its full flowrate range.

A high-pressure filter (Balston DFU, Grade CO filter tube) was placed at the outlet of the plenum to prevent rust scale from the internal walls of the E-cylinder plenum from lodging and interfering with the operation of components downstream of the plenum. A pressure regulator (C.A. Norgren Co., Littleton, CO, P/N R07-100-RNKA) set at 30 psig was interposed between the outlet plenum and the IPFCV (figure 45). This was to ensure that the supply pressure to the valve was constant and independent of small, high frequency pressure fluctuations in the outlet plenum caused by the pulsatile output of the diaphragm compressor. The IPFCV operated in two distinctly different modes during mechanical and spontaneous ventilation which are each separately described in the next two subsections.

6.2.4.1 Mechanical ventilation

No inspiratory waveform shaping was implemented with the valve during mechanical inspiration. The valve delivered only one inspiratory waveform, a constant

flowrate over the set inspiratory period (T$_i$) to achieve the desired VT while the mushroom exhalation valve is pressurized shut during mechanical inspiration (figure 45). There was no feedback control of inspiratory flowrate during mechanical ventilation. The IPFCV was used in an open loop scheme and its triggering was solely time-based during mechanical ventilation (figure 47). The required inspiratory flowrate was determined by dividing the desired VT by the time duration of active inflation which is set by the user's choice of RR, I:E ratio and inspiratory pause.

The flowrate output of the IPFCV was linearly proportional to its current input from the driver circuit when the valve operated in the choked flow regime. The internal geometry of the valve required that the supply pressure be 30 psig or more, for choked flow to occur with outlet pressures of up to 100 cm H$_2$O ($\approx$ 1.5 psig). The proportional voltage input to the IPFCV driver circuit for a predetermined inspiratory flowrate was therefore obtained in the control software of prototype #2 from the equation of the best fitting straight line describing the relationship between input current and flowrate output from a calibration chart supplied by the manufacturer.

Consequently, the open loop scheme for modulating the inspiratory flowrate during mechanical inspiration relied on a choked flow regime persisting throughout inspiration for a P$_b$ or PIP of up to 100 cm H$_2$O for accurate control of VT delivery. As was discussed in section 4.3.3.4 and design objective 6.2 (maximum pressure of the recirculated gases not to exceed 2 psig), the recompression of the recirculating gases to 30 psig caused rainout of moisture in the breathing circuit. This will be discussed further in another section of this chapter.

6.2.4.1.1 Theoretical analysis of choked flow in the inspiratory valve

When it was realized that the minimum supply pressure requirement for choked flow through the IPFCV was causing rainout of moisture from the breathing circuit, a theoretical analysis of the choked flow characteristics of the valve was performed. Previously, a phone call to the manufacturer had revealed that the flow throttling action of the IPFCV was performed by a spherical ball immediately downstream of a straight circular passageway drilled in the internal valve manifold and supplied with high pressure gas. The modulation of current to the valve coil moved the spherical ball relative to the circular outlet, thus producing flowrate modulation. In effect, the internal geometry of the valve was that of an abrupt expansion which is known to have significant pressure losses associated with it (Miller 1990, 375). Due to proprietary concerns, the manufacturer did not elaborate on the actual internal dimensions and geometry of the valve.

The objective of the brief analysis was to theoretically determine if modification of the internal geometry of the valve could reduce the minimum supply pressure requirement of the IPFCV without changing any of the functional operating characteristics of the IPFCV.

Assuming that a gas with a specific heat ratio of 1.4 is isentropically flowing through a valve with a converging nozzle (Shapiro 1953, 91), the theoretical value of P_b/P_o at which the valve will start unchoking is 0.528 (Shapiro 1953, 616). The actual P_b/P_o value at which the IPFCV was unchoking according to the manufacturer's specifications was 1.5 psig/30 psig = 16.2 psia/44.7 psia = 0.362. The valve had

poorer choked flow characteristics than could be practically attained. If the valve had operated in the choked flow regime up to the theoretical P_b/P_o value of 0.528, then the minimum supply pressure requirement (P_o) to the IPFCV would have dropped to $P_b/0.528$ = 16.2 psia/0.528 = 30.7 psia = 16 psig. While this lower theoretical P_o value compared favorably to the actual P_o requirement of the valve, it would still not satisfy design objective 6.2 which requires that the maximum pressure be kept below 2 psig to prevent moisture rainout.

So the problem is turned around to determine what P_b/P_o is required to produce choked flow with a maximum supply pressure, P_o, of 2 psig and a maximum back pressure, P_b, of 1.5 psig. The P_b/P_o value is 1.5 psig/2 psig = 16.2 psia/16.7 psia = 0.97. This P_b/P_o value is theoretically attainable with a valve that has a converging-diverging (CD) nozzle with a weak normal shock downstream of the throat of the CD nozzle (flow regimes II - IV) (Shapiro 1953, 93, 140).

Consequently, the brief theoretical analysis of choked flow in a valve indicates that a valve could be manufactured that would have the desired choked flow characteristics required of the IPFCV in prototype #2 while minimizing humidity loss. However, the reduction to practice of this brief theoretical analysis is not inconsequential and was considered to be beyond the scope of this dissertation.

However, beyond the actual direct application of the theoretical analysis to the IPFCV of prototype #2, it was realized during the theoretical exercise that current valve design, especially of the internal geometry, does not generally attempt to minimize pressure loss across the valve. A reduced pressure loss for any fluid (pneumatic,

hydraulic, liquid, etc.) flow control valve whether proportional or on/off would be beneficial because it would reduce the overall energy consumption of the system (process plant, control system, etc.) in which it is used. For example, a smaller and less expensive pump or compressor facility would be needed for a new factory equipped with valves with reduced pressure loss, providing both reduced capital and operating costs.

6.2.4.1.2 Factors affecting VT delivery during mechanical inspiration

To return to the discussion of mechanical inspiration, it would be ironic to go to the trouble of ensuring choked flow in the IPFCV for precise delivery of VT, if the delivered VT to the patient was then affected by the compliance of the breathing circuit, the FGF, PIP and T_i as in conventional anesthesia delivery systems (see equation 4.4).

With the design of prototype #2, there is no FGF per se as in conventional systems. During mechanical inspiration, the valve opens to a predetermined setting to provide the desired inspiratory flowrate over the T_i duration. The IPFCV setting is then returned to its "FGF" position (0 or 5 l/min default flowrate setting depending on the control software version) when active inflation of the lungs is over, unless an inspiratory pause is present. The IPFCV driver circuit has a 0 written to it from the demultiplexed D/A line (output flowrate = 0) during an inspiratory pause to achieve the defining condition of $Q_{ca} = 0$, while the mushroom exhalation valve is maintained shut.

Consequently, VT augmentation by FGF did not occur with the design of prototype #2 because the IPFCV changes function during a mechanical inspiration. Instead of delivering the "FGF", the IPFCV delivers the required inspiratory flowrate

over the desired T_i such that the FGF, if non-zero, "disappears" during mechanical inspiration. Thus VT delivery became independent of FGF and T_i with the design of prototype #2.

To minimize the effect of circuit compliance and the PIP on VT delivery, a 1 m (3.28 ft) length of stiff, thick-walled silicone tubing with an i.d. of 0.64 cm (0.25") was used as the inspiratory "hose" instead of the regular 22 mm i.d. standard breathing circuit inspiratory hose. Furthermore, the compliance of the exhalation hose (22 mm i.d. standard breathing circuit hose) was effectively removed from the circuit by pressurizing shut the mushroom exhalation valve close to Y-piece, i.e., upstream of the exhalation hose, during mechanical inspiration (figure 45).

As already alluded, an inspiratory pause capability fixed at 25% of T_i was present during mechanical ventilation in prototype #2. The duration of the inspiratory pause was included within the total inspiratory time. In other words, for a given I:E ratio, the duration of expiration was unchanged whether an inspiratory pause was used or not. For example, for a set T_i of 2 seconds, active inflation would occur for 2 seconds without an inspiratory pause. With a 25% T_i pause, the active inflation would last for 1.5 seconds with a constant flowrate higher than the inspiratory flowrate without a pause by a factor of 1.33 so that the same VT is delivered.

In keeping with one of the initial reasons for designing a new anesthesia delivery system (anesthesia delivery during ESWL), HFV was also implemented in prototype #2. The power and flexibility of digital electronics and software was amply illustrated when writing the code for HFV. The code for mechanical ventilation was written in a generic

fashion that enabled HFV to be implemented without any additional effort compared to the time and effort required for the HFJV unit used in prototype #1.

6.2.4.2 Spontaneous ventilation

During spontaneous ventilation without assistance from the system, the IPFCV would simply be set at the default "FGF" setting of 5 l/min while the mushroom exhalation valve was maintained open at all times. Consequently, the collapse of the manual breathing bag during spontaneous inspiration could be felt.

Spontaneous ventilation with assistance from the ventilation system with the objective of reducing the WOB was initially tried on prototype #2 using modulation of the IPFCV. The digital PID modulated the inspiratory flowrate as a function of the error between the desired baseline pressure and the sampled pressure at the ETT distal tip (P_{ett}) with the objective of maintaining P_{ett} at the baseline PEEP level (ambient (PEEP = 0) or above ambient). In physical terms, if the PID controller was perfect, then the PV loop for a spontaneous breath of a given VT would reduce to a vertical straight line of height VT on a pressure volume graph, with zero area and zero WOB. For example, if the P_{ett} was lower than the desired PEEP level, the inspiratory flowrate would be increased to build pressure back up at the ETT distal tip.

Spontaneous inspiration was simulated according to the method described by Lampotang et al. (1986). An Ohmeda 7000 anesthesia ventilator ventilated the left (driver) bellows of a mechanical test lung with two independent bellows (Michigan Instruments Inc., Vent-Aid TTL, Training Test Lung). During inflation by the Ohmeda

7000 ventilator, the driver bellows would lift the right (driven) bellows via a metal bar attached to the driver bellows top mounting plate and slung below the top mounting plate of the driven bellows creating a sub-ambient pressure in the driven bellows during "spontaneous" inspiration. During the exhalation phase of the left (driver) bellows, the metal bar would lose contact with the right (driven) bellows such that the exhalation from the driven bellows was solely determined by the compliance and resistance setting on the driven bellows.

The ventilation system of prototype #2 was connected to the right (driven) bellows. The control of P_{ct} worked well during simulated spontaneous inspiration. For example, the maximum dip below ambient for a simulated 1,000 ml breath with an 8 mm i.d. ETT was reduced from 8 - 10 cm H_2O to only 2 - 3 cm H_2O when the PID controller was active and properly "tuned" (tuning method to be described later).

However, it was noticed during the tests that P_{ct} would overshoot to about 15 cm H_2O above the baseline pressure in spite of the fact that the PID controller would reduce the flowrate output of the IPFCV to zero in an attempt to maintain baseline pressure. Endless hours of tuning the PID by trying different P, I and D coefficients to obtain better damping of the expiratory pressure overshoot proved fruitless.

Eventually, a simple test was performed to explain why the digital PID controller that controlled the IPFCV could not reduce the pressure overshoot during exhalation. The test lung was disconnected from the breathing circuit of prototype #2. The simulated trachea (Imatrach, National Catheter Co.) of the test lung was left intubated with an 8 mm i.d. ETT whose proximal end was open to atmosphere since the ETT was

disconnected from the breathing circuit. The compliance of each lung was set at 0.025 l/cm H_2O. The top mounting plates of the mechanical test lung were manually pulled to aspirate a VT of approximately 1 l (0.5 l in each bellows). The top mounting plates of the right and left bellows were released simultaneously while the pressure in each bellows was observed via the pressure gauges mounted on each bellows. As suspected, the pressure in each lung had a transient peak to 15-18 cm H_2O as the top mounting plates were released to simulate the start of spontaneous exhalation, even though the ETT proximal tip was open to atmosphere.

Thus, the simple test confirmed that the flow resistance of the ETT combined with the compliance and resistance of the test lung was causing the pressure overshoot. More importantly though, the test also demonstrated that if only ambient or above ambient pressures are available in the circuit, then the pressure overshoot during exhalation cannot be avoided because the pressure in the circuit can be set only as low as ambient. Thus, a case was made for the ability to create subambient pressures at the Y-piece if control of P_{ct} to the set baseline pressure is desired, especially for pediatric patients with short exhalation periods and high resistance ETTs because of the narrow bore.

It was noted at the time that it was not possible in the configuration of prototype #2 depicted in figure 45 to generate subambient pressure by modulation of the flowrate from the IPFCV. However, if the actuator for the PID controller P_{ct} is changed from the IPFCV to the exhalation proportional flow control valve (EPFCV), the subambient pressure at the inlet of the diaphragm compressor (or recirculating device) could then be used to assist spontaneous exhalation, i.e., flatten the pressure overshoot during

exhalation. This scheme will be described in more detail in the section describing the EPFCV.

Another experience with the IPFCV deserves mention before leaving this section as it influenced the design of the GRADS prototype (section 4.3.7.2, figure 25). The possibility of using both the IPFCV and EPFCV in a complementary manner as a means of controlling P_{ct} was an intriguing and, at first sight, attractive concept. This was especially true since the maximum flowrate capability of the IPFCV was not quite enough to completely bring P_{ct} back to baseline, during spontaneous inspiration. Consequently, it was postulated that if the PID controller would close the EPFCV slightly while the IPFCV would be delivering an increased flowrate during spontaneous inspiration, P_{ct} could be controlled closer to the set baseline, resulting in even more reduced WOB.

The control code was rewritten with the independent PID for each actuator designed to control P_{ct}. The system behaved erratically because the action of actuator A would create a "disturbance" in P_{ct} to which actuator B would respond and vice-versa. Violent pressure swings of up to 40 cm H_2O about the baseline occurred in a totally random manner. Admittedly, the problem could have been solved by having a single PID controlling both actuators but the control algorithm becomes more complicated. It was based on this experience with dual actuator control of one variable that in section 4.3.7.2, during the design phase of GRADS, a control scheme that uses a single actuator to control P_{ct} was preferably sought.

6.2.5 Humidity Considerations

The test rig normally used dry medical O_2. Therefore there was usually no condensation observed on the water trap at the outlet of the diaphragm pump. However, on a humid summer day when the central AC was not working in the University of Florida Anesthesiology Laboratory where the tests were being performed, the circuit was left open for a while and then reconnected to the test lung and started. It was noticed that condensation began to appear at the water trap at the outlet of the diaphragm compressor.

During the design of prototype #2, the interaction between the increase in the water vapor pressure due to recompression and the saturation vapor pressure at a given temperature had not been considered. Assuming an isothermal compression and that all components of the gas mixture (water vapor, N_2, O_2) act as perfect gases, the water vapor pressure is increased by the same ratio as the absolute pressure compression ratio. The increase in water vapor pressure results in condensation of the water vapor when the its partial pressure increases above the saturation vapor pressure at a given temperature.

Therefore, recompression to pressures exceeding 2 psig (figure 21) in prototype #2 represented a fundamental obstacle towards retaining exhaled humidity in a closed system, one of the basic advantages of closed circuit anesthesia. The unacceptable rainout of humidity in prototype #2 caused by the choked flow requirement of the IPFCV would cause inadequate humidity levels in the circuit or require additional complexity to add humidity back. This would be detrimental to patients under prolonged anesthesia because of the ensuing desiccation of the upper respiratory system (Kleemann 1989).

6.2.6 Exhalation Proportional Flow Control Valve (EPCFV)

During the design process, the need for an electronically controlled, high-flowrate (up to 100 l/min), large orifice (2.54 cm (1") diameter), low flow resistance (≤ 1 cm H_2O pressure drop at 60 l/min O_2) proportional flow control valve on the exhalation hose became evident. Available commercial devices were bulky, expensive (approximately $1,000 to $2,000) and were intended mostly for use with very high pressure differentials in the range of thousands of psi (Tescom 1989). Consequently, the maximum variable orifice opening in these commercially available devices was too small (about 0.32 cm (0.125") diameter at most) for the desired application. Many of the available devices were crudely modified for electronic interfacing by simply mounting an electric motor onto a valve initially designed for manual actuation such that there were also concerns about the frequency response of these valves.

Therefore, a proportional flow control valve meeting the desired specifications was designed from scratch using a woofer speaker (Realistic 10.2 cm (4") woofer, Radio Shack Catalog No. 40-1022A, 55 Hz - 5 kHz, 8Ω, nominal 5 W, maximum 10 W) as the proportional linear motion actuator. The woofer was driven by the demultiplexed D/A output of the 80535 via a custom-designed class B amplifier driver (figure 48). The movement of the woofer diaphragm is proportional to the input current. The woofer speaker was encased in an airtight transparent enclosure made of plexiglas so that proper operation could be conveniently and visually checked at all times. Standard 15 mm i.d. connectors for breathing circuit hoses mounted on the airtight enclosure allow the EPFCV to be readily interposed at any point in the breathing circuit.
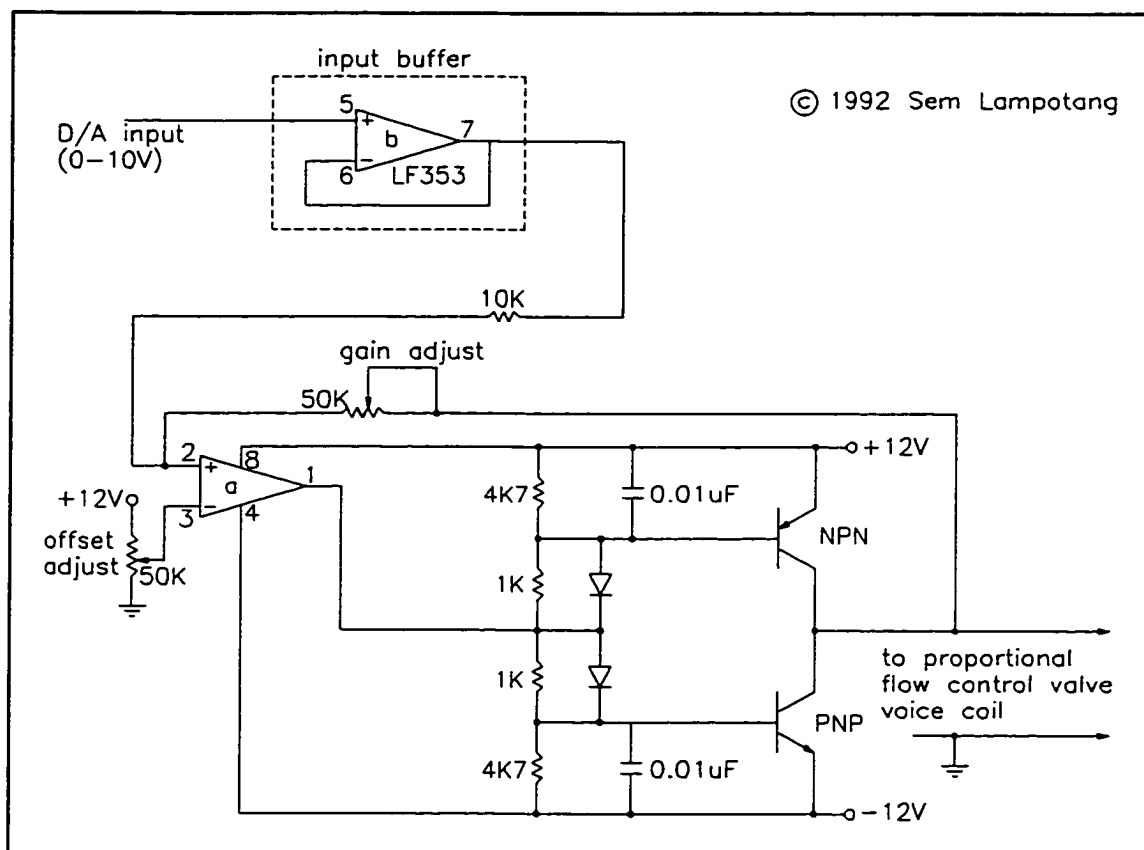
Figure 48. The class B driver circuit for the proportional flow control valve made from a woofer speaker.

The woofer has a maximum throw of 9 mm (0.35") when driven by the amplifier circuit of figure 48. This was determined by writing 0 followed by 4095 (2^{12} - 1) to the amplifier circuit via the demultiplexed 12-bit D/A and measuring the vertical displacement of the diaphragm. A vertical inlet tube (6 cm (2.4") straight length of circular plastic tube with a flow area diameter of 3.0 cm (1.18")) directed the gas flow to the flow throttling location. A cone made out of Delrin with a taper angle (the angle that the tapered side makes with the axis of the cone) of 30° mounted on the woofer diaphragm provided the flow throttling as it is advanced into or retracted from the inlet

tube. Three cones of different taper angle were used: 75°, 45° and 30°. The cone with the 30° taper angle gave the best throttling action over the range of movement of the woofer, i.e., least dead-zone action, a situation where vertical movement of the woofer diaphragm results in no throttling action. The cone with the 75° taper angle gave the most dead-zone action.

The EPCFV had a large current draw (3 A) requiring a substantial power supply because of the low resistance of the voice coil (8Ω) combined with a voltage supply of 24 V (dual power supply of +12V and -12V). The valve would be fully closed and wide open when 0 and 4095 was written to it respectively. The midrange of the D/A output, 2048, was adjusted to correspond approximately to the midrange of the woofer excursion.

6.2.6.1 Valve leakage

One of the fabrication problems of the proportional valve concerned the leakage rate past the throttling cone when the valve is fully closed, with D/A = 4095 written to it. It was anticipated during fabrication of the proportional flow control valve that the valve would also function as a PEEP valve. It would close completely when P_{ca} dropped to the PEEP level thus maintaining P_{ca} at the desired PEEP level. Consequently, a leak at the seal between the throttling cone and the inlet tube would allow P_{ca} to drop below the set PEEP level even if the valve was fully closed. Initially, a 2 mm (0.08") thick layer of soft foam packaging material was glued to the tapered surface of the throttling cone to provide a deformable surface that would provide a good seal. This approach did not provide a good seal because the seal would be provided by a circular line contact

between the inlet tube and the tapered cone which in turn was dependent on the proper alignment of the inlet tube to the throttling cone. Perfect alignment of the inlet tube and throttling cone was difficult to achieve in practice with the proportional valve design.

Consequently, the seal design was changed from a point or line contact to an area contact. A flat doughnut with a concentric width of approximately 1 cm (0.39") was cut out of 1.27 cm (0.5") thick soft black foam rubber used for thermal insulation of hot water pipes. The doughnut was fitted over the straight section of the throttling cone, providing a 1 cm (0.39") wide concentric sealing area between the inlet tube mounting plate and itself (see details of the EPFCV in figure 45).

It was also contemplated that the EPFCV might also be used as an exhalation valve which closes during mechanical inspiration so that all gas flow goes to the patient. That is, the EPFCV would function as the mushroom exhalation valve does in prototype #2. In fact, this is the way in which the EPFCV is used with the GRADS prototype system during mechanical inspiration. Thus, a good seal when the EPFCV is fully closed would be also be required to maintain PIPs of up to 100 cm H_2O during mechanical inspiration.

6.2.6.2 PEEP control actuator

As already alluded in the previous section, the EPFCV was also intended to work as a PEEP valve during mechanical expiration when the mushroom exhalation valve is open. The control of PEEP was performed by a PID controller that was only active during mechanical expiration. The error terms (error, error integral and error rate) were

zeroed after each expiration during mechanical ventilation. The feedback sensor for the PEEP PID controller was the pressure sampled at the ETT distal tip. The PEEP PID controller was consistently able to control PEEP to within 0.5 cm H_2O of the desired PEEP.

Initially, the manual bag that is interposed between the patient and the EPFCV caused consistent undershoot of the PEEP PID controller. That is, the PEEP would end up at 8 cm H_2O instead of the desired 10 cm H_2O, for example. A close examination of the P_{et} trace together with a printout of the control action (i.e., the D/A values written to the EPFCV were captured to a file on hard disk on the PC that was used as a monitor for the DACS board) during mechanical expiration revealed that the PID controller was actually working well. A D/A value of 4095 would be written to the EPFCV as P_{et} dropped to the desired PEEP level. However, once the EPFCV was fully closed, volume would shift from the lungs and be absorbed by the compliance of the manual bag upstream of the EPFCV. The shift in volume from the lungs to the manual bag was causing the PEEP undershoot.

This problem was solved by using an external global variable in the control software that was called 'cone_start_position'. The initial setting of 'cone_start_position' was 2048, the midrange of the EPFCV. After each exhalation, the PEEP offset error is calculated by subtracting the actual end expiratory pressure (eep) from the desired PEEP level. The offset was then used to change the value of 'cone_start_position' after each exhalation until the offset was less than 0.4 cm H_2O while keeping the PID

coefficients for the PEEP controller constant. The C code for this "adaptation" of the starting position of the EPFCV to the offset caused by the manual bag is:

offset = eep - PEEP;

if (offset < - 0.4 ¦¦ offset > 0.4) cone_start_position -= offset*20;

The "adaptation" coefficient of 20 in the control code was derived from experimentation with different coefficients. With the addition of this simple "adaptation" algorithm to the PEEP control PID and an "adaptation" coefficient of 20, end expiratory pressure (eep) would typically undershoot once or twice below PEEP at the start of mechanical ventilation, maybe overshoot once and then would invariably fall within the offset limit of 0.4 cm H_2O within 4 breaths. From that point, the 'cone_start_position' variable would no longer change and the PEEP controller would work to the desired accuracy indefinitely.

6.2.6.3 Assisted spontaneous breathing actuator

Spontaneous inspiration could also be assisted to reduce the work of spontaneous breathing. During assisted spontaneous breathing, the objective was to reduce the dip in pressure below the desired pressure baseline during inspiration and the overshoot above the desired pressure baseline during expiration. The minimization of the area of the PV loop and thus the WOB for a spontaneous breath of a given VT was performed with a digital PID controller. The error signal that drives the discrete-time, digital PID controller was obtained by subtracting the pressure sampled at 20 Hz at the ETT distal

tip (P_{ctt}; p_ett in the control code) from the set PEEP level which could also be zero

(i.e., no PEEP added). The digital PID equations in C code were:

```
last_error = error;          /* definition and calculation of error terms */
error = PEEP - p_ett;        /* every 1/20 second */
integral_error = integral_error + error;
error_rate = error - last_error;

woofer_cone_height = 2048 + ((int) (p*error + i*integral_error + d*error_rate
                  +0.5));                  /* actual PID algorithm */

if (woofer_cone_height < 0) woofer_cone_height = 0;
if (woofer_cone_height > 4095) woofer_cone_height = 4095;
```

The value of 2048 in the PID algorithm is the midrange of the EPFCV. By setting a

baseline shift of 2048 in the control action, it was ensured that the EPFCV actuator could

respond in either direction to a control action request from the controller. In other words,

the EPFCV was not pegged at either extreme (saturated). Saturation of the EPFCV

actuator would have meant that it would not have been able to respond to a control action

request in the direction in which it was pegged.

6.2.7 Exhalation Valve

The exhalation valve is a mushroom valve (Inspiron, Rancho Cucamonga, CA).

A mushroom shaped rubber diaphragm is pressurized with air on one side to close off

an inlet tube with a flow area of 2 cm (0.8") in diameter (low pressure loss). The

mushroom valve is pressurized with compressed air from the E-cylinder regulated down

to 100 cm H_2O by a miniature precision pressure regulator (R100, Air Logic, Racine,

WI). The supply of pressurized air to the mushroom valve is controlled by a 3-way NC

Clippard EV-3 valve. The charging air to the mushroom valve is discharged through the exhaust port of the EV-3 when it is de-energized. A 7.5 cm (3") length of 3.2 mm (0.125") i.d. silicone tubing connects the mushroom valve to the pilot valve (EV-3) for rapid depressurization of the mushroom valve diaphragm when the valve is de-energized.

The mushroom exhalation valve chosen because of its low pressure loss. It was open during mechanical exhalation, spontaneous breathing (both assisted and unassisted) and manually assisted breathing. The mushroom valve was closed during mechanical inspiration (during both active inflation and the inspiratory pause, if present).

6.2.8 O_2 Flush Valve

If a mechanical inspiration is in the process of being delivered when the O_2 flush pushbutton (a manually actuated mechanical valve in conventional anesthesia delivery systems) is depressed, the FGF rate will go as high as 60 l/min so that VT is increased many times over with the risk of barotrauma. In prototype #2, the O_2 flush valve is a 2-way, normally open, 12 V DC, solenoid-actuated electromechanical valve (Humphrey Products, Kalamazoo, MI, 7.4 W, P/N 125E1 3 11 20 35). The O_2 flush valve is triggered by a manually-actuated switch with spring return (figure 49). The occurrence of an O_2 flush is detected by the sensing circuit in figure 49. The I/O line (pin 4.7) of the DACS board that senses the O_2 flush status is normally high (1) and goes low (0) when the O_2 flush pushbutton is depressed. Pin 4.7 is polled at regular interval (0.05 s) by the real-time control software which then aborts mechanical inspiration during an O_2 flush (inspiratory flowrate is reduced to zero by writing a D/A value of 0 to the IPFCV).
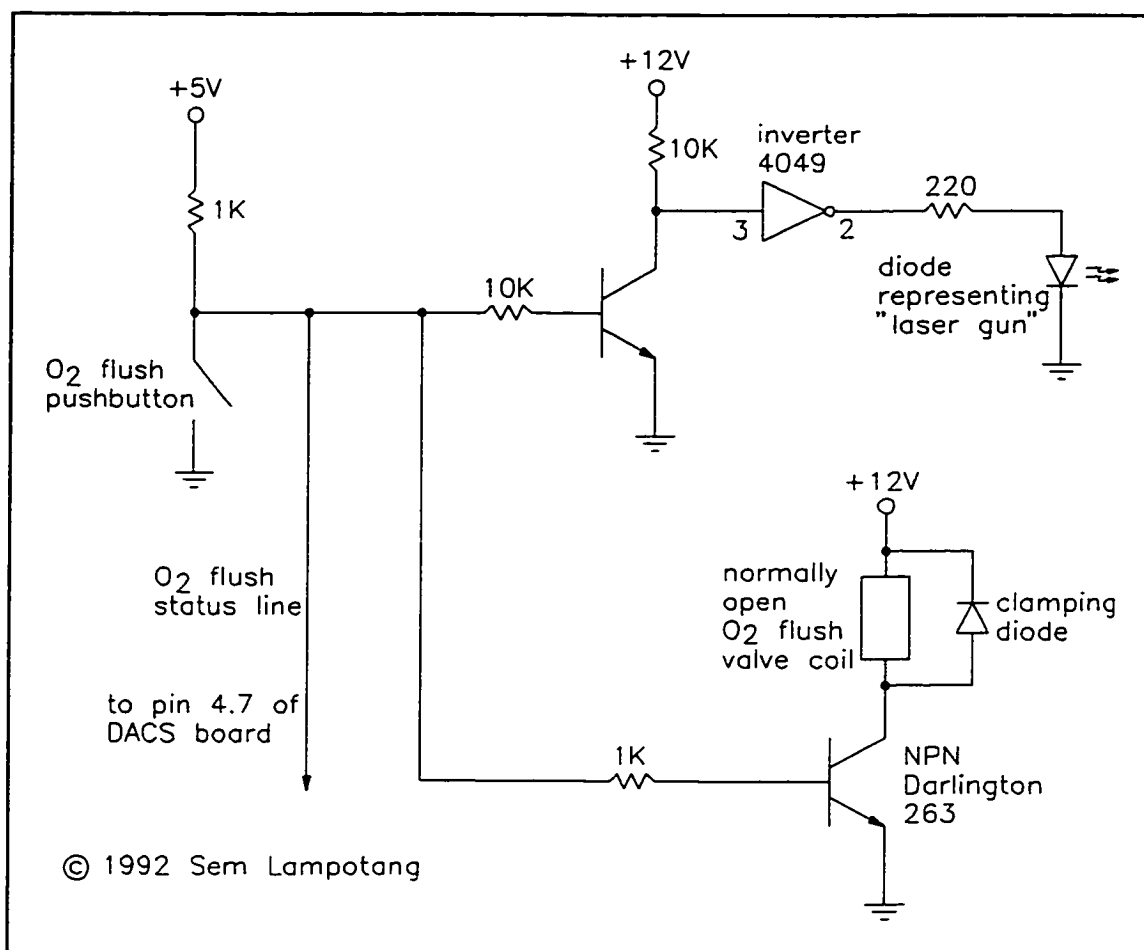
Figure 49. The O_2 flush valve driver circuit, the O_2 flush detection circuit and the concept for the "laser surgery gun" disable during an O_2 flush

Similarly, a condition where P_{cu} exceeds the high pressure limit results in abortion of mechanical inspiration. This is a patient safety feature which, in the author's opinion, should be mandatory but is not implemented in current anesthesia delivery systems. The C code for automatic abortion of a mechanical inspiration during an O_2 flush or if $P_{cu} \geq$ high pressure limit was designed to as readable as possible through extensive use of the #define statement facility provided in C.

```
#define O2_FLUSH_ON      input(P4)>>7 == 0  /* bit 7 on port 4 goes low */
#define HI_PRESS_LIMIT   40    /* 40 cm H2O high pressure limit */
#define INSP_VALVE       0x01   /* demultiplexed D/A channel 0 that */
                                /* controls the inspiratory valve */

.
.


if (p_ett >= HI_PRESS_LIMIT || O2_FLUSH_ON)
        write_da_mux (INSP_VALVE, 0);  /* abort mechanical inspiration by writing */
                                       /* 0 to the inspiratory valve through */
                                       /* channel 0 of the demultiplexer */
else
{
        /* perform normal delivery of a constant flowrate for desired VT in Ti */
}
```

During laser surgery of the airways, the laser might ignite the ETT especially if the O_2 concentration is above 40% (Pashayan et al. 1988). An O_2 flush is therefore an undesirable event during laser surgery of the airway since the O_2 concentration will quickly reach 100% and chances of an airway fire are increased. However, the random nature of an O_2 flush, in the engineering sense, makes it likely that an O_2 flush will eventually occur during the exact time that a surgeon is using a laser surgery gun and accidentally perforates the ETT wall, with disastrous consequences. From an engineering point of view, an O_2 flush is not only random but also a deterministic event, i.e., causally determined by a preceding event(s). Consequently, it was conceived that the deterministic nature of an O_2 flush could be exploited to disable a laser surgery gun whenever an O_2 flush is occurring which would remove the chance of an airway fire.

In the design of prototype #2, the laser disable circuit is hardwired to the O_2 flush valve pushbutton as shown in figure 49. A light emitting diode (LED) represented a "laser surgery unit" in the circuit of figure 49 that was used to demonstrate the concept

that an O_2 flush could be used to systematically turn off a laser surgery unit connected to it during surgery in the tracheal region. The LED "laser gun" was hardwired to the O_2 flush pushbutton and would turn off during an O_2 flush (figure 49). This would improve patient safety since the risk of an "airway" fire during an O_2 flush with laser surgery is diminished. The "laser gun" disable circuit performed as expected and was consistently able to turn off the LED "laser gun" during an O_2 flush. In the design of prototype #2, a time delay (not implemented) would be required to reenable the laser after an O_2 flush. The time delay should be long enough that the FiO_2 has fallen back to a level below 0.4 before the laser is re-enabled. A better solution for interrupting a laser surgery unit during an O_2 flush will be presented in section 6.3.6.

Another objective of the exercise was to convey the advantages of an anesthesia delivery system that can communicate to other real-world devices, if a "real world interface port" is available. In other words, the anesthesia delivery system interacts with other units in the OR and the ability for communication between it and those units is desirable for increased patient safety as demonstrated by the simple circuit of figure 49.

6.2.9 D/A Demultiplexer

The design of prototype #2 required that the microcontroller board control two proportional actuators: the IPFCV and EPFCV. However, the design of the DACS board had only one D/A line available. A demultiplexer board that splits the single D/A line from the DACS into 4 independent D/A lines was therefore designed, built and

successfully tested (figure 50 where only 2 of the 4 demultiplexed channels are shown since all 4 channels are identical in construction and operation).

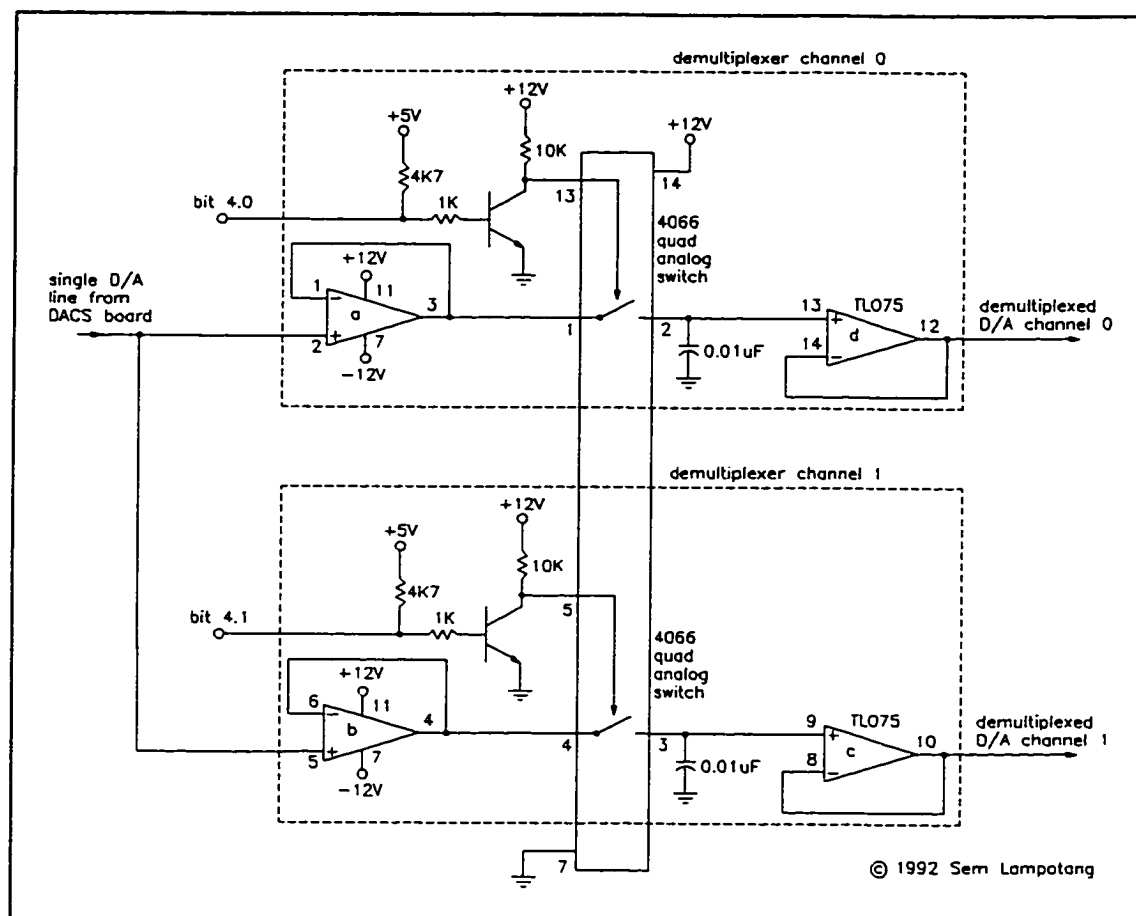Figure 50. The 4 channel demultiplexer for controlling more than one proportional actuator from the single D/A line of the DACS board. Only 2 of the 4 channels are shown.

The operation of the 4 channel demultiplexer is controlled by bits 4.0 to 4.3 of the DACS TTL (transistor transistor logic) I/O port. Essentially, when it is desired to write an analog voltage to, for example, channel 0 to control the IPFCV, the DACS

board first closes the analog switch between pins 1 and 2 of the 4066 quad analog switch IC while the other switches in the 4066 are open.

During initial development of the demultiplexer, direct closing of the 4066 switch without a level shifter via the TTL control signal from the DACS was attempted and performance was erratic. The TTL signal is only at 5 V when high but needs to control analog voltages higher than itself (D/A output of 0 - 10 V). A level shifter that boosts a high TTL signal from 5V to 12 V in the circuit for closing the 4066 analog switch provided reliable and consistent performance when it was added.

With the switch to channel 0 closed, the analog voltage that needs to be written to channel 0 is placed on the D/A output line and gets loaded via the input buffer and through the closed analog switch to the sample and hold (S/H) circuit. The S/H circuit was designed to store the analog voltage for the duration of the control input interval, i.e., 1/20 second. The size of the capacitor in the S/H circuit was optimized by experimentation so that it was not so large that it would take a long time to load it meaning that the analog switch would have to be left closed for a long time. On the other hand, the capacitance had to be large enough, that the analog voltage was sustained without significant decay at the output of the demultiplexed D/A line before the next control input interval.

Once the D/A analog voltage has been loaded into the S/H circuit, the switch for channel 0 opens and the process is ready to repeat itself for either another channel (e.g., channel 1 for writing an analog voltage to control the EPFCV) or the same channel.

The demultiplexer performed to specifications in prototype #2 and provided reliable and independent digital control of both the high pressure IPFCV and the low pressure EPFCV at a control input frequency of 20 Hz from a single 12-bit D/A line.

6.2.10 Ventilation Mode Selector Switch
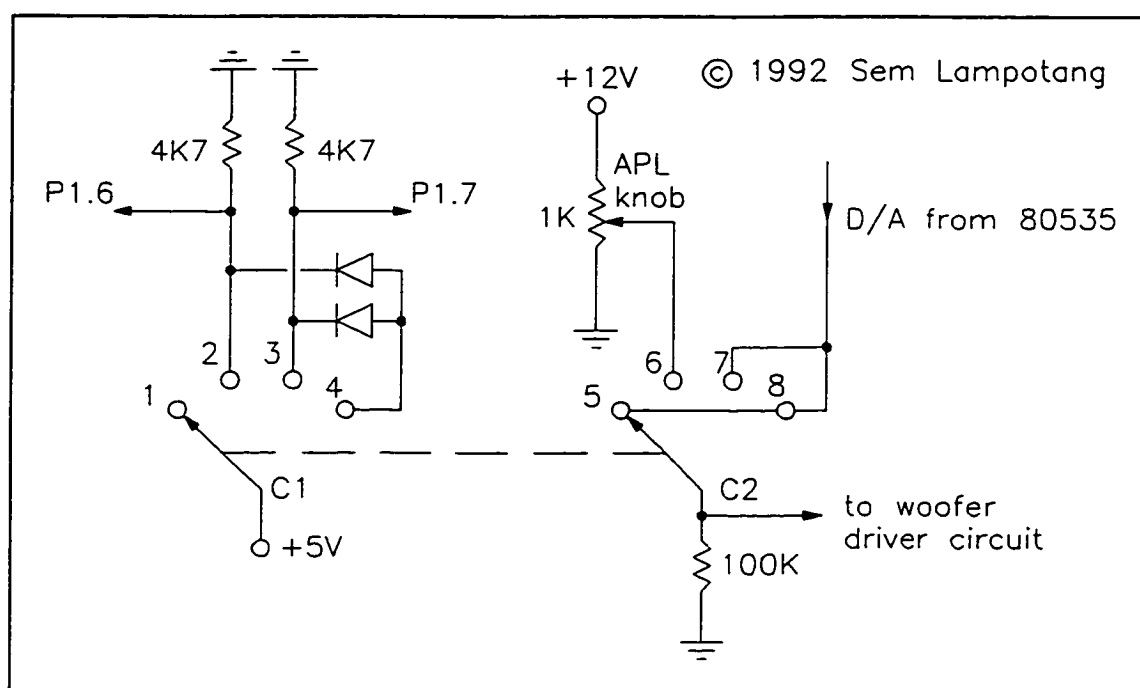
Figure 51.   The ventilation mode selector switch concept and the double-pole, quadruple-throw mechanical switch used for its implementation.

The present user interface on anesthesia delivery systems is not optimal. For example, to switch from manual to mechanical ventilation, the user has to perform as much as 3 separate actions: (a) switch the mode selector knob which is simply a 2-position detented switch with flaps that reroute the path of gas flow in the CO_2 absorber, (b) turn on the mechanical ventilator and (c) close the APL valve. Consequently, in the

design of prototype #2, one of the goals was to achieve a more streamlined way of changing ventilation mode. This goal would also be self-serving form the viewpoint of ease of coding the real-time control software of the prototype since much of the control software is context sensitive, especially relating to the mode of ventilation.

A mechanical double-pole, quadruple-throw switch (Grayhill) recycled from a discarded electronic ventilator monitor (Bourns Life Systems, Model LS160) was used to implement the improved interface concept while also allowing the real-time control software to know at all times any changes in ventilation mode, as soon as they are made. The ventilation mode selector switch is a central feature of the real-time control software as will be seen in the later section on the control algorithm.

One pole of the switch (the left hand one in figure 51) is used solely to determine the ventilation mode. The 7th and 8th bit of port 1 (8 bits) of the DACS board are used to detect the 4 possible switch positions. The diode arrangement and pulldown resistors attached to the left pole of the switch in figure 51 were designed to produce a distinctive and unique bit pattern from bits 1.6 and 1.7 for each of the possible switch positions.

As an additional detail which must not be forgotten because it could potentially affect patient safety, the status of the switch when the wiper is between detent positions was also analyzed and taken into consideration in the initial design. In other words, the microcontroller operating at 12 MHz can sample the status of the switch faster than a human hand can turn the switch from say position 1 to position 2. There will be a finite period of time (indiscernible to a human but noticeable to the microcontroller) during the transition from position 1 to position 2 during which the microcontroller will still be

reading the switch status. If the design of the diode arrangement would for example indicate to the control software that mechanical inspiration mode was on when the switch is really in a transition state, this might cause unnecessary alarms or, even worse, harm to the patient. Consequently, the switch configuration was designed such that all transition states (1-2, 2-3, 3-4) are read as the same, safe ('standby') state.

An electrical analysis of the left pole of the switch shows that bits 1.6 and 1.7 will have the following values for the 4 possible positions and the 3 transition states.

	bit 1.7 (MSB)	bit 1.6 (LSB)
wiper on position 1:	0	0
transition 1-2	0	0
wiper on position 2:	0	1
transition 2-3	0	0
wiper on position 3:	1	0
transition 3-4	0	0
wiper on position 4:	1	1

A bitwise manipulation (shift to the right by 6 bits) is performed after reading port 1. The compact C code for the bitwise shift 6 places to the right of the binary value in port 1 is:

```
ventilation_mode = input(P1) >> 6;
```

This shift clears any preexisting values from bits 1.0 - 1.5 which also results in bits 1.6 and 1.7 becoming bit 1.0 and 1.1 after the shift to the right by 6 bits. The new values for bits 1.2 to 1.7 after the shift to the right are assigned by default to be zeroes (0). Consequently, after the bitwise shift, the value of port 1 can be only 0, 1, 2 or 3.

In the control software, each of the possible values of the integer variable 'ventilation_mode' is assigned to a ventilation mode. Values 1,2,3 and 4 are assigned to standby, manual, mechanical and assisted spontaneous ventilation modes respectively.

The right pole of the switch was used mainly to change control of the EPFCV action from the D/A line of the microcontroller (wiper on position 5, 7 or 8) to the 1K, 10 turn linear potentiometer that functions as the APL knob in a conventional anesthesia delivery system, during manual ventilation (position 2 on the left hand pole of the switch). Therefore, when wiper C2 is on position 6 and wiper C1 is on position 2 indicating manual ventilation, the user can manually control the excursion of the EPFCV throttling cone through the APL knob (pot) to determine how much gas must be "spilled". For example, if the patient has stiff lungs, during manual ventilation, the APL knob would be almost fully closed so that high inflating pressures can be generated at the airway.

The electromechanical "APL valve" potentiometer worked well in combination with the double-pole, quadruple-throw switch and the EPFCV. According to three practicing anesthesiologists who tried it at the time, it provided good manual control of the leak at the APL valve (EPFCV). In the design of prototype #2, the flexibility of the low pressure loss, wide bore, EPFCV was already being demonstrated. The EPFCV was used as (a) a PEEP valve during mechanical exhalation, (b) a backup exhalation valve (backup to the mushroom exhalation valve) during mechanical inspiration, (c) an APL valve during manual and unassisted spontaneous ventilation and (d) a control actuator for the P_{et} feedback loop during assisted spontaneous ventilation.

6.2.11 Software Development Platform

The hardware platform for software development was an IBM PC (8086/8087, 8 MHz, 360K floppy disk drive and 20 MB hard drive, CGA monochrome monitor). A C cross-compiler (C-51 Cross-Compiler Kit v 3.0, Archimedes Software, Inc., CA) that runs on an 8086/8088 system like the PC but generates code for the 8051 family of microcontrollers to which the 80535 of the DACS board belongs was used to compile the code.

The usual software development cycle involved writing the high level code in pseudo code. Next, the pseudo code would be actually implemented in C with liberal use of print statements to facilitate tracking of the program execution and debugging. Upon successful compilation and linking of the text file, the resulting hex file is loaded into the static RAM chip of the DACS board, via a null modem cable and using a terminal emulator program for the PC (Mirror III). A monitor program for the 80535 burned into EPROM handles the I/O functions for the DACS board. Consequently, as the program executes, prompts and alarm messages are displayed on the monitor of the PC. The Mirror terminal emulator program also provides the ability to capture the data stream appearing on the monitor to hard disk, for later analysis. This development platform proved to be convenient and flexible to use, allowing quick modification of the code as the code was being tested.

While the software is still at a developmental stage, the machine code is never burned into EPROM but is always loaded in RAM. Simply turning off the power to the DACS board would erase the machine code loaded into the RAM and allow a modified

version to be loaded. For a simple modification, a typical source code edit, recompile and relink, reload and run cycle could take as little as 3 minutes on an 8 MHz machine which is relatively slow. The machine code was burned into EPROM when the software was stable and no more changes were anticipated.

6.2.12 Real-Time Control Software

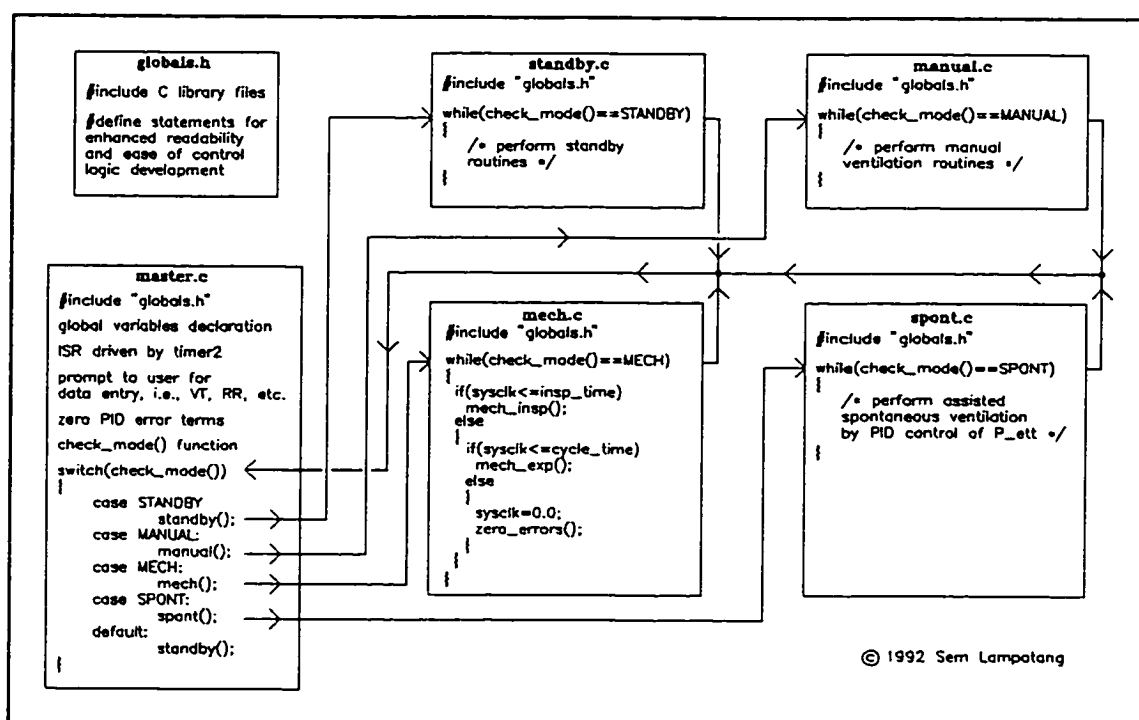Figure 52. The modular structure of the real-time control software that controls the operation of prototype #2. Only the most important lines of code are shown.

The C language (a middle-level language) was chosen over other high level computer languages because of its superior capability for bitwise manipulation and hardware interfacing during development of complex software and portability to other

development systems. The ease of bitwise manipulation and logic in C is especially convenient for interfacing the microcontroller to binary (on/off) actuators.

The control software consisted of 6 modules: a definition header file (globals.h), a master program (master.c) and 4 subprograms (standby.c, manual.c, mech.c, spont.c) for handling each of the 4 different ventilation modes which could be compiled and linked separately (see figure 52). This was convenient for program development since, for example, a minor change in the code in file 'spont.c' meant that only 'spont.c' needed to be recompiled. In contrast, if all 6 modules had been placed in one big file, all the modules would have had to be recompiled which would be inefficient and tedious. Further, the modular structure of the control software was designed to facilitate the addition of more ventilation modes (e.g., CFAV; section 2.3.2) in the future.

6.2.12.1 Header file

The header file was used for inclusion of the necessary C library files for tasks like I/O handling and mathematical functions. It also enhanced ease of coding and control logic development as well as readability by assigning descriptive English names to arcane C commands that address the low level architecture of the 80535 via the #define facility. Some examples are shown below:

```
#define READ_P_ETT   read_ad(1,0x90) /* set input range to 0 - 2.8125 V for D/A */
                                     /* channel 1 which is wired to the pressure transducer */
                                     /* that samples the ETT distal tip pressure */

#define WOOFER  0x02     /* demux D/A channel 1 */
```

```
#define STANDBY   0    /* standby ventilation mode */
#define MANUAL    1    /* manual or unassisted spont. ventilation mode */
#define MECH      2    /* mechanical ventilation mode */
#define SPONT     3    /* assisted spontaneous vent. mode */
```

```
#define CLOSE_EXP_VALVE set_bit(P1_2_bit) /* close mushroom exhalation valve */
#define OPEN_EXP_VALVE clear_bit(P1_2_bit) /* open mushroom exhalation valve */
```

6.2.12.2 Master program

All the global variables used by the control software are declared in the master program. A global float variable, 'sysclk', keeps track of time and is incremented within an interrupt service routine (ISR) that executes every 1/20 second. The ISR is triggered by hardware interrupts from timer 2 of the 80535. Within the ISR, a global integer variable, 'new_data', is also set as a flag that ensures that variables like P_{eu} and execution of the 'while' loops in the control software occurs at a fixed time interval of 0.05 second (1/20 s). The sampling and control action frequency of 20 Hz was determined through experimentation with different time intervals.

The user prompts for data entry (ventilation parameters like RR, VT, I:E, PEEP level, PID coefficients for PID tuning, etc.) are also performed by the master program before program execution starts. Zeroing of the variables representing the error terms of the PID controllers is also done in the master program. The subroutine for checking the ventilation mode selector knob status via port 1 is also coded in the master program.

During execution, the master program continuously checks the status of the ventilation mode selector switch and functions as a "switchyard" redirecting program execution to the appropriate sub-program according to the switch position. In effect, the

master program is simply one 'switch' statement. In C syntax, 'switch' is a control statement that directs program flow and acts as a multiple if-then-else statement; it is analogous to the 'case' control statement in Pascal.

6.2.12.3 Standby ventilation control code

The program for standby ventilation simply places the system in a neutral and safe state. The mushroom exhalation valve is kept open. A demultiplexed D/A value equal to the constant BIAS_FLOWRATE which is defined to a default value of 3000 (approximately 25 l/min) in the 'globals.h' header file is written to the IPFCV. A demultiplexed D/A value equal to the constant MID_POSITION assigned by default to 2048 in the header file is written to the EPFCV. This effectively places the EPFCV throttling cone in mid-position so that its flow resistance combined with the 25 l/min recirculating "FGF" rate around the circuit does not build up pressure at the patient connection to the breathing circuit.

During standby ventilation mode, the pressure sensors are constantly polled at a sampling frequency of 20 Hz and alarms are generated if P_{ct} traverses the pressure limits. A low pressure limit is essential in prototype #2 to ensure that the suction at the compressor inlet is not transmitted to the patient's lungs and to generate an alarm when P_{ct} is below the low pressure limit. The status of the ventilation mode selector switch is also checked within the standby ventilation mode program. The program is simply one big 'while' loop which keeps executing as long as the ventilation mode selector switch is set on standby ventilation or during the finite transition time when the switch is

between any 2 detent positions (figure 52). Thus, the design of the ventilation mode selector circuitry places its transition states in the safe and neutral configuration of the standby ventilation mode.

6.2.12.4 Manual/unassisted spontaneous ventilation control code

The program for manual and unassisted spontaneous ventilation is also one big 'while' loop which keeps on executing as long as the mode selector switch is in the manual position (figure 52). The status of the ventilation mode selector switch is checked at the top of the while loop which executes every 1/20 second. The switchover of control of the EPFCV from the 80535 to the user via the APL valve is done in hardware in the right hand pole of the switch as shown in figure 51. The pressure sensors are constantly polled at a sampling frequency of 20 Hz.

A demultiplexed D/A value equal to the constant MANUAL_FGF_RATE which is defined to a default value of 2000 (approximately 10 l/min) in the 'globals.h' header file is written to the IPFCV. The EPFCV is manually controlled by the user from the APL valve potentiometer. The mushroom expiratory valve is kept open unless P_{ea} is lower than the low pressure limit set at a default value of 5 cm H_2O below ambient in the header file. Closing the mushroom exhalation valve isolates the airway of the patient from the suction of the compressor inlet which it is assumed would be the cause of a P_{ea} more than 5 cm H_2O below ambient.

If P_{ea} exceeds the high pressure limit (default setting of 40 cm H_2O in the 'globals.h' header file), the flowrate output from the IPFCV is throttled back from

MANUAL_FGF_RATE to 0 while an alarm message is printed on the monitor screen. In an actual commercial implementation, audible and visual alarms could be used for the alarm condition. It would simply be a matter of adding some more lines of code to the subroutine that handles the low pressure alarm condition. The goal in the prototype software was to consistently detect an alarm condition whenever it occurs. The actual presentation of the alarm to the user involves human factors and user psychology which, although significant, are beyond the scope of this work.

6.2.12.5 Mechanical ventilation control code

The program for mechanical ventilation is one big 'while' loop which keeps on executing as long as the ventilation mode selector switch is in the mechanical position. In the 'mech.c' file, there are two void functions, mech_insp() and mech_exp() which control the inspiratory and expiratory phases of mechanical ventilation respectively. The mech() void function checks the value of 'sysclk' during program execution and redirects program execution to either of mech_insp() or mech_exp() based on the value of 'sysclk' (see figure 52). At the end of each respiratory cycle, 'sysclk' is reset to zero.

6.2.12.6 Assisted spontaneous ventilation control code

The program for assisted spontaneous ventilation is also one big 'while' loop which keeps on executing as long as the ventilation mode selector switch is in the assisted spontaneous mode position (figure 52). A digital PID is active and provides a control action at a frequency of 20 Hz based on the error between P_{ct} and the desired baseline

P_{ct} level. The control action of the PID controller modulates the position of the throttling cone on the EPFCV. P_{ct} is sampled at 20 Hz. The mushroom exhalation valve is kept open during spontaneous ventilation. A demultiplexed D/A value equal to the constant BIAS_FLOWRATE which is set to a default value of 3000 (25 l/min) in the header file is written to the IPFCV.

6.2.13 PID Tuning Method

The control software consisted of digital PID algorithms because non-linearities and threshold control are more readily handled with digital control. The coefficients of a PID algorithm can also be easily changed compared to an analog PID system.

The tuning method (Astrom & Hagglünd 1988) that was used for the digital PIDs was selected over other tuning techniques because it is practical, systematic and convenient to use. In essence, the technique for tuning a PID consists of starting out with a P controller only, i.e., the I and D coefficients are initially both set at zero. The P coefficient, also known as the gain (Ogata 1970, 155), is adjusted until the system just starts to overshoot in its response to a reference step input. For example, if the system response does not initially overshoot, the P coefficient is increased gradually until an overshoot starts to occur. At this point, the system response will settle to a steady state value which will in general be lower (offset) than the reference step input. The offset is expected because the PID controller is effectively still a P controller at this stage (Ogata 1970, 170) and thus a non-zero error is required for a non-zero control output.

Once the P coefficient that just provides an overshoot is obtained, it is held constant while the I coefficient is gradually increased to get rid of the offset error that resulted with the P controller. A PI controller is in effect at this point because the D coefficient is still zero. The I coefficient is increased until it minimizes the offset error. Further increase of the I coefficient past the optimum usually led to oscillations of the steady state response which is undesirable.

In actual tuning of the PIDs, it was found that the PID (or more correctly the PI) controller would usually meet its performance specifications at this stage. The use of a non-zero D coefficient did not usually bring any benefit or even deteriorated the performance of the controller by introducing more overshoots to the system response before the system would settle to a steady state value. A non-zero D coefficient will also amplify noise from the feedback transducer by responding to it and may thus cause a saturation effect on the actuator (Ogata 1970, 158), e.g., the EPFCV. The use of non-zero D coefficients was recommended for situations where the rate of change of the error signal needed to be controlled (Aström & Hagglünd 1988). Thus, most of the "PIDs" used in prototype #2 were actually PI controllers.

6.2.14 Data Entry and User Selection Menu

Although the keyboard data entry was designed from the viewpoint of ease of use for the system developer rather than the clinical user, its benefits in terms of reduced clutter of the control panel by a multitude of knobs and control settings were noticed during experimentation with the system. Furthermore, the settings used by

anesthesiologists, e.g., flowrate, VT, RR, are pretty much standardized so that an argument can be made that the control software could have default settings for an adult, pediatric and neonate patient which the user could then elect to override through a keyboard. The digital PID coefficients and the ventilatory parameters were entered through the keyboard.

6.2.15 Safety

Safety devices like pressure relief valves were deliberately omitted from the design of prototype #2. The main objective of the study was the proof of concept that the design will work rather than a finished product ready for use on a patient. Further, the safety devices might cut in and compensate for failures of the controller. For example, a safety vacuum relief valve may correct excessive sub-atmospheric pressure without the experimenter being aware of it and could consequently distort the evaluation of system performance.

6.2.16 Mechanical Enclosure

Prototype #2 was not contained in any enclosure. The different components of the system were simply placed on a laboratory bench and assembled together. This was not an optimal situation but at the time the emphasis was on getting the components of the system to work. Because the system was simply laid on top of a bench, it could not be moved easily for testing purposes unless the whole bench was moved. Finally, the components were not as well protected on a bench top as they would have been in a box

enclosure. This was realized after a heavy box on a shelf overhanging the experimental bench fell and shattered the wire wrapped DACS board, rendering it inoperational and beyond repair.

6.2.17 Results and Conclusions

Prototype #2 was a fundamental learning experience without which the GRADS design could never have materialized. The expected loss of humidity from rainout during recompression to pressures above 2 psig was confirmed. Along the same lines, the danger of positive displacement recirculation devices and of pressures higher than the expected maximum required PIP in the breathing circuit was rudely emphasized. It was learned through experimentation that the plenums required to dampen the pressure pulsations of a positive displacement device would add about 15 l of volume to the circuit which is itself only 5 - 7 l. With hindsight, the shutoff head above 2 psig combined with the humidity loss at high recompression pressures and the 15 l volume for the plenums made it become self-evident that a rotodynamic pump (White 1979), e.g., a centrifugal device with a fixed limit to the shut-off head and a non-pulsatile output was required.

The EPFCV fabricated from a woofer worked well in all the different functions in which it was used (PEEP control, exhalation valve, APL valve, assisted spontaneous breathing actuator).

The DACS board proved that it had sufficient processing power to acquire and control the numerous components in prototype #2 in real time. A sampling and control action frequency of 20 Hz was found to work well, by a process of experimentation.

The problems with dual actuator control were identified. The digital PIDs also functioned to specification when the control action frequency was 20 Hz. The Archimedes C compiler proved to be convenient and practical to use and created compact code that would still fit in the 32 Kbytes of RAM storage of the DACS board.

In spite of the many design advantages that prototype #2 already had over conventional systems, e.g., no insidious augmentation of VT by FGF, it had two unacceptable fundamental problems: the rainout of exhaled moisture from the patient and the high shut-off pressure of the diaphragm compressor, both detrimental to the patient's health and safety. Therefore, a third system design iteration was required and was performed. This effort led to the design of the Gainesville Recirculating Anesthesia Delivery System (GRADS) which is described in the next section.

6.3 GRADS Prototype

The GRADS prototype documentation will be shorter than that for the previous prototype since many of the components described in detail for prototype #2 are used in GRADS (figure 53). A complete listing of the components in GRADS will be performed in this section.

The modules in prototype #2 were deliberately designed from the start in a modular fashion so that they could easily be reconfigured into different system layouts. Thus, when the GRADS design was finalized, the existing modules from prototype #2 were readily incorporated into the GRADS prototype by simply rearranging the modules in a different configuration. A single line entry will redirect the reader who reads

section 6.3 ahead of section 6.2 to the appropriate subsection of section 6.2 if the component is already described for prototype #2.
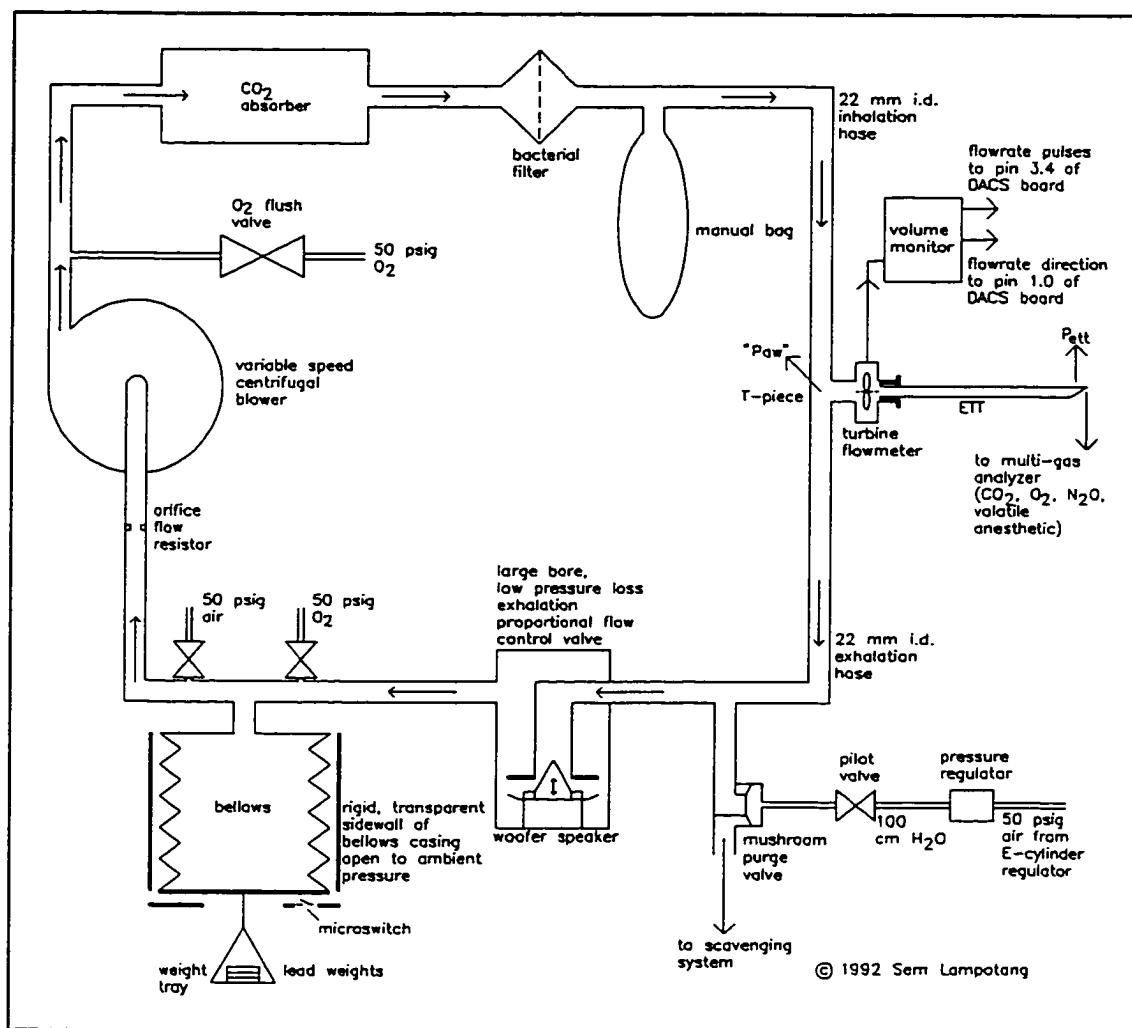

Figure 53. The implementation of the GRADS prototype.

The GRADS design was conceived in June 1991. There was also a concurrent effort at the time to determine the merit of adding inspiratory flowrate shaping during mechanical ventilation to the GRADS design. This investigation grew into a sustained and dedicated two month effort which resulted in the work presented in chapter 5 and

delayed actual implementation of the GRADS design. Preliminary trials of the GRADS concept were performed in October 1991 before starting actual implementation of the ventilation component of the design.

The test was performed by assembling the blower, a circle breathing circuit, a hanging bellows, a 3 l manual bag and another 3 l bag representing the patient's lungs in a bare bones configuration of the GRADS design. Periodically, the 22 mm i.d. exhalation breathing hose was manually pinched to simulate the action of the EPFCV during mechanical ventilation while the blower was circulating gases around the circuit at approximately 40 l/min. The 3 l bag representing the lungs was rhythmically inflated in synchrony with the manual pinching of the exhalation hose. The necessity of having the bellows as a collapsible volume on the subambient side of the circuit was confirmed by removing the bellows from the circuit. On pinching the hose manually to simulate mechanical ventilation, there was almost no inflation of the 3 l bag representing the lungs of the patient. Thus, the prediction of equation 4.10 was confirmed.

The manual bag was also squeezed to simulate manual ventilation and inflated the bag representing the lungs. A decrease in compliance of the "lungs" was also simulated during manual ventilation by squeezing the 3 l bag representing the lungs. In a blind test, the person squeezing the manual bag, i.e., manually ventilating the patient, was always able to tell whenever the "lung compliance" was reduced from the change in the feel of the manual bag. Once the preliminary trial tests of the concept had been performed and had indicated that there was no fundamental flaw in the design, the fabrication of GRADS started in earnest in December 1991.

6.3.1 DACS Board

Following the accidental destruction of the wire-wrapped DACS board in prototype #2, a printed circuit board (PCB) version of the DACS board with the same microcontroller, the 80535, was used. In the PCB version of the DACS board, there were 3 headers (TTL I/O, analog and expansion) which allowed quick and secure interfacing of the board to the system components via ribbon cables. The assignment of the pins in the TTL I/O and analog headers is listed in tables 12 and 13.

Table 12. The pin assignment on the TTL I/O header connector of the DACS board used in the GRADS prototype.

	Gnd	34	33	+5 V	
	Gnd	32	31	+5 V	
Not assigned		30	29	P 3.5	
Flowrate pulse counter	P 3.4	28	27	P 3.2	
	P 1.7	26	25	P 1.6	
	P 1.5	24	23	P 1.4	
	P 1.3	22	21	P 1.2	
	P 1.1	20	19	P 1.0	Flowrate direction
	P 4.6	18	17	P 4.7	Laser disable
	P 4.4	16	15	P 4.5	
Demux CH_2	P 4.2	14	13	P 4.3	Demux CH_3
Demux CH_0	P 4.0	12	11	P 4.1	Demux CH_1
Air make-up activate	P 5.0	10	9	P 5.1	Bellows sensor
O2 make-up activate	P 5.2	8	7	P 5.3	Purge valve activate
O2 flush activate	P 5.4	6	5	P 5.5	O2 flush request
Mode selector bit 0	P 5.6	4	3	P 5.7	Mode selector bit 1
Not assigned		2	1		Not assigned

Table 13. The pin assignment on the analog I/O header connector of the DACS board used in the GRADS prototype.

	-12 V	20	19	+12 V	
Woofer valve	D/A Out	18	17		Not assigned
ETT-tip pressure	AN0	16	15	A Gnd	
Y-piece pressure	AN1	14	13	A Gnd	
Blower speed setting	AN2	12	11	A Gnd	
Vacuum transducer	AN3	10	9	A Gnd	
	AN4	8	7	+ 5 V	
	AN5	6	5	+ 5 V	
	AN6	4	3	D Gnd	
	AN7	2	1	D Gnd	

6.3.2 Centrifugal Blower

The blower is a 2-stage, variable speed centrifugal blower (Ametek, Lamb Electric Division, Model No. 116639-2-E). Its backward curved blades provide a monotonic discharge curve and therefore stable operation without "hunting" or "surging" (Lapina 1982). Wall AC power is regulated by an on-board DC power supply that supplies a brushless DC motor. Speed control is achieved through an 18 kHz pulse width modulated (PWM) controller that accepts an analog DC input voltage ranging from 3V - 10V and is readily interfaced to the D/A output of a microcontroller or the output of a potentiometer. The motor has locked rotor protection as well as automatic over temperature correction. The blower is recommended for use in ambient temperatures between 0 and 40°C and shuts down below the minimum speed of the blower (about 3,000 rpm). At the minimum speed, the blower delivers approximately 2.54 cm (1")

H_2O vacuum per fan stage. At maximum motor speed, the blower can deliver up to 150 cm H_2O in a shutoff condition according to the manufacturer's specifications.

6.3.2.1 Blower speed control

The blower speed control unit inbuilt in the blower will take a DC voltage range of 3 - 10 V. The manufacturer's data sheet recommends that voltages in excess of 10 V should not be supplied to the speed control unit. The blower is manually controlled in the GRADS prototype via a 10-turn, 1KΩ, linear potentiometer that is placed on the front control panel. The knob mounted on the potentiometer shaft is labeled 'PIP limit'. The 1 KΩ pot is connected to the +12V power line via a 200Ω, ¼ W resistor such that its maximum voltage output to the blower speed control unit is 10 V (figure 54).
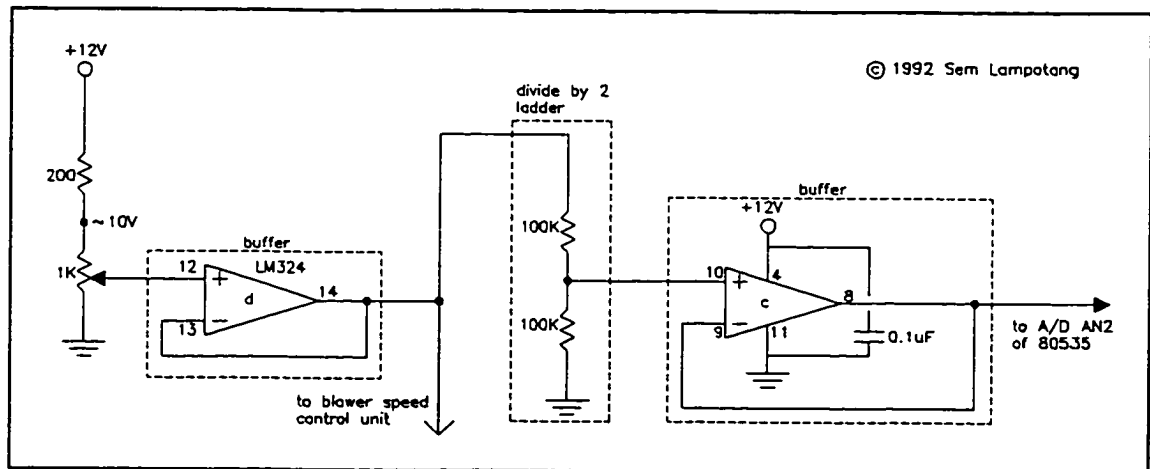

Figure 54. The circuit for manually controlling the blower speed and hence the PIP limit. The input to the blower speed control unit is monitored by the A/D as a safety feature.

The voltage output of the PIP limit pot is monitored via a high impedance divide by 2 ladder. Because the A/D converter of the 80535 can only accept a maximum input range of 0 - 5 V, the divide by 2 ladder is necessary to reduce the 0 - 10 V output range of the PIP limit pot to 0 - 5 V. After the A/D conversion, the value of the input voltage to the blower speed control unit is multiplied by 2 in software to arrive at the true input voltage. The high impedance of the divide by 2 ladder is to ensure that the resistance of the ladder which is effectively in parallel to the potentiometer does not distort the linear output of the pot. The input to the blower speed control unit is monitored as a convenience for experimental data collection when testing system performance. However, the same A/D line could also be used as a safety feature. For example, if the maximum PIP is 20 cm H_2O and the anesthesiologist has the blower speed control set at a maximum PIP of 60 cm H_2O, a caution message could be displayed, warning that the PIP limit is unnecessarily high and could jeopardize patient safety.

For a commercial implementation of this design, a shaft encoder would be preferable to a mechanical pot for increased patient safety. If a conventional pot is set at the maximum PIP limit by accident (e.g., by the cleaning personnel, while wiping the front control panel with bactericidal solution) before the machine is turned on, then the blower will be in the high PIP capability mode as soon as it starts. Thus, the patient could be hurt if a breathing circuit malfunction occurs concurrently (e.g., the EPFCV fails shut). On the other hand, with a shaft encoder (also known as a soft pot or a digital pot), its output can be initialized at a safe value on startup irrespective of its mechanical

"setting". The encoder position would be read by the 80535 using memory mapped I/O and the blower speed controlled via the 80535 through a demultiplexed D/A line.

6.3.3 Pressure Sampling, Transducers and Differential Amplifiers

The pressure transducers, ETT design, sampling site, and differential amplifiers for the GRADS prototype are identical to prototype #2 (section 6.2.3).

6.3.4 Proportional Flow Control Valve

The proportional flow control valve used in the GRADS prototype had to be a low pressure loss, high flow valve so that the recirculating device would not need to recompress to high pressures to make up for the pressure losses. Consequently, the proportional flow control valve is the EPFCV of prototype #2 (section 6.2.6). The same driver circuit was used as in prototype #2 (figure 48).

6.3.5 Purge Valve

The purge valve in prototype #3 (GRADS) is the mushroom exhalation valve of prototype #2 (section 6.2.7). Its large flow area (2.54 cm (1") diameter) was essential for letting the high flowrate of O_2 (60 l/min) during an O_2 flush flow through it without the pressure buildup in the breathing circuit exceeding 1 cm H_2O. The purge valve is piloted through the same Clippard 3-way valve as the exhalation valve of prototype #2.
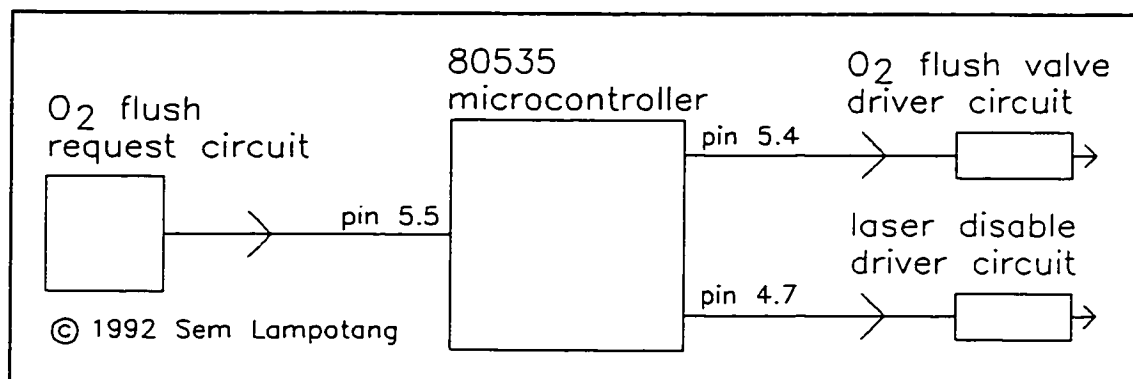
6.3.6 O₂ flush

Figure 55. The control structure of the O₂ flush event in the GRADS prototype. The request for, and execution of, an O₂ flush are linked through the microcontroller.

The O₂ flush feature is implemented in a fundamentally different way in the GRADS prototype. Instead of the electromechanical O₂ flush valve being directly hardwired to the O₂ flush pushbutton like in prototype #2 (figure 49), the O₂ flush is divided into two logical components: the request for an O₂ flush and the actual execution of the request, i.e., delivery of 60 l/min of O₂ in the circuit (figure 55).

The O₂ flush is a highly disruptive and random event during anesthesia and can cause barotrauma and injury to the patient breathing on an experimental closed circuit design or during mechanical inspiration in a conventional anesthesia delivery system. Consequently, although the O₂ flush is an essential and apparently simple feature required of an anesthesia delivery system, incorporating it into the system design can be a deceptively challenging task and requires careful analysis. As an example of the technical difficulty of the O₂ flush, the Physioflex which represents at the time of writing the state of the art in anesthesia delivery system does not have an O₂ flush feature.

Whereas an O_2 flush event was only detected and appropriate patient safety measures taken in the control software design in prototype #2 (figure 49), the design of the O_2 flush in GRADS exploits the speed of the microcontroller and the relatively coarse temporal resolution of humans compared to the machine cycle of the 80535 microcontroller (1 μs). Many advantages derive from decoupling the O_2 flush request from the actual execution of the request.

First of all, the randomness of the O_2 flush event is effectively removed. The O_2 flush request is communicated to the microcontroller which can then prepare the system for the impending activation of the O_2 flush valve. In other words, the O_2 flush is transformed from a random event to a planned event as far as the system is concerned.

Secondly, an O_2 flush subroutine of finite execution time duration can be written which is accessed when the polled O_2 flush request line status is triggered. The sequential activation of the O_2 flush valve within the O_2 flush subroutine removes any possible concerns, like in prototype #2, about the O_2 flush valve being activated before the system has been fully configured for the O_2 flush. The O_2 flush request service subroutine renders the control software significantly more modular and easier to code and modify, e.g., for additional actions that have to be performed before an O_2 flush.

The O_2 flush service routine must be of finite time duration for 2 main reasons: (a) it would not be acceptable for the user to wait, e.g., 15 seconds between the time that the O_2 flush request is depressed and actual activation of the O_2 flush valve and (b) from a human factors point of view, the objective is to make the change in the control structure of the O_2 flush transparent to the user. Therefore, the new O_2 flush design

should have the same look and feel as the conventional O_2 flush designs. Consequently, the delay between the O_2 flush request and activation should not exceed about 0.05 s. This is not as stringent a specification as it might appear at first glance since the 80535 can perform approximately 50,000 operations in 0.05 seconds, i.e., the O_2 flush subroutine can have as many as 50,000 operations in it before any delay will be noticed.

Thirdly, because the microcontroller is interposed between the request and activation circuits, the inherent multi-purpose capability of software provides for more generic and flexible control of the O_2 flush. Fourthly, safety is enhanced because the microcontroller can both activate and deactivate the O_2 flush. Thus, if P_{ct} is above the high pressure limit (e.g. because of the purge valve failing shut), the microcontroller has the ability to abort the O_2 flush sequence to prevent barotrauma to the patient.
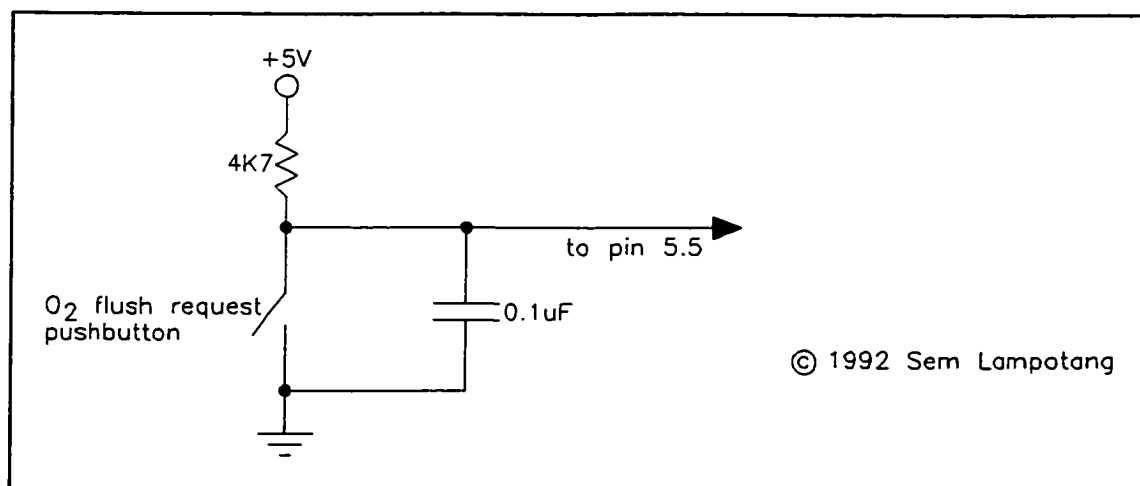
6.3.6.1 O_2 flush request

Figure 56. The O_2 flush request circuit.

The O_2 flush request is simply a spring return, single pole, single throw switch with a 4.7 KΩ pull up resistor and a 0.1 μF debouncing capacitor connected to pin 5.5 of the 80535 as shown in figure 56.

6.3.6.2 O_2 flush subroutine

The O_2 flush in GRADS is performed differently from prototype #2. The status of the O_2 flush request pushbutton is polled every 0.05 second. Pressing the O_2 flush pushbutton simply generates a request for an O_2 flush which the control software services only after it is safe to do so.

The C code for the O_2 flush function is readable and descriptive of the control sequence:

```
#define DISABLE_LASER P4.7=0  /* MOC3010 diode off; no AC flows via triac */
#define ENABLE_LASER  P4.7=1  /* MOC3010 diode on; AC flows via triac */

void O2_flush()
{
        DISABLE_LASER;
        OPEN_PURGE_VALVE;
        delay(2);      /* 2*0.05s = 0.1 second delay */
        write_da(0);   /* woofer prop. flow control valve wide open */
        OPEN_O2_FLUSH_VALVE;

        while (O2_FLUSH_REQUEST)    /* keep executing this while loop */
        {                          /* as long as O2 flush request pushbutton */
                DISABLE_LASER;     /* is depressed.  Suspend all other */
                OPEN_PURGE_VALVE;  /* system processes like mechanical */
                write_da(0);       /* ventilation, etc. */
                OPEN_O2_FLUSH_VALVE;
        }

        CLOSE_O2_FLUSH_VALVE;
        delay(2);
        CLOSE_PURGE_VALVE;
```

```
ENABLE_LASER;   /* this would not be done in an actual implementation
                   because the FiO₂ will still be greater than 0.4
                   immediately after an O₂ flush */
}
```

The 'delay()' function provides the ability to create an adjustable delay between the opening of the purge valve and the O_2 flush valve in case that the response time of the O_2 flush valve is shorter than that of the purge valve. This will obviously be a function of the hardware that will be used in the actual implementation of the system. The delay is adjusted by the integer parameter passed to the function when it is called. The actual time delay is obtained by multiplying the parameter passed to the function by 0.05 s. The resolution of the time delay adjustment is 0.05s.

6.3.6.3 O₂ flush valve and driver circuit

The O_2 flush valve is a normally closed, 12 V DC actuated, 6 W device with an orifice size of 0.16 cm x 0.16 cm (1/16" x 1/16") (Precision Dynamics, Inc., New Britain, CT, 2 MOPD, A5 ident, Valve No: A3314-S8). The O_2 flush valve is a 3-way valve converted into a 2-way valve by plugging the exhaust port and is supplied with 50 psig O_2 from the pressure regulator on the O_2 E-cylinder. The output of the O_2 flush valve is connected through a 0.75 m (2.46 ft) length of 0.32 cm (1/8") i.d., high pressure, low compliance tubing to a standard 15 mm i.d. connector that can be interposed anywhere in the circuit. A 0.127 mm (0.005") diameter orifice is placed inside the tubing to permanently throttle the flowrate of O_2 at 60 l/min when the O_2 flush valve is supplied with 50 psig O_2. The valve was controlled by the microcontroller via the driver circuit in figure 57.
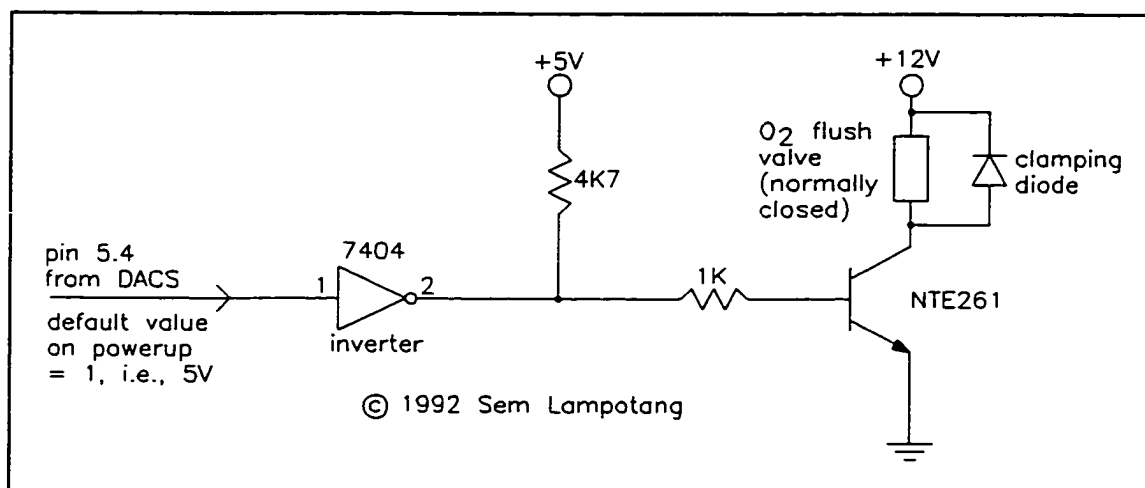
Figure 57. The O_2 flush valve driver circuit.

An inverter was required in the O_2 flush valve driver circuit during prototype development because the O_2 flush valve is normally closed while the default setting on power-up for the TTL I/O pins of the 80535 is '1', i.e., 5V. Therefore, while the machine code for the control software was being loaded into RAM for testing purposes, O_2 was being flushed into the circuit at 60 l/min. A quick solution would have been to immediately write a '0' to pin 5.4 in software as soon as program execution starts. However, this was deemed to be neither a safe nor an elegant solution.

6.3.6.4 Laser disable circuit

A concern with the "laser" disable demonstration board design used in prototype #2 (figure 49) was the possible electrical interaction between the anesthesia machine and the laser surgery unit, e.g., ground loops or an electrical short circuit in the laser surgery unit disabling the anesthesia machine or vice versa. Consequently, during the third

system design iteration loop, this concern was addressed by designing, building and successfully testing the circuit shown in figure 58. The electrical circuits of the anesthesia delivery system and the laser surgery unit are deliberately maintained in electrical isolation from each other. The circuits are coupled optically via the MOC 3010 triac driver IC to ensure that there are no ground loops between the anesthesia machine and the laser microsurgery unit. The design of the AC power interruption device was made generic.
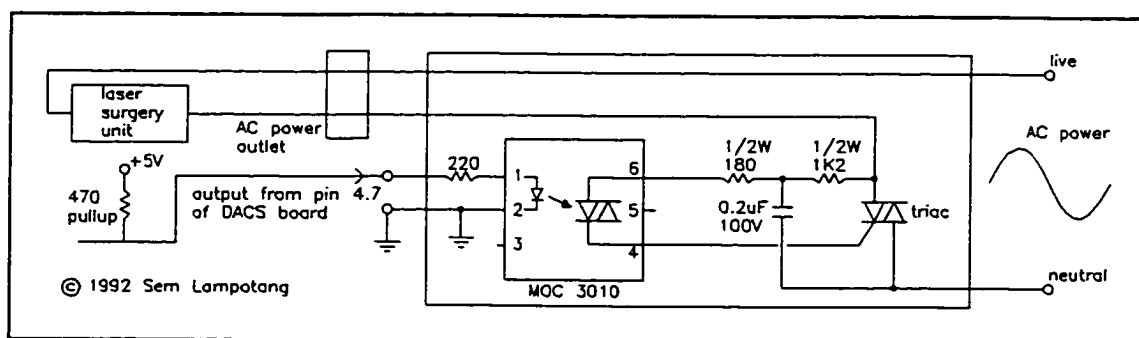

Figure 58. The laser disable circuitry that is triggered from the microcontroller of GRADS. The two circuits are electrically separated; the connection is done optically.

When pin 4.7 is set high, the light emitting diode inbuilt in the MOC3010 IC emits light and energizes the triac inside the MOC3010. This triac in turn energizes the discrete triac in the circuit and allows AC power to flow to the generic AC power outlet to which the laser surgery unit would be connected. Conversely, when pin 4.7 is set low, the LED inside the MOC3010 does not emit light and both triacs (the one in the MOC3010 and the discrete one) do not conduct and AC power cannot flow to the generic power outlet. For demonstration purposes, the laser surgery gun was represented by a

helium-neon laser tube (Siemens LGK 7630, PN 122 P 87143, 6.0 mW Po) recycled from a laser photocopier whose power supply was plugged into the generic AC power outlet. The laser disable circuit worked well and was consistently able to turn off the laser whenever the O_2 flush request pushbutton was depressed.

With some minor modifications which would mainly depend on whether the controlled device is a resistive load, an inductive load or a combination of both, the circuit shown in figure 58 can be used to control any AC powered device from the anesthesia machine and could also be readily adapted to control a DC device. For example, a motorized syringe injector plugged into the generic AC outlet could be turned off by the anesthesia machine if the monitors, e.g., blood pressure monitor, communicate to the anesthesia machine that the syringe has injected too much of a drug that lowers blood pressure into the patient.

6.3.6.5 Generic laser disable

Prototype #2 demonstrated that an O_2 flush button can be readily interfaced with a laser gun. However, the design was hardwired so that the "laser" could only be interrupted by an O_2 flush. But, there are other ways in which FiO_2 could accidentally exceed 0.4. One simple way is if a new resident sets the FiO_2 at 1.0 during laser surgery of the upper airway. The design of prototype #2 would be helpless against this potentially dangerous situation.

Therefore, the laser disable circuit in GRADS was designed in a modular way to address this potential design flaw of prototype #2. By interfacing the microcontroller to

the laser disable circuit, communication has been established between the anesthesia machine and the laser surgery unit in a generic fashion. The FiO_2 can be read from the serial data stream output by a multi-gas analyzer in real time and the laser disable circuit can be activated whenever FiO_2 exceeds 0.4. Because of the modular organization of the control program structure and the flexibility of software, it would require only the addition of a few lines of code in the control software to disable the laser whenever FiO_2 exceeds 0.4.

6.3.6.6 Reenable laser after disable

In the description of the O_2 flush subroutine (section 6.3.6.2), it has already been mentioned that once the laser gun has been disabled, reenabling it as soon as the O_2 flush pushbutton is released would not be advisable since the FiO_2 will still be above 0.4, immediately following the O_2 flush. One possible solution is to reenable the laser by setting pin 4.7 to '1' when FiO_2 drops and stays below 0.4 for more than 30 seconds. Another solution is to have a manual reset button which the anesthesiologist will have to consciously press to reenable the laser gun. Obviously, a combination of both could also be implemented.

6.3.7 Ventilation Mode Selector Switch

The ventilation mode selector switch concept was carried over from prototype #2. Its operation and circuitry is identical to that described in section 6.2.10.

6.3.7.1 APL valve

The APL valve configuration was identical to the one used in prototype #2 (section 6.2.10). The same concerns about the position of the mechanical potentiometer that controls blower speed when the system is started (section 6.3.2.1) also apply to the APL valve pot. For example, if both the mechanical APL valve and the blower speed pots are accidentally set to the fully closed and maximum speed positions respectively, prior to starting the system, the patient could be injured because of the resulting overinflation of the lungs on startup.

The same solution as for the blower speed control pot will also work, i.e., a shaft encoder whose "position" or setting can be initialized as the machine is turned on, irrespective of its position. As with the blower speed control pot, the shaft encoder is read using memory mapped I/O and a demultiplexed D/A line is used to control the APL valve. Thus, the manual "input" of the user when the APL valve knob is turned is reinterpreted via the 80535.

The reinitialization of the APL valve position to, e.g., the mid-position, would be programmed to occur each time that the ventilation mode selector switch is set to manual ventilation and at startup. This would ensure that the APL valve "setting" is always in a safe state at startup and switchover to manual ventilation. Then, any movement of the shaft encoder by the user turning it will be interpreted relative to the position of the shaft encoder when it was initialized at startup or at switchover to manual ventilation. Exactly, the same technique would be used for the blower speed control shaft encoder.

Further, the D/As from the 80535 that control the blower speed and the APL valve setting allow the microcontroller to take over the control of these two components if it is clear that a dangerous situation is developing and the user is not responding in the appropriate manner. In an extreme case, the microcontroller can turn off the blower completely, if the high or low pressure limits are violated.

6.3.8 Software Development Platform

The development platform consisted of the prototype connected to an IBM-compatible personal computer (PC-Craft 80386/80387, 25 MHz microprocessor, 8MB RAM) through a null-modem cable and one serial port (console) of the DACS board. The C compiler was version 4.0 of the cross-compiler kit (Archimedes Software Inc.) that was used in prototype #2. A commercial terminal emulator program for the PC (Mirror 3.0) was used to monitor the flow of data coming from the 80535 and communicate with it. Using the capture facility of Mirror, the data were written directly in data files on the fixed disk (110 MB, Western Digital) of the PC.

6.3.9 Real-Time Control Software

The control software of the GRADS prototype has the same modular structure of prototype #2. One major modification was the addition of the O2_flush() subroutine described in section 6.3.6.2 in the 'master.c' file. The 'standby.c' and 'globals.h' files were renamed 'prime.c' and 'defines.h' which are more accurate descriptions of the function of each file.

Each of the 4 subprograms (prime, manual, mech and spont) was also altered to handle an O_2 flush request in a polled fashion. In each of the 4 subprograms which are effectively 4 big 'while' loops (see figure 52), immediately after the 'while' statement which checks for the ventilation mode selector switch status, an 'if else' statement is interposed before the main body of the 'while' loop. The 'if else' statement redirects program flow away from normal program execution in the event of an active O_2 flush request. For example:

```
#define O2_FLUSH_REQUEST  P5.5==0

while(check_mode()==MANUAL)
{
        if (O2_FLUSH_REQUEST)
                O2_flush();
        else
        {
                /* perform routines for manual ventilation */
        }
}
```

It might seem that an inordinate amount of attention is lavished on the O_2 flush in the software control program. However, one has to remember that to achieve the objective of efficient use of volatile anesthetics, reduced OR pollution and increased humidity and heat retention, the system will have to operate in closed circuit mode most of the time. In a closed circuit, an O_2 flush event can become a lethal feature if the O_2 flush is not handled properly. The high flowrate of O_2 will quickly build up pressure in the circuit and rupture the lungs of the patient.

6.3.10 Pre-Use Check of System

As a troubleshooting facility for software development, a pre-use check program was written in Archimedes C 4.0 that checks the proper operation of each of the components in the system. This program was always run every time that new control software was tested to ensure that the hardware was working properly before the new software was tested. This systematic approach to software development increased the speed and efficiency of debugging the software because it reduces the risk of wasting much time looking for a software bug when the problem really stems from the hardware (e.g., one of the many wires in the system may have broken).

The troubleshooting pre-use check exploits the fact that all the hardware components of the system are intimately interfaced with the computer. The troubleshooting pre-use check was demonstrated to clinicians and obtained favorable reviews. It was made clear to the clinicians that the trouble-shooting pre-use check was intended solely for the use of the software developer.

In most institutions and in accordance with the American Society of Anesthesiology's recommendations, a clinician performs a pre-use check of the anesthesia machine every morning and before each case. The software development tool could be readily converted into a semi-automated clinical pre-use check that the clinician would run on the anesthesia delivery system each morning before starting his case load. Such a semi-automated pre-use check will have the benefits of being systematic, standardized and quicker to perform than the pre-use check recommended by the FDA (Food and Drug Administration; an anesthesia machine is officially classified as a drug).

6.3.11 CO_2 Absorber

The CO_2 absorber was made from a 20.3 cm (8") length of transparent plastic pipe with an internal diameter of 7 cm (2.75"). PVC endcaps (one blank and the other with a threaded end piece) were glued on each end with silicone glue. The threaded end-piece can be unscrewed to allow emptying and refilling of the CO_2 absorbent inside the CO_2 cartridge when it becomes exhausted. A 15 mm i.d. standard connector was inserted and glued with silicone compound inside a hole drilled into the center of each end-piece, thus allowing the CO_2 absorber to be easily interposed at any point inside the breathing circuit. Fine steel mesh screens on the inside of each end piece prevent CO_2 absorbent dust or granules from being blown into the breathing circuit via the 15 mm i.d. connectors. The pressure drop across the CO_2 absorber filled with CO_2 absorbent is 2 cm H_2O at 60 l/min of air.

6.3.12 Gas Make-Up Valves

The gas mixture in the circuit for testing and demonstration will be mostly air and sometimes 100% O_2 mainly because N_2O has to be handled and disposed with care because of the harmful side-effects of breathing waste N_2O. It is more convenient and less noxious to use air and O_2 for testing purposes. Thus, these are the only two gases used in the GRADS prototype for testing and demonstration purposes.

The O_2 and air make up valves are Clippard EV-2 2-way NC valves with a response time of 5 milliseconds (Clippard Instruments Laboratory, Inc.). Because the make-up valves are light and compact, they can be directly mounted onto standard 15

mm i.d. connectors that are interposed into the breathing circuit. The valves were directly mounted onto the standard connectors to minimize the residual volume of gas between the valve and the breathing circuit and also to ensure that the flow resistance of a connecting piece of tubing does not generate back pressure that can unchoke the valve.

The air and O_2 make up valves, the mushroom exhalation valve and the O_2 flush valve are supplied from an O_2 and an air E-cylinder mounted on the right side of the prototype system for easy access by the user. The pressure in a full O_2 cylinder and also in a full air cylinder is approximately 2200 psig. The pressure is regulated down for oxygen through a medical oxygen pressure regulator (Western Enterprises, Model No. M1 870 FG1, Westlake, Ohio) down to 50 psig. The air pressure regulator (Veriflo Corporation, Part No. 707 971, Richmond, CA) also reduces the pressure to 50 psig.

The output of the air and O_2 pressure regulators were set at 50 psig because 50 psig is a common and standardized pressure in most hospitals (relevant when the prototype system is being supplied with gases from the hospital central supply) and also because a supply pressure of 50 psig to the make-up valves will provide choked flow through the make-up valves at back pressures of up to 100 cm H_2O (approx. 1.5 psig).

Frequency modulation at a fixed opening period of 1/20 second is used to vary the flowrate from the O_2 and air gas make-up valves. The volume of gas delivered per 1/20 second burst of the O_2 and air make-up valves was obtained using a short program written in Archimedes C 4.0 that alternately opens and closes the valve being tested for periods of 1/20 s each. The number of bursts can be varied as well as the supply pressure to the valve. The volume delivered by the valve is collected via a breathing

circuit hose into an inverted bell spirometer (Warren E. Collins Inc., Catalog No. P-1300, 13.5 l spirometer, Braintree, MA, Ser. No. 2436). The bell factor was 41.27 ml/mm of vertical displacement. The volume per burst is obtained by dividing the collected gas volume by the number of bursts. The volume of air delivered per 0.05 second burst was 1.4 ml.

6.3.13 Electrical Power Supplies

The prototype system is supplied with electrical power from 3 power supplies. A power strip with an on/off switch brings in wall power which supplies the 3 power supplies, the blower, the DC transformer for the flowrate monitor and the cooling fan. One power supply (Condor DC Power Supplies, Inc., Model No. HTAA-16W-A, Oxnard, CA) was dedicated to supplying +5 and +12V to the DACS board. An identical power supply was used to supply +5, +12 and -12 V to a power bus. Finally, due to the high current draw of the woofer speaker ($\sim$ 3 A), a heavier duty power supply (Condor DC Power Supplies, Inc., Model No. HCC15-3-A+, Oxnard, CA) supplied +12 and -12 V to the power bus. The grounds for all 3 power supplies were connected to a single point ground (the ground line of the power bus made of thick (12 AWG) copper wire).

6.3.14 Mechanical Enclosure

The chassis of the prototype system was recycled from a Puritan-Bennett MA-1 ICU ventilator. The MA-1 was gutted until only a bare chassis on wheels remained.

Three levels that were also functionally distinct were assembled within the chassis. These were the front control panel which had two analog pressure gauges (Bourdon gauges), the O_2 flush request pushbutton, the ventilation mode selector switch, the APL valve and the blower speed control knobs.

Next, there was the electronics and power supply board which held the power supplies, the DACS board, the different driver circuits and a connector panel with DIN-5 and phono jacks for easy disconnection of the electronics board from the chassis for ease of soldering during repairs and modifications. A fan at the back of the chassis drew cooling air over the electronics board. There were also 2 DB9 connectors at the back of the chassis. One was connected to the serial port of the DACS board and was used for serial connection to the monitor PC. The other worked as the "real world interface port". Pin 9 of the interface port DB9 was connected to pin 4.7 of the 80535 which allowed an O_2 flush request to disable a laser surgery unit.

The third level consisted mainly of the pneumatics and housed the blower, bellows, proportional flow control valve fabricated from a woofer speaker, the hoses, the gas make-up valves and the O_2 flush valve. A bacterial/viral filter (Respirgard-II, Marquest Medical Products, Inc., Englewood, CO) was interposed between the CO_2 absorber and the patient.

6.3.15 Bellows

The bellows was reclaimed from the MA-1 ventilator whose chassis houses the prototype system. The weights for creating a sub-ambient atmosphere inside the bellows

were obtained from sawing a circular piece of lead into sectors. The weights were measured with a digital scale for postal use that reads to the nearest 0.5 ounce (Pitney-Bowes, Focus Model 5042, Serial Number 26046, Stamford, CT).

The bellows sensor is connected to pin 5.1 of the TTL I/O header of the DACS board through a low pass filter with a -3 dB cutoff frequency of 340 Hz (4.7 KΩ resistor and 0.1 μF) that perform switch debouncing in hardware. The bellows sensor detects when the bellows is seated. The bellows switch is a NO switch (Matsushita) recycled from the door interlock safety system on a microwave oven (Kenmore). The circuit for interfacing the bellows sensor switch to the 80535 is identical to that in figure 56 for the O$_2$ flush request circuit.

Initially, an optical method of detection of bellows position was tried with an infrared emitter/detector pair (Radio Shack) placed diametrically opposite each other. The bellows would interrupt the beam of light continuously emitted by the emitter when it bottoms out and the voltage at the detector would decrease because of the attenuation caused by the bellows. However, the output of the photodetector was an analog signal such that a comparator would have been necessary to detect bellows position. The output of the photodetector was also dependent on the ambient light such that there were concerns about the feasibility and reliability of the optical method of detecting bellows position.

6.3.16 Back-Up Ventilation System

The GRADS prototype incorporates a back-up ventilation system for emergency use in the event of a power failure. It simply consists of a ball-in-tube flowmeter (Chemetron, Medical Products Division, St Louis, MO, O_2 flowmeter calibrated at 50 psig and 21.1°C (70°F), 0-15 l/min range, Model 3401-0101) directly connected to the O_2 E-cylinder. The output of the emergency O_2 flowmeter is directed into an adult size, single patient use, manual resuscitation bag (Puritan Bennett, Lenexa, KS, model DMR) where it enriches the O_2 supply to the patient.

6.4 Summary

The three different anesthesia delivery platform prototype generations that have resulted from this study have been described. Their weaknesses and strong points were analyzed. The actual method of fabrication, the problems encountered during fabrication and their solutions have been detailed. Further, the inevitable endless enhancements that come to mind while fabricating a given design have been described, e.g., the shaft encoders instead of the mechanical pots for blower speed control and the APL valve pots. The design of the GRADS prototype at the time of writing is in a stable state where a design freeze is appropriate and necessary. A design freeze is required in any design process so that some preliminary system evaluations can be performed rather than endlessly refining components to the extent that there is no one identifiable version of the prototype system. The preliminary system evaluations are described in the following chapter.

CHAPTER 7
PRELIMINARY PROTOTYPE PERFORMANCE EVALUATION

This chapter presents the preliminary performance data of the GRADS prototype. A systematic evaluation and optimization of the interactions of all the parameters, like anesthesia circuit priming volume, bellows volume and loading weight, PID coefficients, blower speed, VT and gas make-up valve and O_2 flush valve orifice size, that affect the performance of a system based on the GRADS concept will be a major undertaking that is beyond the scope of this study. The main objectives of this work were to establish an engineering design methodology and document the design path and the fabrication of the three main system design iterations in detail to facilitate further development. Consequently, this chapter will limit itself to preliminary performance data obtained from the GRADS prototype that demonstrate the stability and feasibility of the GRADS design concepts.

7.1 Method

The performance tests fall into three groups. The first set of tests demonstrates the fundamental characteristics of the GRADS design. The second data set shows the pressure, volume and flowrate traces during manual and mechanical ventilation. The third set of tests addresses safety and human factors considerations and is partially based

on subjective evaluation by three independent observers, all practicing anesthesiologists with a minimum experience of 10 years in clinical anesthesia.

For the preliminary performance tests, the actual blower speed was not measured because the blower was completely encased. The shaft of the blower was not accessible or visible which prevented the use of either a contact or strobe tachometer respectively. The drive unit for the variable speed blower is a brushless DC motor and blower speed is controlled by pulse width modulation at 18 kHz. As expected from the drive unit and the speed control scheme, the manufacturer's performance curves show that blower speed is linearly related to the input voltage to the blower speed control unit (V_{blower}). The minimum blower speed is 3,000 rpm at a V_{blower} of 1.5 V. At the maximum V_{blower} input of 10 V, blower speed is 10,800 rpm for the 2-stage blower in the GRADS prototype. Thus, the blower speed was inferred by reading V_{blower} via channel 2 of the A/D converter on the 80535 and using the linear relationship between V_{blower} and blower speed obtained from the manufacturer.

The data was collected by modifying the control software code for the GRADS prototype with the use of 'print' statements that wrote the desired values, e.g., time, pressure, flowrate and V_{blower}, at intervals of 1/20 s to the monitor screen of the PC. The terminal emulator software (Mirror III) running on the PC was used to capture the numbers for the desired variables to a data file on the hard disk of the PC. The numbers from the data file were then imported into a graphics package (GLE) and plotted.

During the tests, a commercially-available, double compartment, mechanical test lung with independently adjustable compliances and flow resistances (Training Test Lung, Michigan Instruments Inc., Grand Rapids, MI) was used to simulate the patient.

7.2 Fundamental System Characteristics

This set of tests was designed to show the fundamental characteristics of the GRADS system prototype like its safety, stability and controllability. The inherent patient safety benefit of using a centrifugal blower as the recirculating device is illustrated by the curve of shutoff discharge pressure against blower speed. The stability and controllability of pressure (P_{ct}) and circuit gas volume are illustrated by a manual sweep through the entire blower speed range while the digital PID maintains P_{ct} at its user-selected setpoint. The dynamic response of FiO_2 sampled at the Y-piece during an O_2 flush was also acquired to obtain the time constant of the system during an O_2 flush.

7.2.1 Shutoff Discharge Pressure Curve

The inherent safety advantage of the shutoff discharge pressure curve of the centrifugal blower was described in preceding chapters. Figure 59 displays the shutoff discharge pressure at the mechanical test lung, P_{ct}, as a function of the blower speed with a simulated failure of the proportional flow control valve (PFCV) in the fully closed position. In other words, figure 59 shows the maximum PIP that will be generated by the blower in case of system malfunction for a given blower speed. For patient safety, the default blower speed is set at 5,750 rpm (V_{blower} = 4.5 V) such that the blower can

only generate a maximum PIP of 30 cm H_2O for normal lungs. However, from the shutoff pressure discharge curve, it can be seen that if the patient has stiff lungs that require higher PIP capability, e.g., 60 cm H_2O, a blower speed of 7,125 rpm (V_{blower} = 6 V) will allow that PIP to be attained and thus will enable that patient's lungs to be ventilated.
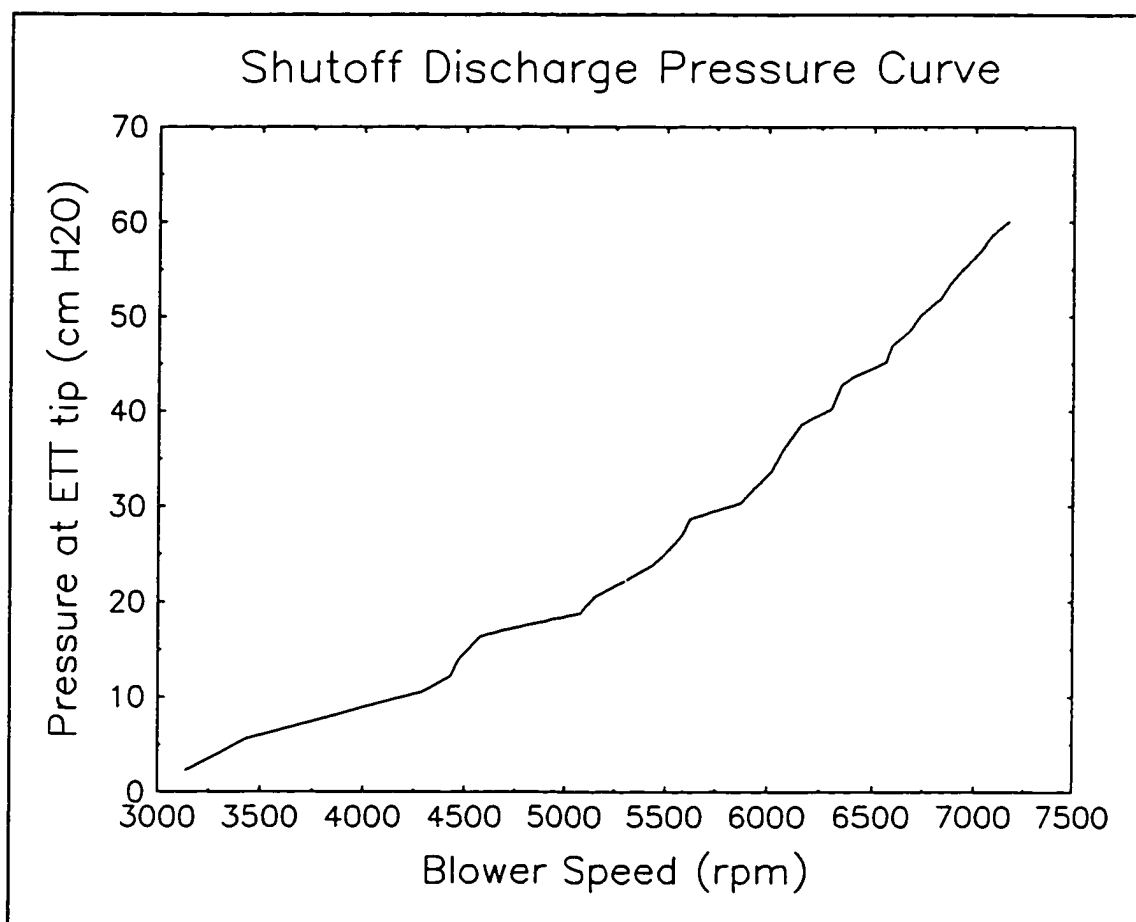

Figure 59. The shutoff discharge pressure curve of the centrifugal blower for different blower speeds

The shutoff discharge curve was obtained by opening the blower inlet to atmosphere while completely blocking the exhalation hose at the point where it connects

to the GRADS prototype chassis to simulate a failure of the PFCV in the completely closed position. The breathing circuit was connected via an 8.0 mm i.d. ETT to a mechanical test lung with the compliance per lung set at 0.01 l/cm H_2O. Shutoff pressure was read from the ETT tip while the voltage input into the blower was manually increased in a gradual fashion.

7.2.2 Sweep Through the Blower Speed Range

The tests depicted in figure 60 were designed to show the ability of the system to maintain a set pressure at the ETT distal tip while the blower speed was being increased at as steady a rate as manually possible through its whole speed range. The blower speed control knob (10 turns, 1 $K\Omega$, linear potentiometer) was manually and steadily rotated from the 0 to the 10 V position in about 2 minutes. The slew rate of V_{blower} was approximately 5 V/minute. Thus, the blower speed axis in figure 60 is also loosely correlated to time, with the 10,800 rpm point approximating a point in time 2 minutes after the start of the test. A constant slew rate of blower speed was considered to be a more stringent test of the stability of the system compared to moving the knob and waiting for the system to settle to the desired pressure setpoint before moving the blower speed control knob again.

The sweep through the entire speed range of the blower in approximately 2 minutes demonstrates the stability of the P_{ett} and circuit volume control loops implemented in the GRADS prototype. The bellows was maintained seated by the control software which was modified for the sweep test. The ventilation mode selector

switch was in the 'prime' position but any switch position, e.g., 'mechanical', that connects the output of the DACS board D/A to the proportional flow control valve could have been used.
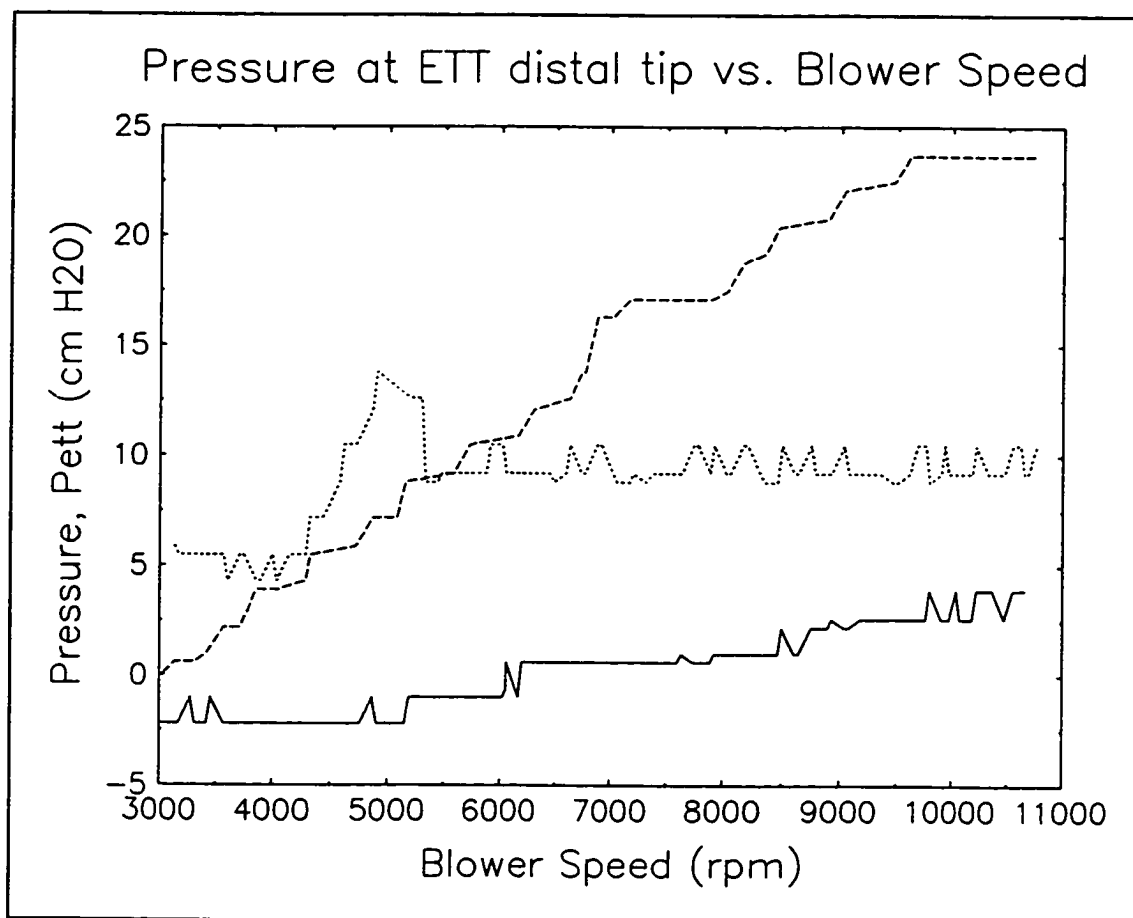
Pressure at ETT distal tip vs. Blower Speed

Figure 60. The effect of blower speed on uncontrolled P_{ett} (dashed line) and the curves when P_{ett} is controlled to 0 (solid) and 10 cm H_2O (dotted) are shown.

The PFCV was able to maintain P_{ett} at the desired set point by modulation of its annular orifice size through the digital PID algorithm. The curves for P_{ett} when it is being controlled at 10 cm H_2O (dotted line) and 0 cm H_2O (solid line) are shown in figure 60. The increase in P_{ett} as the recirculating flowrate around the circuit is

increased, without a digital PID to regulate P_{ct} but with the circuit volume controller active (i.e., the bellows was maintained seated) is also included as the dashed line in figure 60 for comparison. The dashed line in figure 60 demonstrates an inherent characteristic of the closed anesthesia circuit and the recirculating gas flow.

When P_{ct} was controlled at 0 cm H_2O (solid line in figure 60), there was a progressive increase of P_{ct} above the set point of 0 cm H_2O, when the blower speed exceeded 8,500 rpm. It was hypothesized that this increase of P_{ct} past its setpoint was due to the actuator, the PFCV, going into its saturation region. In other words, the limited downward excursion of the throttling cone in the PFCV combined with the higher flowrates at the higher blower speeds resulted in a pressure buildup past the P_{ct} setpoint. The actuator could not physically open any wider to decrease its flow resistance even though the digital PID was instructing the PFCV to open wider. This presumed saturation effect on the PFCV was confirmed by inspecting the control action of the digital PID by modifying the software to print the D/A values that were being written to the PFCV. Beyond blower speeds of 8,500 rpm ($V_{blower} = 7.5$ V), the D/A value written to the PFCV was 0, i.e., the PFCV was wide open but the high recirculating flowrate was causing pressure buildup (~ 3 cm H_2O) at the ETT distal tip through the flow resistance of the wide open PFCV. This conclusion was also visually confirmed by verifying the throttling cone position on the PFCV when the blower speed was greater than 8,500 rpm.

Therefore, to verify that the system is able to control P_{ct} at the desired setpoint throughout the entire blower speed range without the confounding issue of actuator

saturation, the pressure setpoint was increased from 0 to 10 cm H_2O. The pressure buildup at a blower speed of 10,800 rpm when the PFCV was in its saturation region for a P_{ct} setpoint of 0 cm H_2O, was only 3 cm H_2O. Thus, it was expected that the PFCV would not become saturated, even at the maximum blower speed of 10,800 rpm, if the P_{ct} setpoint was increased to 10 cm H_2O.

When P_{ct} was controlled at 10 cm H_2O, there was a large oscillation in the value of P_{ct} in the region where the blower speed was less than 5,300 rpm. This oscillation is explained by figure 59 which graphs the shutoff discharge curve of the blower. At a blower speed less than 4,400 rpm, the shutoff discharge curve cannot be higher than 10 cm H_2O. Consequently, even with the PFCV fully closed, the desired P_{ct} of 10 cm H_2O could not be attained. Once the blower speed exceeds 5,300 rpm, a shutoff pressure of 25 cm H_2O can be generated and the PID controller in combination with the PFCV can drive P_{ct} to the desired set point (10 cm H_2O). Beyond a blower speed of 5,300 rpm, P_{ct} is controlled at 10 cm H_2O within $\pm$ 1.2 cm H_2O.

The coefficients for the digital PID that controlled P_{ct} during the tests were 10, 2 and 0 for the proportional, integral and derivative coefficients respectively. The digital PID was tuned according to the method described in section 6.2.13. The derivative coefficient was set at zero so that no control action would be performed in response to the electrical noise on the P_{ct} signal. The preliminary results shown in figure 60 demonstrate that the PFCV can control P_{ct} to a setpoint selected by the user as long as the PFCV does not get into its saturation region (input D/A value $\leq$ 0 or input D/A value $\geq$ 4095 for a 12 bit D/A).
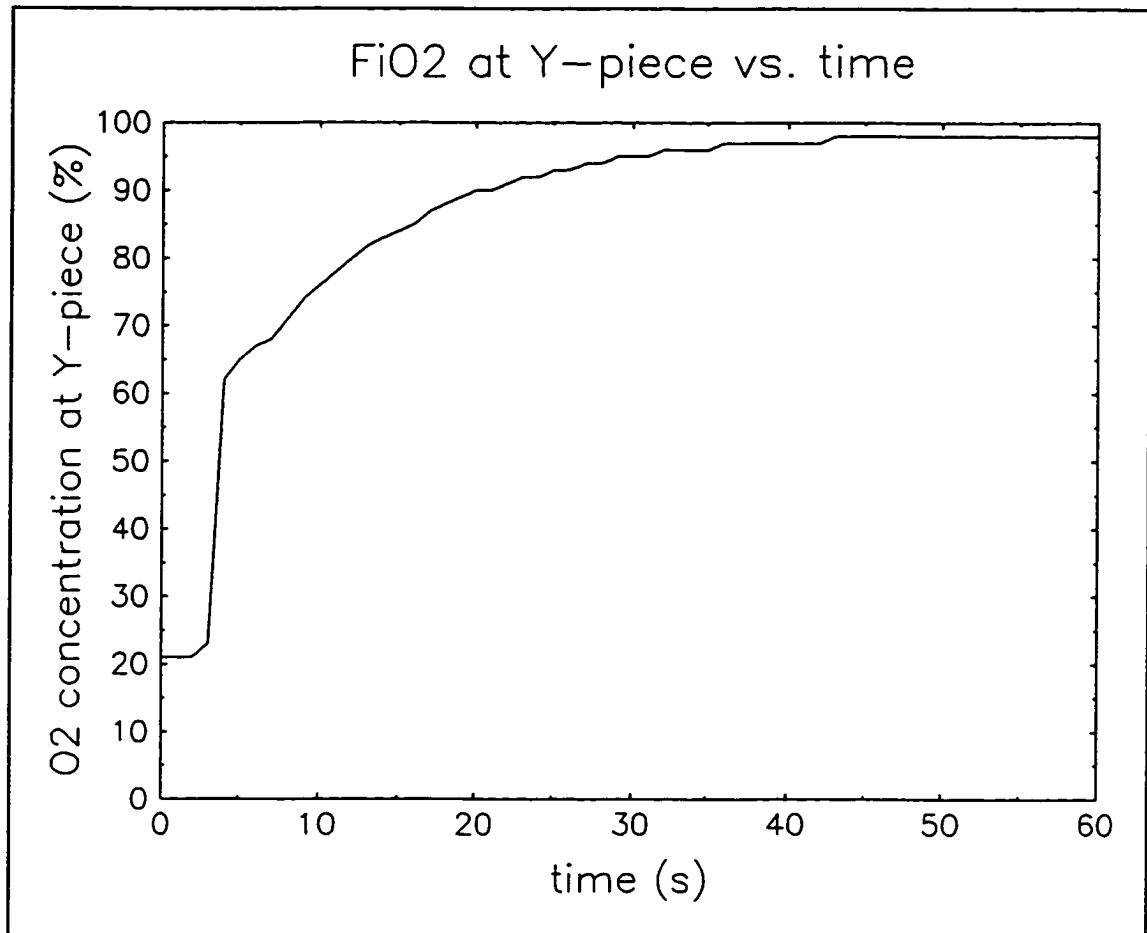
7.2.3 FiO₂ During O₂ Flush

Figure 61. The response of oxygen concentration sampled at the Y-piece during an O₂ flush.

The ability to rapidly attain an FiO_2 of 1.0 in less than 60 s by flushing O_2 through an anesthesia breathing circuit during an emergency situation is a mandatory patient safety feature in an anesthesia delivery system. The rapid attainment of an FiO_2 of 1.0 during an O_2 flush in the GRADS prototype is shown in figure 61.

The FiO_2 was measured by a magneto-acoustic gas analyzer (Hewlett Packard M1025A Anesthetic Gas Analyzer). Serial communication was established between the gas analyzer and a PC via a terminal emulator program (Mirror). The gas analyzer was instructed to output a data stream that contained the FiO_2 value at a fixed time interval of 1.0 second which was captured to a data file on the hard disk of the PC.

The O_2 flush request button was depressed at the '0' s marker. The circuit had already been primed with air and the test lung was being mechanically ventilated with air. Thus, the FiO_2 was 0.21 at the start of the flush event. From the FiO_2 curve, it can be seen that within 5 seconds of requesting an O_2 flush during mechanical ventilation, the FiO_2 had risen to 0.65. At 30 s, the FiO_2 was 0.95.

The FiO_2 curve during an O_2 flush has three distinct regions where the slopes are markedly different. The first region has a slope of zero and spans the 0 - 2 s period. This portion of the FiO_2 curve represents most likely the time delays due to (a) the GRADS control software configuring the system prior to the O_2 flush valve being energized open and the response time of the O_2 flush valve, (b) the time taken for the gas sample to be drawn from the Y-piece via the 2 m (6.6 ft) long sampling line into the gas analysis cell and (c) the response time of the gas analyzer ($\sim$250 ms according to the service manual). There is then a sharp jump in FiO_2 from 0.21 to 0.62 in the time interval between 2 and 4 s. This represents the wavefront of 100% O_2 from the O_2 flush reaching the gas analysis cell. Afterwards (time $>$ 4 s) the FiO_2 slope progressively tapers off as the air initially in the circuit volume between the purge valve and the O_2 flush valve (bellows, proportional flow control valve, etc.) is suctioned by the blower and

is mixed with the 100% O_2 coming from the purge valve. The bellows remained seated throughout the O_2 flush.

The system time constant during an O_2 flush is calculated from figure 61. The time constant is defined as the time for FiO_2 to rise to 0.632 = $(1-e^{-1})$ of the interval between an initial FiO_2 of 0.21 and the desired endpoint FiO_2 of 1.0. The time constant is the point on the time axis in figure 61 where the FiO_2 is 0.21 + 0.632*(1.0 - 0.21) = 0.71. Thus, the time constant of the system during an O_2 flush is approximately 8 seconds. If one removes the time delay of the gas analyzer, estimated at 2 seconds from figure 61, the time constant of the system during an O_2 flush is short at about 6 seconds.

7.3 Ventilation

The performance of the GRADS prototype during mechanical ventilation without and with PEEP is shown in this section. A set of traces for manual ventilation is also included.

7.3.1 Mechanical Ventilation without PEEP

The set of plots of P_{ca}, flowrate and volume with respect to time in figure 62 describes two consecutive breaths during mechanical ventilation of the test lung. The set ventilatory parameters were a VT of 700 ml, RR of 10 bpm and an I:E ratio of 1:2. It can be seen from the flowrate trace that there is initially an oscillation about the constant flowrate value that will give the desired VT over the set inspiratory time, T_i, of 2 s. After about 1 second, the PID controller for the flowrate during mechanical inspiration

locks onto the desired flowrate. Exhalation follows and is completed passively in about

1.5 seconds from the start of exhalation such that a period of about 3.5 s with almost no
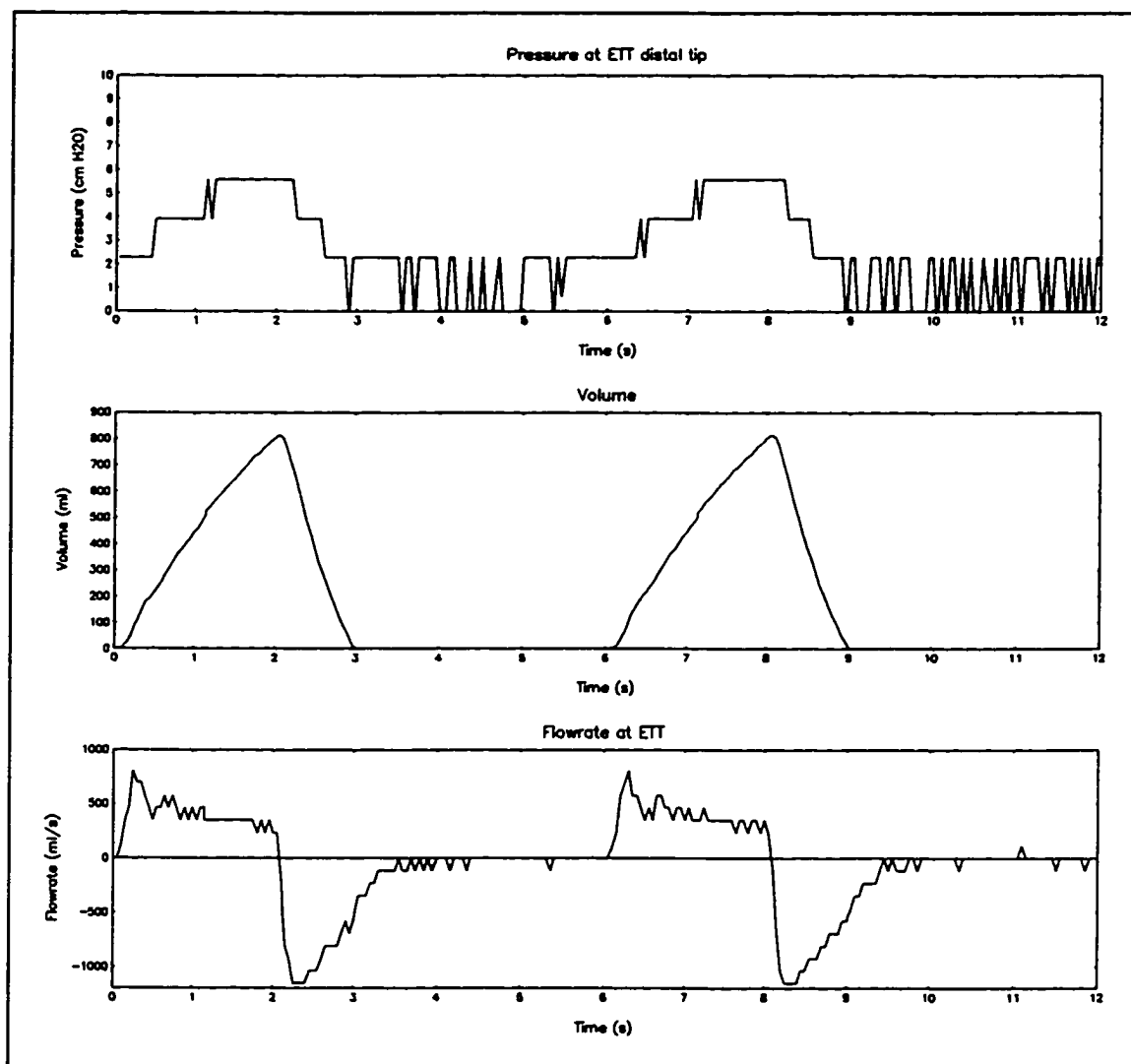
gas flow into or out of the lungs terminates exhalation.

Figure 62. The pressure, volume and flowrate curves for mechanical ventilation at a rate of 10/min, a VT of 700 ml and an I:E ratio of 1:2.

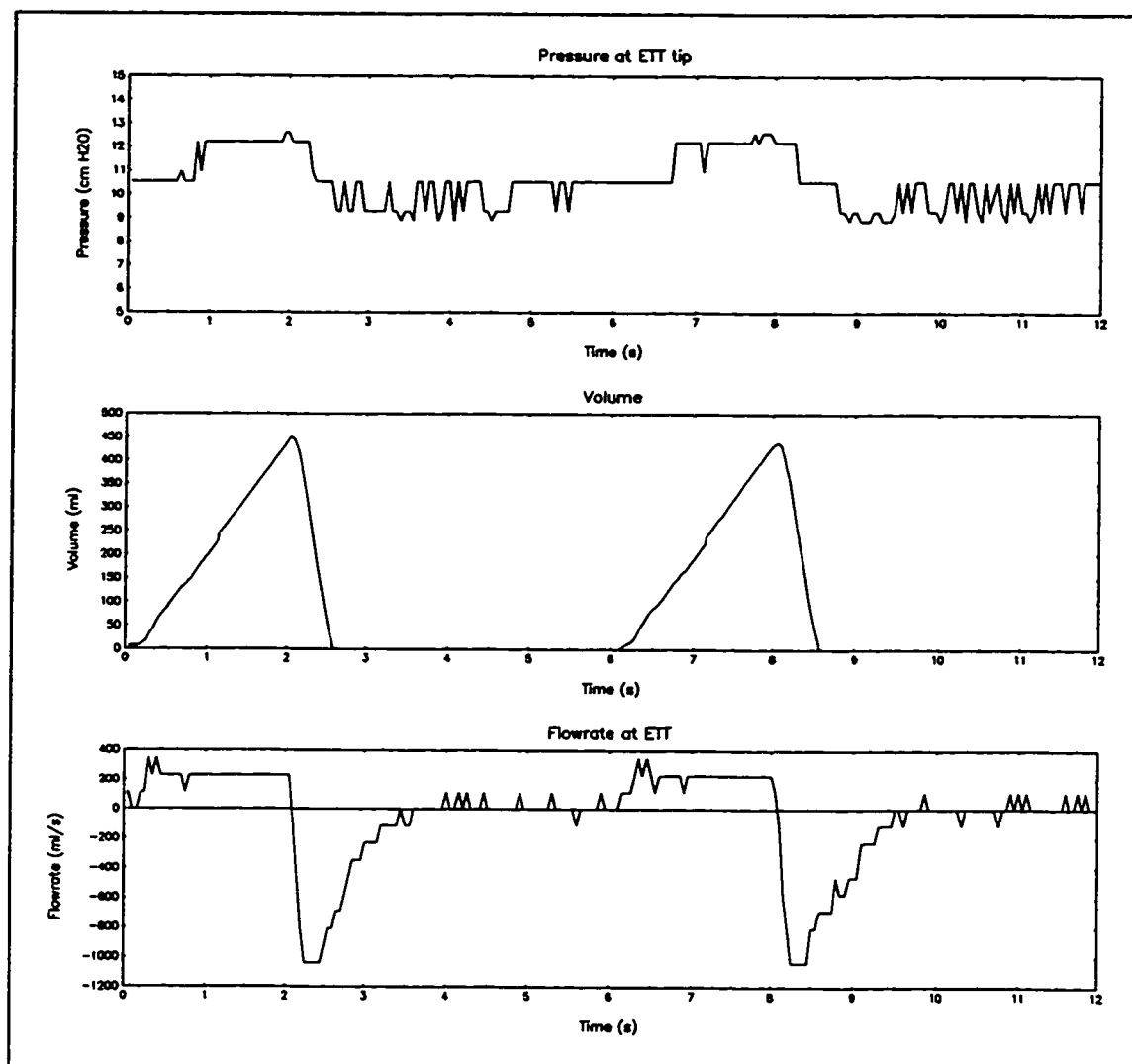## 7.3.2 Mechanical Ventilation with PEEP

Figure 63. Pressure, volume and flowrate traces for 2 breaths during mechanical ventilation with a PEEP of 10 cm H_2O. VT = 700 ml, RR = 10 bpm, I:E ratio = 1:2

Figure 63 shows the performance of the PFCV as a PEEP valve. The desired

PEEP level was 10 cm H_2O and a digital PID algorithm with coefficients of P = 50, I

= 4 and D = 0 maintained Pett at end exhalation at 10 cm H_2O.
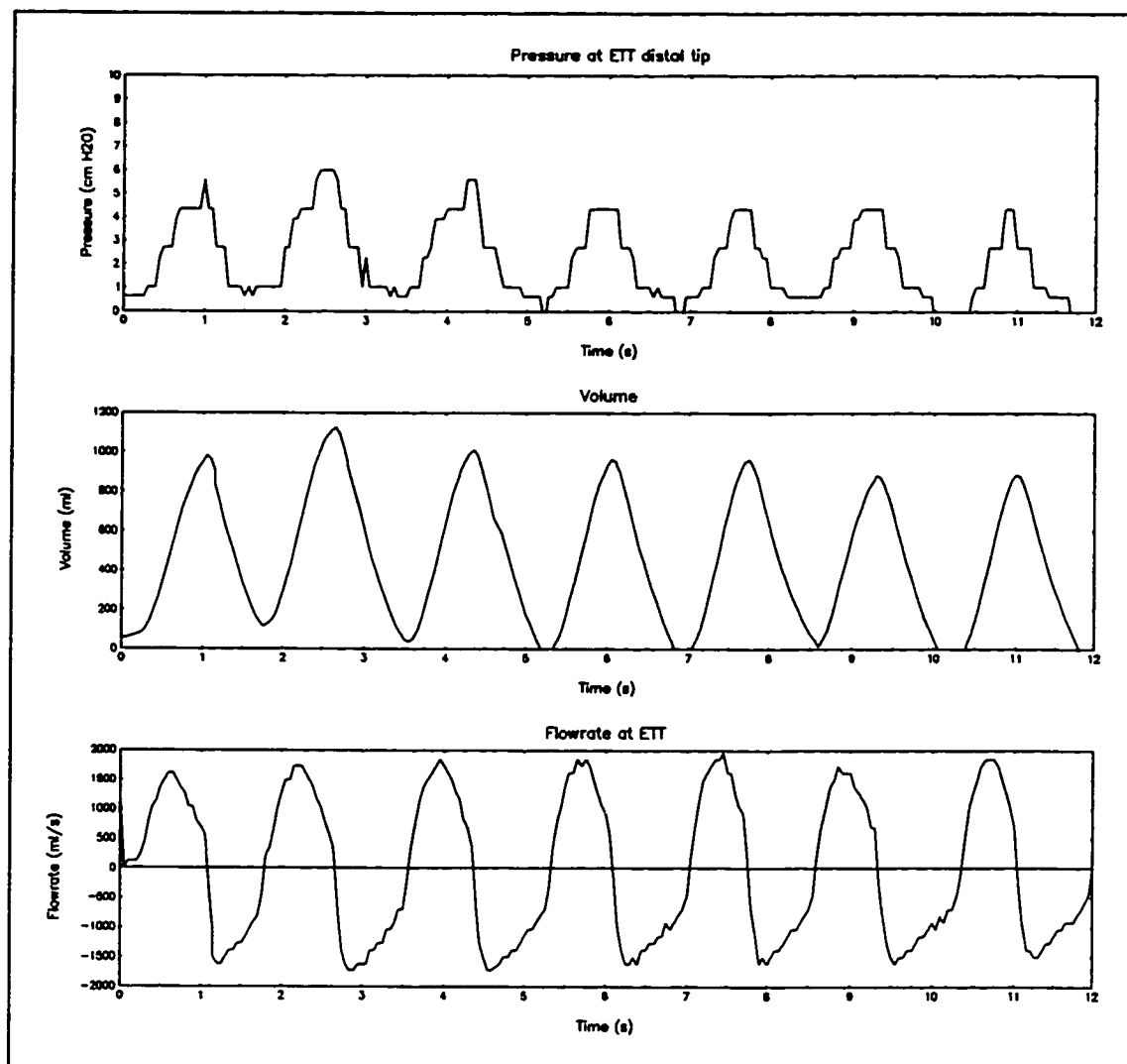
7.3.3 Manual Ventilation

Figure 64. Pressure, volume and flowrate traces during manual ventilation of a mechanical test lung with each lung compartment compliance set at 0.05 l/cm H_2O

The pressure, volume and flowrate traces during manual ventilation are included to demonstrate the ability of the system to operate in manual ventilation. The manual ventilation rate was roughly 35 bpm.

7.4 Safety

The design of the GRADS prototype emphasizes patient safety. Two prominent novel safety features are the automatic abortion of mechanical inspiration and the disabling of a laser microsurgery unit via a data sharing interface during an O_2 flush.

7.4.1 Laser Disable During O_2 Flush

As expected from the deterministic nature of the O_2 flush, the laser disable circuitry was consistently able to turn off the demonstration helium-neon laser that was used to simulate the laser microsurgery unit during an O_2 flush. Thus, the risk of an airway fire caused by an O_2 flush during laser microsurgery of the upper airway of an intubated patient has been eliminated.

7.4.2 O_2 Flush During Mechanical Inspiration

The control software worked as expected and invariably directed program flow away from the normal ventilation mode (manual, mechanical, assisted spontaneous) whenever an O_2 flush occurred. Thus, the risk of barotrauma during an O_2 flush that coincides with mechanical inspiration has been eliminated. Furthermore, on releasing the O_2 flush request button, ventilation resumed at the same mode and settings that were in effect prior to the O_2 flush event.

7.5 Human Factors and Preliminary Clinician Feedback

The GRADS prototype retained the ability, available in conventional systems, to feel the change in compliance during manual ventilation. Further, some human factors features lacking in anesthesia delivery systems in use at the time of writing were identified and were specifically addressed by the GRADS design. These features include (a) the ventilation mode selector knob, (b) the ability to manually ventilate the patient and assess the pulmonary resistance and compliance at all times and in all ventilation modes and (c) the ability to feel a spontaneous breathing effort from the patient at all times and in all ventilation modes. The above features were all successfully implemented in the GRADS prototype.

The GRADS prototype as a whole and the human factors features specifically were subjectively evaluated by three experienced anesthesiologists using a mechanical test lung. The prototype and its novel safety and human factors features were well received and were judged to be an improvement over existing designs, at the time of writing.

7.6 Summary

The preliminary performance data that have been collected indicate that the GRADS prototype is a stable and safe ventilation platform for anesthesia delivery. Its demonstrated ability to operate in a stable mode without constant user input or adjustment predicts that it will use gases and volatile anesthetics efficiently. During development and in the preliminary tests depicted in this chapter, the novel features, methods and

software in the system performed to specification. No major flaw in the design was identified during development or the preliminary performance evaluation.

The consistently predictable and reliable behavior of the GRADS prototype compared to its predecessors (prototypes #1 and #2) is an encouraging sign that the prototype is a strong candidate for conversion into a commercial product. The GRADS prototype in its present state already offers design features that are superior to existing systems in use at the time of writing from the point of view of safety, predicted efficiency of anesthetic usage, simplicity, user-friendliness and data sharing through an open information architecture. Because of its superior design features, a commercial system based on the GRADS prototype will save lives by preventing accidental barotrauma and "airway" fires, will reduce airway desiccation and heat loss through retention of humidity, and will reduce the cost of anesthesia through its ability to operate in closed circuit without constant user supervision.

It is recommended that the GRADS prototype concept be commercialized after incorporation of the necessary modules like anesthetic delivery, monitors, alarms, redundant microcontrollers, etc. and revision of the materials selection and the control software, followed by extensive and comprehensive testing.

CHAPTER 8
CONCLUSIONS AND RECOMMENDATIONS

Due to the extensive scope of this dissertation which deals with the design of a system, there are many conclusions and recommendations for future follow-up work that this study has identified. Some of them have already been described as a form of closure since the chapters are very much self-contained. They are recapitulated briefly in this chapter.

An extensive literature survey confirmed that, at the time of writing, delivery of closed circuit anesthesia without constant attention and adjustments from the user is still not a practical reality. The way in which sampling of "airway pressure" at the Y-piece, in the breathing circuit or in the ventilator creates artifactual data that are dependent on the flowrate in the ETT and the ETT flow resistance was also explained, documented and demonstrated.

A method of sampling airway pressure more accurately at the ETT distal tip was identified and described. Similarly, the design of the GRADS system delivers inspiratory flowrate under feedback control which eliminates the effect of the different parameters on VT delivery during mechanical ventilation. The ETT distal tip pressure and gas analysis sampling and the delivery of inspiratory flowrate under feedback control are examples of the WYSSIWYG (what you set and sample is what you get) design philosophy that matured during this design exercise.

392

The "real world interface port" concept was also described and demonstrated in preliminary form. The "real world interface port" is the gateway for information sharing between an anesthesia delivery system and other equipment in the OR which might interact with it. The O_2 flush disable circuit was used to successfully demonstrate the "open information architecture" design philosophy which the "real world interface port" implementation supports.

The anesthetic delivery module design in chapter 4 (syringe injector, PID or adaptive control of end-tidal anesthetic, charcoal canister) should be implemented. Tests should be performed to verify that there are really no unintended interactions between the anesthetic delivery module and the life support module.

The desirable design features (Peltier module heater/cooler; CO_2 absorber bypass; CO_2 injection; CFAV; open-circuit, room-air operation; unidirectionally compliant manual breathing bag; scavenging system; circulating ETO sterilization process; the breathing circuit module concept) described in chapter 4 should be implemented and tested.

A deliberate and sustained development effort should be directed at making ETT distal tip pressure and gas analysis sampling a practical, routine and safe clinical procedure because the benefits to be derived from it are considerable and have been explained at length. Some possible solutions have already been proposed.

Recommendations for follow-up work with applications beyond anesthesia include research on finding a blunt body cross-section for a bidirectional vortex shedding flowmeter that will shed vortices reliably at Reynolds numbers as low as 50. Such a

vortex shedding flowmeter will find immediate application for flowrate measurement in anesthesia. A low pressure loss, wide flow area, proportional flow control valve that can be readily interfaced to a computer was not commercially available at the time of writing and had to be designed and fabricated. Valve manufacturers should investigate the market potential of such a device.

The energy efficiencies to be obtained from valves, both proportional and on/off, that operate in the choked flow regime at P_b/P_o of 0.8 or higher were discussed. A brief theoretical analysis indicated that such high P_b/P_o ratios can be practically achieved. Valve manufacturers should conduct a market survey and an engineering feasibility study to determine the commercial and economic potential of the improved valve design with a converging-diverging internal flow passage.

The results of this study should also be applicable to other situations where toxic and/or expensive gases have to be confined in a pressure controlled environment. Examples are manufacture of electronic components under an inert or toxic atmosphere, chemical reactions, etc.

An extensive and methodical evaluation of the GRADS prototype design should be performed. Experiments on the algorithms and methods to re-enable the laser after an interruption should be conducted. An expert system shell for intelligent alarms and an automated or semi-automated clinical pre-use check for the GRADS prototype which will be facilitated by the intimate interfacing of the mechanical components with the electronics and the "real world interface port" should definitely be implemented.

Based on its successful application that led to the GRADS prototype, it is concluded that the formalized design methodology and checklist proposed in chapter 4 is practical to use and will most likely assist in the design of anesthesia delivery systems other than GRADS, in the future.

In the application domain of engineering design, a distinct separation exists between structural knowledge (the objects and physical entities) and functional knowledge (how the objects behave and interact). The functional hierarchy and the structural hierarchy are not necessarily isomorphic. In the design knowledge checklist presented in chapter 4, no distinction was made between structural and functional knowledge. A worthwhile exercise would be to derive two checklists (one following a structural hierarchy and the other a functional hierarchy) from the checklist of chapter 4.

A mechanical inspiration hypothesis was developed and will need to be validated. Other papers not included in the literature review of mechanical inspiration in chapter 5 should be reviewed for inconsistencies with the newly proposed hypothesis. The mechanical inspiration hypothesis and its corollaries and the proposed lung class identification algorithms should be validated in mechanical lung models, in pigs and in clinical trials on patients screened to have the same mechanical lung parameters configuration, in that order. The new inspiratory waveforms (both pressure and flowrate) should be incorporated on the GRADS platform and thoroughly evaluated.

Another lesson learned from this project is that an endeavor of this scope has to remain purely in the domain of the experimental. Initially, efforts must not be spent in trying to design a machine for mass market or even experimental patient use. Mass

market safety considerations are important but are distracting to the main objective of building an experimental system and even hamper the creative process since one then immediately has to start with a series of constraints which tend to funnel the designer to existing solutions. Mass market safety considerations like deterioration of valve seal materials by the volatile anesthetics are real issues (e.g., the Challenger space shuttle disaster dramatically demonstrated the importance of attention to details and mundane items like valve seal materials and design). These will need to be addressed at the proper place and time, i.e., during reduction to a commercial product.

To conclude, a prototype for an anesthesia delivery platform was successfully designed according to a newly established engineering design methodology and a mechanical inspiration hypothesis has been formulated that provides a consistent framework in which to interpret the field of inspiratory waveform shaping.

APPENDIX A
UNITS CONVERSION TABLE

Source: Anderson et al. (1976) and derivations

<u>Pressure:</u>

$1 \text{ N/m}^2 = 1 \text{ Pa}$; $1 \text{ bar} = 10^5 \text{ N/m}^2$; $1 \text{ mm Hg} = 1 \text{ torr} = 133.3 \text{ N/m}^2$

$1 \text{ cm H}_2\text{O} = 98.07 \text{ N/m}^2 = 0.74 \text{ mm Hg} = 0.014 \text{ psi} \approx 0.1 \text{ kPa}$

$1 \text{ psi} = 70.31 \text{ cm H}_2\text{O} = 6895 \text{ N/m}^2 \approx 6.9 \text{ kPa}$

$1 \text{ int. atm.} = 1.013 \times 10^5 \text{ N/m}^2 = 14.7 \text{ psia} = 1.013 \text{ bar}$

<u>Length:</u>

$1" = 2.54 \text{ cm}$; $1 \text{ ft} = 12" = 0.3048 \text{ m}$

<u>Volume:</u>

$1 \text{ ft}^3 = 0.02832 \text{ m}^3 = 28.32 \text{ l}$

$1 \text{ in}^3 = 16.39 \text{ cm}^3$

<u>Flowrate:</u>

$1 \text{ scfm} = 28.32 \text{ slpm}$

<u>Temperature:</u>

$^\circ\text{C} = (^\circ\text{F} - 32)/1.8$

$^\circ\text{K} = ^\circ\text{C} + 273.15 ^\circ\text{C}$

$^\circ\text{R} = ^\circ\text{F} + 459.67 ^\circ\text{F}$

397

APPENDIX B
MACH NUMBER IN THE ANESTHESIA CIRCUIT

The maximum Mach number in the anesthesia breathing circuit is calculated assuming that the maximum recirculation flowrate is 100 l/min. For a 22 mm i.d. corrugated breathing hose which makes up the majority of the breathing circuit, the velocity of gas in the circuit will be Q/A where Q is the flowrate in m^3/s and A is the cross-sectional flow area in m^2.

$Q = 100 \text{ l/min} = 0.1 \text{ m}^3/\text{min} = 0.1/60 \text{ m}^3/\text{s} = 0.001667 \text{ m}^3/\text{s}$

$A = \pi d^2/4 = \pi(2.2)^2/4 = 3.8 \text{ cm}^2 = 3.8 \times 10^{-4} \text{ m}^2$

$V \approx 4.4 \text{ m/s}$

The speed of sound in the anesthetic gas mixture assumed to be at 38°C (311 K) and 100% N_2O (for ease of calculation of k) is obtained from the equation (Shapiro 1953, 47):

$$c = \sqrt{(kRT)}$$

where k is the specific heat ratio (1.31), T is the temperature in Kelvin (311) and R is the specific gas constant. The specific gas constant of N_2O (188.96 J/kg K) is obtained by dividing the universal gas constant (8314.3 J/kmol K) by the molecular weight of N_2O (44).

398

The speed of sound in N_2O at 311 K is therefore 277 m/s. Consequently, the maximum Mach number in the breathing circuit is 4.4/277 = 0.016 which is much lower than the threshold of Mach 0.2 where the assumption of incompressible flow will start breaking down.

APPENDIX C
EFFECT OF GAS MIXTURE DENSITY ON VOLUMETRIC FLOWRATE
MEASUREMENT IN A VENTURI FLOWMETER

The effect of varying anesthetic gas mixture densities on the <u>volumetric</u> flowrate

measurement accuracy of a venturi flowmeter is calculated.

Assuming that the calibration gas mixture for the venturi flowmeter was 50% O_2

(ρ = 1.331 kg/m^3) and 50% N_2O (ρ = 1.843 kg/m^3), the calibration gas density (ρ_{cal})

will be (0.5*1.331 + 0.5*1.843) = 1.587 kg/m^3. Therefore, with a 70% Xe (ρ = 5.85

kg/m^3) and 30% O_2 gas mixture, the effective density is (0.7*5.85 + 0.3*1.331) =

4.494 kg/m^3. For a 70% He (ρ = 0.166 kg/m^3) and 30% O_2 mixture the mixture density

is (0.7*0.166 + 0.3*1.331) = 0.516 kg/m^3. For a given ΔP, the ratio (R) of the

apparent flowrate (Q_{app}) to the real flowrate (Q_{real}) can be approximated to R =

(Q_{app}/Q_{real}) = (ρ_{real}/ρ_{cal})$^{1/2}$. Consequently, $R_{70\%Xe,30\%O2}$ = 1.68 and $R_{70\%He,30\%O2}$ = 0.57.

400

APPENDIX D
MINIMUM EXPECTED REYNOLDS NUMBER AT THE ENDOTRACHEAL TUBE

The pipe Reynolds number (Re) is obtained from the equation $Re = \rho Vd/\mu$ where ρ is the density in kg/m^3, V is the gas velocity in m/s, d is the internal diameter of the pipe in m and μ is the viscosity of the gas in $N.s/m^2$. To obtain the minimum Re for each mode, the largest bore ETT is used, i.e., d is fixed at 0.5 inches (12.7 mm) for Re calculation purposes.

$$V = \frac{Q_{min}}{A} = \frac{Q_{min}}{\pi d^2/4}$$

$$Re = \frac{\rho Vd}{\mu} = \frac{\rho \dfrac{Q_{min}}{\pi d^2/4} d}{\mu} = \frac{4\rho Q_{min}}{\pi \mu d}$$

$$Re_{min} = \frac{4\rho Q_{min}}{\pi \mu d_{max}} = \frac{4 Q_{min}}{\pi \nu d_{max}} \quad where \quad \nu = \frac{\mu}{\rho}$$

The gas velocity, V, is obtained by dividing the minimum volumetric flowrate, Q_{min} by the cross-sectional area, $A = \pi d^2/4$, of the ETT with internal diameter, d. For O_2, the kinematic viscosity at 300K is 16.14×10^{-6} /s (Incropera & DeWitt 1985, 770). For a Q_{min} of 0.05 l/s (RR range is limited to 5-40), $Re = 4*0.05x10^{-3}/(\pi*16.14x10^{-6}*12.7x10^{-3}.) = 311$ for an ETT of 12.7 mm bore with O_2.

REFERENCES

Adriani J: The chemistry and physics of anesthesia (2nd ed). Springfield, Charles C Thomas, p 204, 1979

Advanced Micro Devices: Microcontrollers 1988 data book / handbook. Sunnyvale, CA, 1988

Al-Saady N, Bennett ED: Decelerating inspiratory flow waveform improves lung mechanics and gas exchange in patients on intermittent positive pressure ventilation. Intensive Care Medicine 11:68, 1985

American National Standards Institute: American National Standard ANSI Z79.8-1979: Minimum performance and safety requirements for components and systems of continuous-flow anesthesia machines for human use. New York, 1979

American National Standards Institute: American National Standard ANSI Z79.11-1982 for anesthetic equipment-scavenging systems for excess anesthetic gases. New York, 1982

Andersen BW: The analysis and design of pneumatic systems (reprint). New York, John Wiley & Sons, Inc., p 15, 1976

Anderson JC, Hum DM, Neal BG, Whitelaw JH: Data and engineering formulae for engineering students (2nd ed). Oxford, Pergamon Press, 1976

Andrews JJ: Inhaled anesthetic delivery systems in Miller RD (ed): Anesthesia vol. 1, (3rd ed). New York, Churchill Livingstone, p 218, 1990

Aström KJ, Hagglünd T: Automatic tuning of PID controllers. Research Triangle Park, NC, Instrument Society of America, 1988

Atwater RJ, Good ML: A low-cost laboratory data acquisition and control system. Computers in Anesthesia X, New Orleans, LA, October 18-21, 1989

Baker AB, Colliss JE, Cowie RW: Effects of varying inspiratory flow waveform and time in intermittent positive pressure ventilation II: Various physiological variables. British Journal of Anaesthesia 49:1221, 1977

402

Baker AB, Hahn CEW: Models of the lung. British Journal of Anaesthesiology 43:816, 1971

Baker AB, Hahn CEW: An analogue study of controlled ventilation. Respiration Physiology 22:227, 1974

Baker AB, Wilson AM, Hahn CEW: Alveolar pressure response to top-hat gas flow or pressure waves in artificial ventilation. Respiration Physiology 22:217, 1974

Banner MJ, Boysen PG, Lampotang S, Jaeger MJ: End-tidal CO_2 affected by inspiratory time and flow waveform - time for a change (abstract). Critical Care Medicine 14:374, 1986

Banner MJ, Lampotang S: Clinical use of inspiratory and expiratory waveforms in Kacmarek RM, Stoller JK (eds): Current respiratory care. Philadelphia, B.C. Dekker Inc., 1988

Banner MJ, Lampotang S: Mechanical ventilators - Fundamentals in Perel A, Stock MC (eds): Handbook of mechanical ventilatory support. Baltimore, Williams & Wilkins, 1992

Banner MJ, Lampotang S, Blanch PB: Mechanical ventilation, in Civetta JM, Kirby RR, Taylor RW (eds): Critical care, Philadelphia, J.B. Lippincott Co., (in preparation), 1992

Banner MJ, Lampotang S, Boysen PG, Hurd TE, Desautels DA: Flow resistance of expiratory positive-pressure valve systems. Chest 90:212, 1986

Beneken JEW, Gravenstein N, Gravenstein JS, van der AA JJ, Lampotang S: Capnography and the Bain circuit I: A computer model. Journal of Clinical Monitoring 1:103, 1985

Beneken JEW, Gravenstein N, Lampotang S, van der Aa JJ, Gravenstein JS: Capnography and the Bain circuit II: Validation of a computer model. Journal of Clinical Monitoring 3:165, 1987

Bergman NA: Fourier analysis of effects of varying pressure waveforms in electrical lung analogs. Acta Anaesthesiologica Scandinivica 28:174, 1984

Bersten AD, Rutten AJ, Vedig AE, Skowronski GA: Additional work of breathing imposed by endotracheal tubes, breathing circuits, and intensive care ventilators. Critical Care Medicine, p 671, 1989

Bhansali PV, Dempsey JA, Chosey L, Iber C, Musch T, Webster JG: Sensitivity of frequency dependence of lung compliance in detecting uneven time constants. IEEE Transactions on Biomedical Engineering BME-30:625, 1983

Bickford RG: Automatic electroencephalographic control of general anesthesia. EEG & Clinical Neurophysiology 2:93, 1950

BOC Health Care: Ohmeda model 5400 volume monitor: Operation maintenance. Madison, The BOC Group Inc., Publication No. 0178 1740 000, 06 84 A 07 20 13, p 4, 1984

Bolder PM, Healy TEJ, Bolder AR, Beatty PCW, Kay B: The extra work of breathing through adult endotracheal tubes. Anesthesia Analgesia 65:853, 1986

Boquet G, Bushman JA, Davenport HT: The anaesthetic machine - a study of function and design. British Journal of Anaesthesia 52:61, 1980

Brown AC, Canosa-Mas CE, Parr AD, Pierce JMT, Wayne RP: Tropospheric lifetimes of halogenated anesthetics. Nature 341:635, 1989

Cameron JR, Skofronick JG: Medical physics. New York, John Wiley & Sons, p 575, 1978

Chemical Rubber Company Handbook of Chemistry and Physics: A ready-reference book of chemical and physical data 1989-1990 (70th ed). Boca Raton, FL, CRC Press Inc., 1990

Cheney FW: Anesthesia: Potential risks and causes of accidents in Gravenstein JS, Holzer JF (eds): Safety and cost containment in anesthesia. Boston, Butterworths, p 12, 1988

Cheremisinoff NP, Cheremisinoff PN: Flow measurement for engineers and scientists. New York, Marcel Dekker, Inc., 1988

Chilcoat RT: An adaptive technique for programmed anaesthesia. British Journal of Anaesthesia 45:1235, 1973

Circle Seal Controls: Brunswick Corporation, Industrial valves and controls, Anaheim, CA, 1984

Clippard Instrument Laboratory: Clippard Minimatic valves. Catalog 181-R1. Cincinnati, Ohio, 1981

Cohen EN, Belville JW, Brown BW: Anesthesia, pregnancy and miscarriage: A study of operating room nurses and anesthetists. Anesthesiology 35:343, 1971

Cohen EN, Brown BW, Bruce DL, Cascorbi HF, Corbett TH, Jones TW, Whitcher CE: Occupational disease among operating room personnel: A national study. Anesthesiology 41:321, 1974

Coles JR, Brown WA, Lampard DG: Computer control of respiration and anaesthesia. Medical and Biological Engineering, p 262, 1973

Conway CM: Anaesthetic breathing systems in Scurr C, Feldman S: Scientific foundations of anaesthesia (3rd ed). London, William Heinemann Medical Books Limited, p 557, 1982

Cooper JB, Newbower RS: The anesthesia machine: An accident waiting to happen in Pickett RM, Triggs TJ (eds): Human factors in health care. Lexington, Lexington Books Co., p 345, 1975

Cooper JB, Newbower RS, Kitz RJ: An analysis of major errors and equipment failures in anesthesia management: Considerations for prevention and detection. Anesthesiology 60:34, 1984

Cooper JB, Newbower RS, Long CD, McPeek B: Preventable anesthesia mishaps: A study of human factors. Anesthesiology 49:399, 1978

Cooper JB, Newbower RS, Moore JW, Trautman ED: A new anesthesia delivery system. Anesthesiology 49:310, 1978

Cooper JB, Newbower RS, Trautman ED: An electronic injector for metering volatile anesthetics. Proceedings of the 28th Annual Conference on Engineering in Medicine and Biology (ACEMB), New Orleans, p 415, 1975

Cowles AL, Borgstedt HH, Gillies AJ: Digital computer prediction of the optimal anaesthetic inspired concentration. British Journal of Anaesthesia 44:420, 1972

Cullen DJ: Anesthetic depth and MAC in Miller RD (ed): Anesthesia (2nd ed). New York, Churchill Livingstone, p 554, 1986

Cullen SC, Gross EG: The anesthetic properties of xenon in animals and human beings, with additional observations on krypton. Science 113:580, 1951

de Jong RH, Eger EI: MAC expanded, AD50 and AD95 values of common inhalation anesthetics in man. Anesthesiology 42:384, 1975

Dammann JF, McAslan TC, Maffeo CJ: Optimal flow pattern for mechanical ventilation of the lungs. 2. The effect of a sine versus square wave flow pattern with and without an end-inspiratory pause on patients. Critical Care Medicine 6:293, 1978

Doebelin EO: Measurement systems: Application and design (4th ed). New York, McGraw Hill Publishing Co., p 568, 1990

Dorsch JA, Dorsch SE: Understanding anesthesia equipment: Construction, care and complications (2nd ed). Baltimore, Williams & Wilkins, 1984

Dripps RD, Eckenhoff JE, Vandam LD: Introduction to anesthesia: The principles of safe practice (6th ed). Philadelphia, W.B. Saunders Co., 1982

du Moulin GC, Hedley-White J: Bacterial interactions between anesthesiologists, their patients and equipment. Anesthesiology 57:37, 1982

Dupuis YG: Ventilators: Theory and application. St Louis, MO, C.V. Mosby Co., 1986

Edsall DW: Economy is not a major benefit of closed-system anesthesia. Anesthesiology 54:258, 1981

Eger EI: Isoflurane: A compendium and reference. Madison, WI, Anaquest, BOC Health Care, p 1, 1985

Eger EI: Uptake and distribution of inhaled anesthetics in Miller RD (ed): Anesthesia (2nd ed). New York, Churchill Livingstone, p 626, 1986

Eger EI, Epstein RM: Hazards of anesthetic equipment. Anesthesiology 25:494, 1964

Eger EI, Ethans CT: The effects of inflow, overflow and valve placement on economy of the circle system. Anesthesiology 29:93, 1968

Eger EI, Bahlman SH: Is the end-tidal anesthetic partial pressure an accurate measure of the arterial anesthetic partial pressure? Anesthesiology 35:301, 1971

Erdmann W, Prakash O, Schepp R: Closing the loop from sensor to therapy. Anesthesia - Safety for all. International Congress Series 637, 595, Excerpta Medica, Amsterdam, 1984

Erdmann W, Veeger AI, Verkaaik APK: Narkosebeatmungsgeräte: Gegenwart und Zukunft in Jantzen JPAH, Kleemann PP (eds): Narkosebeatmung, low flow, minimal flow, Geschlossenes System. Stuttgart, Schattauer, pp 14-16, 1989

Feeley TW, Hamilton WK, Xavier B, Moyers J, Eger EI: Sterile anesthesia breathing circuits do not prevent postoperative pulmonary infection. Anesthesiology 54:369, 1981

Forrest JB: Assessment of the risk of anesthesia: Analysis of outcomes in Gravenstein JS, Holzer JF (eds): Safety and cost containment in anesthesia. Boston, Butterworths, p 25, 1988

Fox RW, McDonald AT: Introduction to fluid mechanics (2nd ed). New York, John Wiley & Sons, p 452, 1978

Fuleihan SF, Wilson RS, Pontopiddan H: Effect of mechanical ventilation with end-inspiratory pause on blood-gas exchange. Anesthesia and Analgesia Current Researches, vol 55, No. 1, 1976

Gaba DM: Human error in anesthetic mishaps. International Anesthesiology Clinics, 27:139, 1989

Gaba DM, DeAnda A: The response of anesthesia trainees to simulated critical incidents. Anesthesia Analgesia 68:444, 1989

Gaba DM, Maxwell M, DeAnda A: Anesthetic mishaps: Breaking the chain of accident evolution. Anesthesiology 66:670, 1987

Gal TJ: Effects of endotracheal intubation on normal cough performance. Anesthesiology 52:324, 1980

Garibaldi RA, Britt MR, Webster C, Pace NL: Failure of bacterial filters to reduce the incidence of pneumonia after inhalation anesthesia. Anesthesiology 54:364, 1981

Good ML, Blaschke UT, Lampotang S: Simultaneous failure of an anesthesia gas machine and the backup ventilation equipment. Submitted for publication, 1992.

Good ML, Lampotang S, Gibby GL, Gravenstein JS: Critical events simulation for training in anesthesiology (abstract). Journal of Clinical Monitoring 4:140, 1988

Gravenstein JS: Training devices and simulators (editorial). Anesthesiology 69:295-297, 1988

Gravenstein N, Banner MJ, McLaughlin G: Tidal volume changes due to the interaction of anesthesia machine and anesthesia ventilator. Journal of Clinical Monitoring 3:187, 1987

Gravenstein N, Lampotang S: Ventilation during anesthesia in Kirby RR, Banner MJ, Downs JB (eds): Clinical applications of ventilatory support. New York, Churchill Livingstone p 297, 1990

Gravenstein N, Lampotang S, Beneken JEW: Factors influencing capnography in the Bain circuit. Journal of Clinical Monitoring 1:6, 1985

Grodin WK, Epstein MAF, Epstein RA: Mechanisms of halothane adsorption by dry soda lime. British Journal of Anaesthesia 54:561, 1982

Groß-Alltag F, Marx T, Friesdorf W: An experimental approach to recycling volatile anesthetics. Meeting Proceedings Second Annual Meeting of Society for Technology in Anesthesia (STA), San Diego, CA, Jan 30 - Feb 1, 3-11.1, 1992

Guyton AC: Textbook of medical physiology (7th ed). Philadelphia, W.B. Saunders Co., p 471, 1986

Hameroff SR, Watt RC: Microtubules: Biological microprocessors? in Carter FL (ed): Molecular electronic devices. New York, Marcel Dekker Inc., p 341, 1982

Hamilton Medical: Veolar operator's manual. Part number 610 233. Reno, NV: Hamilton Medical, 1988

Hatch DJ: Tracheal tubes and connectors used in neonates - dimensions and resistance to breathing. British Journal of Anaesthesia 50:959, 1978

Hawes DW, Ross JAS, White DC, Wloch RT: Servo-control of closed circuit anaesthesia. British Journal of Anaesthesia 54:229P, 1982

Hawkins GA: Thermal properties of substances and thermodynamics in Baumeister T, Avallone EA, Baumeister T (eds): Marks' standard handbook for mechanical engineers (8th ed). New York, McGraw-Hill, pp 4-17, 1978

Hayes JK, Westenskow DR, East TD, Jordan WS: Computer-controlled anesthesia delivery system. Medical Instrumentation 18:224, 1984

Hedenstierna G, Johansson H: Different flow patterns and their effect on gas distribution in a lung model study. Acta Anaesthesiologica Scandinivica 17:190, 1973

Herscher E, Yeakel AE: Nitrous oxide-oxygen based anesthesia: The waste and its cost. Anesthesiology Review. 4:29, 1977

Herzog P, Norlander OP: Distribution of alveolar volumes with different types of positive pressure gas flow patterns. Opusc. Med. Bd 13, nr 1, 1968

Hill DW: Physics applied to anaesthesia. London, Butterworths, pp 148-154, 1967

Holman JP: Experimental methods for engineers (4th ed). New York, McGraw-Hill Book Co., p 237, 1985

Hornbeck RW: Numerical methods. Englewood Cliffs, NJ, Prentice-Hall, 1975

Incropera FP, De Witt DP: Fundamentals of heat and mass transfer (2nd ed). New York, John Wiley & Sons, p 770, 1985

Jackson DE: Anesthesia equipment from 1914 to 1954 and experiments leading to its development. Anesthesiology 16:953, 1955

Jansson L, Jonson B: A theoretical study on flow patterns of ventilators. Scandinavian Journal of Respiratory Disease. 53:237, 1972

Jantzen JPAH, Kleemann PP: Narkosebeatmung Low flow, Minimal flow, Geschlossenes System. Stuttgart, Schattauer, 1989

Johannigman JA, Branson RD, Campbell R, Hurst JM: Laboratory and clinical evaluation of the MAX transport ventilator. Respiratory Care 35:952, 1990

Johansson H, Löfström JB: Effects on breathing mechanics and gas exchange of different inspiratory gas flow patterns during anesthesia. Acta Anaesthesiologica Scandinivica 19:8, 1975

Johnson DE, Hilburn JL, Johnson JR: Basic electric circuit analysis (3rd ed). Englewood Cliffs, NJ, Prentice-Hall, p 308, 1986

Jones CS: A new look at old anesthesia circuits (letter). Anesthesiology 56:486, 1982

Jones PL, Prosser J: An assessment of the Neff circulator. Canadian Anaesthetists Society Journal 20:659, 1973

Kacmarek RM, Dimas S, Reynolds J, Shapiro BA: Technical aspects of positive end-expiratory pressure (PEEP): Part 1. Physics of PEEP devices. Respiratory Care 27:1478, 1982

Kernighan BW, Ritchie DM: The C programming language. Prentice Hall, Englewood Cliffs, NJ, 1978

Kirby RR, Perry JC, Calderwood HW, Ruiz BC, Lederman DS: Cardiorespiratory effects of high positive end-expiratory pressure. Anesthesiology, 43:533, 1975

Kleemann PP: Tierexperimentelle und klinische Untersuchungen zum Stellenwert der Klimatisierung anästhetischer Gase im Narkosekreissystem bei Langzeiteingriffen. Wiesbaden, Wissenschaftliche Verlagsabteilung Abbott GmbH, 1989

Koblin DD, Eger EI: How do inhaled anesthetics work? in Miller RD (ed): Anesthesia (2nd ed). New York, Churchill Livingstone, p 593, 1986

Lachmann B, Armbruster S, Schairer W, Landstra M, Trouwborst A, van Daal GJ, Kusuma A, Erdmann W: Safety and efficacy of xenon in routine use as an inhalational anesthetic. The Lancet, v 335, p 1413, 1990

Lampotang S: Microprocessor-controlled ventilation systems and concepts in Kirby RR, Banner MJ, Downs JB (eds): Clinical applications of ventilatory support. New York, Churchill Livingstone, 1990a

Lampotang S: Microprocessor and control systems in mechanical ventilators in Banner MJ (ed): Positive pressure ventilation. Problems in Critical Care, vol. 4, No. 2, Philadelphia, J.B. Lippincott Co., 1990b

Lampotang S, Good ML, Gibby GL, Milsap J, Peickert W, Braatz R, Gravenstein JS: The Gainesville anesthesia simulator I: Design considerations. Submitted for publication to the Journal of Clinical Monitoring, 1992a

Lampotang S, Good ML, Gibby GL, Milsap J, Peickert W, Braatz R, Gravenstein JS: The Gainesville anesthesia simulator I: Engineering and hardware. Submitted for publication to the Journal of Clinical Monitoring, 1992b

Lampotang S, Gravenstein N, Banner MJ, Jaeger MJ, Schultetus RR: A lung model of carbon dioxide concentrations with mechanical or spontaneous ventilation. Critical Care Medicine 14:1055, 1986

Lampotang S, Nyland ME, Gravenstein N: The cost of wasted anesthetic gases (abstract). Anesthesia Analgesia 72:S151, 1991

Langill AW, Friedland H, Limbacher DL: New control valve accepts digital signals. Control Engineering 16:95, 1969

Lapina RP: Estimating centrifugal compressor performance. Houston, Gulf Publishing Co., p 107, 1982

Laycock CH: Applied electrotechnology for engineers. London, Macmillan Press Ltd., p 18, 1976

Loeb RG, Brunner JX, Westenskow DR, Feldman B, Pace NL: The Utah anesthesia workstation. Anesthesiology 70:999, 1989

Lough MD, Chatburn R, Schrock WA: Handbook of respiratory care. Chicago, Year Book Medical Publishers, Inc., 1983

Lyager S: Influence of flow pattern on the distribution of respiratory air during intermittent positive pressure ventilation. Acta Anaesthesiologica Scandinavica 12:191, 1968

Lyndon B Johnson Space Center: Apparatus circulates sterilizing gas. NASA Tech Briefs, Official Publication of National Aeronautics and Space Administration, Vol. 15, No. 10, p 116, October 1991

Macintosh R, Mushin WW, Epstein HG: Physics for the anaesthetist including a section on explosions (3rd ed). Philadelphia, F.A. Davis Co., 1963

Mapleson WW, Allott PR, Steward A: A non-feedback technique for programmed anaesthesia. British Journal of Anaesthesia 46:805, 1974

Mapleson WW, Chilcoat RT, Lunn JN, Blewett MC, Khatib MT, Willis BA: Computer assistance in the control of depth of anaesthesia. British Journal of Anaesthesia 52:234P, 1980

Mayhew YR, Rogers GFC: Thermodynamic and transport properties of fluids (SI units; 2nd ed). Oxford, Basil Blackwell, 1977

Merkel G, Eger EI: A comparative study of halothane and halopropane anesthesia. Anesthesiology 24:346, 1963

Miller DS: Internal flow systems: Design and performance prediction (2nd ed). Houston, TX, Gulf Publishing Company, 1990.

Morris LE: The circulator concept in Wyant GM (ed): Problems in the performance of anesthetic and respiratory equipment. International Anesthesiology Clinics 12:181, p 192, 1974

Morris P, Tatnall ML, Montgomery FJ: Controlled anaesthesia: A clinical evaluation of an approach using patient characteristics identified during uptake. British Journal of Anaesthesia 55:1065, 1983

Mushin WW, Galloon S: The concentration of anaesthetics in closed circuits with special reference to halothane. III. Clinical effects. British Journal of Anaesthesia 32:324, 1960

Mushin WW, Jones PL: Physics for the anaesthetist (4th ed). Oxford, Blackwell Scientific Publications, p 387, 1987

Mushin WW, Rendell-Baker L, Thompson PW, Mapleson WW: Automatic ventilation of the lungs (3rd ed). Oxford, Blackwell Scientific Publications, p 7, 1980

National Institute for Occupational Safety and Health: Development and evaluation of methods for the elimination of waste anesthetic gases and vapors in hospitals. DHEW Publication No. (NIOSH) 75-137. Cincinnati, US Department of Health, Education and Welfare, p Vlll-1, 1975

Neff WB, Burke SF, Thompson R: A venturi circulator for anesthetic systems. Anesthesiology 29:838, 1968

Neff WB, Sullivan MT, Poulter TC: A magnetic-drive circulator designed for completely closed carbon dioxide absorption systems. Anesthesiology 51:169, 1979

Norreslet J, Friberg S, Nielsen TM, Romer U: Halothane anaesthetic and the ozone layer (letter). The Lancet, vol i:719, 1989

Nunn JF: Applied respiratory physiology (3rd ed). London, Butterworths, p 160, 1987

Ogata K: Modern control engineering. Englewood Cliffs, NJ, Prentice-Hall, Inc., p 233, 1970

Ohmeda: 5250 respiratory gas monitor. Operation and maintenance manual. Publication 6050 0001 051 06 90 G 10 11 13, Madison, WI, 1990a

Ohmeda 7800 ventilator: Software version 1.x operation and maintenance manual. 1500-0062-000 08/15/90, Madison, WI, p 3-15, 1990b

Ohmeda: 7810 anesthesia ventilator manual. Madison, Ohmeda Anesthesia Systems, BOC Health Care, 1988

Ohmeda Modulus II anesthesia machine: Preoperative checklists operation and maintenance manuals. Madison, Ohmeda Anesthesia Systems, Division of The BOC Group Inc., 205-5168-300, 1986

Orkin FK: Anesthetic systems in Miller RD (ed): Anesthesia (2nd ed). New York, Churchill Livingstone, p 135, 1986

Otis AB, McKerrow CB, Bartlett RA, Mead J, McIlroy MB, Selverstone NJ, Radford EP: Mechanical factors in distribution of pulmonary ventilation. Journal of Applied Physiology 8:427, 1956

Pashayan AG, Gravenstein JS, Cassisi NJ, McLaughlin G: The helium protocol for laryngotracheal operations with CO_2 laser: A retrospective review of 523 cases. Anesthesiology 68:801, 1988

Patel A, Milliken RA: Costs of delivery of anesthetic gases examined I (letter). Anesthesiology 55:710, 1981

Petrucci RH: General chemistry: Principles and modern applications (5th ed). New York, Macmillan Publishing Co., p 584, 1989

Petty C: The anesthesia machine. New York, Churchill Livingstone Inc., p 82, 1987

Physio Medical Systems: Gesloten anaesthesie ventilator. Physio B.V., Hoofddorp, The Netherlands, 1990

Portex Publication LT-046 REV. 10/90: Endotracheal tubes. Concord Portex, Keene, New Hampshire, 1990

Puritan-Bennett: 7200 series microprocessor ventilator service manual. Part number 31052, rev E 12-84, Overland Park, Kansas, Puritan-Bennett Corporation, 1984

Quasha AL, Eger EI, Tinker JH: Determination and applications of MAC. Anesthesiology 53:315, 1980

Quinlan D, Modell JH: Painless cost containment (abstract). Anesthesiology 51:S354, 1979

Ream AK: New directions: The anesthesia machine and the practice of anesthesia (editorial). Anesthesiology 49:307, 1978

Rehder K, Knopp TJ, Brusasco V, Didier EP: Inspiratory flow and intrapulmonary gas distribution. American Review of Respiratory Disease 124:392, 1981

Rehder K, Knopp TJ, Sessler AD, Didier EP: Ventilation-perfusion relationship in young healthy awake and anesthetized-paralyzed man. J Appl Physiol: Respirat Environ Exercise Physiol 47:745, 1979

Rendell-Baker L: On the promise of economy denied (editorial). Anesthesiology 29:5, 1968

Revell DG: A circulator to eliminate mechanical dead Space in circle absorption systems. Canadian Anaesthetists' Society Journal 6:98, 1959

Revell DG: Am improved circulator for closed circle anaesthesia. Canadian Anaesthetists' Society Journal 6:104, 1959

Ritchie RG, Ernst EA, Pate BL, Pearson JD, Sheppard LC: Closed-loop control of an anesthesia delivery system: Development and animal testing. IEEE Transactions on Biomedical Engineering, BME-34:437, 1987

Rodgers RC, Hill GE: Equations for vapor pressure versus temperature: Derivation and use of the Antoine equation on a hand-held programmable calculator. British Journal of Anaesthesia 50:415, 1978

Rodgers RC, Ross JAS: Anaesthetic agents and the ozone layer (letter). The Lancet, vol i:1209, 1989

Roffey PJ, Revell DG, Morris LE: An assessment of the Revell circulator. Anesthesiology 22:583, 1961

Ross JAS, Wloch RT, White DC, Hawes DW: Servo-controlled closed circuit anaesthesia: A method for the automatic control of anaesthesia produced by a volatile agent in oxygen. British Journal of Anaesthesia 55:1053, 1983

Salamonsen RF: A vaporizing system for programmed anaesthesia. British Journal of Anaesthesia 50:425, 1978

Schepp R, Erdmann W, Westerkamp B, Faithfull NS: Automatic ventilation during closed circuit anesthesia in Droh R, Erdmann W, Spintge A (eds): Anaesthesia innovations in management. Berlin, Springer, 1985

Schreiber P: Anaesthesia equipment: Performance, classification and safety. Berlin, Springer-Verlag, p 118, 1972

Shapiro AH: The dynamics and thermodynamics of compressible fluid flow (volume 1). New York, John Wiley and Sons, 1953

Smith RB: Continuous-flow apneic ventilation. Respiratory Care 32:458, 1987

Smith RB, Babinski M, Bunegin L, Gilbert J, Swartzman S, Dirting J: Continuous flow apneic ventilation. Acta Anaesthesiologica Scandinivica 28:634, 1984

Spain JA: Costs of delivery of anesthetic gases examined III (letter). Anesthesiology 55:711, 1981

Spiegel MR: Mathematical handbook of formulas and tables. New York, McGraw Hill Book Co., p 104, 1968

Steward A, Allott PR, Cowles AL, Mapleson WW: Solubility coefficients for inhaled anesthetics for water, oil and biological media. British Journal Of Anaesthesia 45:282, 1973

Stoecker WF, Stoecker PA: Microcomputer control of thermal and mechanical systems. New York, Van Nostrand Reinhold, pp 78-90, 1989

Strauß JM, Bannasch W, Hausdörfer J, Bang S: Die Entwicklung von Carboxyhämoglobin während Langzeitnarkosen im geschlossenen Kreissystem. Der Anaesthetist 40:324, 1991

Sullivan M, Saklad M, Demers RR: Relationships between ventilator waveform and tidal volume distribution. Respiratory Care 22:386, 1977

Sykes MK, Sugg BR, Hahn CEW, Jackson RK, Palayiwa E: A new microprocessor-controlled anaesthetic machine. British Journal of Anaesthesia 63:45, 1989

Tatnall ML, Morris P, West PG: Controlled anaesthesia: An approach using patient characteristics identified during uptake. British Journal of Anaesthesia 53:1019, 1981

Tescom Corporation: Pressure Controls Division, Elk River, Minnesota, Form 1583, 1/89, 35M GL; 1989

Thomas KB: The development of anesthetic apparatus. Oxford, Blackwell Scientific Publications, p 5, 1975

Titel JH, Lowe HJ: Rubber-gas partition coefficients. Anesthesiology 29:1215, 1968

Ulyatt DB, Judson JA, Trubuhovich RV, Galler LH: Cerebral arterial air embolism associated with coughing on a continuous positive airway pressure circuit. Critical Care Medicine 1991

US Patent 4,702,241; Gravenstein JS, Lampotang S: Self-contained jet pump breathing apparatus

US Patent 4,573,462; Baum M: Respiratory system

US Patent 4,543,951; Phuc TN: Respirator with two jet gas injection tubes

US Patent 4,520,812; Freitag L, Wendt M, Dankwart FJ: Method and apparatus for controlling a pressure level in a respirator

US Patent 4,481,944; Bunnell JB: Apparatus and method for assisting respiration

US Patent 4,463,756; Thuc TN: Ventilation apparatus for artificial respiration

US Patent 4,281,652; Miller DM: Control member for anaesthesia apparatus

US Patent 4,245,633; Erceg GW: PEEP providing circuit for anesthesia systems

US Patent 4,188,946; Watson RL, Rayburn RL: Controllable partial rebreathing anesthesia circuit and respiratory assist device

US Patent 4,082,093; Fry SE, Hurd CC: Compensator valve

US Patent 4,007,737; Paluch BR: Anesthesia breathing system

US Patent 3,815,593; Baumont G: Static respirator for artificial ventilation

US Patent 3,485,243; Bird FM, Pohndorf HL: Respirator with improved exhalation and control means

US Patent 3,385,295; Beasley NF: Apparatus for use in administering intermittent positive pressure breathing therapy

US Patent 3,378,005; Smith RM: Anesthetic apparatus

US Patent 3,033,196; Hay WW: Artificial respiration apparatus

US Patent 2,830,583; Finney RP: Electrically controlled breathing apparatus

US Patent 2,325,049; Frye HH, Behnke AR: Breathing apparatus

US Patent 1,635,101; von Hoff C: Oxygen respiratory apparatus

US Patent 1,630,501; Steese MC: Life-saving apparatus

van der AA, JJ: Intelligent alarms in anesthesia: A real time expert system application (PhD dissertation). The Hague, CIP-Gegevens Koninklijke Bibliotheek, 1990

Verkaiik APK, Erdmann W: Respiratory diagnostic possibilities during closed circuit anesthesia. Acta Anaesthesiologica Belgica 41:178, 1990

Versichelen L, Rolly G: Mass-spectrometric evaluation of some recently introduced low flow, closed circuit systems. Acta Anaesthesiologica Belgica 41:230, 1990

Virtue RW, Aldrete JA: Costs of delivery of anesthetic gases examined II (letter). Anesthesiology 55:711, 1981

Wark K: Thermodynamics (4th ed). New York, Mc Graw-Hill, Inc., p 485, 1983

Waterson CK: The Anesthesia Machine: Current design and alternatives. Medical Instrumentation 17:379, 1983

Waterson CK: Recovery of waste anesthetic gases in Brown BR, Calkins JM, Saunders RJ (eds): Future anesthesia delivery systems. Philadelphia, F.A. Davis, pp 115-117. 1984

West JB: Respiratory physiology - the essentials. Baltimore, Williams & Wilkins Co., p 19, 1974

Westenskow DR, Johnson CC, Jordan WS, Gehmlich DK: Instrumentation for measuring continuous oxygen consumption of surgical patients. IEEE Transactions on Biomedical Engineering BME-24:31, 1977

Westenskow DR, Jordan WS, Hayes JK: Feedback control of enflurane delivery in dogs - inspired compared to end-tidal control. Anesthesia Analgesia 62:836, 1983

Westenskow DR, Jordan WS, Hayes JK: Uptake of enflurane: A study of the variability between patients. British Journal of Anaesthesia 55:595, 1983

Whelan JP, Gravenstein N, Welch JL, Lampotang S, Newman RC, Finlayson B: Simulation of ventilatory-induced stone movement and its effect on stone fracture during extracorporeal shock wave lithotripsy. Journal of Urology 140:405, 1988

White FM: Fluid mechanics. New York, McGraw Hill Book Co., p 633, 1979

BIOGRAPHICAL SKETCH

Samsun Lampotang was born on August 28, 1957 in Port Louis, Mauritius, Indian Ocean. He graduated from the Royal College, Port Louis in 1976 and apprenticed in engineering at Forges Tardieu, Port Louis, Mauritius. In August 1977, he was awarded a scholarship from the Government of Mauritius to study at Brunel University, England. He obtained a bachelor's degree (Honors) in mechanical engineering in June 1981. As part of his bachelor's degree, he worked for 18 months in England and Scotland.

He started graduate studies in mechanical engineering at the University of Florida in January 1982 and received a Master of Engineering in May 1984. Since August 1982, he has performed research at the University of Florida Department of Anesthesiology.

During a summer externship in 1987 at Ohmeda Anesthesia Systems Engineering R&D Lab in Madison, WI, he designed and built an anesthesia simulator together with Michael L. Good, MD and Joachim S. Gravenstein, MD, Dr. h.c., which received the first prize for best scientific exhibit at the American Society of Anesthesiologists' 1987 annual meeting. Working with Michael J. Banner, PhD, RRT and Paul B. Blanch, BS, RRT, he also designed and built an adult/pediatric transport ventilator that is currently being sold worldwide. Together with Dietrich Gravenstein, MD and other inventors, he has patented a device for detection of esophageal intubation and a method for non-invasive determination of hemoglobin concentration. He plans to work in the general area of research and development of medical technology after graduation.
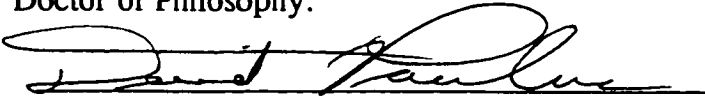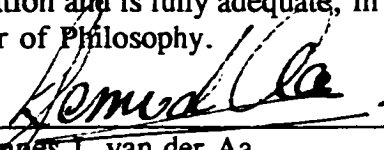
418

I certify that I have read this study and that in my opinion it conforms to acceptable standards of scholarly presentation and is fully adequate, in scope and quality, as a dissertation for the degree of Doctor of Philosophy.

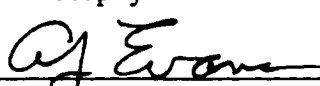Vernon P. Roan, Chairman
Professor of Mechanical Engineering

I certify that I have read this study and that in my opinion it conforms to acceptable standards of scholarly presentation and is fully adequate, in scope and quality, as a dissertation for the degree of Doctor of Philosophy.

Joachim S. Gravenstein
Graduate Research Professor in Anesthesiology

I certify that I have read this study and that in my opinion it conforms to acceptable standards of scholarly presentation and is fully adequate, in scope and quality, as a dissertation for the degree of Doctor of Philosophy.

Harold W. Doddington
Engineer of Aerospace Engineering, Mechanics, and Engineering Science

I certify that I have read this study and that in my opinion it conforms to acceptable standards of scholarly presentation and is fully adequate, in scope and quality, as a dissertation for the degree of Doctor of Philosophy.

David A. Paulus
Associate Professor of Mechanical Engineering

I certify that I have read this study and that in my opinion it conforms to acceptable standards of scholarly presentation and is fully adequate, in scope and quality, as a dissertation for the degree of Doctor of Philosophy.

John K. Schueller
Associate Professor of Mechanical Engineering

I certify that I have read this study and that in my opinion it conforms to acceptable standards of scholarly presentation and is fully adequate, in scope and quality, as a dissertation for the degree of Doctor of Philosophy.
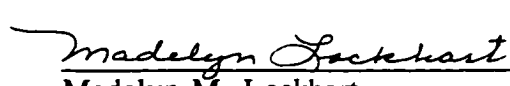
Johannes J. van der Aa
Assistant Professor of Anesthesiology

This dissertation was submitted to the Graduate Faculty of the College of Engineering and to the Graduate School and was accepted as partial fulfillment of the requirements for the degree of Doctor of Philosophy.
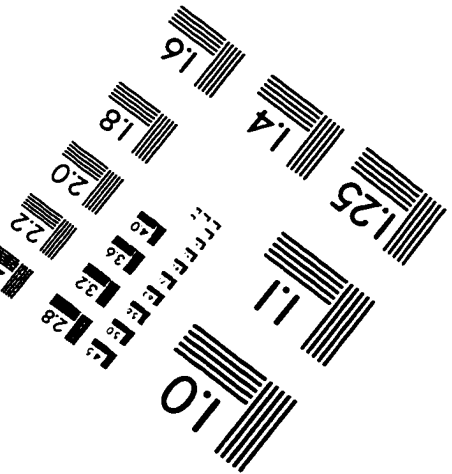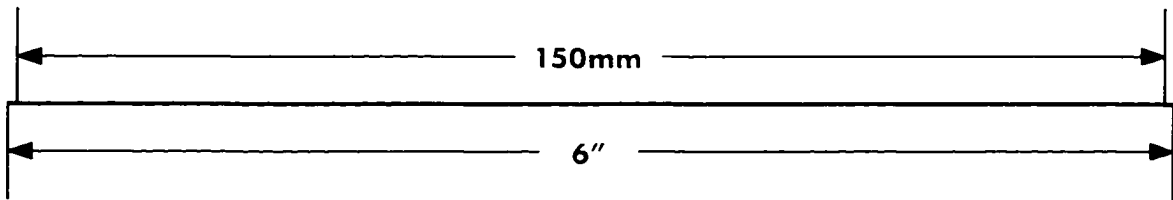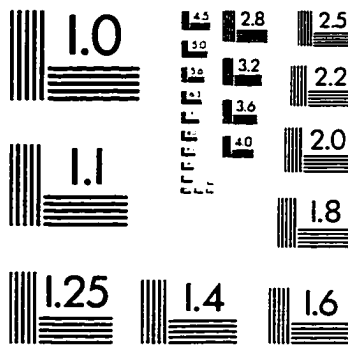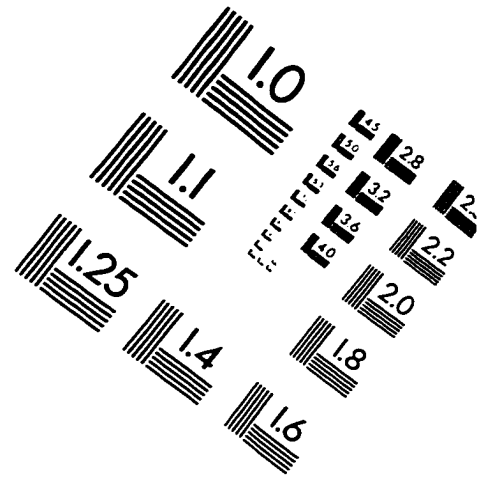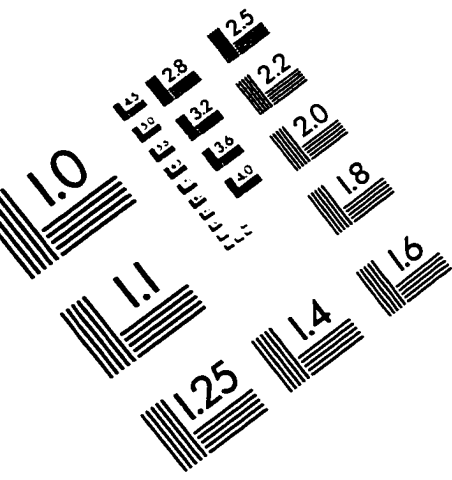
August 1992

Winfred M. Phillips
Dean, College of Engineering

Madelyn M. Lockhart
Dean, Graduate School

IMAGE EVALUATION
TEST TARGET (QA-3)

150mm

6"

APPLIED IMAGE . Inc
1653 East Main Street
Rochester, NY 14609 USA
Phone: 716/482-0300
Fax: 716/288-5989